CZECH TECHNICAL UNIVERSITY IN PRAGUE
Faculty of Nuclear Sciences and Physical Engineering

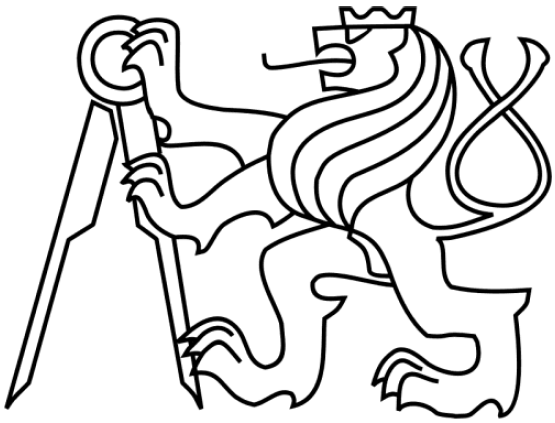

DISSERTATION

Mgr. Ing. Martin Malachov

Chaotic dynamics of purification protocols

Supervisor: prof. Ing. Igor Jex, DrSc.

2023 Prague

ČESKÉ VYSOKÉ UČENÍ TECHNICKÉ V PRAZE
Fakulta jaderná a fyzikálně inženýrská

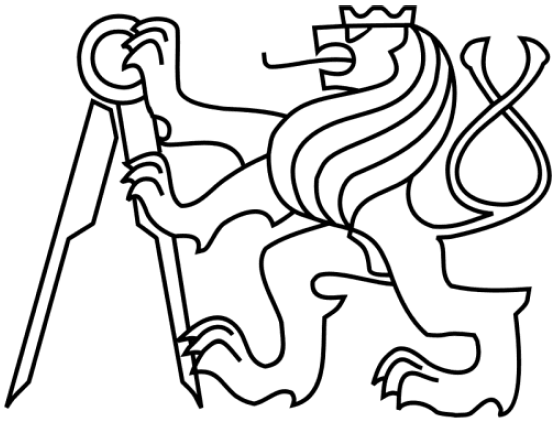

DISERTAČNÍ PRÁCE

Mgr. Ing. Martin Malachov

Chaotická dynamika purifikačních protokolů

Školitel: prof. Ing. Igor Jex, DrSc.

2023 Praha

Declaration

I declare that I carried out this dissertation independently, and only with the cited sources, literature and other professional sources.

I understand that my work relates to the rights and obligations under the Act No. 121/2000 Sb., the Copyright Act, as amended, in particular the fact that the Czech Technical University has the right to conclude a license agreement on the use of this work as a school work pursuant to Section 60 of the Copyright Act.

Prohlášení

Prohlašuji, že jsem svou disetační práci vypracoval samostatně a použil jsem pouze podklady uvedené v přiloženém seznamu.

Nemám závažný důvod proti použití tohoto školního díla ve smyslu §60 Zákona č. 121/2000 Sb., o právu autorském o právech souvisejících s právem autorským a o změně některých zákonů (autorský zákon).

In Prague, date 31st March 2023
V Praze, dne 31. března 2023

signature of the author
podpis autora

Dedication

Author would like to express his deepest thanks to all his family and friends, for their unending support. Author would also like to thank his supervisor for all his tolerance and help.

Poděkování

Autor by rád vyjádřil nejhlubší díky své rodině a přátelům, za jejich podporu bez konce. Autor by též rád poděkoval svému vedoucímu za všechnu jeho toleranci a pomoc.

Bibliographic entry

Title:	Chaotic dynamics of purification protocols
Author:	Mgr. Ing. Martin Malachov
Affiliation:	Department of Physics, Faculty of Nucler Sciences and Physical Engineering, Czech Technical University in Prague
Degree programme:	Aplication of natural sciences
Field of study:	Mathematical engineering
Supervisor:	prof. Ing. Igor Jex, DrSc.
Supervisor's affiliation:	Department of Physics, Faculty of Nucler Sciences and Physical Engineering, Czech Technical University in Prague
Academic year:	2022/2023
Number of pages:	192
Keywords:	quantum information, purification, entanglement, chaos, fractal, dimension

Bibliografický záznam

Název práce:	Chaotická dynamika purifikačních protokolů
Autor:	Mgr. Ing. Martin Malachov
Instituce:	Katedra fyziky, Fakulta jaderná a fyzikálně inženýrská, České vysoké učení technické v Praze
Studijní program:	Aplikace přírodních věd
Studijní obor:	Matematické inženýrství
Školitel:	prof. Ing. Igor Jex, DrSc.
Instituce školitele:	Katedra fyziky, Fakulta jaderná a fyzikálně inženýrská, České vysoké učení technické v Praze
Akademický rok:	2022/2023
Počet stran:	192
Klíčová slova:	kvantová informace, purifikace, provázání, chaos, fraktál, dimenze

Abstract

Quantum information and communication are modern and promising branches of science. The improvement they offer exploits quantum entanglement, the key resource to interesting applications e.g. quantum teleportation, searching algorithms etc. The entangled states suffer from decoherence, noise, in realistic physical setting; one of the protocols proposed lately uses particular measurement-based modification on a copy of the state to restore the state and its entanglement. The action of the protocol is nonlinear and it has been shown that in certain states it induces chaotic dynamics.

Chaos means sensitiveness to initial conditions and perturbations and is often connected to fractal structures. In this work, we propose a simple chaotic model which is completely analysed. Many of found phenomena are documented for the first time in this level of quantum physics, they have no analogy in classical physics. We also propose whole classes of other protocols and try to investigate their dynamical regimes. Most of all, we focus on the fractal structures of the sensitive states. We decide to characterise the structures by their dimension which is the key structural characteristic of fractals. Using numerical methods we estimate the dimension of fractal structures and discover surprising features related both to nonlinear dynamics and quantum physics. The change of the structure with respect to the purity of initial states can be understood as a phase transition. Besides the numerical, we also use analytical methods where possible to demonstrate presence of characteristic features of nonlinear dynamics in the context of purely quantum systems. Motivated by physical and informational background we also make notes on the practical aspects of our results. We also set questions and future directions of this exciting interdisciplinary research.

Abstrakt

Kvantová informace a komunikace jsou slibná odvětví věd. Pokrok, který představují, využívá kvantového provázání, které je klíčovým zdrojem k aplikacím jako např. kvantová teleportace, vyhledávací algoritmus aj. Provázané stavy podléhají dekoherenci, šumu v realistickém fyzikálním prostředí; jeden z nedávných protokolů využívá modifikaci založenou na měření na kopii stavu k obnovení jeho a jeho provázání. Akce protokolu je nelineární a ukázalo se, že na určitých stavech vyvolává chaotickou dynamiku.

Chaos znamená citlivost k počátečním podmínkám a poruchám a je často spojen s fraktálními strukturami. V této práci představujeme jednoduchý chaotický model, který plně analyzujeme. Nacházíme mnohé jevy, které dosud nebyly v této formě v kvantové fyzice objeveny. Dále navrhujeme celou řadu dalších protokolů a zkoumáme jejich dynamické režimy. Zejména se pak soustředíme na fraktální struktury citlivých stavů. K popisu těchto struktur užíváme dimenzi, která je základní strukturální charakteristikou fraktálů. Využitím numerických metod odhadujeme dimenze fratkálních struktur, což vede k řadě objevů v oblasti jak nelineární dynamiky, tak kvantové fyziky. Změna struktury jakožto funkce purity vstupních stavů může být chápána jako fázový přechod. Kromě numerických se snažíme využívat i analytické metody, abychom prokázali charakteristické jevy nelineárních dynamik v kontextu čistě kvantových systémů. Pro motivaci z pomezí fyziky a informatiky také interpretujeme výsledky praktickým směrem. Nakonec formulujeme otázky a směrujeme budoucí práci v tomto zajímavém interdisciplinárním výzkumu.

Contents

1. Introduction

In the last decades, quantum physics and the theory of information and computation joined to give rise to a new branch of promising and surprising improvements to contemporary science. Starting with new quantum protocols that can solve some tasks in polynomial time and so surpass today's algorithms requiring exponential time [59, 13] and ending in whole new protocols beyond the classical physics, e.g. quantum teleportation, [7]. New findings offer crucial improvements in various fields of applications, not only in computing and information storage but also stretching to cryptography or medicine.

Recent papers [35, 36] have shown that there is a new unknown area of study with great potential. Chaos. a new form of chaotic evolution which is induced by quantum description itself. Naturally, one can assume that chaos must be present within the quantum theory at least by the correspondence principle. There must be a quantum description to systems like three body problem etc. However, this type of chaos is a consequence of certain types of evolution equations and not the quantum nature itself. There is a whole branch that aims on studying quantum description of (semi)classicaly chaotic systems. This branch is today usually reffered to as quantum chaology. But in this thesis, we aim for something different. More profound description of certain systems that exhibits chaotic features thanks to the quantum laws themselves. The chaos studied in our work neither has any correspondence to classical chaotic systems nor is related to the field of quantum chaology.

The fundamental cause of the chaos, i.e. exponential sensitivity of the quantum system to its initial conditions [16], lies in its nonlinear evolution. The roots of the nonlinearity originate from an interaction of the physical system with environment. The topic of open quantum systems is usually restricted to special statistical systems (gas and reservoir etc.) but the issue studied in this work presents a very simple and exact interaction of two qubits where one manifests (via measurement-based selection) as the environment which results in seemingly simple nonlinear evolution. However, even such a simple system goes beyond accessible mathematical theories, these offer no description of the asymptotic dynamics at the moment. Furthermore, because there is no analogy to classical systems, we start to study this field of multidimensional quantum chaos from the very beginning and give some fundamental knowledge for future research.

However, the task of studying this new type of chaos has a few fundamental problems. First, the foundation of the topic combines knowledge of many advanced branches including theory of information and computation, quantum physics, the theory of complex functions and the theory of chaos. Each of these branches is quite extensive and requires a different mentality and approach to be handled successfully. In this work we must join them all to offer our readers some new interesting findings and move on with the research with great potential.

The particular quantum information protocol we study was proposed in [4] and improved and modified in [1]. Briefly said, its purpose is to sacrifice some copies of a piece of information to repair damage that is typically caused by transmission through environment on other copies. The protocol uses measurement-based selection to modify the quantum states. While one copy of the state is taken

as a reservoir, this particular environment action can cause a specifical nonlinear evolution. The protocol is constructed in the way that it manifests on the density matrix elements as a function $z \to z^2$. The dynamics can be further modified by an additional unitary operator called twirling operator. In consequence, we describe a new set of quantum dynamical regimes.

Amongst these regimes the prominent position is taken by the chaotic ones. So far, the exponential sensitiveness to initial conditions has been revealed for a particular class of pure states and Hadamard gate as the twirling operator [36]. Inspired by this, we aim for following goals in this thesis. The chaotic behaviour is probably not present only for the particular states. We want to examine asymptotic dynamical regimes for general input states. Special attention must be dedicated to mixed states which - from their definition of statistical ensembles - may exhibit fundamentally different behaviour than pure states. The chaos in [36] has been related to a fractal structure encountered when studying a function of a single complex variable. The chaos is often connected to fractal structures, whence we dedicate particular effort to study such structures in the context of the purification protocols. To do so, we implement a numeric approach of dimension estimation known as box-counting. Introducing the fractal dimension to the topic of the purification protocol is one of the biggest contribution of this thesis.

We also want to investigate whether the evolution induced by the proposed protocol possesses other interesting features connected to nonlinear dynamics. That would be a novel finding for this type of quantum state evolution. We will try to give a complete characterisation of the asymptotic evolution, in an analytic approach where possible. However, the topic of multidimensional chaos is very intricate and so we will have to utilise numerical methods too. One of the side goal of our thesis is to implement the numerical machinery for the purpose of analysis of chaos in quantum purification. Particular attention will be devoted to the box-counting algorithm, as already mentioned.

The next natural step to take is to generalise the protocol [36] and we set up two main directions based on outlines from [1, 35]. These two generalisations are another goal achieved in our thesis. One of them relies on using different twirling operators; we will study the change of the asymptotic evolution based on the parameters of the protocol. The other direction is based on using a system of multiple copies to induce nonlinear behaviour of type $x \to x^n$. Both of the generalisations will be proposed in detail with the exact description elaborated. Both of the generalistions will also be merged together to offer whole new classes of purification protocols. For these we will give basic overview of dynamical and chaotical features and compare them to the original protocol.

The results of our work could be of high importance for the practical applicability of the protocol with an impact to more effective quantum information transmission, e.g. for quantum key distribution, [6, 9, 54]. Even more, our work could initiate new algorithms exploiting discovered nonlinear features. We will also give suggestions on next research and will discuss practical aspects of our theoretical findings.

The framework of this thesis follows a natural line of thoughts outlined in previous paragraphs. In this work we bring together the indispensable pieces of the theories. Therefore, in the second chapter 2 the quantum description of

the physical system is presented together with fundaments of the chaos theory. Particular attention is then paid to the box-counting method and the topic of dimension which we exploit in our work. We also introduce parameterisations and mathematical conventions that will be used for the rest of the work to comprehensively transfer the results to the wider scientific community. The theoretical background will be developed with respect to the fact that our readers may not be experienced enough in all the specific branches. We believe that for them we should offer a comprehensible introduction to basic concepts and instruments. Even at the cost that a reader familiar with e.g. quantum physics will consider some passages trivial and not worth of mentioning. We believe that our approach is appropriate for an interdisciplinary work.

The chapters presenting our results start with the protocol modification for single qubits. This proposal may be considered a toy model but it is complex enough to demonstrate the fundamental properties of more general protocols that will be discussed later. Evolution equations for general (i.e. mixed) input states are derived. By analytic and numeric means we uncover interesting results including features related to nonlinear dynamics that have not yet been observed. One of the conclusions relates to the fractal dimension which undergoes sudden changes which we interpret as a phase transition. The purity of the state (in the sense of pure - mixed states) is not a necessary criterion to observe chaotic features, the mixed states can also exhibit deterministic chaos and form fractal patterns despite their statistical uncertainty. Other findings including remarks on convergence speed are related to the practical use of the protocol.

The fourth chapter 4 generalises the protocol by modifying the twirling operator. We do not analyse all the protocols in detail but at the moment we focus on basic characterisation, similarities and differences and mainly to support that the phase transition in the fractal structure is not unique for the Hadamard gate protocol only. The change of the operator can shift the temperatures of the transitions and possibly also change the number of phases. Our main goal is to demonstrate that the twirling gates can affect the chaotic evolution; we want to present (in)dependence of convergences rates and other nonlinear dynamical features on the protocol parameters.

The next chapter 5 is dedicated to another generalisation of the previously defined toy model of the single qubit evolution to implement more involved evolution maps including higher polynomial functions by introducing more copies of the qubit as the generalised environment. We introduce the concept of the general protocol implementation and put forward the mathematical representation of evolution equations. Furthermore, we reproduce previous results for these newly defined protocols and compare them with the original protocol. In addition, we discuss the practical applicability of the protocol, especially in the context of the convergence speed which is an important aspect for the future use.

Since the original protocol was designed to purify the quantum entanglement in pairs of qubits, in chapter 6 we come back to the protocol defined on two-qubit systems and employ the just studied toy model which has a direct analogy in the two-qubit states evolution; previous results can then be easily recounted in the context of the two-qubit protocols as well as the capabilities of purifying the quantum entanglement. We recapitulate the findings focusing on the newly present effect of entanglement which we measure within the concept of concurrence.

The final chapter is dedicated solely to a recapitulation of the results and questions and proposals for the next research.

Results from our third chapter were published as *Phase Transition in Iterated Quantum Protocols for Noisy Inputs* in Chaos journal - the paper got a particular attention as an editor's pick. The author discovered the topic of phase transitions, provided methodology, box-counting algorithm and results, co-author Orsolya Kálmán provided calculations of backward iterations. Other co-authors Igor Jex and Tamás Kiss helped with the text of the paper. The article can be found in

- *Chaos*, **29**, 033107 (2019); `https://doi.org/10.1063/1.5082946`
- arXiv database: `https://doi.org/10.48550/arXiv.1809.00140`

Further results from the fourth chapter onwards are solely the work of the author and are currently prepared to be published.

2. On the frontiers of theories

The future of quantum information is very promising. This branch of science builds the theory of information upon quantum laws of the Universe, [14, 15]. Although there are many similarities with the classical information theory founded by Shannon, [57] (built upon classical physics), the quantum version is richer. It offers phenomena like quantum entanglement [18] to benefit from. Protocols proposed in the last decades have exploited the exotic nature of quantum physics to implement new algorithms supreme to the current state of the art. The key entity to all parts of the quantum information is the qubit. This quantum analogue of classical bit contains the quantum essence which is essential to the wonderful applications while keeping many properties of the classical bit. However, the most important part of this thesis comes with introducing theory of chaos and joining it to the quantum information. This chapter serves to recapitulate important pieces of theory, so they can be put together into the whole mosaic and easily referred in the later chapters. Also, this basic overview introduce our readers to the ideas which they may not be familiar with. In this way they get acquaintanced with the setting of our topic in the conflux of many distant pieces of knowledge. Reader skilled in a particular topic can probably skip corresponding section and refer to it only when needed in later chapters.

First after the notation overview, we present a brief overview of quantum physics. We focus on its axiomatic construction, terms like quantum state and measurement are formalised so we can later easily watch their role in our problem. Then we focus on the quantum information branch with detailed description of qubit and qubit manipulation. The quantum information and communication protocols often use Fourier transform, Pauli gate, Hadamard gate and other linear elements. But the most important element for our thesis is the CNOT (controlled-not) gate. The quantum analogy of the classical CNOT gate combined with measurement performs nonlinear evolution of qubit which is crucial to our studies. Although the CNOT gate is a linear operator on a pair of qubits, we can understand the system of target and control qubit as an open system where the target qubit serves de facto as the environment. The control qubit modified by this measurement-based modification is then subject to nonlinear evolution. From this we can see that the protocol goes beyond standard courses of quantum physics because it involves quantum physics of open systems. This theory crosses with the theory of information, so we make a few notes on the branch.

Since we aim to study the chaotic features of the protocol, we also need to explore the theory of chaos. This field is very intricate and offers only few tools to manage the general task. Both the theory of chaos and the quantum physics are still developing but at the moment their cross-section usually focuses on quantum description of classically chaotic systems. This is commonly referred to as quantum chaology, [8]. However, the nature of the chaos in our problem is different - it emerges from deep inside the quantum description of the system and has no analogy in classical physics. To introduce our readers to the chaos we set up a definition of chaotic dynamical system followed by manifestation within physical systems. To use the analytic approach to the chaos we focus

then on complex functions of a single complex variable. Knowledge of chaos generated by these functions has direct use in qubit evolution under protocol of our interest. The chaos in these functions is contained in sets of points called Julia sets which often form peculiar fractal structures. These structures usually exhibit self-similarity and their primary and characteristic property is that their dimension is not an integer. We devote a section to fractals, concept of the dimension and the numerical dimension estimation of box-counting approach.

At the end of this theoretical chapter, we finally describe the purification protocol we are interested in, motivation for its proposal, its basic features and current state of knowledge. It is the start point of our study that widely extends our knowledge of nonlinear quantum protocols. At this moment, we only mention that the original protocol [4] was designed as a nonlinear protocol preserving the Bell state. We will first offer a different model that is inspired but simplifies the situation to a single qubit protocol. The results are later generalised to the original protocol but the single qubit space is much more accessible and still surprising model.

Because our topic is built upon three stones - quantum theory, theory of information, and theory of chaos, it is very demanding on completing the pieces of knowledge into the whole mosaic. In this review, we do not present these pieces at full details as they can be studied in many books [44, 45, 47, 10, 61]... In this text we focus on presenting only the crucial and fundamental pieces which fit in the mosaic built in the next chapter. Of course, we repeat many basic and well-known concepts. Some readers may find certain passages of the text too simple and not appropriate for a doctoral thesis but we present them for others that do not. We expect not only quantum physicist to be interested in the chaos inside quantum physics but a mathematician to be interested in the quantum physics inside chaos too. Taking the multidisciplinary topic, we take it as our duty to give the elementary overview, even though some may consider it unnecessary. If our readers belong to the experienced society, we hope they will be lenient to our intentions. On contrary, we hope that any person trying to replicate and improve our results will use this overview as a brief yet nice introduction.

There is also another reason to rewrite things that have been already written a hundred times already besides collecting the pieces of the mosaic to one place. We want to show that our research is based on the very fundaments of the theories. This is interesting for two reasons - the topic itself is seemingly simple and possibly can be introduced to wide community to make an impact in multiple fields. On the other hand, the topic is very delicate and requires precise work and the ostensible simplicity disappears when the topic is studied deeply.

2.1 Notation

$\mathscr{H}$	Hilbert space	$\mathscr{H}^*$	dual space to $\mathscr{H}^*$
$\|\alpha\rangle$	ket, vector $\in \mathscr{H}$	$\langle\beta\|$	bra, dual vector $\in \mathscr{H}^*$
$\langle\beta\|\alpha\rangle$	scalar (inner) product	$\mathcal{L}(\mathscr{H})$	space of linear operators on $\mathscr{H}$

$\|\beta\rangle\langle\alpha\|$	outer product, operator $\in \mathcal{L}(\mathscr{H})$, $\|\beta\rangle\langle\alpha\|(\|x\rangle) := \langle\alpha\|x\rangle\|\beta\rangle$
ρ	density operator, corresponding density matrix

$\odot$	Hadamard (elementwise) product	$\otimes$	tensor product
$\bar{\rho}$	complex conjugate of ρ	$\rho^\dagger$	Hermitian conjugate
$\|\|\psi\|\|$	norm of vector $\|\|\psi\|\| := \sqrt{\langle\psi\|\psi\rangle}$	$\mathbb{C}$	field of complex numbers
$\mathcal{F}_f$	Fatou set of function f	$\mathcal{J}_f$	Julia set of function f

$$\sigma_0 := \begin{pmatrix} 1 & 0 \\ 0 & 1 \end{pmatrix} \tag{2.1}$$

$$\sigma_1 := \begin{pmatrix} 0 & 1 \\ 1 & 0 \end{pmatrix} \tag{2.2}$$

$$\sigma_2 := \begin{pmatrix} 0 & -i \\ i & 0 \end{pmatrix} \tag{2.3}$$

$$\sigma_3 := \begin{pmatrix} 1 & 0 \\ 0 & -1 \end{pmatrix} \tag{2.4}$$

$\mathbb{1}$	identity operator, identity matrix
$\mathrm{Tr}\rho$	trace of operator/matrix ρ
$\hat{n}$	set $\{1, 2, 3, \ldots, n\}$
$\{a_i\}_{i=1}^n, \{a_i\}_{i=1}^\infty, \{a_i\}_i$	unordered sets; index set depending on context
$(a_i)_{i=1}^n, (a_i)_{i=1}^\infty, (a_i)_i$	sequences; index set depending on context
∂S	border of set S
$(a; b)$	open interval $\{x \in \mathbb{R} \| a < x < b\}$
$[a; b]$	closed interval $\{x \in \mathbb{R} \| a \leq x \leq b\}$
$[a; b), (a; b]$	half-closed intervals
$(a, b), (a, b, c), \begin{pmatrix} a \\ b \\ c \end{pmatrix}$	point from $\mathbb{R}^2, \mathbb{R}^3$ or depending on context

Ranges of sum indices or set unions/intersections are omitted when apparent

$\rho \to \rho'$	evolution induced by one protocol iteration upon state ρ
$\mathcal{C} = (\rho_1, \rho_2, \ldots, \rho_n)$	cycle; $\rho_1 \to \rho_2, \ldots, \rho_n \to \rho_1$
$\rho \overset{\infty}{\to} \mathcal{C}$	asymptotic convergence of state ρ to a state or cycle $\mathcal{C}$

2.2 Quantum physics

Quantum physics was established more than a hundred years ago. The revolution in physics is connected to names like Planck, de Broglie, Bohr. Further development was carried out by Schrödinger, Heisenberg and Dirac. But for the purpose of this thesis we stress the names of Einstein, Podolsky and Rosen who pointed out a famous paradox [18] in 1935. Decades later, in 1964 their proposition of hidden variable theory was refuted by work of John Stewart Bell [5] and the nonlocality, exotic nature of quantum physics, was confirmed by his inequalities. The nonlocal character is today embraced in the term of *quantum entanglement* which became a peculiar yet important resource of quantum computers. Still, quantum theory of information had few years ahead to be settled at that time. Starting with work of David Deutsch in [14], new horizons have been discovered

allowing for significant improvement in many branches, not only computation. Still, we find fascinating that the field developed from its very beginnings to an applied and advanced science bringing new and amazing technologies in less than a century. How deeply can our lives change in the next hundred years?

2.2.1 Axiomatic foundation of quantum physics

Strict axiomatic construction of quantum physics makes it a precise, logical and analytical theory. Since the fundaments of the theory are available in vast number of sources, we only highlight pieces we need to put later work into context, to befriend reader with notation and mathematical framework. We follow construction in [10] as we did in [39] but here we skip mathematical formalism unnecessary for this work. No doubt the text will be familiar for all people that went through courses of quantum physics, some information may be even taken for too trivial but we present them mainly for people of mathematical disciplines. Physicists can probably skip the following section without any negative consequences.

The very first postulate finds a suitable mathematical structure able to carry the physical world together with its basic properties. It represents a physical state as an element of the structure.

Axiom 1. *There is a separable complex Hilbert space $\mathscr{H}$ corresponding to the given quantum system. There is a ray in $\mathscr{H}$ corresponding to the given state of considered system.*

This space $\mathscr{H}$ from 1 is called the *state space*. Mathematically, it is a complete topological space equipped with a scalar product. The product plays a crucial role in the probability character of quantum physics. Physical state is not represented by a vector but by a one-dimensional subspace Ψ; the state can be represented by arbitrary vector $|\psi\rangle \in \Psi$, usually a unit vector $||\psi|| = 1$ is taken. It is possible to define the state space as a projective space. Note that the state space is complex and therefore there are infinitely many unit vectors, they differ in phase $e^{i\varphi}$. The optionality of the phase will be exploited in this work. For simplicity and without loss of generality, we will not distinguish a state and its arbitrary representative in this thesis $|\psi\rangle \equiv e^{i\varphi}|\psi\rangle \equiv z|\psi\rangle \equiv \Psi$, with arbitrary $\varphi \in \mathbb{R}, z \in \mathbb{C}$.

Formalism of measurements in quantum physics must respect the crucial idea of quantum physics that measuring affects the state. Lets consider state Ψ transformed into Φ because of the measurement of an observable. Taking unit representatives $|\psi\rangle, |\phi\rangle$ the number $P(\Psi, \Phi) = |\langle\psi|\phi\rangle|^2$ has the meaning of so called *transition probability*, probability that the state Ψ is turned to Φ because of the measurement. Taking orthonormal basis $(|\phi_j\rangle)_j$ of $\mathscr{H}$ any vector can be decomposed to

$$|\psi\rangle = \sum_j \langle\phi_j|\psi\rangle |\phi_j\rangle \overset{label}{=} \sum_j c_j |\phi_j\rangle . \tag{2.5}$$

The transition probabilities of $|\psi\rangle \to |\phi_j\rangle$ are $p_j = |c_j|^2$ and of course $\sum_j |c_j|^2 = 1$. Numbers $(c_j)_j$ are called *Fourier coefficients* of vector $|\psi\rangle$ with respect to the basis $(|\phi_j\rangle)_j$.

To properly introduce observables and their connections to values that can be measured we have to mention the concept of resolution of the identity also called completeness relation. Please find more details in [10].

Axiom 2. *An observable of the physical system is represented as some self-adjoint operator on the corresponding $\mathscr{H}$. Possible values for measurement of observable A are elements of the spectrum of A.*

It is mathematically possible to define an operator on $\mathscr{H}$ from arbitrary two vectors $|\alpha\rangle, |\beta\rangle \in \mathscr{H}$ using outer product in a following way:

$$P = |\alpha\rangle \langle\beta| \Leftrightarrow (\forall |\psi\rangle \in \mathscr{H})(P|\psi\rangle = \langle\beta|\psi\rangle|\alpha\rangle) \tag{2.6}$$

When an orthonormal basis $(|\phi_n\rangle)_n$ of $\mathscr{H}$ is chosen, particular operators $P_{ij} = |\phi_i\rangle \langle\phi_j|$ can be constructed according to 2.6 and combined, we obtain so called *completeness relation*:

$$\sum_n |\phi_i\rangle \langle\phi_i| = \mathbb{1}. \tag{2.7}$$

With two orthonormal bases $(|\phi_i\rangle)_i$ and $(|\psi_i\rangle)_i$ of $\mathscr{H}$ one can construct similarly $P_{ij} = |\phi_i\rangle \langle\psi_j|$, any given operator A on $\mathscr{H}^N$ can be expressed as

$$A = \mathbb{1}A\mathbb{1} = \sum_{i,j} |\phi_i\rangle \langle\phi_i| A |\psi_j\rangle \langle\psi_j| = \sum_{i,j} \langle\phi_i| A |\psi_j\rangle |\phi_i\rangle \langle\psi_j|, \tag{2.8}$$

A is then said to have matrix elements $\langle\phi_i| A |\psi_j\rangle$ with respect to input basis $(|\psi_i\rangle)_i$ and output basis $(|\phi_i\rangle)_i$. Operator A can be thus represented as a matrix $\mathbb{A}$ with elements $\mathbb{A}_{ij} = \langle\phi_i| A |\psi_j\rangle$. The matrix can be used to evaluate image of $|\alpha\rangle$: $A|\alpha\rangle = \sum_{i,j} \mathbb{A}_{ij}\langle\psi_j|\alpha\rangle|\phi_i\rangle$.

In our thesis, the basis will be given by experimental setting, experimental realisation, e.g. with vertical/horizontal polarisation of photons. All the calculations will be performed in this *computational basis* and we will identify coordinates/matrix elements in this basis with the states/operators.

In the quantum information context of this thesis, observabels with continuous values of measurement will not be discussed. For that reason we now restrict to observables with purely discrete spectrum $\sigma(A) = \{a_i\}_i$. Corresponding eigenvectors $A|\alpha_i\rangle = a_i|\alpha_i\rangle$ form an orthonormal basis $(|\alpha_i\rangle)_i$. Previous relations can be directly reduced to this single basis.

Axiom 3a. *For operator A, the probability that a value a_i corresponding to unit vector $|\alpha_i\rangle$ is measured on a state described by unit vector $|\psi\rangle$, is equal to $p = \langle\alpha_i|A|\psi\rangle$. When measurement A has the result a_i, the system is transformed due to the measurement to the state described by $|\alpha_i\rangle\langle\alpha_i|\psi\rangle$. If the measured result is not a_i, the system ends up in a state determined by $(\mathbb{1} - |\alpha_i\rangle\langle\alpha_i|)|\psi\rangle$.*

Axiom 3b. *The mean value of an observable A on a state given by unit vector $|\psi\rangle$ is $\langle A\rangle_\psi = \langle\psi| A |\psi\rangle$.*

Natural need of physics is to transfer to statistical ensembles of states. States we studied so far, rays in $\mathscr{H}$, are called *pure states*. When they are represented by a unit vector $|\alpha\rangle$ they can be associated to operator $|\alpha\rangle\langle\alpha|$. Such operator satisfies certain conditions that lead to the definition of *statistical operators*. First, we note that operators $P_{ij} = |\alpha_i\rangle \langle\alpha_j|$ satisfy $P_{ij}^\dagger = P_{ji}$ and P_{ii} suit definition of projection as well as arbitrary operator $|\alpha\rangle\langle\alpha|/\langle\alpha|\alpha\rangle$ for any $|\alpha\rangle \in \mathscr{H}$ does.

Definition 2.2.1 (Projection)**.** Projection *is such an operator* P *on* $\mathscr{H}$ *that* $Dom(P) = \mathscr{H}$, $P = P^\dagger$ *and* $P = P^2$.

Note that projection is self-adjoint by definition. The eigenvalues of projection are $\{0, 1\}$ which makes them positive operators. The last condition on statistical operators comes from the requirement on probability distribution. When we have a system that can be in one of normalised states $|\alpha_i\rangle$ with probability p_i, the statistical operator associated to this - so called *mixed state* - is identified with

$$\rho = \sum_i p_i \left|\alpha_i\right\rangle \left\langle\alpha_i\right|, \tag{2.9}$$

where naturally $\sum_i p_i = 1$. Person not used to the bra-ket notation should be now pointed out to enjoy that for non-normalised states $|\alpha_i\rangle$ one has to replace the ket-bra product with normalisation factor $\frac{|\alpha_i\rangle\langle\alpha_i|}{\langle\alpha_i|\alpha_i\rangle}$ that will certainly make obvious the reason why physicists love this notation so much. We conclude the line of thoughts with formal definition of statistical operator.

Definition 2.2.2 (Statistical operator)**.** ρ *linear operator on* $\mathscr{H}$ *is* statistical operator *when it satisfies*

1. $\rho = \rho^\dagger$ *(*ρ *is self-adjoint),*
2. $\rho = \rho^2$ *(*ρ *is idempotent),*
3. $Tr(\rho) = 1$.

The statistical operator expressed as a matrix in a given orthonormal basis is also called *density matrix* and we will use the symbol ρ for both the operator and its matrix. The pure states satisfy $Tr(\rho^2) = 1$ as the result of the fact that there is a single vector with corresponding probability 1 while other states contribute with 0 probability. The mixed states (where the probabilities satisfy $\forall i : p_i < 1$) are then distinguished with $Tr(\rho^2) < 1$. We define a quantity to measure the purity/mixedness:

Definition 2.2.3. *Purity of the state* ρ *is*

$$P(\rho) = Tr(\rho^2) \tag{2.10}$$

Prominent place is taken by so called maximally mixed state which correspond to a statistical mix with uniform probabilities, $(\forall i \in \hat{d})(p_i = \frac{1}{d})$ in d-dimensional $\mathscr{H}$. The operator assigned to this state is identity up to the dimension factor $\rho = \frac{1}{d}\mathbb{1}$. For simplicity, we will omit the factor and identify the maximally mixed state as well as the matrix of its matrix elements solely with $\mathbb{1}$, the renormalisation will be mentioned if needed.

Now, we can extend previous axioms to statistical ensembles of states:

Axiom 1b. *For a state of the physical system* $\mathscr{H}$*, there is a corresponding statistical operator* ρ *on* $\mathscr{H}$.

Axiom 3a. *For observable* A*, probability of measuring value* a *with corresponding eigenvector* α *is equal to* $p = Tr(|\alpha\rangle\langle\alpha|\rho)$*. If the measurement result is* a *the state after measurement is described by statistical operator* $\rho' = \dfrac{|\alpha\rangle\langle\alpha|\rho|\alpha\rangle\langle\alpha|}{Tr(|\alpha\rangle\langle\alpha|\rho)}$.

Axiom 3b. *The mean value of an observable A on a state given by ρ is $\langle a \rangle_\rho = Tr(A\rho)$.*

Note that the trace cyclic property simplified the formula in 3a

$$\mathrm{Tr}(|\alpha\rangle\langle\alpha|\rho|\alpha\rangle\langle\alpha|) = \mathrm{Tr}((|\alpha\rangle\langle\alpha|)^2\rho) = \mathrm{Tr}(|\alpha\rangle\langle\alpha|\rho). \tag{2.11}$$

These axioms describe a static state (in both pure and mixed states variant). To evolve the state in time we need to settle a new axiom which leans on a definition of so-called propagator.

Definition 2.2.4. *A class of unitary operators $\{U_{t,s}|t,s \in \mathbb{R}\}$ on $\mathscr{H}$ is called* unitary propagator *when following conditions are fulfilled.*

1. $(\forall r,s,t \in \mathbb{R})(U_{t,s}U_{s,r} = U_{t,r})$*; in particular: $U_{t,t}$ is identity for $\forall t \in \mathbb{R}$.*
2. *Map $(t,s) \to U_{t,s}$ is strongly continuous in $\mathbb{R}^2$.*

The unitarity is a crucial condition which results in reversibility property $U_{t,s} = U_{s,t}^{-1}$.

Axiom 4. *Time evolution of a closed system through time interval $\mathcal{J}$ is described by unitary propagator: $\rho(t) = U_{t,s}\rho(s)U_{t,s}^{-1}$ resp. $|\psi(t)\rangle = U_{t,s}|\psi(s)\rangle$ for all times $s,t \in \mathcal{J}$.*

Stone theorem, refer [10], guarantees that the propagator is generated by a self-adjoint operator. Its physical interpretation for conservative systems is the Hamiltonian H. The dynamical postulate can be then expressed with $U_{t,s} \equiv e^{-iH(t-s)}$. Direct deduction leads to famous Schrödinger equation

$$i\frac{d}{dt}\rho = H\rho - \rho H \text{ , resp. } \quad i\frac{d}{dt}|\psi\rangle = H|\psi\rangle. \tag{2.12}$$

However, for our purposes of discrete quantum evolution induced by iterations of certain unitary operator (i.e. $U^\dagger = U^{-1}$) we will use in this thesis solely following form

$$\rho \to U\rho U^\dagger. \tag{2.13}$$

2.2.2 Open quantum systems

The reversibility of time evolution is a direct consequence of the unitarity of the evolution. The basic property of such evolution is isometry, two states cannot converge to a common state under unitary evolution. a standard process of statistical ensembles of particles is to reach certain equilibrium, this process is not compatible with the isometry. The nonunitary (and therefore irreversible) evolution can be reached by considering multipartite systems with interaction. While the evolution is unitary on the composite system, particular subsystem can exhibit nonunitary evolution. The other systems can be understood as environment, thermal baths etc., in this way we can stretch the theory towards statistical physics. We now introduce description of composite quantum system, [12].

First, we have to assign the Hilbert space to the composite system as the axiom 1 requires. With this we finish the axiom fundament of the quantum theory.

Axiom 5. *The state space of the composite system is the tensor product of the subsystem spaces:* $\mathscr{H} = \mathscr{H}_1 \otimes \mathscr{H}_2 \otimes \cdots \otimes \mathscr{H}_n$.

This axiom can be even used in the opposite way to decompose a physical system into virtual parts, i.e. electron to its position-momentum and its spin system. For simplicity, we will use following notation of bases. Taking $(|\alpha_i\rangle)_i$, $(|\beta_j\rangle)_j$, $(|\gamma_k\rangle)_k, \ldots$ orthonormal bases of the subsystems, it can be shown that tensor products of these vectors form the basis of the composite systems. For the sake of simplicity we designate these vectors with $|ijk\ldots\rangle \equiv |\alpha_i\beta_j\gamma_k\ldots\rangle \equiv |\alpha_i\rangle \otimes |\beta_j\rangle \otimes |\gamma_k\rangle \ldots$ where the context would not allow a confusion.

Consider now system with $\mathscr{H}$ composed of two subsystems with corresponding $\mathscr{H}_1, \mathscr{H}_2$. While it is easy to create the composed state from the known states of the subsystems $\rho = \rho_1 \otimes \rho_2$, we can ask the opposite question: what are the states of the subsystems $\rho_{1,2}$ when we know the state ρ. The answer rises from the concept of partial trace and formalism of observables. Given observables A_i on the subsystems $\mathscr{H}_i$ one can construct observables on the composite state $A_1 \otimes \mathbb{1}, \mathbb{1} \otimes A_2$ which ignore the other state.

Proposition 2.2.5. *For* ρ *density operator of a system* $\mathscr{H} = \mathscr{H}_A \otimes \mathscr{H}_B$ *there is exactly one pair of density operators* $\rho_{A,B}$ *such that for all observables* $O_{A,B}$*:*

$$\begin{aligned} Tr((O_A \otimes \mathbb{1})\rho) &= Tr_A(O_A\rho_A)\,, \\ Tr((\mathbb{1} \otimes O_B)\rho) &= Tr_B(O_B\rho_B), \end{aligned} \tag{2.14}$$

where the traces act over corresponding subspaces, as suggested by notation.

These unique subsystem density operators can be extracted using orthonormal bases $(|\alpha_i\rangle)_i, (|\beta_j\rangle)_j$ of spaces $\mathscr{H}_A, \mathscr{H}_B$ respectively.

$$\rho_A \equiv \mathrm{Tr}_B\rho = \sum_j (\mathbb{1}\otimes\langle\beta_j|)\rho(\mathbb{1}\otimes|\beta_j\rangle),\ \rho_B \equiv \mathrm{Tr}_A\rho = \sum_i (\langle\alpha_i|\otimes\mathbb{1})\rho(|\alpha_i\rangle\otimes\mathbb{1}) \tag{2.15}$$

The lower index notes the system that is traced out. These equations could stand as definitions of the partial trace over subsystem B, resp. A; however, they lack normalisation property that is guaranteed by the density operators with trace equal to 1. Our readers can easily convince themselves that for general composite operator $O_A \otimes O_B$:

$$\begin{gathered} \mathrm{Tr}_A(O_A \otimes O_B) = \mathrm{Tr}_A(O_A) \cdot O_B,\ \mathrm{Tr}_B(O_A \otimes O_B) = \mathrm{Tr}_B(O_B) \cdot O_A \\ \mathrm{Tr}(O_A \otimes O_B) = \mathrm{Tr}_B(\mathrm{Tr}_A(O_A \otimes O_B)) = \mathrm{Tr}_A(\mathrm{Tr}_B(O_A \otimes O_B)) = \mathrm{Tr}_A(O_A) \cdot \mathrm{Tr}_B(O_B) \end{gathered} \tag{2.16}$$

However, the crucial point of the composite systems lies in the fact that there are states in $\mathscr{H} = \mathscr{H}_A \otimes \mathscr{H}_B$ that cannot be expressed as so called *product states* $\rho_A \otimes \rho_B$. Such states are called *entangled states* and their exact nature was a source of a mystery for a time. The measurement performed on one subsystem causes instantaneous collapse of the state of the other subsystem. a famous paper by Albert Einstein, Boris Podolsky and Nathan Rosen from 1935, [18] argued that such situation interpreted as instantaneous transfer of information is in contradiction with the theory of relativity. The explanation was searched in so-called hidden parameters that are not involved in the quantum description. Classical correlations could then explain the seeming contradiction. Yet in 1964

John Bell presented a set of inequalities, [5] that would have to be satisfied in arbitrary hidden variable theory. Such inequalities can be experimentally verified, e.g. considering spin particles or polarised photons and the experimental results confirmed that there are no hidden variables. As we write this thesis, it happens that Nobel prize was awarded to A. Aspect, J.F. Clauser and A. Zeilinger for this verification. The quantum physics truly allows for entangling two systems beyond classical correlations. Entanglement has become an important phenomenon, a resource that can be used for surprising applications. An example of an entangled system will be shown in the next paragraphs dedicated to quantum information.

We complete the quantum theory text with a final proposition that sheds a different light on mixed states.

Proposition 2.2.6 (Mixed state purification)**.** *For given mixed state $\rho = \sum_i p_i|\alpha_i\rangle\langle\alpha_i|$, statistical operator on $\mathscr{H}_1$ with orthonormal basis $(|\alpha_i\rangle)_i$, it is possible to introduce another system with the same state space $\mathscr{H}_2 = \mathscr{H}_1$ with orthonormal basis $(|\omega_i\rangle)_i$ such that state*

$$|P\rangle := \sum_i \sqrt{p_i}|\alpha_i\rangle|\omega_i\rangle \tag{2.17}$$

is pure on $\mathcal{H}_1 \otimes \mathcal{H}_2$ and its partial trace over added subsystem yields $Tr_2 P = \rho$.

The construction is merely a mathematical trick, with the added subsystem being virtual without any physical meaning. But still, the state P, called purification of ρ, can be used to simplify some deductions because some considerations are simpler for pure states. We warn now that we will not use this process in our work. We will work with mixedness of a state, modify it, but we will change the state itself by discrete time evolution. The evolutions function will be induced by measurement on a subsystem of composed system. To avoid misunderstanding, we stress that we do not introduce any virtual systems and purify a state in the sense of changing its purity due to its time evolution.

There is also another source of possible confusion, caused by using the word purification for purification of entanglement. Although both processes concerning entanglement and mixedness are called purification, their meaning is very different. The purification in context of mixed states is taken from the aspect of state's purity/mixedness. Purification of entanglement which will be discussed in the next part aims for, of course, increasing the entanglement in a quantum state.

It is quite natural to study the composite systems because the basic concept of thermodynamics lies in interaction of multiple systems, usually introducing reservoir/bath system. a basic idea developed in the theory is that Hamiltonian of the composite system is determined by addition of subsystem Hamiltonians together with the interaction Hamiltonian. However, our research does not go in this direction so we leave the topic of statistical and thermodynamic branches of quantum physics and proceed to our field of interest.

2.2.3 Quantum information

Theory of quantum information and communication is a relatively new branch of science that is supreme to classical information theory in certain way - tasks

requiring amount of resources exponential to the size of input can be executed with only polynomial-dependent amount of resources. This relates to NP complete tasks, [11]. There are also completely new quantum algorithms that have no analogy in classical theory, [59, 7] a wide and comprehensible introduction to the field is given in [47] from where we extract following overview and where we took inspiration for the last subsection.

The quantum computation is based on a very simple idea - to build the theory on the physical laws which are quantum, not classical. David Deutsch in 1985 attempted to construct a machine capable of simulating efficiently any (quantum) physical system, [14, 15]. A quantum analogue of Turing machine, [62] - *universal quantum computer* - has been proposed but the construction does not guarantee it to be more efficient than a classical universal computer. During later years, Deutsch, Shore and others proposed algorithms, e.g. for a search in an unstructured list or number factorisation [59] that are proven to best the classical ones. The unusual character of quantum physics gives a rise to a new resource, quantum entanglement, which we have already mentioned. a great amount of popularity was gained by quantum teleportation protocol [7] which exploits the entanglement but is not the only one. Quantum information and communication will rely on entanglement.

Now we outline only vital terms and mathematical concept that we will use later. The essential concept of the whole theory is a *qubit*, quantum analogue of the bit. Qubit is a physical system with two possible states of existence, let us call them 0 and 1, naturally. The corresponding Hilbert space is $\mathbb{C}^2$, the basis vectors corresponding to the states 0, 1 will be marked $|0\rangle, |1\rangle$ and they form an orthonormal basis, the *computational basis*. a general pure state qubit is given as a superposition of the basis states

$$|\psi\rangle = \alpha\,|0\rangle + \beta\,|1\rangle\,. \tag{2.18}$$

An additional condition $\alpha^2 + \beta^2 = 1$ is usually set to constrain the qubit representation. However, we do not do so always because suitable reparametrisation of qubits may lead to significant simplifications when handling polynomial equations. For the sake of simplicity, we shall identify $|0\rangle = \begin{pmatrix} 1 \\ 0 \end{pmatrix}, |1\rangle = \begin{pmatrix} 0 \\ 1 \end{pmatrix}$.

A two-qubit system is then corresponding to $\mathbb{C}^2 \otimes \mathbb{C}^2$ with a natural orthonormal basis

$$|00\rangle = \begin{pmatrix} 1 \\ 0 \\ 0 \\ 0 \end{pmatrix}, |01\rangle = \begin{pmatrix} 0 \\ 1 \\ 0 \\ 0 \end{pmatrix}, |10\rangle = \begin{pmatrix} 0 \\ 0 \\ 1 \\ 0 \end{pmatrix}, |11\rangle = \begin{pmatrix} 0 \\ 0 \\ 0 \\ 1 \end{pmatrix} \tag{2.19}$$

formed naturally by qubit pairs with corresponding values.

As we promised, now we show an example of an entangled state. Taking $|\Phi^+\rangle = \frac{1}{\sqrt{2}}(|00\rangle + |11\rangle)$ one can easily see that it cannot be decomposed into any product $(\alpha|0\rangle + \beta|1\rangle) \otimes (\gamma|0\rangle + \delta|1\rangle)$. If the first qubit is measured with result 0, the other qubit necessarily also must yield 0 when measured; vice versa, when one of the qubits is measured to 1, the other would yield the same output too. This fact can be used to implement surprising applications, i.e. quantum teleportation [7].

The particular state $|\Phi^+\rangle$ is not the only one with such properties. Other significant states are $|\Phi^-\rangle = \frac{1}{\sqrt{2}}(|00\rangle - |11\rangle)$ and $|\Psi^\pm\rangle = \frac{1}{\sqrt{2}}(|01\rangle \pm |10\rangle)$. The importance of these states lies in the fact that they contain maximal amount of entanglement. Such states are called Bell states and can be distinguished thanks to following property. Performing the partial traces over (any) one qubit yields maximally mixed state: $\mathrm{Tr}_A|\Phi^+\rangle\langle\Phi^+| = \mathrm{Tr}_B|\Phi^+\rangle\langle\Phi^+| = \frac{1}{2}\mathbb{1}$. In general, if each subspace $\mathscr{H}$ of the composed system has dimension d, the *maximally entangled state* in the product space $\mathscr{H}^{\otimes n}$ traced over all but one of the subsystems yields $\frac{1}{d}\mathbb{1}$.

Measuring the amount of entanglement generally is not an easy question, [52]. While a universal approach can be defined, there is no straightforward method of its evaluation because it requires finding a minimum of a complicated expression; for qubit pairs the approach can be fortunately simplified. The general approach is based on the concept of entropy which we will explore below, now we focus particularly on *binary entropy function*:

$$h(x) = -x\log x - (1-x)\log(1-x) \tag{2.20}$$

Given a two-qubit state ρ it can be shown that operator $\rho(\sigma_2 \otimes \sigma_2)\bar{\rho}(\sigma_2 \otimes \sigma_2)$ is positive. Its eigenvalues are used to defined *concurrence* which is the key ingredient to entanglement measurement.

Definition 2.2.7 (Entanglement of formation)**.** *Given a two qubit state ρ, its concurrence is defined as*

$$C(\rho) = max\ \{0, \sqrt{\lambda_1} - \sqrt{\lambda_2} - \sqrt{\lambda_3} - \sqrt{\lambda_4}\}, \tag{2.21}$$

where $\lambda_1 \geq \lambda_2 \geq \lambda_3 \geq \lambda_4$ are decreasingly ordered eigenvalues of $\rho(\sigma_2 \otimes \sigma_2)\bar{\rho}(\sigma_2 \otimes \sigma_2)$.

The entanglement of formation is given by the binary entropy function

$$I(\rho) = h\left(\frac{1+\sqrt{1-C^2(\rho)}}{2}\right) \tag{2.22}$$

As an example, for the Bell state $|\Phi^+\rangle$ the eigenvalues of $|\Phi^+\rangle\langle\Phi^+|(\sigma_2 \otimes \sigma_2)|\Phi^+\rangle\langle\Phi^+|(\sigma_2 \otimes \sigma_2)$ are $\lambda_1 = 1, \lambda_2 = \lambda_3 = \lambda_4 = 0$ resulting into concurrence $C(|\Phi^+\rangle\langle\Phi^+|) = 1$ and entanglement of formation $I(|\Phi^+\rangle\langle\Phi^+|) = 1$ which is the maximal value of the binary entropy function. In contrast, factorisable state $|00\rangle$ has all the concurrence eigenvalues equal to zero, that gives $C(|00\rangle\langle 00|) = 0$ and $I(|00\rangle\langle 00|) = 0$. a trivial consequence is that for arbitrary ρ: $I(\rho) \in [0; 1]$.

Entropy is a celebrity of the information sciences as well as thermodynamics and other branches of physics and mathematics. Shannon's definition can be straightforwardly implemented in quantum information theory:

Definition 2.2.8 (von Neumann's entropy)**.** *For given density operator ρ its entropy is defined as $S(\rho) = Tr(-\rho\log\rho)$.*

Expressing eigenvalues $\{\lambda_i\}_i$ of ρ the definition reduces to $S(\rho) = \sum_i -\lambda_i \log\lambda_i$ which is the Shannon entropy of the probability distribution. The entropy also allows comparing two states:

Definition 2.2.9 (Relative entropy)**.** *For given density operators ρ, σ their relative entropy is defined as*

$$S(\rho||\sigma) = Tr\,(\rho \log \rho - \rho \log \sigma). \tag{2.23}$$

The values of relative entropy are always non-negative (but can be infinite) and zero is reached if and only if $\rho = \sigma$; this statement is usually called Klein's inequality. This type of positivity suggests us to use it as an indicator of how close two quantum states are. However, the relative entropy is not symmetrical and does not satisfy the triangle inequality. Although it is not a metric, it is still used to compare two states for other useful properties like convexity and monotonicity. We leave details to [47] and present another indicator of closeness of two quantum states. Widespread use has been acquired by approach based on overlap of quantum states:

Definition 2.2.10 (Fidelity)**.** *For two density operators ρ, σ their* fidelity *is*

$$F(\rho, \sigma) = Tr\sqrt{\sqrt{\rho}\sigma\sqrt{\rho}}. \tag{2.24}$$

This quantity is symmetrical and $0 \geq F(\rho, \sigma) \geq 1$ while $F(\rho, \sigma) = 1 \Leftrightarrow \rho = \sigma$. Often, one can find value $F^2(\rho, \sigma)$ to be used and called fidelity while the value $F(\rho, \sigma)$ is called square-root fidelity.

There are of course other ways to measure similarity of two states, with their own pros and contras. Of course, a good way of measuring is always reached with properties of a metric. One such metric can be defined based on tracing.

Definition 2.2.11 (Trace distance)**.** *For two density operators ρ, σ their* trace distance *is*

$$T(\rho, \sigma) = \frac{1}{2} Tr\sqrt{(\rho - \sigma)^\dagger(\rho - \sigma)}. \tag{2.25}$$

This quantity clearly yields 0 if and only if $\rho = \sigma$. On the other hand, the maximal obtainable value is 1. For the fidelity, the converse is true: $F(\rho, \sigma) = 1 \Leftrightarrow \rho = \sigma$ while $F(\rho, \sigma) = 0$ can be reached for states sharing no common information.

All three quantities are invariant on unitary transformation of the states: $S(\rho||\sigma) = S(U\rho U^\dagger||U\sigma U^\dagger), F(\rho, \sigma)$=$F(U\rho U^\dagger, U\sigma U^\dagger), T(\rho, \sigma) = T(U\rho U^\dagger, U\sigma U^\dagger)$ for any unitary operator U. This fact can be used when unitary evolution of a closed system is considered - the distance, the similarity of the states is not changed. While contemporary papers usually prefer fidelity, we will use the approach of the trace distance not only because it is a metric but mainly for its useful properties that will be discussed later. There is a relationship between the two quantities

$$1 - F(\rho, \sigma) \leq T(\rho, \sigma) \leq \sqrt{1 - F^2(\rho, \sigma)} \Leftrightarrow 1 - T(\rho, \sigma) \leq F(\rho, \sigma) \leq \sqrt{1 - T^2(\rho, \sigma)} \tag{2.26}$$

which allows for estimating the fidelity from the trace distance if our reader wants to.

When we have described qubits, we can advance to use them for computation. Qubit processing is inspired by classical information processing too. NOT gate is responsible for swapping bit states $|0\rangle \leftrightarrow |1\rangle$ forming computational basis. Its

action on $|\psi\rangle$ can be written as a matrix multiplication where the NOT gate is represented by matrix $\mathbb{X}$:

$$X = \sigma_1 = \begin{pmatrix} 0 & 1 \\ 1 & 0 \end{pmatrix}; |\psi\rangle \to \mathbb{X} \cdot |\psi\rangle = \alpha\,|1\rangle + \beta\,|0\rangle\,. \tag{2.27}$$

Another important gate is so-called Hadamard gate. It is usually called H in the literature but for our purposes where we will deal with similar gates, we will use H_1 equally. The matrix representation of the gate is

$$H_1 = H = \frac{1}{\sqrt{2}} \begin{pmatrix} 1 & 1 \\ 1 & -1 \end{pmatrix}. \tag{2.28}$$

Its importance lies in its direct application in above mentioned protocols of quantum teleportation, number factorisation, searching algorithm and many others. The reason is in its ability to create equal superpositions from the basis states:

$$H|0\rangle = \frac{1}{\sqrt{2}}(|0\rangle + |1\rangle)\,,\ H|1\rangle = \frac{1}{\sqrt{2}}(|0\rangle - |1\rangle) \tag{2.29}$$

This gate is new to the information processing since such superpositions do not exist for classical bits. One can ask what matrices $\mathbb{U}$ (or corresponding operators U) can serve as qubit processing gates.

Proposition 2.2.12. *Unitarity is a sufficient property for a matrix $\mathbb{U} \in \mathbb{C}^{2,2}$ to serve as a valid single-qubit gate.*

This can be even strengthened with following efficiency statement to describe qubit processing completely.

Proposition 2.2.13. *It is possible to build up any single qubit gate using finite set of gates.*

Computation necessarily needs more qubits to perform even the simplest tasks. a crucial example of a two-qubit gate is the CNOT gate which flips the value of *target* qubit when *control* bit has value 1, otherwise the target qubit is not modified. The quantum version of the gate can then be written in matrix representation as

$$CNOT \equiv \begin{pmatrix} 1 & 0 & 0 & 0 \\ 0 & 1 & 0 & 0 \\ 0 & 0 & 0 & 1 \\ 0 & 0 & 1 & 0 \end{pmatrix} \tag{2.30}$$

when the first qubit is the control qubit while the second is the target one. The matrix multiplication reflects the gate action $\alpha|00\rangle + \beta|01\rangle + \gamma|10\rangle + \delta|11\rangle \overset{CNOT}{\to} \alpha|00\rangle + \beta|01\rangle + \gamma|11\rangle + \delta|10\rangle$. One can see that the value of the target qubit after the CNOT gate can be expressed as addition modulo 2, symbolically: $|ij\rangle \overset{CNOT}{\to} |i, i \oplus_2 j\rangle$. In classical theory of information, thegate performing such addition is called XOR. It is an irreversible gate in the sense that the result cannot be used to reconstruct the values of the added qubits. However, CNOT gate performs the operation no matter whether the control state is measured or not. The collapse of the wave function effectively happens with the measurement of the qubit and

until that moment the gate can be reversed by applying it once more - the gate is inverse to itself.

The importance of this gate is stressed in a following statement that claims any task can be implemented without a need for three or more qubit gates.

Proposition 2.2.14. *Any multiple qubit gate may be made composed of the CNOT and single qubit gates. Two-qubit states are thus able to simulate any system.*

Two-qubit systems can contain the entanglement which makes them vital objects to quantum information and communication protocols. Before we dive into two-qubit entanglement description we study mixed qubit states that will play the central role in our research.

The statistical operator corresponding to a single qubit can be represented with a 2×2 matrix ρ which must satisfy conditions according to 2.2.2 - self adjointness, positivity and unit trace. It can be shown that there is one-to-one correspondence between qubits and matrices

$$\rho = \frac{1}{2}\begin{pmatrix} 1+w & u+iv \\ u-iv & 1-w \end{pmatrix} ; \text{where } w,u,v \in \mathbb{R} \text{ satisfy } u^2+v^2+w^2 \leq 1, \quad (2.31)$$

these are certain combinations of Pauli matrices.

$$\rho = \frac{1}{2}(\sigma_0 + u\sigma_1 + v\sigma_2 + w\sigma_3) \quad (2.32)$$

Reason for the conditions on u, v, w comes from the eigenvalues of ρ that are $\frac{1}{2}(1 \pm \sqrt{u^2+v^2+w^2})$ while $\mathrm{Tr}\rho = 1$ and self-adjointness are automatically guaranteed from the matrix structure for arbitrary w, u, v. We conclude there is a geometrical representation, called Bloch representation or Fano representation, [20], for a qubit as a point from a unit ball in a three-dimensional Euclidean space w, u, v. We will identify the state with its coordinates $\rho \equiv (w, u, v)$, sometimes in a column form purely for spatial reasons. In this thesis we will use both names Fano and Bloch for this representation, coordinates, the latter more frequently.

The pure states form a subset of the unit ball determined by $\mathrm{Tr}\rho^2 = 1$. That translates to $u^2 + v^2 + w^2 = 1$: pure states form the unit sphere, the border of the unit ball; it is usually called the *Bloch sphere*. The mixed states, which can be expressed as convex combinations of pure states as suggested from their construction as probabilistic mixtures of pure states, then constitute the interior of the unit ball which we will call analogically *Bloch ball*. The maximally mixed state is represented as the identity matrix $\mathbb{1}$ (up to normalisation factor), the centre of the ball. To give a deeper insight of the representation we now express important qubit states writing Bloch coordinates into usual vector of Euclidean space $\rho \equiv (w, u, v)$.

$$\begin{gathered} |0\rangle \Leftrightarrow (w,u,v) = (1,0,0)\,, \quad |1\rangle \Leftrightarrow (-1,0,0) \\ \tfrac{1}{\sqrt{2}}(|0\rangle \pm |1\rangle) \Leftrightarrow (0,\pm 1,0) \\ \mathbb{1} \Leftrightarrow (0,0,0) \end{gathered} \quad (2.33)$$

The purity of the state ρ can be calculated straight as

$$P(w,u,v) = \mathrm{Tr}\rho^2 = \frac{1+u^2+v^2+w^2}{2}, \quad (2.34)$$

this formula relates the purity/mixedness of the state geometrically to the radius, Euclidean distance from the origin; in the geometrical representation in Bloch ball: $\sqrt{w^2+u^2+v^2} = \sqrt{2P(\rho)-1}$. This relation is a bijection of the interval of physically relevant radii $\in [0;1]$ and possible purity values $\in [\frac{1}{2};1]$. The maximally mixed state corresponding to the origin has the purity $\frac{1}{2}$; note that more generally, if the Hilbert space has dimension d the maximally mixed state has purity $\frac{1}{d}$. We conclude an important statement that all states with given purity form a sphere in the Bloch space, we will keep in mind there is a one-to-one relation between the abstract radius and the purity with actual physical meaning.

The action of a computation gate (unitary operator) U on the qubit is given according to axiom 5.16 $\rho' = U\rho U^\dagger$. Such action does not change the purity due to the cyclic property of trace: $\mathrm{Tr}\rho'^2 = \mathrm{Tr}(U\rho U^\dagger U\rho U^\dagger) = \mathrm{Tr}(U^\dagger U\rho\mathbb{1}\rho) = \mathrm{Tr}\rho^2$.

The entropy of a qubit can be directly expressed in the Fano coordinates $\rho \equiv (w,u,v)$ using the binary entropy function 2.20; this relation is claimed in [29]:

$$\begin{aligned} S(\rho) = \quad & -\tfrac{1+\sqrt{u^2+v^2+w^2}}{2}\log\left(\tfrac{1+\sqrt{u^2+v^2+w^2}}{2}\right) - \\ & -\tfrac{1-\sqrt{u^2+v^2+w^2}}{2}\log\left(\tfrac{1-\sqrt{u^2+v^2+w^2}}{2}\right) \end{aligned} \tag{2.35}$$

Since the input depends on the radius in the Bloch space (which is directly related to the purity), it is a remarkable fact that the entropy is solely a function of the purity of the state. The trace distance of two qubits in terms of Fano coordinates is actually (half of) Euclidean distance in Fano space. Taking $\rho \equiv (w_1,u_1,v_1), \sigma \equiv (w_2,u_2,v_2)$ one can calculate

$$T(\rho,\sigma) = \frac{1}{2}\sqrt{(w_2-w_1)^2+(u_2-u_1)^2+(v_2-v_1)^2}, \tag{2.36}$$

which means that maximal distance of two qubits is 1 which happen for pure states located antipodally on the Bloch sphere. In our work for the simplicity and the intuitive geometrical meaning we will use $t(\rho,\sigma) = 2T(\rho,\sigma)$, directly the Euclidean distance in the Bloch space. The rescaling does not change any metric properties.

The geometrical approach can be generalised to two-qubit systems. As component systems, they are described according to axiom 5.17 with 4×4 matrix which can be analogically expressed as combinations of tensor products of Pauli matrices:

$$\rho = \sum_{i,j=0}^{3} \alpha_{ij}\,\sigma_i \otimes \sigma_j \tag{2.37}$$

where $\alpha_{00} = \frac{1}{4}$ (to satisfy $\mathrm{Tr}\rho = 1$) while other parameters satisfy $\alpha_{ij} \leq 1$. Last condition - positivity requirement implies very complicated polynomial inequalities for α_{ij}. We now only mention that the geometrical representation space of qubit pairs is a convex set in 15-dimensional Euclidean space.

Coming back to the single qubits, the spheres of constant purity suggest using a reparametrisation of the Bloch space from Cartesian-like coordinates to

spherical coordinates

$$\begin{aligned} w &= \sqrt{2P-1}\cos\vartheta & P &= \frac{u^2+v^2+w^2+1}{2} \\ u &= \sqrt{2P-1}\sin\vartheta\cos\varphi \quad , & \vartheta &= \arccos\frac{w}{\sqrt{2P-1}} \\ v &= \sqrt{2P-1}\sin\vartheta\sin\varphi & \varphi &= \arctan\frac{v}{u} \end{aligned} \tag{2.38}$$

where the purity P is purposely used instead of the radius for its physical meaning. Singularity for $u = 0$ is avoided by setting $\varphi = \mathrm{sgn}(v)\,\frac{\pi}{2}$ in such case. We will usually plot the w-axis as the vertical while u, v would span the equatorial plane. This choice is a usual when Cartesian axes x, y, z are discussed in literature but it is not so usual to put z into the first position in the vector notation (z, x, y) like we do with (w, u, v). However, there is also another, less obvious parameterisation involving stereographic projection with respect to the south pole:

$$\begin{aligned} P &= \frac{u^2+v^2+w^2+1}{2} & w &= \sqrt{2P-1}\frac{1-(x^2+y^2)}{1+x^2+y^2} \\ x &= \frac{u}{\sqrt{u^2+v^2+w^2}+w} = \frac{u}{\sqrt{2P-1}+w}\,, & u &= \sqrt{2P-1}\frac{2x}{1+x^2+y^2} \\ y &= \frac{v}{\sqrt{u^2+v^2+w^2}+w} = \frac{v}{\sqrt{2P-1}+w} & v &= \sqrt{2P-1}\frac{2y}{1+x^2+y^2} \end{aligned} \tag{2.39}$$

This transformation projects rectangles $\varphi \in [0; 2\pi), \vartheta \in [0; \pi]$ to planes $x, y \in \mathbb{R}$. Such transformation is less suitable to visualise dynamics because effects occurring in the proximity of the north pole are projected towards infinity. However, it can be used to represent pure qubit as a complex number $z \equiv x + iy$ (with $P = 1$), its evolution than can be described via complex function and this allows to apply known theory of chaos in [36] and our work.

The final note concerns a generalisation of the qubit called *qudit*. It is a d-level system with Hilbert space generated by computational base $|i\rangle, i \in \{0, 1, 2, \ldots, d-1\}$. Qubits form a special case with $d = 2$. Density matrices of a qudits get more complicated - while the trace condition can be guaranteed by composing it of analogues to Pauli matrices, the positivity condition imposes complicated equations on the combination coefficients. The state space of analogous Fano representation is a convex object in $2^d - 1$ Euclidean space. We will not pursue this line of thought in our thesis but we will outline future direction of research towards this general situation.

2.3 Theory of chaos

At the end of 19$^{\text{th}}$ century, Poincaré investigated the problem of three bodies [53] introducing the *chaos* as a new physical phenomenon appearing even in simple models. The definitions of chaos vary in the literature but all have the main feature in common, it is the exponential sensitivity to initial conditions. This means that even the smallest perturbations in the initial conditions can dramatically influence the evolution of the system.

2.3.1 Chaotic dynamical systems

In this thesis we follow definition as given in Devaney's book [16] adjusted for metric spaces as done in [**?**]. We also find a good source in [61]. First we must define mathematical structure, where chaotic behaviour will occur.

Definition 2.3.1 (Dynamical system)**.** *Let $X = (\mathcal{X}, \rho)$ be a complete metric space, $\mathbb{F}$ be one of $\mathbb{R}$, $\mathbb{R}^+$, $\mathbb{Z}$, $\mathbb{N}_0$. a pair $(\{S_t\}, X)$ is called a* dynamical system *when $\{S_t\}$ is a set of continuous maps from X into itself such as following conditions are satisfied:*

1. $(\forall m, n \in \mathbb{F})(S_{m+n} = S_m \circ S_n)$,
2. $S_0 = \mathbb{1}$ *is identical map.*

Set S_t forms the evolutionary operator while parameter t has the role of time. According to $\mathbb{F}$ we call dynamical system to be reversible continuous, irreversible continuous, reversible discrete or irreversible discrete respectively.

The protocol of our interest is a scheme that mathematically acts as a map on a state space (Hilbert space is a complete metric space) corresponding to qubit or qubit n-tuples or qudits. The scheme is iterated and the iterations of the map form the discrete time evolutionary operator. At this moment, we list important yet universal terms needed for general understanding and correct definitions.

Definition 2.3.2. *Let $f : X \to X$, $g : Y \to Y$ be maps of metric spaces. f and g are said to be* topologically conjugate *if there is a homeomorphism h such that $f \circ h = h \circ g$. Homeomorphism h is then called topological conjugacy.*

Definition 2.3.3. *Let X be a metric space and $f : X \to X$ a map. a point $x \in X$ is* periodic*, if $(\exists n \in \mathbb{N})(f^n(x) = x)$. a point $x \in X$ is* preperiodic *if $(\exists j \neq k \in \mathbb{N})(f^j(x) = f^k(x))$ but x is not periodic.*

Definition 2.3.4. *$f : X \to X$ map on a metric space is* topologically transitive *if for any nonempty open sets $U, V \in X$ there exists such $k > 0$ that $f^k(U) \cap V \neq \emptyset$*

Definition 2.3.5 (Chaotic dynamical system)**.** *Let (X, ρ) be a complete metric space with metric ρ, f be a map $f : X \to X$. The dynamical system (X, f) is* chaotic *if*

1. *set of preperiodic points of f is dense in X,*
2. *f is topologically transitive.*

The original Devaney's definition contained one more point:

3. f has sensitive dependence on initial conditions.

This point means that there is ε such that, for any $x \in X$ and any its neighbourhood U, there exist $y \in U$ and $n \in \mathbb{N}$ so that $\rho(f^{\circ n}(x), f^{\circ n}(y)) > \varepsilon$. Later it was proven, see [45], that this point is a consequence of the first two points and thus not needed in the definition. Nevertheless, this point is crucial because it is responsible for unpredictability which is one of three characteristics of chaos. The

other two are regularity (existence of dense set of periodic points) and indecomposability (system cannot be divided into noninteracting subsystems). Chaotic evolution is well understood for a very particular system - metric space $\mathbb{C}$ and evolution functions being iterations of a holomorphic function, or more specifically a rational polynomial function. We will introduce reader to this field later.

So far the definitions are very abstract but our work is focused on a protocol that is iteratively applied to a physical state. In this way we deal with a discrete time evolution where time corresponds to the number of iterations executed. The metric space will be either $\mathbb{R}^n$ or complex space $\mathbb{C}$ with Euclidean metric. Therefore, we restrict now ourselves to these spaces and discrete evolution for the rest of the work.

One of our interest besides proving chaotic properties will also be to determine stable regimes (fixed points or cycles). We now resume classification based on Jacobi matrices for discrete dynamical systems. This theory is slightly different from the theory for continuous time evolution which is studied far more extensively. Therefore, the discrete version is a little more difficult to search for. We can recommend sources like [56, 61] to find more details. Nonetheless, our readers will do well through the rest of this work with only our brief overview.

In following paragraphs consider map $f : \mathbb{R}^n \to \mathbb{R}^n$ that is applied on a vector $(x_1, x_2, \ldots, x_n) = x \in \mathbb{R}^n$ yielding

$$(x'_1, x'_2, \ldots, x'_n) = x' = f(x) = (f_1(x), f_2(x), \ldots, f_n(x)). \tag{2.40}$$

The question of stability aims at disturbing the initial state. The evolution can increase the perturbation, decrease it over time, even oscillations without any converging trend can occur. The basic approach inspired by derivatives and Taylor expansions for functions of a single variable, i.e. $n = 1$, performs linearisation of the dynamical system.

Definition 2.3.6. *For a map f we call x_0 fixed point whenever $f(x_0) = x_0$. This fixed point is asymptotically stable when $(\exists U$ neighbourhood of $x_0)(\forall x \in U)(\lim_{j\to\infty} f^j(x_0) = x_0)$, otherwise it is unstable.*

Labelling the perturbation with ε at the point x_0, for differentiable f we can expand

$$f(x_0 + \varepsilon) = f(x_0) + \mathbb{J}\varepsilon + \mathcal{O} \tag{2.41}$$

where $\lim_{\varepsilon\to 0} ||\varepsilon|| \cdot ||\mathcal{O}|| = 0$ holds. The matrix $\mathbb{J} = \mathbb{J}(x_0)$ is called Jacobi matrix (at the point x_0) and is given by

$$\mathbb{J}_{ij} = \left.\frac{df_i}{dx_j}\right|_{x_0} \tag{2.42}$$

where the derivatives are evaluated at the fixed point.

The crucial role in the stability is played by eigenvalues and eigenvectors of the Jacobi matrix, note that they may be complex. The difference $f(x) - f(x_0)$ can be related to the perturbation $x - x_0$ which can be decomposed into eigenvector basis, if such exists. The action of the Jacobi matrix then clearly shows the contractions when corresponding eigenvalues are of magnitude < 1.

Proposition 2.3.7. *For the map f with the fixed point x_0 and corresponding Jacobi matrix with eigenvalues $\lambda_i, i \in \hat{n}$ we call the fixed point*

1. hyperbolic *when* $(\forall i \in \hat{n})(|\lambda_i| \neq 1)$, *in particular*
   (a) superattractive *when* $(\forall i \in \hat{n})(\lambda_i = 0)$
   (b) attractive *when* $(\forall i \in \hat{n})(|\lambda_i| < 1)$ *with* $(\exists i \in \hat{n})(|\lambda_i| > 0)$
   (c) repelling *when* $(\forall i \in \hat{n})(|\lambda_i| > 1)$
   (d) saddle point *when* $(\exists i, j \in \hat{n})(|\lambda_i| < 1 \wedge |\lambda_j| > 1)$
2. nonhyperbolic *otherwise.*

There is another widely used concept of Lyapunov stability which relaxes the condition of the asymptotical stability. That allows to include the nonhyperbolic states to be included into stable regimes.

Definition 2.3.8. *The fixed point x_0 of map $F : \mathbb{R}^n \to \mathbb{R}^n$ is Lyapunov stable when $(\forall U$ neighbourhood of $x_0)(\exists V$ neighbourhood of $x_0)(\forall x \in U)(\forall n \in \mathbb{N})$ $(F^n(x) \in V)$. Otherwise, we say it is unstable.*

In this way, the stability can be attributed to a much wider set of states where eigenvalues with $|\lambda| = 1$ emerge. Note that each asymptotically stable state is also Lyapunov stable while the converse is not true, the behaviour of Lyapunov stable but asymptotically unstable state is usually indifferent, i.e. the orbit of a perturbed state oscillates in the vicinity of the unperturbed orbit in a certain sense. The higher orders of the perturbation must usually be taken into account to decide properly the local dynamics of such states.

The asymptotic stability on the other hand can be narrowed to the concept of exponential stability where the rate of convergence is exponential and is described by Lyapunov coefficients, but for the moment we take that to be beyond the scope of this work. We only mention to our readers the basic idea - consider a fixed point that is perturbed by sufficiently small distance in a direction of an eigenvector corresponding to eigenvalue λ of Jacobi matrix. After n iterations, the perturbed and original point differ by factor approximately

$$\lambda^n = e^{n \ln \lambda}. \tag{2.43}$$

We take formal definition of the Lyapunov numbers from [34]. When $(\lambda_i)_i$ is a sequence of eigenvalues of matrix $\mathbb{A}\mathbb{C}^{n,n}$ in decreasing order of magnitudes, $|\lambda_1| \geq |\lambda_2| \geq \ldots |\lambda_n|$ we define $\Delta_j(\mathbb{A}) = |\lambda_1 \lambda_2 \ldots \lambda_j|$.

Definition 2.3.9. *Lyapunov numbers δ_j for orbit of x_0 under map f are*

$$\delta_j = \lim_{k \to \infty} \sqrt[k]{\Delta_j \left(\prod_{n=0}^{k-1} \mathbb{J}(x_0^{(n)}) \right)}, \tag{2.44}$$

if the limit exists. Symbol $x_0^{(n)}$ stands for n-th iterate of point x: $f^n(x_0)$. Lyapunov exponents are $\lambda_j = \ln \delta_j$.

The connection to stability is typically following, attractive behaviour is implied by negative Lyapunov exponent, repelling behaviour by positive Lyapunov exponent. There can be exceptions, counterexamples to this naive thought are offered by Perron, [51].

In this thesis we aim at purification, i.e. desired state subject to perturbation will be demanded to converge back to the original one. In this context we will usually speak of attractive, repelling or saddle points in the sense of the first definition. The speed of convergence is coded in the magnitude of the eigenvalues. Eigenvectors corresponding to the real eigenvalues define subspaces at which the perturbation is simply reduced/increased by the factor of the eigenvalue, complex eigenvalues encode rotation making the fixed point a vertex. Negative eigenvalues typically mean oscillations. We show an overview in a figure below.

The fixed points which we take for an obvious concept are not the only important states. To settle down the terminology and generalise previous concepts, we now discuss the periodic orbits.

Definition 2.3.10. *The orbit of the point $x \in X$ in dynamical system is a sequence $(x, f(x), f^2(x), \dots) = (f^n(x))_{n=0}^{\infty}$. When the point is periodic with period n, we call arbitrary sequence $\mathcal{C} \equiv (f^m(x), f^{m+1}(x), \dots, f^{m+n-1}(x))$ cycle and all these cycles initiated at arbitrary $m \in \mathbb{N}$ are taken as equivalent.*

The stability of the length n cycles is then given by a product of Jacobi matrices corresponding to all the members of the cycle

$$\mathbb{J}|_{f^{n-1}x} \cdot \mathbb{J}|_{f^{n-2}(x)} \cdot \dots \cdot \mathbb{J}|_{f(x)} \cdot \mathbb{J}|_{x} \tag{2.45}$$

in the same way as in 2.3.7. The evolution for complex eigenvalues of cycles can be very complicated and we do not need to discuss them in detail because it is not relevant for the purpose of our work aimed at the purification.

2.3.2 Chaos in physics

Weather and climate are ones of well known examples of chaotic systems driven by few simple differential equations. Another physical dynamical system is fluid dynamics where chaos manifests as turbulences. Other applications can be found in stock exchange price evolution, population growths and other branches of science. We shall now return to celestial mechanics where the topic started, [28, 53]. Lagrange and Hamilton mechanics system is manipulated via phase space. Equations of motion restrict physical evolution to a certain manifold in the phase space. For an integrable system this manifold has topological structure of toroid, canonical action-angle variables can be defined so that the motion is represented as orbiting the toroid. Chaos breaks this structure.

To give a taste we consider now three-body system where one body serves as a perturbation to the two particle system. Phase space of two bodies will be deformed due to perturbation. When the third body is small enough (like in Sun - Earth - Moon situation), the toroid in phase space is slightly deformed, but under rough measures the main toroidal structure is preserved. When the perturbation is big, the structure of toroid is shattered and does not resemble toroid in any measure. The small deformation case is usually called soft chaos while the distorted manifold structure is reason to call this situation hard chaos.

There is an interesting statement from the soft chaos theory. This so-called KAM theorem (named after Kolmogorov, [38], Arnold, [2], and Moser, [46]) says that for very small perturbation there exist regions, 'stability islands', in the phase space where motion is realised almost like in the non-perturbed case. These are

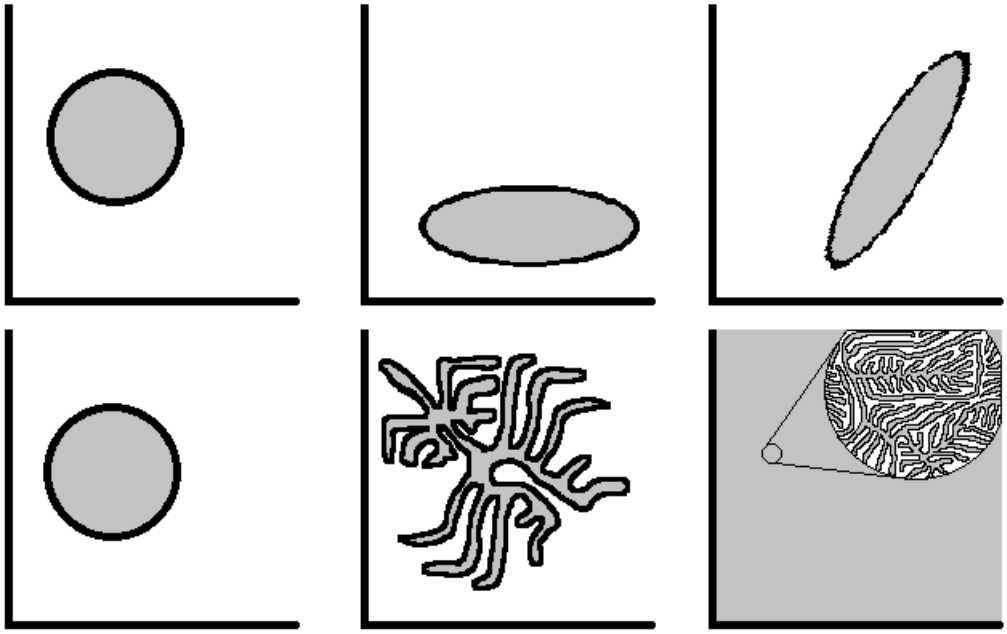

Figure 2.1: Evolution of a 'bubble' of initial conditions for integrable systems (*top*) and chaotic systems (*bottom*) in the phase space.

the reason for our solar system not to be torn into pieces by gravity. The Moon could be catapulted away from Earth instead of being forced to orbit almost Kepler ellipses if it had possessed much more mass.

Evolution in the phase space is different for integrable systems and chaotic systems, as it is illustrated in figure 2.1. In both cases, the Liouville theorem holds. That means that a set of initial conditions represented as some 'bubble' in the phase space evolve as incompressible liquid. For integrable system this initial-state-bubble will preserve relatively decent shape while for chaotic system this bubble would fill uniformly vast region, possibly even whole phase space in the limit of infinite time. Two arbitrarily close starting points will eventually get as far away as wanted - this is the sensitivity to initial conditions, token of chaos.

This thesis deals with quantum information theory which turns trajectories in phase space into an obsolete approach. Where is chaos hidden in quantum physics? Construction in 5.16 leads to unitary evolution which is linear and preserves distance. Such condition is in contradiction with the sensitivity to initial conditions. However, the unitarity of quantum state evolution follows from requirement of closed systems. Open systems allow for nonunitary evolution and so in principle, chaos. They are usually studied with a statistical approach, a system is described only by mean values which can wash chaotic features. The protocol of our interest considers a qubit subject to a very specific environment action which allows to exactly describe its nonlinear evolution precisely.

The evolution map will be multidimensional, and thus no mathematical background is available to draw results straight from mathematical theorems. However, under certain restrictions it has been shown [36] that systems of two qubits

is represented by a complex number and its evolution is described by iterations of a complex function of a single complex variable which truly induces chaos. The asymptotic dynamics generate a fractal structure that contains the points sensitive to initial conditions, the chaotic points. Such fractal structures will be shown to be a characteristic feature for general protocols and general input states. We will now present brief overview of the complex functions theory and fractals because they will be key instruments to understand the purification protocol.

2.3.3 Complex function of a single complex variable

The topic of chaotic maps in mathematics started with works of Gaston Julia and Pierre Fatou [21, 33] at the beginning of the last century. Without a big responses at first. With an advance of computers and work of Benoît Mandelbrot, [40] the theory got popular thanks to visualisation of the results which include fractals. Since than, many books have been dedicated to the mathematical analysis of the chaotic maps, yet the progress has not been general. Narrow branches can give very interesting findings in particular systems but no complex analytical theory is available for general chaotic dynamical systems. We will use the knowledge obtained about dynamical systems defined by complex functions of a single complex variable and for more complicated systems we will be left to numerical effort.

The theory of complex functions of a single complex variable results into a main idea of separating the function's domain into two disjoint sets - Fatou and Julia set - which contain points with regular and chaotic behaviour respectively. The Julia set usually forms a fractal and it contains the points of seemingly random evolution, yet it is deterministic. These points evolve through the whole Julia set chaotically, exhibiting no convergence, while the points from the Fatou set are drawn to some attractors. The Julia set is then representing states of troubling behaviour for quantum information protocols aiming at repairing a quantum state, i.e. making it converge to a certain specific state. In this view, the Julia set (respectively its analogue in higher dimensions) contains states for which the protocol fails. That is a natural and practical reason to focus on this topic. On the other hand, there is a curiosity coming from the fractals that can emerge in quantum physics in a novel way. But first we introduce the basics of the theory of complex functions of a single complex variable. It is impossible to encompass all the works on the topic but for a basic overview we refer to [44, 19, 3, 45, 23] books which are suitable for a beginner. Some definitions are a straightforward analogy of before-mentioned; still we write it to settel down notation and show similarities as well as slight nuances.

First of all, let us settle the manifold which will serve as a domain. The pillar of our work in the context of the complex functions is in identification of the Bloch sphere with so called *Riemann sphere* through stereographic projection 2.39 and setting $z = x + iy$. Riemann sphere $\hat{\mathbb{C}} = \mathbb{C} \cup \infty$ is topologically a sphere, a simple connected manifold in particular. It is one of three canonical models of simple connected complex manifolds.

Proposition 2.3.11 (Uniformisation theorem)**.** *Every simple connected Riemann surface is conformally isomorphic (i.e. there exists a manifold isomorphism holomorphic also with its inverse) to one of following manifolds:*

1. *a field* $\mathbb{C}$*,*

2. *a disk* $\mathbb{D}$,

3. *a Riemann sphere* $\hat{\mathbb{C}}$.

While the pure qubit can be represented as a point of $\hat{\mathbb{C}}$, the application of the protocol of our concern or generally qubit evolution will be represented as a function $f : \hat{\mathbb{C}} \to \hat{\mathbb{C}}$ as long as pure qubit remains pure. Protocols of our concern satisfy this condition, furthermore their application responds to an iteration of a rational polynomial functions.

Definition 2.3.12. *$f : \hat{\mathbb{C}} \to \hat{\mathbb{C}}$ is* rational polynomial *if it can be expressed as $f(z) = P(z)/Q(z)$ where P, Q are polynomial without a common root. The* degree *of rational polynomial function $deg(f)$ is the maximum of the degrees of its corresponding polynomials.*

Definition 2.3.13 (Normal family of functions)**.** *Suppose X, Y be Riemann surfaces, $\mathcal{A}$ be a set of continuous maps $X \to Y$. $\mathcal{A}$ is called a normal family of functions, if for any infinite sequence of functions $\{f_n\}_{n=1}^{\infty} \in \mathcal{A}$ there exists a subsequence which converges locally uniformly to a continuous map $f : X \to Y$.*

This important property of existence of the locally uniformly convergent subsequence in iterated function implies regular dynamics, i.e. absence of sensitivity to initial conditions, chaos. This proposition is applied to chained iterations of the evolution function in our work.

Definition 2.3.14 (Julia set & Fatou set)**.** *Let $f : S \to S$ be a nonconstant holomorphic map on a Riemann surface S. For a point $z_0 \in S$ there is following dichotomy:*

1. *There exists a neighbourhood U of z_0 such that f^n restricted to U forms a normal family of functions. We say that point z_0 is regular or normal.*

2. *Such the neighbourhood does not exist.*

Set of regular points forms Fatou set*, $\mathcal{F}(f)$. The points satisfying the second condition form* Julia set*, $\mathcal{J}(f)$.*

The Julia set is a crucial object in the theory of complex variables because it is connected to chaotic behaviour. The Julia set has many properties that earned it its popularity amongst wide public. The most interesting is its self-similarity feature, fractal-like structure which adds to this thesis inomittable element of aesthetic value. Of course, following properties of Julia set are much more important for this thesis.

Theorem 2.3.15. *The Julia set is fully invariant. This means: $(\forall n \in \mathbb{Z})$ $(f^n(\mathcal{J}(f)) = \mathcal{J}(f))$. Furthermore, Julia set of a function and its n-fold iterate coincide. That means:*
$(\forall n \in \mathbb{N})(\mathcal{J}(f)) = \mathcal{J}(f^n))$.

Corollary 2.3.16. *Because $\mathcal{F}(f) \cup \mathcal{J}(f) = \mathbb{C}$ from the definition, the same statement holds for $\mathcal{F}(f)$ too.*

Proposition 2.3.17. *For function f of degree at least 2, the Julia set has following properties: $\mathcal{J}(f) \neq \emptyset$, $\mathcal{J}(f) = \overline{\mathcal{J}(f)}$ and $\mathcal{J}(f)$ has no isolated points.*

Following definition is special case of more general definitions 2.3.3, 2.3.10

Definition 2.3.18. *An orbit of a point z is the sequence of its forward images, i.e. $\mathcal{O}(z) = (f^n(z))_n$. If $(\exists n \in \mathbb{N})(f^n(z) = f(z) \wedge (\forall k \in \widehat{n-1})(f^k(z) \neq z))$, orbit is said to be periodic, we call subset of orbit $\mathcal{C} \equiv (f^n(z))_m^{m+n-1}$ for arbitrary $m \in \mathbb{N}$ a cycle; smallest number n satisfying the condition is called the* period *of the cycle. The number $\lambda = (f_n)'(z)$ is called the* multiplier *or eigenvalue of the cycle.*

Definition 2.3.19. *A cycle whose multiplier is*

1. *$\lambda = 0$, is called superattractive,*
2. *$0 < |\lambda| < 1$, is called attractive,*
3. *$|\lambda| = 1$, is called indifferent,*
4. *$|\lambda| > 1$, is called repelling.*

A cycle for which $\lambda = 1$ but none of f^n is identical map (i.e. $\lambda = e^{i\varphi}$, $\varphi \in \mathbb{R} \setminus \mathbb{Q}$) is called parabolic. If the orbit is not periodic but $(\exists m, n \in \mathbb{N})(f^m(z) = f^n(z))$, we call it preperiodic. The eigenvalue characteristics are defined the same way after omitting the preperiodic part.

Note the similarity with previously stability classification 2.3.7 which is basically enhanced within the indifferent case. The definition leads us to ideas that attractive cycles of f belong to $\mathcal{F}(f)$, perturbation to the cycle is effaced by the function iterations. The repelling cycles are part of $\mathcal{J}(f)$ as the perturbed and original orbits diverge. When an indifferent cycle is perturbed, it evolves differently but stays close to the original one; it cannot be a priori assigned to neither Julia nor Fatou set. More exactly, these thoughts are summarised and extended after following definition.

Definition 2.3.20. *For each attractive cycle, there is a nonempty open set of points, whose orbits tend in limit to some point of the cycle. This set is called* basin of attraction, Ω. *Each point $z \in \mathcal{F}(f)$ can be associated with one connected component Ω_z of some basin of attraction, so that $z \in \Omega_z$. This component is called* immediate basin of attraction. *The immediate basin of attraction of a cycle is meant to be a union of immediate basins of all points of the cycle.*

Theorem 2.3.21. *Each attractive cycle is contained in the Fatou set. Each parabolic and each repelling cycle is contained in the Julia set. a whole basin of attraction Ω of an attracting cycle is contained in the Fatou set. But the boundary of the basin $\partial\Omega$ is a part of the Julia set. Even, the topological boundary of basin of attraction of any single attractive cycle is equal to the entire Julia set.*

Proposition 2.3.22. *Rational polynomial function of degree $d \geq 2$ has at most $2d-2$ attractive or parabolic cycles. There is only a finite number of non-repelling cycles.*

The last proposition is useful as it simplifies search for members of the Julia/Fatou sets by restricting the number of possible cycles. However, there is another simplification based on so-called critical points.

Definition 2.3.23. Critical point *z is any point such that the first derivative of f vanishes there, i.e. $f'(z) = 0$.*

Proposition 2.3.24. *Let f be a rational polynomial function of degree $d \geq 2$. Each immediate basin of attraction contains at least one critical point. Forward orbit of critical points converge to an attractive or parabolic cycle, if it converges at all.*

Thanks to these propositions one can find cycles, determine their character; in that way one can find members of the Julia set. The invariance of the Julia/Fatou set can be augmented to following statements that give a recipe to discover the whole Julia set from some of its members.

Definition 2.3.25. *A property is said to be true for* generic *$x \in \mathcal{M}$ if it is true for all points in some countable intersection of dense open subsets of $\mathcal{M}$.*

Theorem 2.3.26. *For each $z_0 \in \mathcal{J}(f)$: $\overline{\{z|(\exists n \in \mathbb{N}_0)(f^n(z) = z_0)\}} = \mathcal{J}(f)$.*

Theorem 2.3.27. *For generic $z_0 \in \mathcal{J}(f)$: $\overline{\{z|(\exists n \in \mathbb{N}_0)(f^n(z_0) = z)\}} = \mathcal{J}(f)$.*

Briefly, Julia set is sufficiently approximated by preimages of an arbitrary one of its members found thanks to critical points. We add that while the iteration of the evolution function on the members of the Julia set causes divergence under the slightest perturbation, the inverted function must guarantee convergence of the preimages of points from the Julia set. As the polynomial functions typically have many preimages of a single point, this backward iteration is often capable of finding the Julia set very quickly and precisel,y even with low numerical requirements.

The last proposition to be mentioned serves to accent that the Julia set will be nonempty in our research, it can take various forms with seemingly different structures. Yet the structures cannot be arbitrary.

Proposition 2.3.28. *If the Julia set has an interior point, then $\mathcal{J}(f) = \mathbb{C}$.*

This proposition guarantees that there are no 'islands' of chaos. If such island is found somehow, then all the points exhibit chaotic evolution. This property and many others are in general lost when the evolution in more complicated manifolds like three-dimensional Euclidean space of Fano representation is studied.

The topic of complex functions is tightly connected to fractals. There is one that gained much of popularity, it is the Mandelbrot set [40, 41, 58] which is constructed in a following way. Consider a family of complex functions $f_c(z) = z^2 + c$ with c complex parameter. All such functions have infinity for th attractive critical point. And for that reason, following definition is correct, even for generalisations to polynomial functions of higher degrees:

Definition 2.3.29 (Filled Julia set)**.** *For a polynomial function f, set of points that do not escape infinity,*

$$\mathcal{K}(f) = \{z \in \mathbb{C} | \lim_{n\to\infty} f^n(z) \infty\}, \tag{2.46}$$

is called filled Julia set*.*

Proposition 2.3.30. *For any polynomial function of degree ≥ 2, $\mathcal{K}(f)$ is non-empty compact set. The border of the filled Julia set equals its Julia set, $\partial\mathcal{K}(f) = \mathcal{J}(f)$.*

Theorem 2.3.31. *There is dichotomy - for each polynomial function f of degree ≥ 2, $\mathcal{K}(f)$ is either path-connected or totally disconnected, in the latter case $\mathcal{K}(f) = \mathcal{J}(f)$*

Definition 2.3.32. *Mandelbrot set is defined based on the structure of the Julia set*

$$\mathcal{M} = \left\{c \in \mathbb{C} | f_c(z) = z^2 + c \text{ has connected Julia set}\right\} \tag{2.47}$$

Mandelbrot himself gave a clue how to describe the set easily.

Proposition 2.3.33.

$$\mathcal{M}_f = \{c \in \mathbb{C} | \{f^{\circ n}(0) | n \in \mathbb{N}\} \text{ is bounded}\}\} \tag{2.48}$$

This suggests an algorithm that decides whether a point $c \in \mathbb{C}$ belongs to the Mandelbrot set. Iterations of initial point 0 are executed. Whenever $|z| > 2$ it can be shown that $|f(z)| > 2|z|$ and thus when an iteration of zero escapes ring $|z| < 2$ the constant c is assigned to the Mandelbrot set.

There are quite a few reasons why we speak of the Mandelbrot set. One is to demonstrate that the structure of the Julia set can be disconnected, such case is problematic for numerical work and will be a major issue in the fourth chapter of our work. Second reason is that the topic got popular and let to new discipline which tries to study how that Julia set change when the parameters of functions are changed. This led to a concept of J-stability,[42], and showed that there are regions where the structure of the Julia set is stable and there are sudden changes to it when the regions are crossed. This advanced field is very interesting because we will encounter similar behaviour. The last reason is that Mandelbrot set is that its border is a fractal with dimension equal to 2, proven here [58]. With this fact we connect to the next section.

2.3.4 Dimension

We mentioned that the evolution can induce fractal structures. These structures will be of our interest as they contain states of chaotic or more complicated behaviour that goes beyond theory of complex functions. In the Fano space or a more general space the state can be attractive in one direction while repelling in another direction, as a saddle point. But probably the most interesting feature related to chaos is the fractal structure itself. The fundamental characteristic of fractals is their non-integer dimension. We now present the dimension concept and ways to estimate the dimension of a set.

General definition was given in [30] by Hausdorff who put together and further developed previous thoughts of Caratheodory and others. He proposed a class of measures on arbitrary metric space.

Definition 2.3.34 (Hausdorff d-dimensional measure)**.** *In metric space X for each $0 \leq d \in \mathbb{R}$ and $Y \subset X$ we define* Hausdorff d-dimensional measure*:*

$$\mathcal{H}^d(Y) = sup_{\varepsilon>0}\left\{inf_{\{U_i\}}\left\{\sum_i |U_i|^d \middle| Y \subseteq \bigcup_i U_i \wedge \forall i \in \mathbb{N} : |U_i| \leq \varepsilon\right\}\right\} \tag{2.49}$$

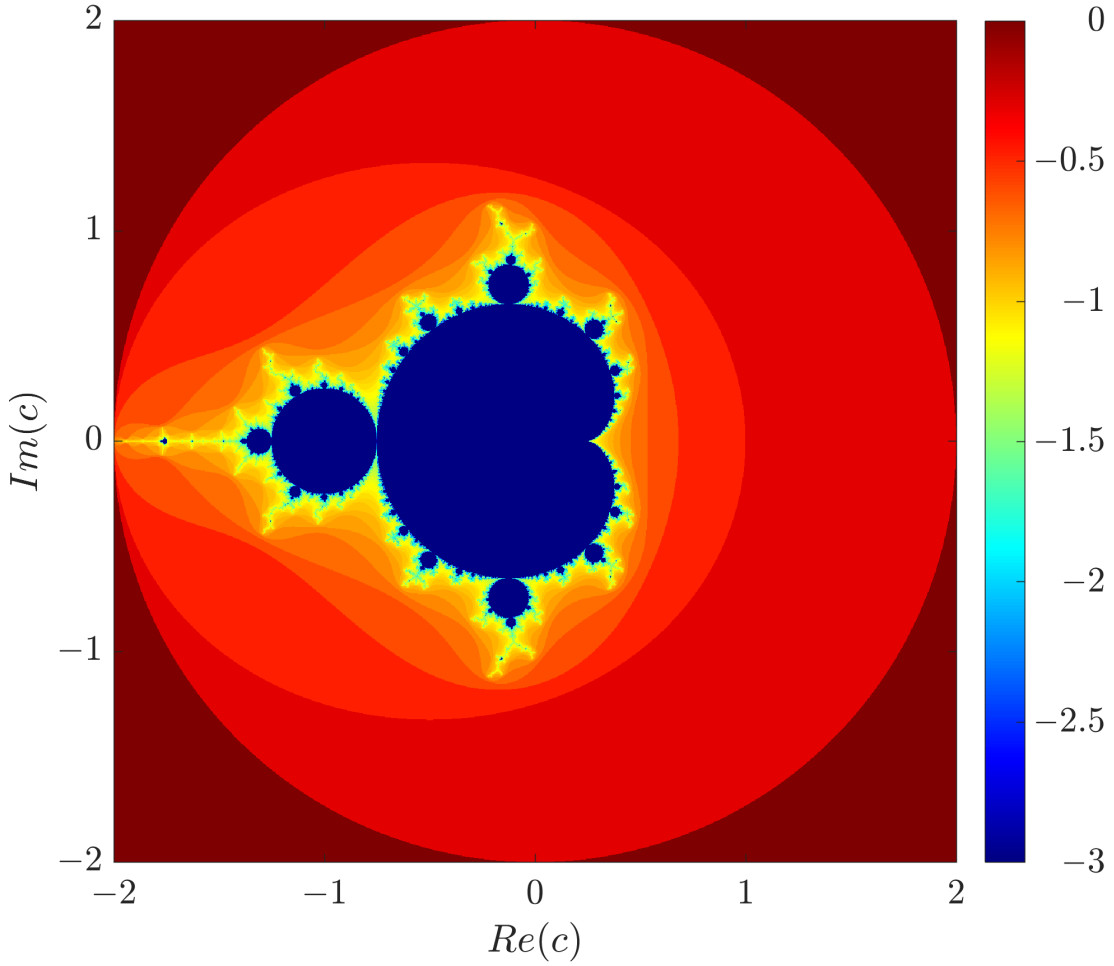

Figure 2.2: Our implementation of the algorithm to determine the Mandelbrot set. Complex plane of constants c; when $|f_c^n(z)| \geq$ for the first iteration n, the point c is assigned value n. The value of logarithm $-\log_{10} n$ is coded in colour. The maximum threshold was set to $n = 10^3$, when the state remains in the circle $|z| < 2$ for this number of iterations, its orbit is taken for bounded.

Value $|U|$ is the diameter of set U determined by the metric of the space. This measure typically attains value 0 or infinity. It can be easily seen that for given set Y if there is d_0 such that $\mathcal{H}^{d_0}(Y) = 0$, then $(\forall d > d_0)(\mathcal{H}^d(Y) = 0)$. On the other hand, $\mathcal{H}^{d_0}(Y) = \infty \Rightarrow (\forall d < d_0)(\mathcal{H}^d(Y) = \infty)$. But furthermore, there is a unique value of $\mathscr{D} \in \mathbb{R}$ separating these two options, typically the $\mathscr{D}$-measure values a finite nonzero number (but not always, for some cases it can be zero) while $\forall d < \mathscr{D} : \mathcal{H}^d(Y) = \infty$ and $\forall d > \mathscr{D} : \mathcal{H}^d(Y) = 0$. This is the core idea of the dimension definition.

Definition 2.3.35 (Hausdorff dimension)**.** *Dimension of set $Y \subset \mathcal{X}$ is:*

$$dim(Y) = inf\Big\{d \geq 0 | \mathcal{H}^d(Y) = 0\Big\} \tag{2.50}$$

To give our readers an intuition for the seemingly complicated definition, we apply it to basic objects. We do not aim for full correctness and leave finding the infima and suprema to intuitive understanding. Taking a length 1 line segment (which of course has dimension equal to 1), its optimal covering of maximal

diameter ε is attained by touching $\lceil \frac{1}{\varepsilon} \rceil$ spheres of diameter ε. To find the supremum of quantity $\sum_i |U_i|^d$ it is useful to introduce particular values $\varepsilon = \frac{1}{n}$ for integer $n > 0$. One then needs n balls (basically line segments too) yielding $\sum_i |U_i|^d = n \cdot n^{-d} = n^{1-d}$. The supremum over all values n which can be without loss of generality taken real, $n, \in \mathbb{R}$ is then equal to zero only when $d > 1$. The infimum of such values d is then 1, the dimension of the line. Taking a square of unit size, one can cut it into n^2 squares with side $\frac{1}{d}$. The Hausdorff measure in such case is taking the supremum of quantity (leaving the correct argumentation of supremum and coverings to mathematical papers) n^{2-d}. Hausdorff measure is then equal to zero for $d > 2$ which gives the dimension of (classically understood two-dimensional) surface to be equal to 2. Going to higher dimensions one can catch the idea that the dimension confronts the coverings which are refined to smaller scales to compare them with the amount of covering sets needed. This agrees not only with a laic perception of the dimension but also definition of dimension for vector spaces etc.

However, the general definition 2.3.35 cannot be used straightly to determine the dimension of a general set, the optimisation of the covering cannot be usually given/proven. It would not be a simple task even for our simplest toy models of a line and a square. a practical way to estimate the dimension has been proposed with an alternative definition. It picks the crucial idea of comparing coverings of the set as we have just shown. Taking a set of dimension $\mathscr{D}$ and series of its optimal coverings with precise diameters ε from the definition, the Hausdorff $\mathscr{D}$-measure values a finite number $\mathcal{H}^{\mathscr{D}}(Y) = \sum \varepsilon^{\mathscr{D}} = N_\varepsilon \varepsilon^{\mathscr{D}}$ where we marked number of members of the ε-covering with N_ε. This relation can be re-expressed:

$$\mathscr{D} = \frac{\ln \frac{\mathcal{H}^{\mathscr{D}}(Y)}{N_\varepsilon}}{\ln \varepsilon} = \frac{\ln N_\varepsilon}{\ln \frac{1}{\varepsilon}} - \frac{\ln \mathcal{H}^{\mathscr{D}}(Y)}{\ln \frac{1}{\varepsilon}} \tag{2.51}$$

Since Hausdorff's definition contains another optimisation, supremum over $\varepsilon > 0$, the alternative definition of the dimension takes this into account with realising that the credible value is obtained in limit $\varepsilon \to 0$ as the coverings embrace the set more precisely. Fraction $\frac{\ln \mathcal{H}^{\mathscr{D}}(Y)}{\ln \frac{1}{\varepsilon}}$ vanishes in such limit.

Definition 2.3.36 (Box-counting dimension)**.** *For set Y subset of metric space X its* box-counting dimension *is given by*

$$\mathscr{D}_{BC} = \lim_{\varepsilon \to 0} \frac{\ln N_\varepsilon}{\ln \frac{1}{\varepsilon}} \tag{2.52}$$

when the limit exists; N_ε is the minimal number of open sets of diameter $< \varepsilon$ requiered to cover Y.

In the case that the limit does not exist, it is possible to define *upper* and *lower box-counting dimension.* There are inequalities amongst the upper/lower box-counting dimensions and the Hausdorff dimension, see [61]. However, we will implement the idea in a numerical way where we obtain approximation of the dimension without elaborating limits or limes superior/inferior. In this approach an estimate is given; its fidelity is determined by many factors which will be discussed below and in appendix A.

The importance of this concept is in the availability of practical realisation. The definition can be implemented on a computer in a following way: An image (space X) capturing object (subset Y) is divided into a grid of *boxes* (covering sets), disjoint sets of prescribed diameter (alternatively: volume, surface). For a two-dimensional image, it can be understood as a kind of pixelisation of the image. The number of boxes containing the desired set Y is counted to obtain N_ε with ε determined by the size of the pixel. Such pair creates a point $(-\ln\varepsilon, \ln N_\varepsilon)$. These points for smaller and smaller values of ε (i.e. image pixelised to more detailed box-grid) lean to a line with slope $\mathscr{D}_{BC}$. The dimension estimate is taken from a linear fit of the points. Full description of our own box-counting algorithm is presented in the appendix A with all the details explained and with some performance enhancements proposed for our purpose. More notes on the topic of the box-counting dimension with its relation to Hausdorff dimension and other dimension definitions etc. can be found in [61].

At this place, we only mention that the box-counting method can be seemed as an instrument of easy implementation. However, one must be very careful about its proper realisation. The dimension value obtained by the box-counting scheme can disagree with the Hausdorff dimension. The reason is that the limit in the definition does not have to exist. Even more, the limit is only computationally approximated. However, for most objects the box-counting approach gives a good dimension estimate because for very small ε the box-counting covering gets closer to the optimal covering. One can also reason that the limit does not have to be taken and for practical purposes certain scales of epsilons should be considered. Such argumnets can be found when discussing measuring a length of a coastline in [40]. The consequences for physical applications should go hand in hand with physical assumptions.

For our work, the box-counting will be the main idea to estimate the dimension of fractal structures. More detailed information on exact implementation and caveats are provided in appendix A. But to give another perspective on the dimension of fractal structures and to show that the actual concept of dimension is very complex and intricate, we now give even one more definition. It is illustrative and highlights another typical property of fractals, *self-similarity*. However, our definition of self-similarity dimension will be a genuine compromise because very precise mathematical definition requires several theorems on maps of metric sets. An over-simplified definition is usually presented as in [61] to calculate the dimension of very simple self-similar sets. We create a definition usable on a much wider class of objects, although not fully universal. It is not usable for objects that are composed of objects that continuously change structural properties, including dimension that can change over its substructures. a more general approach with its own advantages and disadvantages is called fat fractal [27] in contemporary literature but we do not go in this direction because we do not expect to encounter such objects in our research.

Definition 2.3.37 (Self-similarity dimension)**.** *Y subset of metric space is* self-similar *if there is a finite set of affine isometries $\{f_i\}_i$ and scaling factors $\{\gamma_i\}_i$ such that $Y = \bigcup_i f_i(\gamma_i Y)$ and all sets $f_i(\gamma_i Y)$ are disjoint. The* self-similarity dimension *of Y is then such number $\mathscr{D}_S$ that*

$$\sum_i \gamma_i^{\mathscr{D}_S} = 1. \tag{2.53}$$

The simple variant of the similarity dimension is usually done with setting $\forall i : \gamma_i = \gamma$. In that case the dimension is given simply $\mathscr{D}_S = \frac{\ln n}{\ln \gamma}$[1] where n is the number of scaled copies composing to the original set. However, we find amusing to think of a more general approach to which we connect the Hausdorff measure again. The object Y of the dimension $\mathscr{D}$ can be evaluated to have certain finite Hausdorff measure $0 < \mathcal{H}^{\mathscr{D}}(Y) < \infty$. This measure is by definition scalable: $\mathcal{H}^{\mathscr{D}}(\gamma Y) = \gamma^{\mathscr{D}} \cdot \mathcal{H}^{\mathscr{D}}(Y)$ which can be seen from considering optimal coverings of the original and scaled sets. The other ingredient is additivity: for any sets Y_1, Y_2 of the dimension $\mathscr{D}$ the definition also implies $\mathcal{H}^{\mathscr{D}}(Y_1 \cup Y_2) = \mathcal{H}^{\mathscr{D}}(Y_1) + \mathcal{H}^{\mathscr{D}}(Y_2)$. These two conditions are responsible for correctness of our own formula in the definition.

For readers' comfort, we can now evaluate the self-similarity of well-known Koch's flake, [37]. This set is created from a line segment by iterating following procedure infinitely many times: Each line segment is divided equally to three parts, an equilateral triangle is drawn above the middle part and its original base is erased. Thanks to this procedure, the length of the shape increases by factor $\frac{4}{3}$ with each iteration. The length (Hausdorff 1-measure) is infinite. Evaluation of the similarity dimension is easy as each side of the flake is composed of its 4 copies scaled by factor $\frac{1}{3}$. We solve $1 = 4\left(\frac{1}{3}\right)^{\mathscr{D}_{\mathscr{S}}}$ to get $\mathscr{D}_{\mathscr{S}} = \frac{\ln 4}{\ln 3} = \log_4 3 \doteq 1.262$. This result matches the box-counting dimension where one intuitively needs 4^n covering sets (number of sides) of diameter $\varepsilon = 3^{-n}$ (length of the side). For this reason, when we take for obvious the covering optimality, there is a relation

$$\frac{\ln N_\varepsilon}{\ln 4} = n = -\frac{\ln \varepsilon}{\ln 3} \Rightarrow N_\varepsilon = \frac{\ln 4}{\ln 3} \ln \frac{1}{\varepsilon} \tag{2.54}$$

from which $D_{BC} = \log_4 3$.

Let us now present a more difficult example based on the Koch flake where we use our enriched definition. Consider similar iterative procedure with replacing a line segment with 5 lines of $\frac{1}{4}$ length and 2 lines of $\frac{1}{8}$ length according to following figure 2.3. In such case, we solve $1 = 5 \cdot 2^{-2\mathscr{D}} + 2^{1-3\mathscr{D}}$. The solution is $\mathscr{D}_{\mathscr{S}} = \frac{\ln(1+\sqrt{2})}{\ln 2}$.

Furthermore, we can even invert the question - can we find such an iterative replacement scheme to obtain an object with dimension 2? The answer is positive but it is not trivial to avoid self-intersections. The answer and more fun can be found when Peano curves are searched for, [49]. Now let us cut this interesting topic as it goes beyond the scope of our work. We conclude this section with statement that the topic of the dimension is very interesting on itself. We cannot encompass even a small part, especially about relations between presented definitions. But there are many papers and books on even more concepts and their mutual relations. We will further restrict to box-counting approach as precisely described in appendix A for its practical usability. In the appendix we also present short contemplation on the topic of rough numerical approach versus exponential instability of the chaos.

[1] Please note that logarithm properties allow to choose any base b to be applied in the equation $\mathscr{D}_S = \frac{\log_b n}{\log_b \gamma}$.

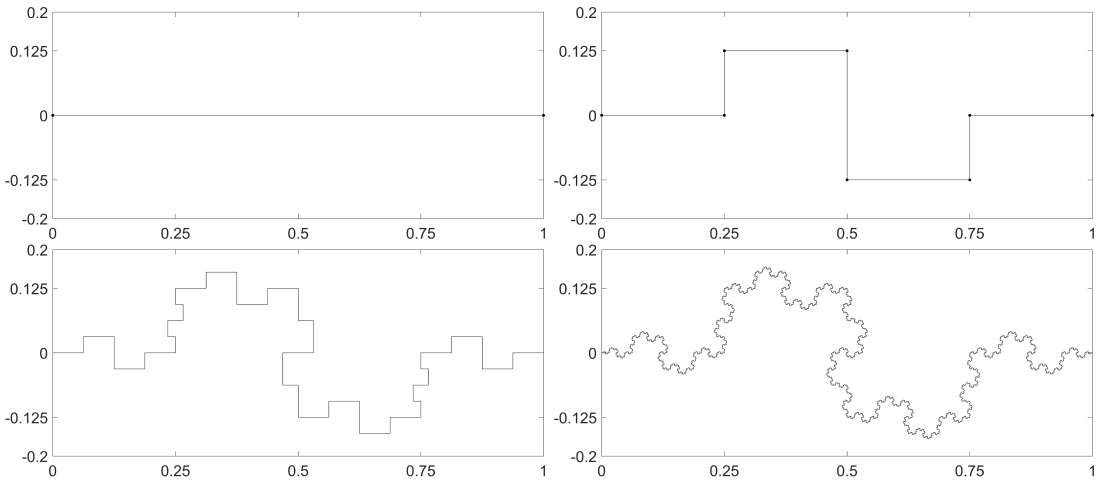

Figure 2.3: The iteration of object à la Koch snowflake with multiple scaling factors. In the *top left* plot the initial substrate - line segment - is transformed into a set of lines drawn in the *top right* figure. Newly created border points are accented with dots, so it is obvious that the object is composed of 5 lines of length $\frac{1}{4}$ and 2 copies scaled to $\frac{1}{8}$, not 12 copies scaled to $\frac{1}{8}$. *Bottom* plots show the object after 2 (left) and 6 (right) iterations. By the iterative scaling, the longest line segment in the bottom right plot has length of $4^{-6} \doteq 2 \cdot 10^{-4}$ which is below the resolution of human eye in the image; for that reason the fractal is well simulated.

2.4 Chaotic purification protocol

Let us now finally join the previous sections together to introduce our readers to our own research. The protocol of our concern intents to modify - to repair - a physical state which typically suffers from decoherence inflicted by its environment. As the protocol should work on a wide set of damaged states, no unitary operation is capable of such reconstruction making the whole set of states converge to a single attractor - remember that unitary operators are isometric, we also discussed the unitary transform when entropy and trace distance were introduced 2.2.11. Therefore, our protocol defines a special open system with the environment being a copy of the qubit system. The dynamics defined globally is unitary on a system of joint two copies but when caring for the target system only, the evolution is nonlinear and can be interpreted as a specific environment interaction. This nonlinearity is the reason for the sensitiveness to the initial conditions, i.e. chaos. The core of the protocol was proposed in [4, 1] while its chaotic features were noted in [35, 36]. We dig deeper into the properties and we modify the protocol to investigate the quantum chaos in a more general situation, but that will come in the next chapter. At this place, we describe the original protocol construction and its action on qubits.

In the paper [1] the crucial concept is proposed with generalised exclusive OR gate, called *GXOR gate*. The action of the usual XOR gate defined by modular addition can be written as

$$\mathrm{XOR}_2 \left|i, j\right\rangle = \left|i, i \oplus_2 j\right\rangle . \tag{2.55}$$

Please note that this gate is exactly the CNOT gate mentioned earlier 2.30, we stick to the CNOT name in this thesis. However, the XOR gate can be defined generally for qudits of dimension D:

$$\mathrm{XOR}_D \left|i,j\right\rangle = \left|i, i \oplus_D j\right\rangle \tag{2.56}$$

This gate is unitary but not self-adjoint for $D > 2$. Inverse gate to this XOR_D has to be expressed by iteration $\mathrm{XOR}_D^{-1} = \mathrm{XOR}_D^{D-1}$ (while CNOT satisfies $\mathrm{CNOT} = \mathrm{CNOT}^{-1}$). This inconvenience can be bypassed by redefining the gate to generalised GXOR using modular subtraction:

$$\mathrm{GXOR}_D \left|i,j\right\rangle := \left|i, i \ominus_D j\right\rangle \tag{2.57}$$

Such a modified operator is unitary and self-adjoint for arbitrary D. We let it act on a system composed of two parts in so called *control* and *target* states, $\rho_c \otimes \rho_t$ and then we perform projection (measurement) according to axiom 3a on a chosen state $\left|s\right\rangle_t$ of the target state. Mathematically, this can be written thanks to the axioms and 2.2.1 as

$$\mathcal{S}(\rho_c, \rho_t) = \frac{[(\mathbb{1}_c \otimes \left|s\right\rangle_t \left\langle s\right|_t)\mathrm{GXOR}][\rho_c \otimes \rho_t][(\mathbb{1}_c \otimes \left|s\right\rangle_t \left\langle s\right|_t)\mathrm{GXOR}]^\dagger}{\mathrm{Tr}([(\mathbb{1}_c \otimes \left|s\right\rangle_t \left\langle s\right|_t)\mathrm{GXOR}][\rho^c \otimes \rho^t][(\mathbb{1}_c \otimes \left|s\right\rangle_t \left\langle s\right|_t)\mathrm{GXOR}]^\dagger)} \tag{2.58}$$

where indices mark operators or vectors of individual subsystems. This operator is a map $\mathscr{H}_c \otimes \mathscr{H}_t \to \mathscr{H}_c$ and in particular, the original protocol was interested in taking the target and control systems to be identical copies of systems, $\rho_c = \rho_t \in \mathscr{H}_c = \mathscr{H}_t = \mathbb{C}^2$. If the projection state is chosen $\left|s\right\rangle_t = \left|0\right\rangle$, the measurement base selection applied to a density matrix (in computational basis) changes it in following manner:

$$\rho = \begin{pmatrix} \rho_{11} & \rho_{12} & \cdots & \rho_{1n} \\ \rho_{21} & \rho_{22} & \cdots & \rho_{2n} \\ \vdots & \vdots & \ddots & \vdots \\ \rho_{n1} & \rho_{n2} & \cdots & \rho_{nn} \end{pmatrix} \to \rho' \equiv \frac{\rho \odot \rho}{\mathrm{Tr}(\rho \odot \rho)} = \frac{1}{\sum_i \rho_{ii}^2} \begin{pmatrix} \rho_{11}^2 & \rho_{12}^2 & \cdots & \rho_{1n}^2 \\ \rho_{21}^2 & \rho_{22}^2 & \cdots & \rho_{2n}^2 \\ \vdots & \vdots & \ddots & \vdots \\ \rho_{n1}^2 & \rho_{n2}^2 & \cdots & \rho_{nn}^2 \end{pmatrix} \tag{2.59}$$

Surprisingly, the operation takes a form of Hadamard (elementwise) matrix multiplication, $\odot$. Obviously, the application of the protocol imposes nonlinear (nonunitary) evolution which has a very simple form of squaring the matrix elements. This nonlinear map is the core of our research.

We remind that this evolution takes this simple form thanks to the choice of the computational basis. And it is also important to note that the measurement demands renormalisation as written in axiom 3a, this will be a typical feature of following equations too. However, when an additional unitary operation is applied, the trace does not change, the trace renormalisation can thus be mathematically performed before or after the additional unitary gate, at will. For this reason, we will sometimes not write the normalisation factor explicitly. We can finally write a general form of the protocol of our interest for pure and mixed states:

$$\left|\psi\right\rangle \to \left|\psi'\right\rangle = U(\left|\psi\right\rangle \odot \left|\psi\right\rangle), \quad \rho \to \rho' = U(\rho \odot \rho)U^\dagger \tag{2.60}$$

The unitary gate U will determine characteristics of the protocols, we will investigate how the choice of U modifies the behaviou; we will refer to it as the *twirling gate* or *twirling operator*.

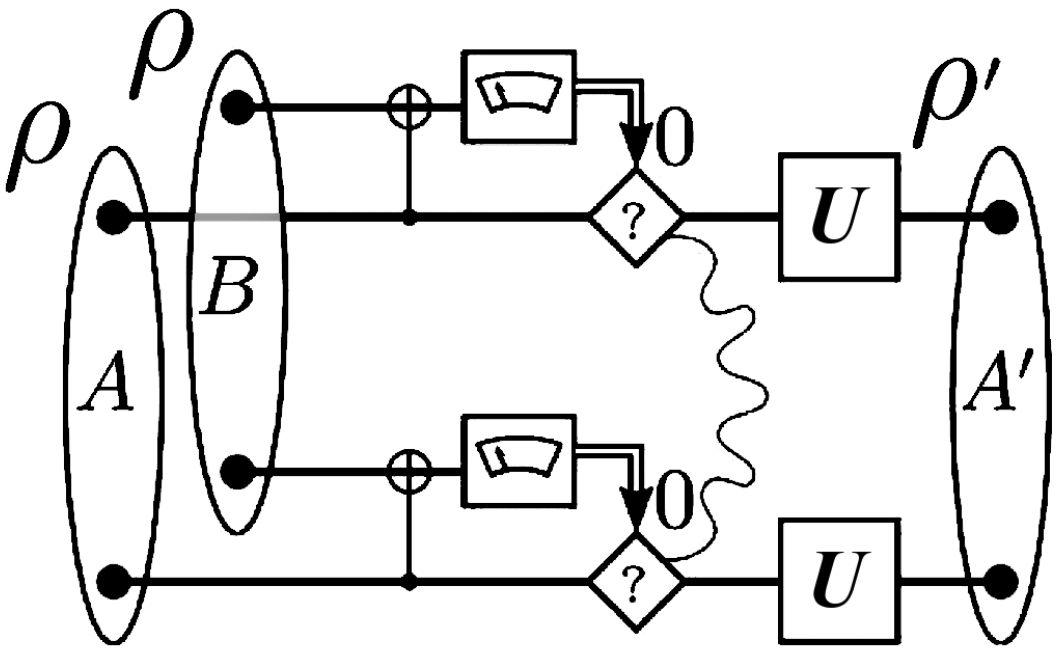

Figure 2.4: The nonlinear protocol for two-qubit states based on CNOT gate enhanced with twirling gate $U \otimes U$.

The papers [35, 36] study the protocol with choosing pairs of qubits for the physical system, i.e. $n = 4$ in 2.59. And enhances the protocol with Hadamard twirling gate 2.29

$$H \otimes H = \frac{1}{2} \begin{pmatrix} 1 & 1 & 1 & 1 \\ 1 & -1 & 1 & -1 \\ 1 & 1 & -1 & -1 \\ 1 & -1 & -1 & 1 \end{pmatrix}. \tag{2.61}$$

This protocol is schemed in figure2.4. The paper [36] notices that the action of the protocol on a particular invariant set of pure states takes a simple form expressible in terms of rational polynomial complex functions. However, two iterations of the protocol must be executed.

$$|\psi\rangle \equiv \begin{pmatrix} 1 \\ 0 \\ 0 \\ z \end{pmatrix} \rightarrow |\psi'\rangle = H \otimes H \left(|\psi\rangle \odot |\psi\rangle\right) = \begin{pmatrix} 1+z^2 \\ 1-z^2 \\ 1-z^2 \\ 1+z^2 \end{pmatrix} \rightarrow \tag{2.62}$$

$$\rightarrow |\psi''\rangle = H \otimes H \left(|\psi'\rangle \odot |\psi'\rangle\right) \equiv \begin{pmatrix} (1+z^2)^2 + (1-z^2)^2 \\ 0 \\ 0 \\ (1+z^2)^2 - (1-z^2)^2 \end{pmatrix} \equiv \begin{pmatrix} 1 \\ 0 \\ 0 \\ \frac{2z^2}{1+z^4} \end{pmatrix}$$

Of course, we use the property settled in axiom 1 and take suitable norm of the vector representing the ray in $\mathbb{C}^4$. The evolution function $z \rightarrow \frac{2z^2}{1+z^4}$ can be composed of two iterations of

$$f(z) = \frac{1-z^2}{1+z^2}, \quad f^2(z) = \frac{2z^2}{1+z^4} \tag{2.63}$$

This function f is studied using the apparatus of the Julia sets from previous section proving for the first time a new chaotic regime of quantum evolution. In particular, there is a fractal structure (Julia set) of qubit pairs that undergo deterministic chaos. Of course, these findings are restricted to a very specific protocol setting and a very specific set of states. In this thesis, we discover what happens for a wider set of protocols and states. We will see that the fractal structures are a general property and chaos is not an exclusive phenomenon in systems formed of pairs of qubits.

The importance of the results from [36] lies in the fact that the Bell state $|\Phi^+\rangle$ is an attractive fixed state and states close to it (and belonging to the mentioned invariant set of states) are purified by the protocol, i.e. if the Bell state is disturbed by decoherence or some error due to the transition through realistic physical channels, this protocol is capable of repairing the damage. Unfortunately, the paper could not claim that this kind of repair works for a general state because of considering only the particular invariant set. Yet, we come to the process of *entanglement purification*. Such processes aim exactly on restoring the dissipated entanglement. In this moment, we remind the concurrence based measure entanglement of formation 2.2.7 and the trace metric 2.2.11 on states to note that we can measure how much is a state disturbed from $|\Phi^+\rangle$.

At this place, we would only like to emphasize that this protocol uses a copy of the qubit as a particular environment and the twirling is the tensor product, meaning that both qubits are modified with single qubit Hadamard gates separately. In consequence, the protocol is LOCC. This abbreviation stands for *local operation and classical communication*. The protocol decomposes into two identical subprocesses which are independently performed on each qubit of the pair. The pair members do not have to be spatially or temporally close to each other. This allows this protocol to be used for the quantum communication. Protocols without LOCC property would require both qubits from the pair to be processed together in one physical computer. But then they cannot be sent to two communication parties.

We have put together basic pieces of the puzzle from quantum physics and theory of chaos so we can discover new results and build a systematic overview of a new class of quantum protocols. We encourage our readers to find themselves more detailed works dedicated to the single branches that are wound here together to rather an overview than a full-fledged book. But we are prepared to not drown in wild waters of chaotic dynamics of quantum systems. We can now start our own thinking on the topic trying to discover subtle features of chaos in more general protocols applied to more general states. Before we jump into fresh waters of discovery, we now present our key methods that will be used throughout the rest of the thesis.

2.5 Attractor maps

The application of the introduced protocol is represented by a map on Riemann sphere $\mathbb{C}$ that makes a single step of discrete time evolution, an iteration. The map is iterated, its asymptotic evolution can be considered. Originally in an attempt to purify entanglement in a particular set of two-qubit states. The instantaneous question arises to analyse asymptotic iterated dynamics on much wider set of

states; that is the main goal of this thesis.

At this moment, we stand to an interesting task: *'How to illustrate asymptotic evolution of general states under repetitive protocol iteration?'* At this place our own work starts but we keep the text in the theoretical chapter as we create an intuitive concept which is used as a common instrument in the later text. In the following, we consider a mixed state of a single qubit to be our input state of the protocol.

To answer the question, we now present a natural and pictorial concept that will be called *attractor map* throughout the thesis. The purity of the state plays an important physical role and the states of constant purity P form a sphere of radius $\sqrt{2P-1}$ in the geometric representation of Bloch coordinates 2.39. The position on a sphere is canonically given by two coordinates, e.g. spherical as expressed in 2.39 too. These two angular coordinates run through finite intervals which can be formally merged to a rectangle $[0; 2\pi) \times [0; \pi]$. We identify a point in such rectangle (for given purity) as a representative of the initial state ρ to be iterated. Alternatively, the Riemann sphere can be used in projection to Gauss plane as complex numbers $z = x+iy$ derived in 2.39. Or, another two-dimensional set can be used as the grid of states to be iterated.

The initial state is therefore coded by two numbers that can be taken for a position in the attractor map, a pixel in the image. After the protocol is applied iteratively to the state and its asymptotic evolution is estimated, its asymptotic regime must be differentiated visually. a natural and easy way to do so is using colours. The asymptotic state (determined by three coordinates in the Bloch space) can be assigned a colour in RGB code. However, we must keep in mind such colours offer no intuitive understanding. Also, optically indistinguishable colours could mark quite different asymptotic dynamics. Still, for more involved dynamics where a high number of alternative regimes must be differentiated, the RGB coding is convenient. We choose to use following code: the components of RGB vector belong to interval $[0; 1]$ in Matlab, vector $(0, 0, 0)$ means black colour while $(1, 1, 1)$ stands for white. We assign each state with Bloch coordinates (w, u, v) its RGB vector using following map:

$$(r, g, b) = \frac{1}{2}(1 - u, 1 + v, 1 + w) \tag{2.64}$$

We sum up that the attractor map is an image (typically rectangular) where a position of the pixel represents the initial state and its colour refers to the asymptotic dynamics of the state. As an example, we show now such attractor map for identity map. This map has trivial evolution, each state converging to itself asymptotically.

The reason why we introduce the attractor map is not only to make an easier understanding of the iterated map action, but also to reveal the structure of the immediate basins of attraction, 2.3.20. These sets are formed by areas of the same colour in the attractor map. Their border is then naturally formed of states that are sensitive - their evolution is drawn to different attractors under the smallest perturbation. We will refer to these always as the (set of) *sensitive states* through the rest of the work. For the complex functions these states form the Julia set and the sensitiveness is exponential for its generic states. In general, nothing can be said about the actual evolution of the mixed qubits in the Bloch ball,

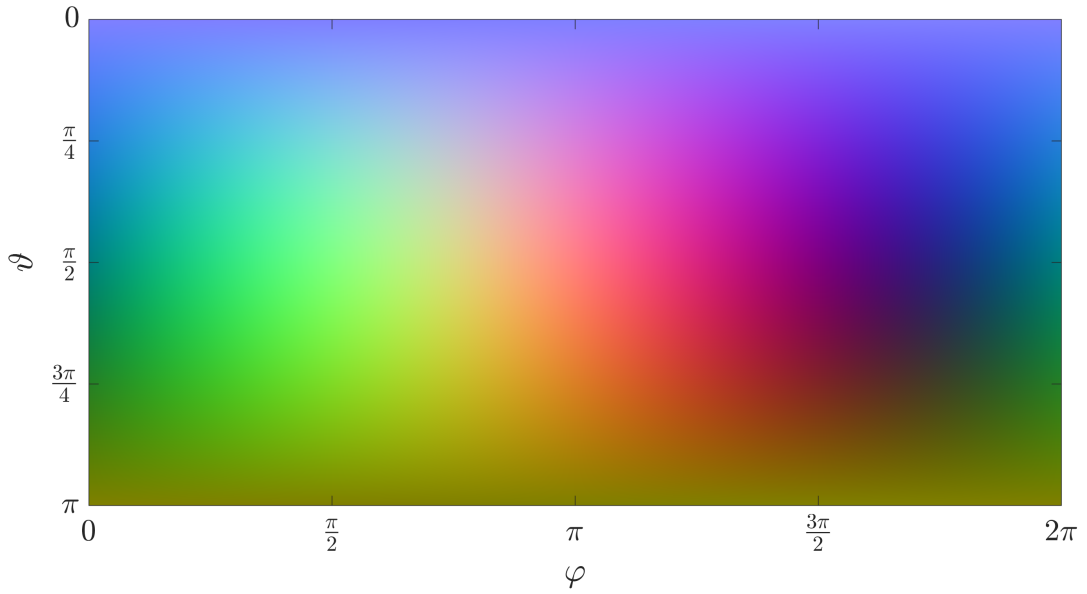

Figure 2.5: RGB code of the pure states. At the same time, the image is the attractor map of identity operator. North pole $\vartheta = 0$ corresponds to state $|0\rangle$ with Bloch vector $(w, u, v) = (1, 0, 0)$ and rgb colour $(r, g, b) = (0, 0, \frac{1}{2})$ of light blue. South pole $\vartheta = \pi$ represents the $|1\rangle$ with Bloch vector $(-1, 0, 0)$ and light green colour with $(0, \frac{1}{2}, 0)$. State $\frac{1}{\sqrt{2}}(|0\rangle + |1\rangle)$ with Bloch vector (0, 1, 0) is found under spherical coordinates $\vartheta = \frac{\pi}{2}, \varphi = 0$ with turquoise colour $(0, \frac{1}{2}, \frac{1}{2})$ and $\frac{1}{\sqrt{2}}(|0\rangle - |1\rangle)$ with Bloch vector $(0, -1, 0)$ is found at $\vartheta = \frac{\pi}{2}, \varphi = \pi$ with colour $(1, \frac{1}{2}, \frac{1}{2})$ in a shade of salmon colour.

but for cases where we iterate a complex function, i.e. pure states, the theory confirms deterministic chaos is present. These border structures are the states of our interest, even for protocols that are not represented as complex functions. The structure is typically a fractal when we deal with complex functions, but for multidimensional maps we cannot generally expect this. We also have to take into account that the attractor maps as planar images show only two-dimensional slices of multidimensional basins of attraction. And in general there might even be no basins of attraction as there could be a continuum of attractive regimes and iterating complicated evolution functions could go beyond the standard behaviour present in known systems. That will not be our case because we will deal with rational polynomial functions which even in multidimensional space offer only a restricted set of critical points and attractors. But of course, the sensitive states could form complicated fractal bodies that might interfere with the experimental applicability of the protocol. This is one of the reasons to study such structures, the other is rather a mathematical curiosity unable to guess the evolution of the sensitive states. Do they share some features known to e.g. logistic function, [43], or other known chaotic models?

Back to the attractor maps, the structure of the sensitive states visualised as the border of single-coloured regions can take the fractal form which is characterised by its dimension. Therefore, the next step we introduce is the box-counting dimension estimation. The borders of the coloured regions in the attractor map can be detected and we obtain a pixelised image of the structure. The pixels can easily be understood as points in space if desired. In this way we obtain the

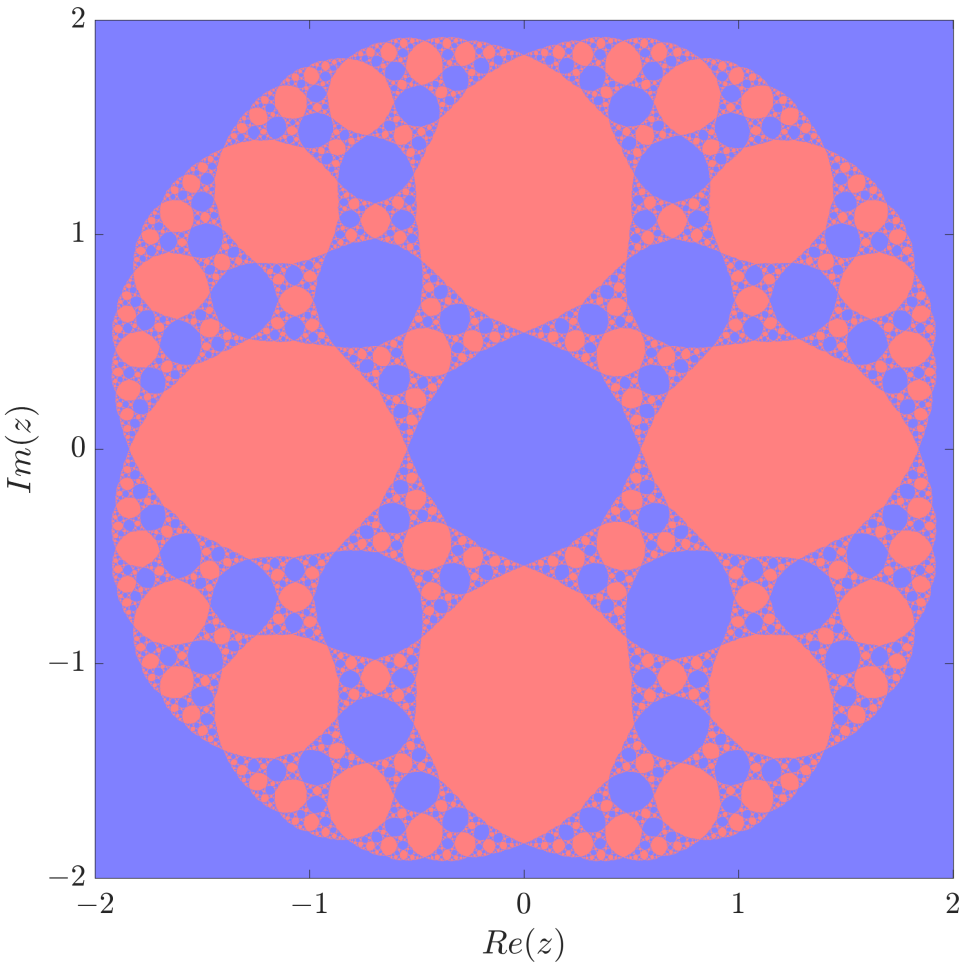

Figure 2.6: Attractor map for the protocol [36], 2.63 in complex z; the Julia set of the evolution function 2.63, is the border between red and blue regions; blue colour codes states converging to $|00\rangle$ after even number of iterations, red colour codes states converging to the Bell state $|\Phi^+\rangle$ after even number of iterations.

structure for which we want to determine its dimension.

We apply the box-counting method - detailed information of the algorithm is provided in appendix A - and we obtain the dimension of a slice of the analogue of the Julia set. Typically, the slicing will be performed by the spheres of constant purity as mentioned. It is also possible to compile the attractor maps to obtain three-dimensional structure but we do not use this approach because it does not induce uniform distribution of states.

For the introduced protocol with evolution function 2.63 we obtain dimension value $\mathscr{D} \doteq 1.56$. This is our first result, the noninteger dimension indicates how complicated the structure of the sensitive states is. The Hadamard gate protocol acting on pure states induces chaotic behaviour in a fractal structure of states. Even without the theoretical background of the complex functions [44] we could state now that this structure of borders of self-similar blocks of islands is a fractal curve of infinite length but zero area.

For the actual result part of our thesis, we will use this procedure for different protocols which induce different evolution maps of $\mathbb{R}^3 \to \mathbb{R}^3$. The fractal structure will be also estimated by box-counting algorithm in three dimensions but

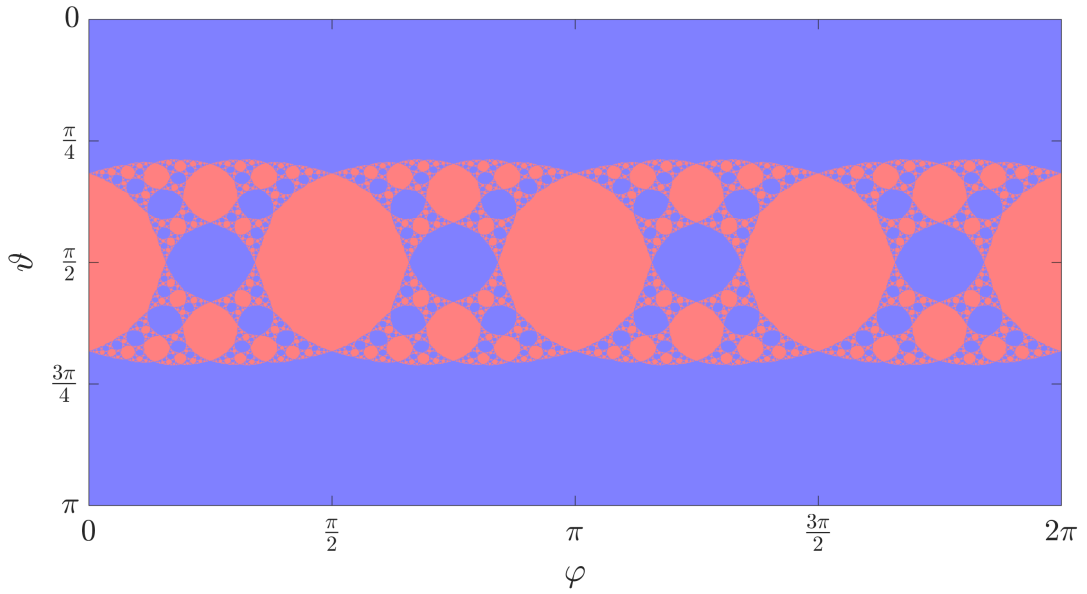

Figure 2.7: Attractor map for the protocol [36] translated to spherical coordinates. The equator $\vartheta = \frac{\pi}{2}$ is the unit circle $|z| = 1$ in previous figure, 2.6.

our main interest will be in slicing the space into attractor maps with respect to the physically relevant parameter, purity. We have it for a natural choice to deal with multidimensional evolution. The purity can be viewed as a measure for the disturbance (typically induced by transmission through the environment) and it is mostly convenient that the states with the same purity form a sphere. The dynamics can stir the states inside the ball wildly and carry them from the sphere of initial states away during the evolution, so we stress that the attractor map represents asymptotic states for states that have initially the same purity but their attractors can be pure, maximally mixed state or have any other asymptotic regime. This approach of slicing the ball of states to spheres with respect to the purity cannot inherently capture the sensitiveness of the states to perturbation in the radial direction. This effect can be observed by comparing attractor maps for different values of P or other attractor maps based on another cuts of the ball of mixed states. The fact that the pure states can be translated to the complex function theory where chaos can be proven analytically is strongly motivating to dive into the mixed states with respect to the initial purity of the state. This approach of ours is a novel and unique characterisation of the dynamics of a quantum system. Following the idea: We know what dynamics governs the pure states of a particular protocol; now, we also want to explore what happens for mixed states.

3. Properties of CNOT based chaotic protocol

The protocol studied in [36] was first to reveal inherent chaos in the iterative dynamics of quantum systems in a very particular case of input states. Such fact was denied years earlier, [8] The primary intent of the protocol was a practical purpose of purifying entanglement of a two qubit system. a $n-$qubit system is fully described as a point from $2^n - 1$ dimensional Hilbert space - as such, their multidimensional dynamical regimes get too complicated to be feasibly calculated and studied. To uncover subtle features of the iterative quantum dynamics, we first propose a very simple model of single-qubit protocol that is based on the original two-qubit protocol. The mathematical description of our model coincides with the originally studied protocol, and thus can be directionally transferred to generalise the new results to the original protocol and extend our knowledge of the nonlinear quantum dynamics. Our model takes only a single qubit into consideration and keeps the crucial element: CNOT operator. Even in spite of its simplicity, this toy model contains surprisingly rich and counterintuitive chaotic features that go beyond contemporary knowledge.

3.1 Protocol action on a single mixed qubit

Inspired by the protocol [36] we introduce the scheme of our protocol in 3.1. The CNOT gate is applied to two identical copies of the input state ρ. After the conditional flip on the target qubit it is measured and based on the result the state function of the control qubit collapses. The twirling operator U in the original protocol [36] is chosen to be the Hadamard gate H_1, 2.28. For the later purposes we choose at this moment slightly different operator determined by rotation matrix with similar properties

$$H_2 = \frac{1}{\sqrt{2}} \begin{pmatrix} 1 & 1 \\ -1 & 1 \end{pmatrix} \tag{3.1}$$

In [39], we have given evidence that such exchange of the twirling gates preserves crucial features of asymptotic behaviour, we will discuss such changes precisely later, in the sixth chapter 6. Mathematically, the action of the protocol iteration reads as

$$\rho = \frac{1}{2} \begin{pmatrix} 1+w & u-iv \\ u+iv & 1-w \end{pmatrix} \to \rho' = \frac{1}{2} \begin{pmatrix} 1+w' & u'-iv' \\ u'+iv' & 1-w' \end{pmatrix} \tag{3.2}$$

where matrix ρ' is obtained through elementwise product

$$\rho' = \frac{H_2(\rho \odot \rho)H_2^\dagger}{Tr(H_2(\rho \odot \rho)H_2^\dagger)}. \tag{3.3}$$

Calculation yields following evolution equations:

$$w' = \frac{u^2 - v^2}{1+w^2}, \qquad u' = -\frac{2w}{1+w^2}, \qquad v' = \frac{2uv}{1+w^2} \tag{3.4}$$

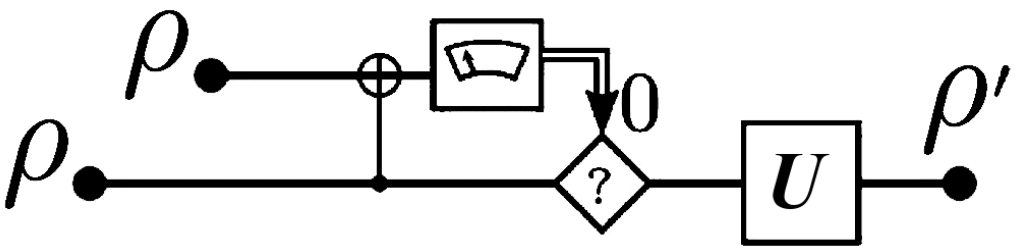

Figure 3.1: Scheme of the single-qubit purification protocol. Now, H_2 is used in place of U.

From these we gain the first interesting statement which was in more general context mentioned in [1].

Proposition 3.1.1. *Pure states remain pure after the protocol iteration. Mixed states remain mixed.*

Proof. The proof is based on simple evaluation

$$\begin{aligned} w'^2 + u'^2 + v'^2 &= \tfrac{1}{(1+w^2)^2}(u^4 - 2u^2v^2 + v^4 + 4w^2 + 4u^2v^2) = \\ &= \tfrac{1}{(1+w^2)^2}(4w^2 + (u^2+v^2)^2) = \tfrac{1}{(1+w^2)^2}(4w^2 + (1-w^2)^2) = \\ &= \tfrac{1}{(1+w^2)^2}(1 + 2w^2 + w^4) = 1 \end{aligned} \tag{3.5}$$

using the purity condition $u^2 + v^2 + w^2 = 1$ at places marked in gray. □

This statement seems to impair the protocol with an unpleasant property - mixed state can never be repaired to a pure one. In the context of the original two-qubit protocol, the Bell state cannot be never reached exactly if the state is disturbed to a mixed one. However, this statement does not impose any limits on a convergence, mixed states can converge (and very fast) towards their attractors leaning on them with arbitrarily small error demanded by experimental setup. In consequence, the proposition does not mean any practical inconvenience.

The dichotomy of the previous statement possesses an advantage - the pure states form an invariant set which can be studied separately. Of course, originally in the research the dynamics of pure states were investigated; now we aim at the (more complicated) rest, the evolution of the mixed states. That is a formidable task, thus we look for other possible invariant sets that might allow for precise analysis. Before we do so, we make an important remark. Much more information can be said about protocol iterated twice. The regime of single repetitions of the protocol exhibits typically non-monotonic behaviour, certain flip that will be discussed later. Pairwise iterations exhibit much more simple trends, including monotonicity. The two iteration evolution function follows.

$$\begin{gathered} w'' = 4\frac{w^2 - u^2v^2}{(1+w^2)^2 + (u^2-v^2)^2}\,, \\ u'' = \frac{-2(1+w^2)(u^2-v^2)}{(1+w^2)^2 + (u^2-v^2)^2}\,,\ v'' = \frac{-8uvw}{(1+w^2)^2 + (u^2-v^2)^2} \end{gathered} \tag{3.6}$$

3.2 Attractors and invariant subspaces

Starting with dynamics in the three-dimensional space, we look for attractors and invariant subsets that can give fundamental and analytical results. We have suggested that for general mixed states it is natural to examine evolution on a hypersurface of even purity, spheres $P = const$. Not only the spheres can be easily mathematically handled but the purity has physical meaning. However, the evolution drags the states across the Bloch ball to create complicated orbits raising and reducing the purity of the state. Brief calculations have shown that there is no simple universal rule to determine which states increase their purity through the evolution. That leads us to formulate our observations into following.

Conjecture 3.2.1. *There are initial states (w, u, v) with purity exhibiting very non-monotonic behaviour for arbitrarily long series of iterations before converging to the corresponding attractor.*

We will provide numerical evidence later on this topic when critical states will be analysed and illustrate with 3.5. For now, we present another statement that will be proved later. It is fundamental for the global view of the mixed state evolution which is highly nontrivial and does not allow for the same approach using complex functions as for pure states.

Proposition 3.2.2. *There is no other invariant surface of constant purity besides $P = 1$ and $P = 0$ that is an invariant set.*

We excluded the situation of $P = 0$ intentionally. Such set of states contain only a single one, the maximally mixed state $\mathbb{1}$. The completely mixed state is found to be a new attractor. It is easy to see from 3.4 that it is a fixed point. Its attractivity comes from analysis of the Jacobi matrix of the evolution map. Reminding that we order the variables in (w, u, v), the Jacobi matrix at that point reads

$$\mathbb{J}(w,u,v) = \begin{pmatrix} \frac{-2w(u^2-v^2)}{(1+w^2)^2} & \frac{2u}{1+w^2} & \frac{-2v}{1+w^2} \\ \frac{2(w^2-1)}{(1+w^2)^2} & 0 & 0 \\ \frac{-4uvw}{(1+w^2)^2} & \frac{2v}{1+w^2} & \frac{2u}{1+w^2} \end{pmatrix}. \tag{3.7}$$

For the maximally mixed state $u = v = w = 0 \leftrightarrow \mathbb{1}$ the Jacobian matrix has triple degenerated eigenvalue 0 which proves the state is superattractive. Furthermore, we give an estimate of the radius of the convergence. To do so, we consider pairwise iteration of the protocol.

Proposition 3.2.3. *Qubit satisfying $|w|, |u|, |v| < 1/8$ converges to the maximally mixed state. The convergence is exponentially fast in pairwise iterations.*

Proof. The rough assumption of a cube $|w|, |u|, |v| < 1/8$ gives after two iterations $|w''| \leq 4w^2 \leq |w|/2$, $|u''| \leq 4u^2 \leq |u|/2$, $|v''| \leq 8|uvw| \leq |v|/2$; the equality trivially occurs iff $w = u = v = 0$. If $|w| + |u| + |v| > 0$ we consider $2n$ iterations of the protocol: we obtain $|w^{(2n)}| < |w|/2^n, |u^{(2n)}| < |u|/2^n, |v^{(2n)}| < |v|/2^n$ which means that after even number of iterations the state converge to $\mathbb{1}$ in terms of w, u, v at least as the function $2^{-n}, 2n \to \infty$ in each parameter. We have not shown yet anything about the odd iterations which could perform some oscillations and could allow the state to escape in the odd iteration regime. We

show now this does not happen. From 3.4 and assumption $|u| < \frac{1}{8}$ it is obvious that after $2n+1$ iterations $|v^{(2n+1)}| < |v^{(2n)}| < 2^{-n}$ so we can claim stronger statement: $|v|$ monotonically decreases to 0. Also, $|u^{(2n+1)}| < 2|w^{(2n)}| < 2^{-n+1}$ and finally $|w^{(2n+1)}| < \max\{(u^{(2n)})^2, (v^{(2n)})^2\} < \max\{|u^{(2n)}|, |v^{(2n)}|\} < 2^{-n}$. We differentiate iterations from powers with the parentheses here to avoid confusion.

This means the all subsequences $w^{(2n)}, w^{(2n+1)}, u^{(2n)}, u^{(2n+1)}$ converge to 0. In total, (w, u, v) converges to $(0, 0, 0)$. The convergence of $w^{(n)}, u^{(n)}$ is not necessarily monotonic but the subsequences of odd and even iterations are. From the point of view of attractivity/repelling, the perturbation decays exponentially in pairwise iterations. The exponential rate is relevant experimentally and is additional information added to the fact that the maximally mixed state is truly an attractor. □

To finish with the attractors, we claim there is only one more attractor besides $\mathbb{1}$. More precisely, the other attractor is length-two cycle which will be called $\mathcal{A} := (|0\rangle, \frac{1}{\sqrt{2}}(|0\rangle - |1\rangle))$.

$$|0\rangle \equiv (1, 0, 0) \leftrightarrow (0, -1, 0) \equiv \frac{1}{\sqrt{2}}(|0\rangle - |1\rangle). \tag{3.8}$$

This pure cycle is already known from the previous papers but working as an attractor for the pure states. We now answer positively that the cycle is also the attractor for mixed states. To prove it we write Jacobi matrix of twofold iteration $\mathbb{J}^{(2)}$:

$$\begin{pmatrix} \frac{8w(1+u^4+v^4+2u^2v^2w^2-w^4)}{((1+w^2)^2+(u^2-v^2)^2)^2} & \frac{-8u(v^6+2u^2w^2+v^2-v^2u^4+v^2w^4)}{((1+w^2)^2+(u^2-v^2)^2)^2} & \frac{-8v(u^6+2v^2w^2+u^2-u^2v^4+u^2w^4)}{((1+w^2)^2+(u^2-v^2)^2)^2} \\ \frac{-4w(u^2-v^2)((u^2-v^2)^2-(1+w^2)^2)}{((1+w^2)^2+(u^2-v^2)^2)^2} & \frac{4u(1+w^2)((u^2-v^2)^2-(1+w^2)^2)}{((1+w^2)^2+(u^2-v^2)^2)^2} & \frac{-4v(1+w^2)((u^2-v^2)^2-(1+w^2)^2)}{((1+w^2)^2+(u^2-v^2)^2)^2} \\ \frac{-8uv((u^2-v^2)^2+1-2w^2-3w^4)}{((1+w^2)^2+(u^2-v^2)^2)^2} & \frac{-8vw((u^2+v^2)^2-4u^4+(1+w^2)^2)}{((1+w^2)^2+(u^2-v^2)^2)^2} & \frac{-8uw((u^2+v^2)^2-4v^4+(1+w^2)^2)}{((1+w^2)^2+(u^2-v^2)^2)^2} \end{pmatrix} \tag{3.9}$$

For the considered attractor cycle by inserting $w = 1, u = v = 0$ or $u = 1, w = v = 0$ we obtain zero matrix proving the cycle is superattractive in the mixed states. We resume, there are two attractors, both superattractive.

We now make a remark on the pairwise iteration - for the pure states it can be shown that the basin of attraction of the unique attractor composes of two parts which are mapped one on another with one or odd number of iterations and back onto itself for even number of iterations. This flip will proliferate even into mixed dynamics and will be obvious in further stability discussions. This flip is responsible for the odd/even regimes above in the proof of 3.2.3. It will also be present in dynamics of other invariant sets in further text; we conclude that this flip is a general characteristic of the protocol.

No other attractor or attractor cycle of higher lengths has been found. We continue with searching for all fixed states or cycles, though unstable. Solving $w = w', u = u', v = v'$ one can obtain four new states (besides $\mathbb{1}$). To describe them easily yet analytically we introduce constant μ which we define as the real root of polynomial $1 - x - x^2 - x^3$. Its value can be expressed analytically

$$\mu = \frac{1}{3}\left(-1 - \frac{2}{\sqrt[3]{17+3\sqrt{33}}} + \sqrt[3]{17+3\sqrt{33}}\right) \doteq 0.543689012692076 \tag{3.10}$$

and satisfies $\frac{1-\mu}{1+\mu} = \mu^2$ from its definition. Obsession for such detailed description of the number comes from the fact that the root of the polynomial $1 - x - x^2$ is $\frac{1}{2}\left(\sqrt{5}-1\right)$ which is reciprocal value of golden ratio $\phi = \frac{1}{2}\left(\sqrt{5}+1\right)$ (root of $1 + x - x^2$ satisfying $1 + \phi = \phi^2$) and this number μ can be suggested as a degree higher analogue (with the ratio-analogue μ^{-1} being root of $1+x+x^2-x^3$ and satisfying $\frac{\mu^{-1}+1}{\mu^{-1}-1} = \mu^{-2}$). Number μ^{-1} is the limit ratio of two consecutive members of any sequence $(T_n)_{n=1}^{\infty}$ satisfying reccurence relation $T_{n+3} = T_{n+2} + T_{n+1} + T_n$ for all $n > n_0 \in \mathbb{N}$. Such sequences are called tribonacci sequences today thanks to Feinberg, [22]. Thanks to this, μ^{-1} can be found as tribonnaci number in literature, without physical relations though. Probably the first and last person to use it in practical applications was Charles Darwin in his famous On the Origin of the Species to explain elephant population growths. Anyway, the analogy between ϕ^{-1} and μ is not complete and we will not need any more than the above written relations in following text.

Back to the topic of the fixed states, there is a triplet of pure states

$$\mathcal{B} := (\mu, -\tilde{\mu}, 0), \mathcal{B}_{\pm} := (-\mu^2, \mu, \pm\sqrt{1-\mu^2-\mu^4}) \tag{3.11}$$

where number

$$\tilde{\mu} \equiv \sqrt{1-\mu^2} = \frac{2\mu}{1+\mu^2} = \frac{1+\mu^2}{1+\mu} = \mu + \mu^2 = \frac{1}{\mu} - 1 = 1 - \mu^3 \doteq 0.839287 \tag{3.12}$$

can be expressed analytically as the real root

$$\frac{1}{3}\left(-2 + \sqrt[3]{19+3\sqrt{33}} + \sqrt[3]{19-3\sqrt{33}}\right)$$

of polynomial $-2 + 2x^2 + x^3$. Taking state $(\mu, -\tilde{\mu}, 0)$ one can analyse Jacobi matrix that has double degenerated repelling eigenvalue $-1-\mu^2$ (the real root of $4 + 4x + 2x^2 + x^3$) with eigenvectors $(0, 0, 1), (\tilde{\mu}, \mu, 0)$ and the last eigenvalue is attractive $\tilde{\mu} > 0$ with eigenvector $(-1, 1, 0)$. We conclude that this fixed state is a saddle point repelling on the sphere (the eigenvectors span tangential space to the fixed point on the Bloch sphere) but attractive from the direction of mixed states. Negative sign of the repelling eigenvalues marks the parity flip, the state gets flipped to the other side of the fixed point (and repelled). Studying two-fold iteration, we find eigenvalues $2\tilde{\mu}$ (real root of $-16 + 4x^2 + x^3$) with double degeneracy and the same set of eigenvectors marking repelling directions. The last eigenvalue marks the attractive direction as earlier, now with the value $1 - \mu^2 \doteq 0.704402$ (the real root of $-4 + 8x - 4x^2 + x^3$). The positivity of the eigenvalues now mark that the disturbed state remains in the same direction and does not flip over.

The other two remaining fixed points can be analysed similiarly. However, their eigenvalues become complex uncovering nontrivial twist, state with such character is usually called focus. Yet all the eigenvalues satisfy $|\lambda| > 1$ and the states are repelling in all directions (eigenvectors span the tangential plane to Bloch sphere again and one aiming inside the mixed states). The points act as repelling vortices.

There is one more fixed state, now mixed: $\mathcal{R} := (\chi, \chi - 1, 0)$ where

$$\chi = \frac{1}{3}\left(1 - \frac{8}{\sqrt[3]{1+3\sqrt{57}}} + \sqrt[3]{1+3\sqrt{57}}\right) \doteq 0.361103080528647 \tag{3.13}$$

is the real root of $1-3x+x^2-x^3$. The analysis of the Jacobi matrix uncovers three eigenvalues with $|\lambda|>1$ proving the state is repelling. With value $1-\chi \doteq 0.638897$ we can determine the purity of $\mathcal{R}$

$$P_1 = \frac{1}{1}(1+\chi^2+(1-\chi)^2) = 1-\chi+\chi^2 \doteq 0.769292 \tag{3.14}$$

which will play an important role later.

With the fixed states done we discover new mixed 2-cycle $\mathcal{C}$ by solving $u''=u, v''=v, w''=w$:

$$\mathcal{C} := (\mu^2,0,0) \leftrightarrow (0,-\mu,0) \tag{3.15}$$

Both of these states naturally share eigenvalues of the two-fold iteration Jacobi matrix. It is double-degenerate value zero marking superattractivity from directions $(0,0,1)$ and $(0,1,0)$ for $(\mu^2,0,0)$ resp. $(1,0,0)$ for $(0,-\mu,0)$. The last eigenvalue is again the value $2\tilde{\mu} \doteq 1.678574$ marking repelling direction $(1,0,0)$ for $(\mu^2,0,0)$, resp. $(0,1,0)$ for $(0,-\mu,0)$. The purity of the state $(\mu^2,0,0)$

$$P_2 = \frac{1+\mu^4}{2} = \mu \tag{3.16}$$

will also play an important role with P_1.

Let us summarise the fixed states and 2-cycles in following table. No other cycles of any lengths were found. This is in accordance with theory of complex functions which allows only a limited number of attractive or parabolic cycles. The numerically based statement for mixed states is nontrivial.

At this moment, let us stray from the topic for a brief yet interesting remark. The number μ repeats itself through the text. That is because of its minimal polynomial which repeats itself in the calculations. We illustrate it with the saddle fixed state $(w,u,v)=(\mu,-\tilde{\mu},0)$. If we take stereographic projection as explained in 2.39 we obtain point $(x,y)=(\mu,0)$. This property is illustrated in following figure.

Relations that were mentioned earlier when $\mu,\tilde{\mu}$ were defined, are now to be completed with the equations depicted in figures 3.3,3.4. We note that all the eigenvalues and the eigenvectors can be expressed analytically, yet such form is too complicated and unnecessary to be explicitly written. All the numerical values in table 3.1 can possibly be related to $\mu,\tilde{\mu}$, e.g. $1+\mu-\frac{1}{\tilde{\mu}} = \frac{\mu^2}{\tilde{\mu}} = \frac{1-\mu^2}{2} = \frac{\tilde{\mu}^2}{2} \doteq 0.352201$ while the square of magnitude of the eigenvalues $\doteq -0.352 \pm 1.720i$ being numerically identical to $2(1+\mu)$. We have only proven presence of $\frac{\tilde{\mu}^2\mu}{\mu-\tilde{\mu}} = \tilde{\mu}^2-2 = -1-\mu^2 \doteq -1.295598$ as degenerate eigenvalue of the pure fixed state $(\mu,-\tilde{\mu},0)$. Components of the eigenvectors contain values identical up to multiplications by imaginary unit i and/or -1 to values to the complex roots of polynomials x^3+x^2+x-1, x^3-x^2-x-x, but we do not find any benefit that could come from precise formulation of such relations at the moment. We conclude that all numbers (by the way, they are non-constructible) probably posses many mathematically interesting properties and only finish with mentioning relation $1-\mu^2-\mu^4 = \mu^2(1+2\mu)$ that will be used below; our readers might use it if they try to reproduce our results.

Returning to the protocol action, lets now ascend from the simple cases of fixed points and 2-cycles towards more complicated invariant sets. One can notice from the table 3.1 as well as from numerical calculations that the mixed states seem

Fixed state	Eigenvalues	Min. polynomial	Eigenvector
$\begin{pmatrix} w \\ u \\ v \end{pmatrix} \equiv \begin{pmatrix} 0 \\ 0 \\ 0 \end{pmatrix}$	0 0 0	x x x	$(w,u,v) \equiv (1,0,0)$ $(0,1,0)$ $(0,0,1)$
$\begin{pmatrix} \mu \\ -\tilde{\mu} \\ 0 \end{pmatrix}$	$-1-\mu^2$ $-1-\mu^2$ $\tilde{\mu}$	$4{+}4x{+}2x^2{+}x^3$ $4{+}4x{+}2x^2{+}x^3$ $-2{+}2x^2{+}x^3$	$(0,0,1)$ $(1+\mu,1,0)$ $(-1,1,0)$
$\begin{pmatrix} -\mu^2 \\ \mu \\ \mu\sqrt{1+2\mu} \end{pmatrix}$	$-0.352{+}1.72i$ $-0.352{-}1.72i$ $1{+}\mu$	$4{+}4x{+}2x^2{+}x^3$ $4{+}4x{+}2x^2{+}x^3$ $2{-}2x{+}2x^2{-}x^3$	$(0.606{+}1.420i, -1.115{+}0.772i, 1)$ $(0.606{-}1.420i, -1.115{-}0.772i, 1)$ $(-0.534231, -0.534231, 1)$
$\begin{pmatrix} -\mu^2 \\ \mu \\ -\mu\sqrt{1+2\mu} \end{pmatrix}$	$-0.352{+}1.72i$ $-0.352{-}1.72i$ $1{+}\mu$	$4{+}4x{+}2x^2{+}x^3$ $4{+}4x{+}2x^2{+}x^3$ $2{-}2x{+}2x^2{-}x^3$	$(-0.606{-}1.420i, 1.115{-}0.772i, 1)$ $(-0.606{+}1.420i, 1.115{+}0.772i, 1)$ $(0.534231, -0.534231, 1)$
$\begin{pmatrix} \chi \\ \chi-1 \\ 0 \end{pmatrix}$	$-1-\chi$ $+1.130395$ -1.130395	$6{+}8x{+}4x^2{+}x^3$ $4{-}2x^2{-}x^3$ $4{-}2x^2{+}x^3$	$(1,1,0)$ $(-0.830500, 1, 0)$ $(0,0,1)$

Cycle	Eigenvalues	Minimal polynomial	Eigenvector
$\begin{pmatrix} 1 \\ 0 \\ 0 \end{pmatrix} \leftrightarrow \begin{pmatrix} 0 \\ -1 \\ 0 \end{pmatrix}$	0 0 0	x x x	$(1,0,0)$ $(0,1,0)$ $(0,0,1)$
$\begin{pmatrix} \mu^2 \\ 0 \\ 0 \end{pmatrix} \leftrightarrow \begin{pmatrix} 0 \\ -\mu \\ 0 \end{pmatrix}$	$2\tilde{\mu}$ 0 0	$-16+4x^2+x^3$ x x	$(1,0,0) \leftrightarrow (0,1,0)$ $(0,1,0) \leftrightarrow (1,0,0)$ $(0,0,1)$

Notation	State/cycle	Character
$\mathcal{A}$	$(1,0,0) \leftrightarrow (0,-1,0)$	pure superattractive sink
$\mathbb{1}$	$(0,0,0)$	mixed superattractive sink
$\mathcal{B}$	$(\mu,-\tilde{\mu},0)$	pure saddle
$\mathcal{B}_\pm$	$(-\mu^2,\mu,\pm\mu\sqrt{1+2\mu})$	pure repelling foci
$\mathcal{C}$	$(\mu^2,0,0) \leftrightarrow (0,-\mu,0)$	mixed saddle
$\mathcal{R}$	$(\chi,\chi-1,0)$	mixed source

Table 3.1: Table of fixed points and cycles. The Bloch coordinates (w,u,v) are organised into columns or rows for spatial reasons as suggested at the top of the table. Eigenvalues responsible for repelling behaviour marked in red. Review of notation and character in the table at the bottom.

to tend to plane (circle) $v=0$. Also, all attractors satisfy $v=0$. Easily from the evolution equations 3.4 $|v'| < \left|\frac{2uv}{1+w^2}\right| < |v|$ whenever $u < \frac{1}{2}$. Furthermore, the Jacobi matrix gives

$$\mathbb{J}(w,u,0)\cdot\begin{pmatrix}0\\0\\1\end{pmatrix} = \begin{pmatrix}0\\0\\\frac{2u}{1+w^2}\end{pmatrix} \tag{3.17}$$

marking that at least the region enclosed by parabolas $2|u| = 1+w^2$ acts in the attractive way. We are unable to give analytical evidence that all states eventually converge to the plane $v=0$ as we numerically find states that oscillate while increasing their v for arbitrary amount of iterations before starting to converge

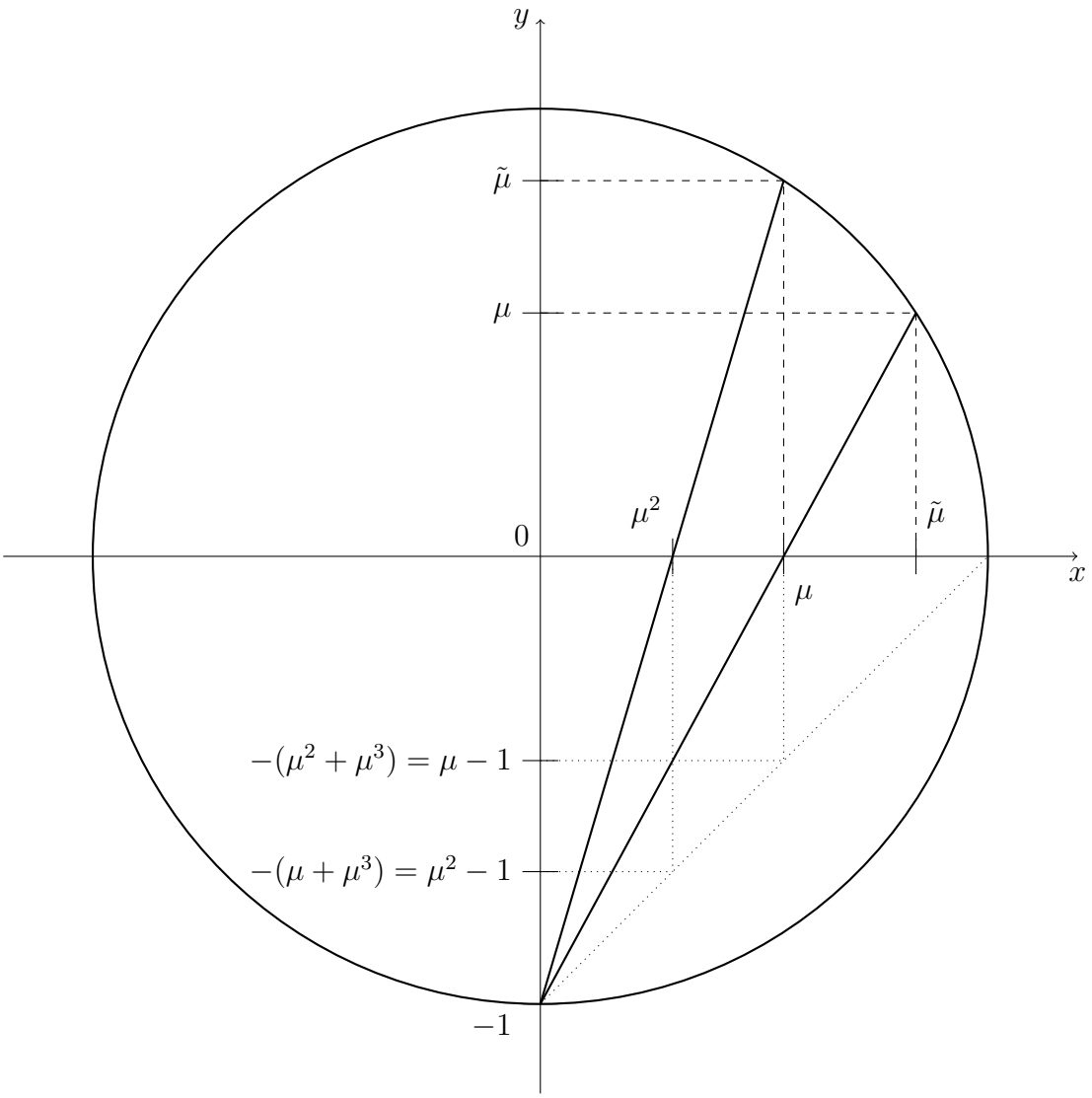

Figure 3.2: Geometrical interpretation of μ and $\tilde{\mu}$, for simplicity in plane. Point $(\tilde{\mu}, \mu)$ is projected to $(\mu, 0)$ by stereographic projection with the pole in $(0, -1)$. At the same time, point $(\mu, \tilde{\mu})$ is projected onto $(\mu^2, 0)$. Dotted lines in bottom right quadrant represent the definition of μ as a polynomial root, $\mu^3 + \mu^2 + \mu - 1 = 0$.

to $v = 0$. To show such example we analyse iterations of perturbed repelling state $(-\mu^2 - \varepsilon, \mu - \varepsilon, \mu\sqrt{1+2\mu})$ where we choose small value $\varepsilon > 0$. The results can be seen in figure below.

These numerical data connect to our first hypothesis 3.2.1 which we now support with an example of the convergence resisting state. The observation also represents an important fact that a quantum physical system may resist the converging dynamics for a vast number of iterations making the protocol ineffective for certain inputs. We touch this issue of practical applications in the overview at the end of this chapter. Now we note that restricting ourselves to plane $v = 0$, the state evolution remains restricted to this plane. We claim the circle

$$K = \{(w, u, v) | u^2 + w^2 \leq 1 \wedge v = 0\} \tag{3.18}$$

is invariant. In this circle previous results about the attraction may be repro-

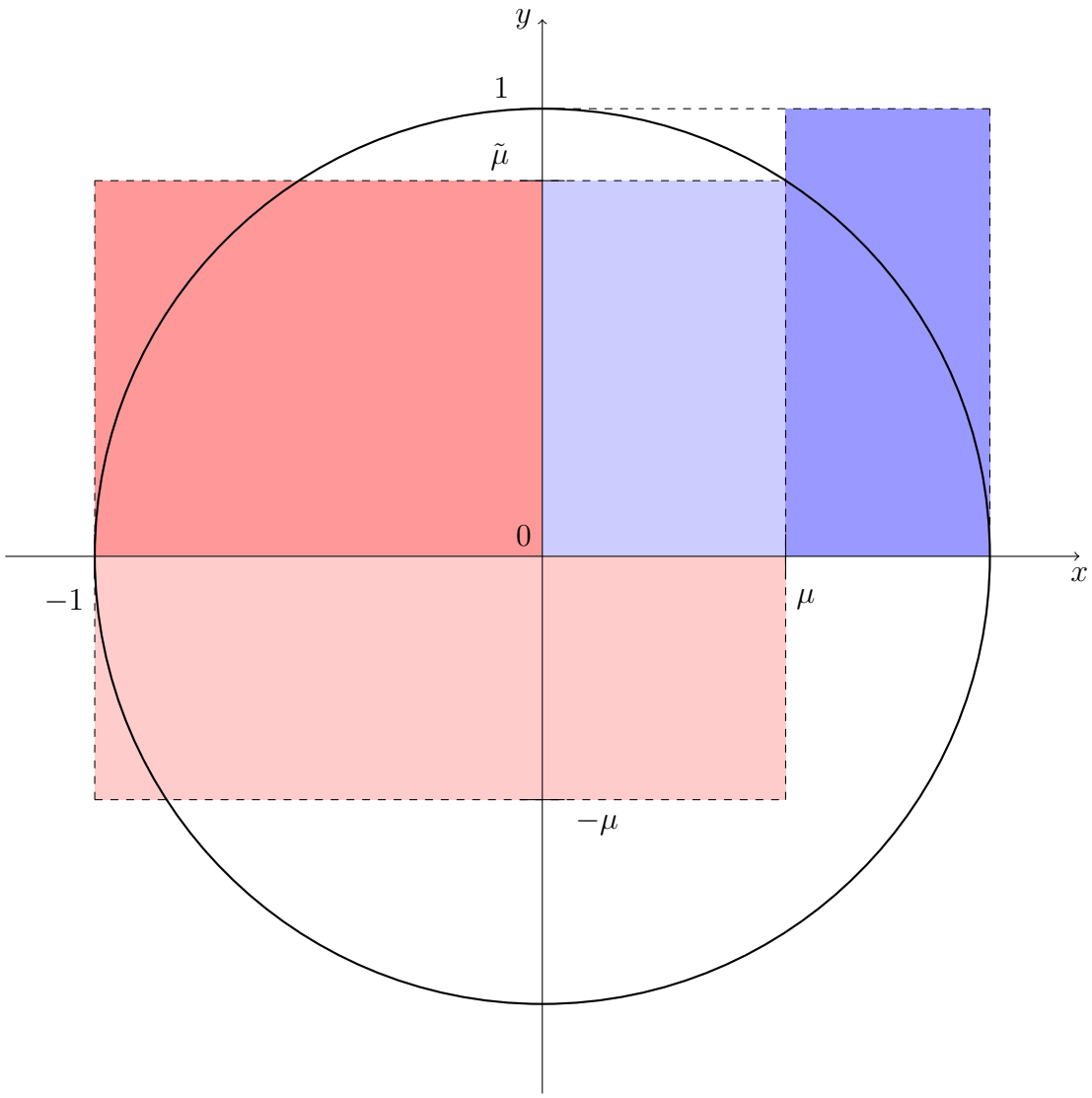

Figure 3.3: Some relations between $\mu, \tilde{\mu}$ can be visualised in rectangles - the blue rectangles have the same area $\mu\tilde{\mu} = 1 - \mu$, both the red rectangles have area $\mu(1 + \mu) = \tilde{\mu}$.

duced for the reason that the dynamics is trivially reduced to evolution function $(w, u) \to (\frac{u^2}{1+w^2}, \frac{-2w}{1+w^2})$. Most states converge towards $\mathbb{1}$ or the pure cycle $\mathcal{A} \equiv |0\rangle \leftrightarrow \frac{1}{\sqrt{2}}(|0\rangle - |1\rangle)$ in even or odd regime of reaching $|0\rangle$. These regions of the asymptotic dynamics are separated by a curve passing through all the repelling and saddle critical states. We can visualise the convergence tendencies in figure 3.6. Only one quadrant $w \geq 0, u \leq 0$ is shown, other quadrants are mapped onto this quadrant during the first two iterations at most. This fact can be seen from evolution equations in the plane; when $v = 0$ is put into 3.6, then obviously

$$w'' = \frac{4w^2}{(1 + w^2)^2 + u^4} \geq 0,\ u'' = \frac{-2u^2(1 + w^2)}{(1 + w^2)^2 + u^4} \leq 0. \tag{3.19}$$

Therefore, we could restrict ourselves to a smaller invariant set, quartercircle $K' = (w, u, v) \in K | w \geq 0 \wedge u \leq 0$. Thanks to the powers in the evolution functions, the

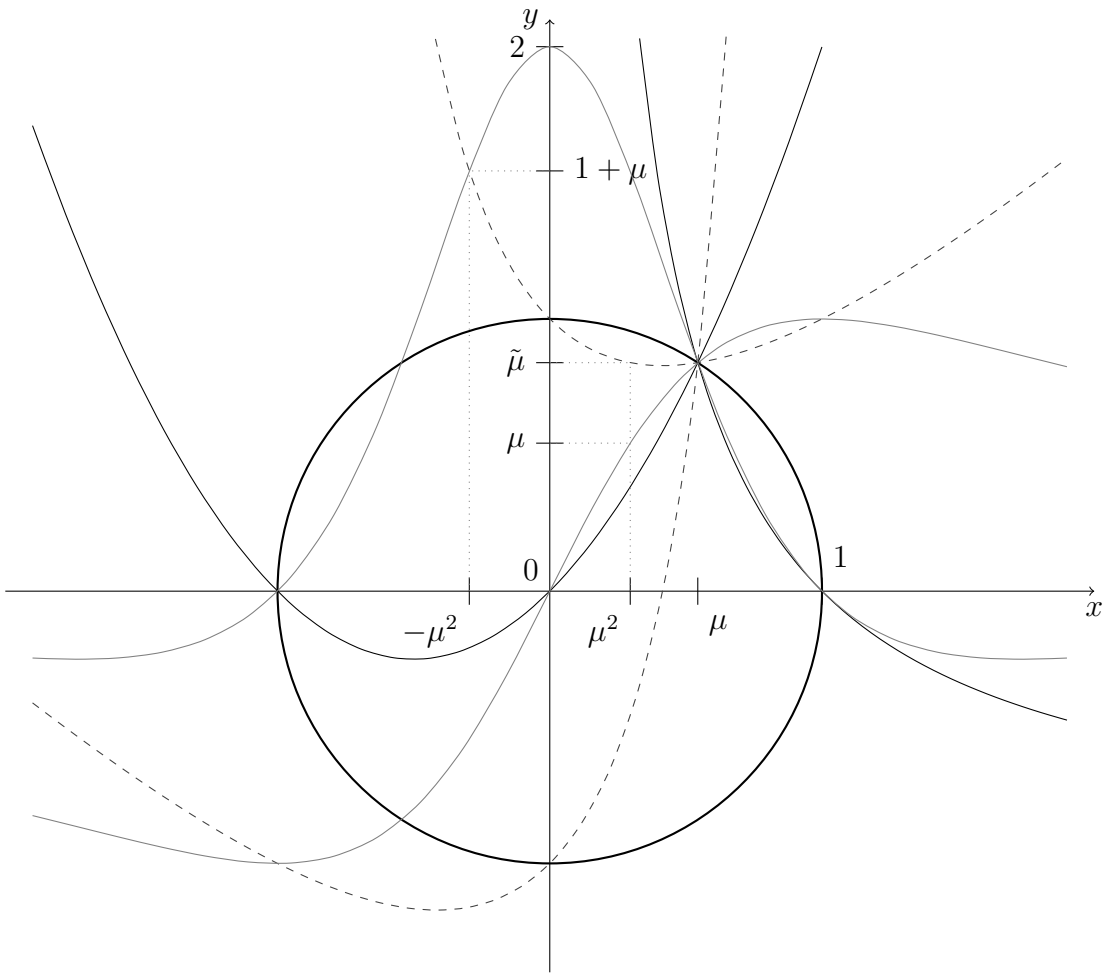

Figure 3.4: Relations between μ and $\tilde{\mu}$ can be visualised by curves passing through the point $[\mu, \tilde{\mu}]$. First, there is parabola $y = x + x^2$ and hyperbola $y = \frac{1}{x} - 1$. But we can find more complicated curves, e.g. $y = \frac{2x}{1+x^2}, y = 2\frac{1-x^2}{(1+x^2)^2}$ drawn in gray and $y = \frac{1+x^2}{1+x}, y = \frac{x^2+2x-1}{1-x}$ dashed in gray. Of course, there are infinitely many curves meeting at $(\mu, \tilde{\mu})$ but these could be taken as canonical due to other properties, e.g. character of the formula, integer coefficients and other intersections.

asymptotic equations will be shared symmetrically in other quarter circles. With this finding we discover certain symmetry that will be in our scope in the next section.

We now bring forth another invariant set that can be visually identified in the image 3.6. It is the line segment $L_1 = \{(w, u, v) | u^2 + v^2 + w^2 \leq 1 \wedge v = 0 \wedge w - u = 1\}$ as can be easily verified using $u = w - 1$ in

$$w' - u' = \frac{u^2 + 2w}{1 + w^2} = \frac{(w-1)^2 + 2w}{1 + w^2} = \frac{1 + w^2}{1 + w^2} = 1. \tag{3.20}$$

This line segment as a one-dimensional object offers a great opportunity to perform detailed and precise analysis. The evolution function takes simpler form when expressed in w which gives

$$w' = \frac{(1-w)^2}{1+w^2},\ w'' = l(w) = \frac{2w^2}{1 - 2w + 4w^2 - 2w^3 + w^4} \tag{3.21}$$

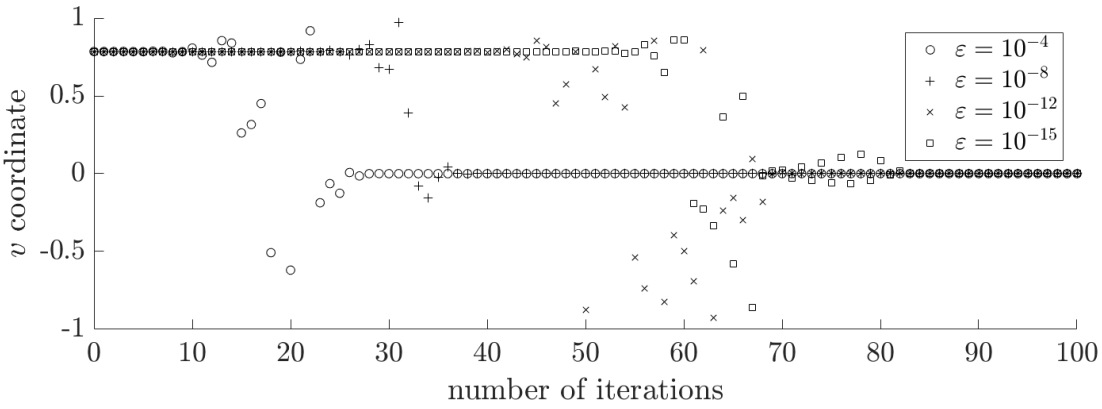

Figure 3.5: v coordinate of evolved state $(-\mu^2-\varepsilon, \mu-\varepsilon, \mu\sqrt{1+2\mu})$. Initial states with different values of ε are chosen, as legend indicates.

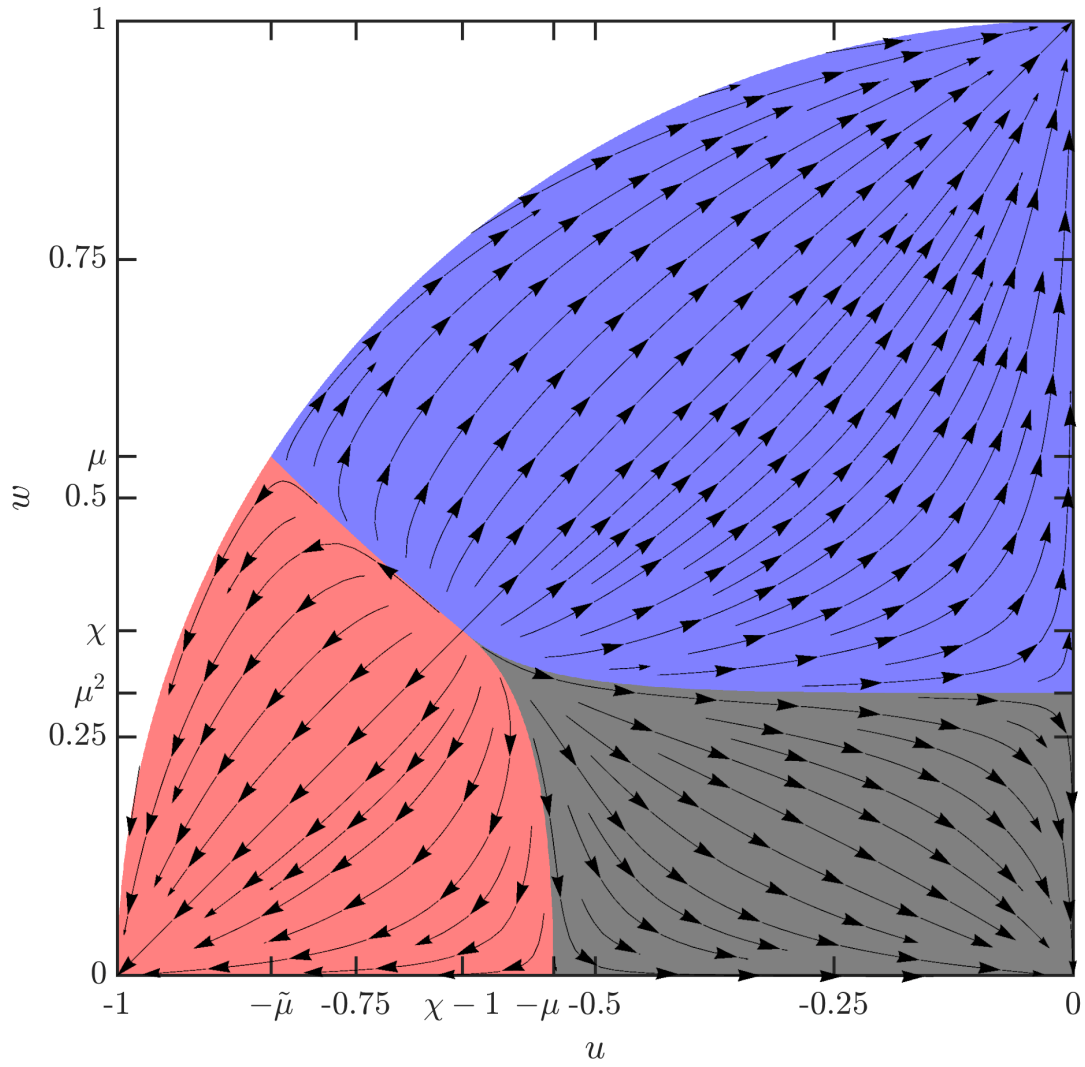

Figure 3.6: Illustration of evolution flow in the attractor map in the $v = 0$ plane. Only quadrant $w \geq 0, u \leq 0$ considered thanks to symmetries, reflections across the axes. *Blue*: convergence to $|0\rangle$ in even number of iterations; *red*: in even number; *gray*: convergence to $\mathbb{1}$, *white*: non-physical points outside the Boch ball.

We encourage our readers to note that the function domain is restricted to $w \in (0;1)$ and the map l or its multiple iterates are maps of the unit interval onto itself. The flip of the odd-even convergence to the cycle $\mathcal{A}$ manifests as a map of segment with $w \in (0;\chi)$ onto segment with $w \in (\chi;1)$ and vice versa. The cycle $\mathcal{A}$ and fixed states can be included in the interval if desired. In the next image we can check differences $w''-w$ which are more simple to understand because the odd-iteration flip does not interfere. As has been told, the point $w=\chi$ is fixed and repelling - for higher values $w>\chi$: $w''>w$ tending to $w-1$ while for $w<\chi$ the point gets further to zero, $w''<w$. We can describe the repelling rate with the slope of the difference function $\Delta l(w) = w''-w = -\frac{w(1-2w+w^4)}{1+w^4}$. Calculating the derivative at the fixed point $\frac{dl}{dw}(\chi) = (1+\chi)^2 \doteq 1.852602$ one can also find that the difference function has slope $(1+\chi)^2-1 = \chi(2+\chi) \doteq 0.852602$. This fact means that a perturbation to the fixed point (with restraint to the invariant set) is magnified by factor $(1+\chi)^2$ proving the repulsion. Actually, we already know this because in table 3.1 we listed the eigenvalue $\lambda = -(1+\chi)$ which corresponds to eigenvector $(1,1,0)$ which spans the set L_1. For two iterations, the eigenvalue must be λ^2. Similarly, the attraction of the attractive cycle is encrypted in $\frac{dl}{dw}(0) = \frac{dl}{dw}(1) = 0$ making them superattractive. The superattraction means that perturbation of order ε is eliminated up to higher orders of at least ε^2.

The last invariant set we identify is more complicated due to the iteration flip: $L_2 = L_2^{(w)} \cup L_2^{(u)}$ where

$$L_2^{(w)}=\{(w,u,v)|w\in[0;1]\wedge u=v=0\},\ L_2^{(u)}=\{(w,u,v)|u\in[-1;0]\wedge w=v=0\} \tag{3.22}$$

These sets are line segments on the half axes. They are mapped one onto the other with a single iteration. In other words, $L_2^{(w)}$ is mapped onto itself with two iterations while $L_2^{(u)}$ is mapped onto itself. The evolution map of state (w,u,v) reduces in these sets to

$$\begin{aligned}(w,0,0)\to(0,\tfrac{-2}{1+w^2},0)\to(\tfrac{4w^2}{(1+w^2)^2},0,0)\equiv(w'',0,0)=:(l_1(w),0,0),\\ (0,u,0)\to(u^2,0,0)\to(0,\tfrac{-2u^2}{1+u^4},0)\equiv(0,u'',0)=:(0,l_2(u),0).\end{aligned} \tag{3.23}$$

To not confuse our readers with analysing function w'' which is different now for L_2 than for L_1, we focus on $u''=l_2(u)=\frac{-2u^2}{1+u^4}$. The function maps $[-1;0]$ onto itself, the border points of the attractive cycle can be excluded if desired. Its fixed point (besides 0 and -1) is, as has been already found, $-\mu$ and the derivative $\frac{dl_2}{du}(-\mu) = 2\tilde{\mu} \doteq 1.678573$ has also been found as the repelling eigenvalue in the table 3.1. Both sets $L_{1,2}$ share the property that they are line segments with attractive border points and one repelling point matching formerly discovered critical points.

Thanks to the analysis of the dynamics in L_1, L_2 we can prove proposition 3.2.2:

Proof. For arbitrary value $P \in (0;1) \setminus P_2$, we recall that $P_2 = \mu$ was defined earlier 3.16, choose state $(\sqrt{2P-1},0,0)$. This state belongs to L_2 and evolves (with the flip of odd-even iterations) towards the pure cycle or $\mathbb{1}$. For value P_2 we would obtain the mixed cycle which would means no change in purity in two iterations. But choosing state $(0,\sqrt{2P_2-1},0)$ with purity $P_2=\mu>\mu^2$, this one is forced to converge to pure cycle $\mathcal{A}$. All the states converge to one of the

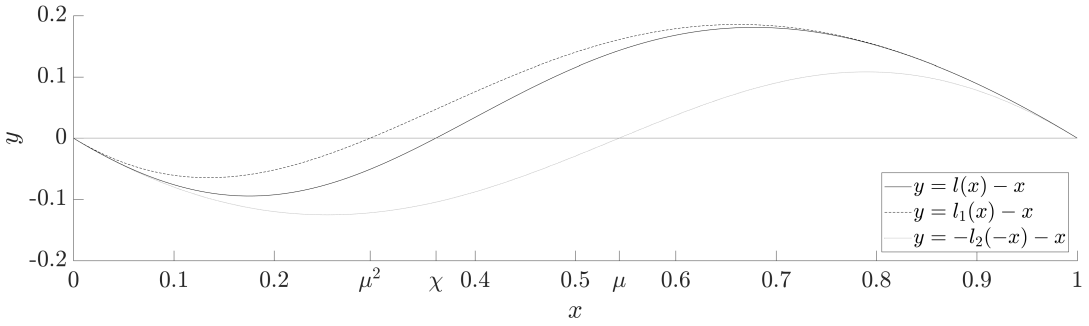

Figure 3.7: Fixed points of functions l, l_1, l_2 can be found as intersections of difference functions $l(x) - x$ etc. with x-axis. Mixed fixed points corresponding to $\mathcal{C}, \mathcal{R}$ determined by $x = \mu^2, x = \chi, x = \mu$ are unstable because difference functions are increasing. Pure fixed points of $\mathcal{C}$ are stable because the difference functions in $x = 0, x = 1$ are decreasing. l_2 map on $[-1; 0]$ flipped symmetrically to act on $[0; 1]$ too.

attractors, whence in each sphere of constant purity there is a state that leave this sphere when evolved. □

From the proof we can make the proposition even stronger: there is no $n \in \mathbb{N}$ that there could be a sphere of purity $0 < P < 1$ that would be mapped onto itself after n iterations. I.e. there is no sphere invariant on two iterations where we could think that the parity flip could lead to some purity oscillations.

We sum up the analysis of invariant sets with a statement that many features of the nonlinear evolution of our model of single qubit chaotic protocol can be expressed analytically. For the first time as far as we know, the nonlinear feature of a saddle point (attractive and repelling at the same time depending on perturbation) is proven in a regime that is present in pure quantum world without any analogue to classical physics. This is a natural piece of mosaic but has not yet been discovered. We have presented all fixed states and cycles and analysed their properties analytically as well as some interesting invariant subsets.

3.3 Symmetries and backward iterations

After finding the important states, we wish to understand the dynamics of general states better; symmetries can be very useful to that. The protocol action performs squaring in terms of the Bloch coordinates and as such there is a multiplet of states mapped on the same state. For our protocol involving squaring of matrix elements we find two preimages[1] for a general state. To do so, we first rearrange the map 3.4 yielding equation

$$w^{(-1)} = \frac{-1 \pm \sqrt{1 - u^2}}{u} \tag{3.24}$$

which has discontinuity that must be formally cared of by defining $w^{(-1)} = 0$ for $u = 0$. And we also must take the + sign in the solution to satisfy $|w| \leq 1$

[1]There are two more formal solutions to the equation system but those are non-physical because the corresponding states would have purity $P > 1$.

and guarantee the physical meaning of the qubit. In this way a unique value of $w \in [-1;1]$ is determined and can now be used to express the other variables. Finally, we get

$$\begin{aligned} u^{(-1)} &= \pm \frac{\sqrt{w+iv}+\sqrt{w-iv}}{\sqrt{1+u}+\sqrt{1-u}} = \pm\sqrt{2}\, \frac{\sqrt{\sqrt{w^2+v^2}+w}}{\sqrt{1+u}+\sqrt{1-u}} \\ v^{(-1)} &= \frac{\pm 1}{i} \frac{\sqrt{w+iv}-\sqrt{w-iv}}{\sqrt{1+u}+\sqrt{1-u}} = \pm\sqrt{2}\,\mathrm{sgn}(v)\, \frac{\sqrt{\sqrt{w^2+v^2}-w}}{\sqrt{1+u}+\sqrt{1-u}} \end{aligned} \tag{3.25}$$

The relationship between the two solutions could be seen from the original equations when simultaneously $u \to -u, v \to -v$ are substituted. Current preimage equations just confirmed there is no other preimage. We now interpret this relation of preimages: the points on the Bloch space that are reflected over the w axis are mapped onto the same state. This means that we can restrict our focus e.g. only on hemisphere $v \geq 0$. When obtaining a state with $v < 0$ we only change the sign of u, v components, such artificial sign flip does not burden the asymptotic dynamics of the system, any result can be mirrored over w axis without loss of any information, dynamical features etc. This symmetry also proliferates into attractor maps. In terms of the spherical angles 2.38 the two mirror states have their azimuthal angle changed by $\varphi \to \varphi + \pi$. Attractor maps will contain two identical images in both halves $\varphi \in [0;\pi]$ and $\varphi \in [\pi;2\pi]$.

Now, consider two states $(\pm w, u, v)$, these evolve to $(w'', u'', \pm v'')$ when two iterations are applied, 3.6. Additionally, states $(w, u, \pm v)$ evolve into $(w'', u'', \pm v'')$. When we add the hypothesis 3.2.1 that all states converge to the plane $v = 0$, we conclude that both states $(\pm w, u, v)$ share their asymptotic regime. Translated to the geometric picture of the ball of Bloch coordinates, there is symmetry of reflection with respect to plane $w = 0$ and also reflection with respect to plane $v = 0$. For this reason alongside with the axial symmetry mentioned earlier we also claim there is symmetry of reflection with respect to the plane $u = 0$, this can also be seen from the equations 3.6. Finally, the compositions of the symmetries lead to central symmetry with respect to the centre of the ball, maximally mixed state. In other words, states

$$(w,u,v), (-w,u,v), (w,-u,v), (w,u,-v), (w,-u,-v), (-w,-u,-v)$$

converge to t=the same attractor, note that for the case of convergence to the cycle, the convergence has the same parity regime, i.e. all listed states converge to e.g. $(1,0,0)$ after odd number of iterations. The evolution is symmetrical in all 8 octants of the Bloch space, whence we can restrict ourselves to only e.g. $w \geq 0, u \leq 0, v \geq 0$ if we desire. This restriction significantly reduces parameter space for the computational work and also imposes symmetries in the attractor maps - the maps for chosen purity when drawn for whole range of spherical parameters of the state, $\varphi \in [0, 2\pi), \vartheta \in [0, \pi]$ does not change when flipped from left to right, upside down or combined; in total, states with $\vartheta \to \pi - \vartheta, \varphi \to 2\pi - \vartheta, \varphi \to \pi + \vartheta$ or any of combination of these transformations evolve to the same asymptotic regime. The restriction is therefore such that $\varphi \in [0, \frac{\pi}{2}], \vartheta \in [0, \frac{\pi}{2}]$ can be considered only. The rest of the attractor map can be reconstructed by corresponding flips and shifts.

The reason why we have expressed the backward iterations is in 2.3.26. It is not difficult to realise that when iterations with inverse maps must change

repelling behaviour to attractive and vice versa. This idea is proceeded to proposition 2.3.26 in the theory of complex functions but must be true even for mixed states. We can use the backward iterations to numerically approximate the structure of the sensitive states inside the Bloch sphere but this approach naturally has a drawback - the structure of the sensitive points exhibits the saddle point behaviour, the forward-stable iterations change to backward-unstable and the numerical approximation trying to identify the saddle point can fail just like for forward iterations. The exponential sensitiveness of the Julia set is the essence for the numerical estimate of the Julia sets; this property is now lost in the multidimensional calculus.

In spite of the unsure results, we can try to identify the backward-stable states and identify them as certain sources while the found (forward) attractors work as sinks. These terms are widely used in nonlinear dynamics and for their illustrative meaning we do not explain them in detail, readers can check [61]. We can set up a question: are the sources and sinks also related to exponential trends similarily to exponential sensitiveness of dynamics of the Julia sets? Is such evolution bound to some particular states?

The answer is positive in the sense explained below. We studied numerically evolution (in forward and backward directions) of disturbed fixed points and cycles $\mathcal{A}, \mathcal{B}, \mathcal{C}, \mathcal{R}, \mathbb{1}$; we have found that they work as sources/sinks as expected based on the table 3.1. The agreement of analytic and numerical results supports following results. All the states are related to exponential trend in evolution of disturbed states, such trend is not bound to the closest vicinity of the states but is a general property in the structure of the sensitive states.

As an example to demonstrate the evolution in the structure of the sensitive states, we have chosen state

$$(0.454533790051990, -0.746052079769224, 0) \tag{3.26}$$

that has been found by evolving perturbed state $\mathcal{B}$ in the (forward repelling) direction determined by corresponding eigenvector 3.1; then this state was iterated backwards. This chosen initial state has been evolved by 50 iterations, both in forward and backward evolution. This approach guarantees numerical stability when approaching the forward-stable fixed point $(\mu, -\tilde{\mu}, 0)$ and also backward-stable towards $(\chi, 1-\chi, 0)$.

Please note that $v = 0$ guarantees also $v = 0$ for all backward and forward iterations. Because a state with $v = 0$ always evolve to one with $w \geq 0$. We cannot search for preimages of states with $w < 0$, the equations 3.24, 3.25 would yield completely mixed state but such option is not physical but a mathematical artefact of the equations form. The existence of multiple preimages of a point is a natural effect of squaring imposed by CNOT operator. For the sake of simplicity we restrict the backward images to the quadrant $w \geq 0 \wedge u \leq 0$, the other preimages would create symmetrical branches by reflection around w-axis, u-axis and combined.

When numerical evolution of 3.26 is determined, we are concerned in the speed of convergence. And we confirm the rate is exponential by fitting the coordinates in Gnuplot software. As an example we choose w coordinate plotted in 3.8 together with exponential fits 3.8. The evolution functions have been

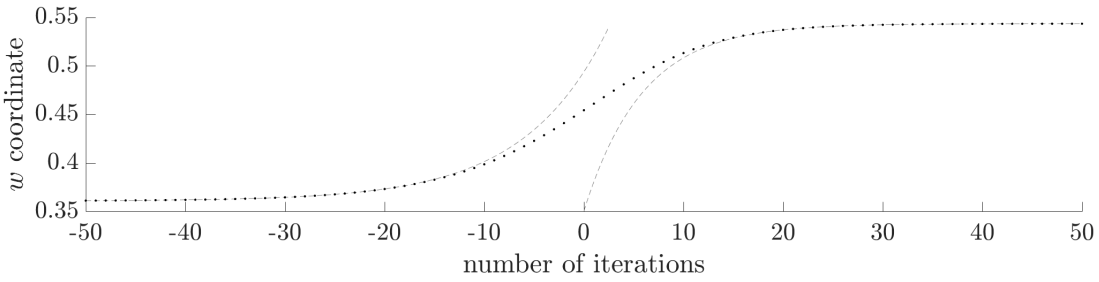

Figure 3.8: Evolution of the point 3.26 from the sensitive structure. w coordinate plotted for 50 forward and backward iterations (dots). Exponential fits 3.3, 3.28 marking the convergence to the critical states are dashed.

derived

$$w(n) = e^{An+B} + C; \quad \begin{array}{rcl} A & = & 0.1189 \pm 0.0002 \\ B & = & -2.0172 \pm 0.0036 \\ C & = & 0.36107 \pm 0.00001 \end{array} \tag{3.27}$$

for n forward iterations when $n \in [20; 50]$ forward images were used to fit the dependence and

$$w(n) = -e^{-An+B} + C; \quad \begin{array}{rcl} A & = & 0.1702 \pm 0.0003 \\ B & = & -1.6441 \pm 0.0058 \\ C & = & 0.54370 \pm 0.00001 \end{array} \tag{3.28}$$

for n backward iterations when $n \in [20; 50]$ was used for the fit.

Similar behaviour is observed for all other critical states that belong to the structure of sensitive points in the $v = 0$ invariant set. We do not feel necessary to publish other fits precisely. Instead, let us make a note on the topic of Lyapunov exponents. These numbers are defined as exponents in the diverging trends, we remind definition 2.3.9. As an example we take state $(\mu^2, 0, 0)$ for pairwise iteration (remember function $l_1(w)$). The Lyapunov exponents of this fixed state can be calculated from the definition because eigenvalues of the Jacobi matrix are $0, \mu^2$ as already known and the Jacobi matrix of n-th iterate equals to n-th power of the Jacobi matrix of singel iteration, this follows from the fact that the point is fixed (for two iterations). We redeem

$$\delta_1 = 2\tilde{\mu}, \quad \delta_2 = 0 \tag{3.29}$$

Using the logarithm we obtain theoretical value of Lyapunov exponent $\lambda = \log 2\tilde{\mu} \doteq 0.5179$. This value has been confirmed by numerical fit of 20 forward images of point $(\mu - 10^{-6}, 0, 0)$ with exponent $\doteq 0.5100$. The Lyapunov exponent for the case of evolution of 3.26 (drawn in 3.8) towards state $\mathcal{B}$ is theoretically drawn from eigenvalue $\tilde{\mu}$ from 3.1, i.e. $\delta = \log \tilde{\mu}^{-1} \doteq 0.1752$, the numerical fit offered value 0.1702. It is important to realise that the numerical fit is deduced from an orbit that is calculated for perturbed state while the theoretical value concerns the fixed point precisely. In the case of the orbit, the formula for the Lyapunov exponent must use eigenvalues of Jacobi matrices at subsequent points of the orbit, not the fixed point. However, we demonstrated that both values - theoretical and numerical - differ only a little, this justifies the use of numerical methods and serves as a self-control for our results.

The Lyapunov exponent approach can be useful tool for next studies but for us it will be too demanding to apply it in the rest of the thesis. We leave the topic for future research. Now, we want to come back to the concept of sources and sinks. Last paragraphs showed that the critical states work as sources/sinks and naturally their role swaps when backward iterations are substituted with forward iterations. The numerical calculations confirmed attracting/repelling properties of the sources/sinks in forward and backward directions and uncovered exponential trends of convergence.

However, to our surprise, we are speaking of convergence in the structure of sensitive states in plane $v = 0$. The behaviour of all the points is regular, meaning no chaos is present in the circle K. There is a continuum (curve) of states that contradicts expectation of behaviour following the chaos of Julia sets. Julia sets allow only Lebesgue measure zero set of points that resist chaos. We have shown with functions $l_{1,2}$, 3.23 that such states are one-dimensional analytically, the rest of the curve connecting state $\mathcal{R}$ with cycle $\mathcal{C}$ and state $\mathcal{B}$ was examined numerically with the same result of regular behaviour. The states, although at least 1 dimensional still have Lebesgue measure zero. In the rest of the Bloch ball, the structure of sensitive points never (numerically) form a subset of nonzero Lebesgue measure that would defy convergence to the global attractors $\mathcal{A}, \mathbb{1}$.

When we do not restrict ourselves to the particular sets in $v = 0$ plane and evolve general states numerically, we reach following statement where we also consider backward iterations. The convergence in exponential rate is a dominant feature of the dynamics induced by our purification protocol.

Statement 3.3.1. *Almost every state of the Bloch ball converges to on of attractors $\mathcal{A}, \mathbb{1}$. For backward iterations, almost every state of the Boch ball converges to attractor $\mathcal{R}$. The convergences are exponential.*

We also present an interesting corollary: in the forward iterations, there are three attractive regimes (towards $\mathbb{1}$, towards cycle - to $|0\rangle$ in odd number or even number of iterations) with two basins of attraction associated. In the backward iterations, there is only one basin of attraction, of the universal attractor $\mathcal{R}$, which equals to the union of the previous. In addition, there is the structure of sensitive states which works as universal repeller, similarly to the Julia set in the complex functions theory.

3.4 Phase transition

While almost all states converge, we now ask whether there is truly chaotic evolution in the mixed states; the token of chaos is the non-converging trend. For that reason we inspire from the Julia set where chaos is guaranteed and take following approach.

We recall that like in 2.63, we can reduce the evolution in pure states to a complex function of a single complex variable. In our case in analogy to 2.63, again

$$z' = f(z) = \frac{z^2 - 1}{z^2 + 1} \tag{3.30}$$

From the attractor map corresponding to the pure states $P = 1$ we obtain positions of sensitive points, these numerically approximate the Julia set $\mathcal{J}(f)$. We

know backward iterations map the Julia set onto Julia set, 2.3.26.

Let us now recall here are two preimages of each state, now expressed as

$$z^{(-1)} = f^{(-1)}(z) = \pm\sqrt{\frac{1+z}{1-z}}. \tag{3.31}$$

Looking for preimages of each state, let us now choose only the solution with negative real part. In this way we obtain a unique inverse map. While the theory claims that the preimage of the Julia set is the Julia set, all preimages must be taken into account; the theory does not offer any predictions for particular preimages of the Julia sets. In this case, all states of the Julia set converge towards $\mathcal{B}$. If we consider only preimages with negative real part, all states converge towards state $\mathcal{B}$; when only preimages with positive real part are considered, all states converge to one of $\mathcal{B}_{\pm}$. The variations of all preimages are responsible for generation of the whole structure of the Julia set.

Now, let us repeat the approach for the mixed states. First, let us consider restriction on preimages with $u \leq 0$ which corresponds to previous choice of z with negative real part. If we take initially all states of chosen value of purity P and iterate backwards, as soon as $P < 1$, all the states converge to $\mathcal{R}$. This state takes over the role of singular repeller. The reason is in the saddle character of the point $\mathcal{B}$ mentioned in 3.1, now repelling for the mixed states in backward iterations. Even for values $P \doteq 1$ the attraction towards this state is overwhelmed by repelling towards $\mathcal{R}$. When the preimages with positive real part are chosen, all the states again converge to one of $\mathcal{B}_{\pm}$.

We just recapitulate that the character of asymptotic behaviour for chains of positive/negative preimages is the same for pure and mixed states. The converging exponential trends in the previous section were achieved by taking always the $u \leq 0$ preimage; such artificially selected branches exhibit converging behaviour on all states. Now, the combination of all possible preimages of the sensitive states of given initial purity follows the same trend. The structure, even when simple for lower purity, creates fractal patterns when iterated backwards. The fractal structure emerges together with its chaotic behaviour!

We have numerically confirmed when considering all preimages that the sensitive states in backward iterations proliferate through the structure of sensitive states, see 3.9. But there is a new and important discovery. The backward iterations do not constitute the whole set of sensitive states. This is a major and significant difference compared to the pure states where the preimages are dense in the Julia set. For mixed states the preimages always (with the exception of mixed cycle $\mathcal{C}$) converge to $\mathcal{R}$ or chaotically jump across a substructure of sensitive states with purity $P_1 \leq P < 1$. The following is based on numerical observations. There are two fundamental types of behaviour for sensitive points which probably makes the set split into two parts. One of the subset is complete analogy of the Julia set meaning the subset is equal to its preimage, this set possesses fractal shape. The backward iteration restricted to the other subset is not surjective, the states are not accessible with backward iterations and possibly exhibit converging dynamics either $\mathcal{R}$ or Julia set on the Bloch sphere. Such convergence has been proven for curves in sets L_1, L_2 analytically earlier. The subset of the non-returning states seems to form regular curves but such statement is difficult to prove numerically. This leads us to following formulation.

Conjecture 3.4.1. *The set of sensitive states consists of two disjoint subsets.* Accesible states *are fully invariant on back-iterations and contain chaos in Devaney's definition, and thus form an analogue to the Julia set.* Inaccesible states *form regular curves and the inverse evolution function restricted to these states is not topologically transitive.*

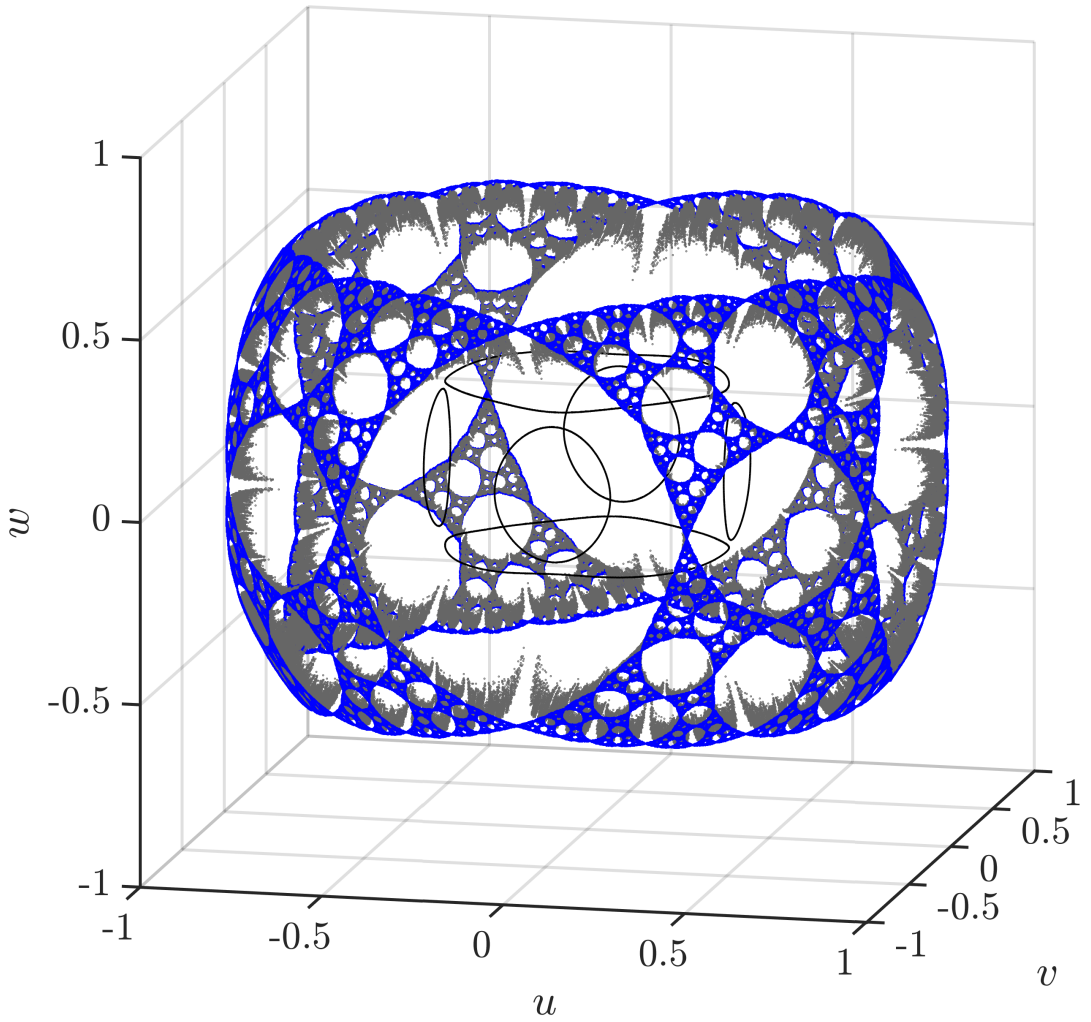

Figure 3.9: Sensitive states with purity $P = 0.7$ (black) iterated backwards (gray) do not form a dense subset of sensitive states. They proliferate into fractal bounded by $P_1 \leq P < 1$. Julia set on Bloch sphere (blue) is connected to the structure of the preimages.

Concluding that the structure of sensitive states seems to be a complicated, fractal shaped set with devious dynamics, we seek to prove and characterise the fractalness with calculating the dimension (in the three-dimensional Bloch space) $\mathscr{D}_3$. Using the third approach to box-counting as explained in A we determined the sensitive points in $2500\times2500\times2500$ uniform Cartesian grid in octant $w, u, v \geq 0$. By the box-counting fitting with scaling factors $100 \leq \lambda \leq 250$ we arive to

$$\mathscr{D}_3 = 2.20 \pm 0.01 \tag{3.32}$$

We have already introduced the spheres of initial states of fixed purity, now let us take a look at the structure of sensitive states with respect to this slicing.

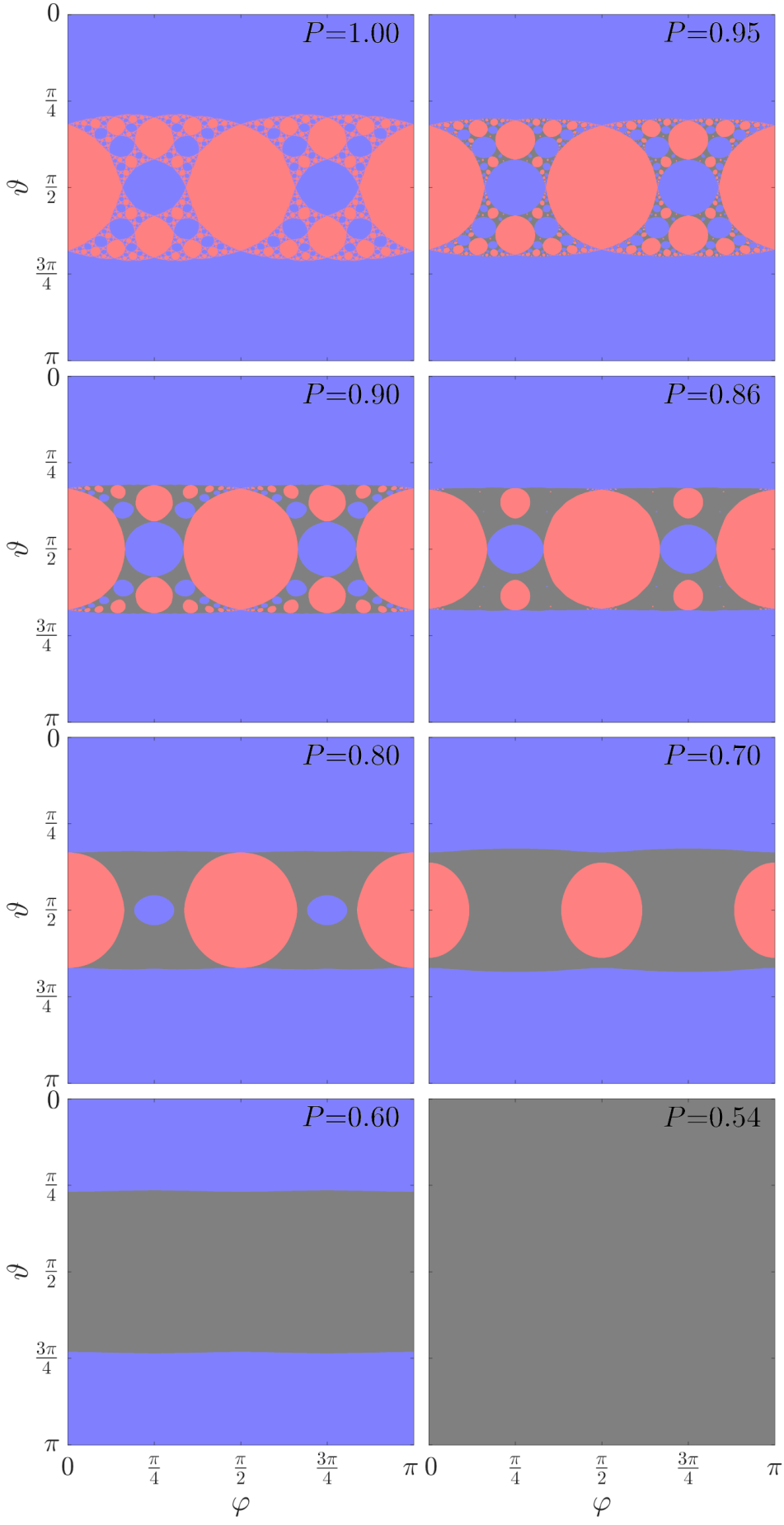

Figure 3.10: Attractor maps on spheres of initial states of constant purity P marked in the figures; all maps in spherical coordinates and with the same axis system, i.e. top of each plot corresponds to $|0\rangle$, bottom to $|1\rangle$. Blue colour - states converging to $|0\rangle$ under even number of iterations. Red - states converging to $|0\rangle$ under odd number of iterations. Gray - states converging to $\mathbb{1}$.

I.e. we choose P and find sensitive states in the sphere of radius $\sqrt{2P-1}$. In this way we obtain a slice of the fractal which we now illustrate in the attractor maps constructed upon the spheres. For the reason of the symmetry in the input states $(w, \pm u, \pm v)$, we restrict the maps only to $\varphi \in [0; \pi)$, equivalently $u \geq 0$.

In case $P = 1$ we have the Julia set for which the chaos and fractalness are typical. We now aim for calculating the fractal dimension in the two-dimensional space $\mathscr{D}_2$. We used the second box-counting approach in A. We used 50 randomised boxings with resolution of up to 7000^2 boxes and we worked in spherical angles 2.38 in range $\varphi \in [0; 2\pi], \vartheta \in [0.8994; 2.2422]$. This range cuts off the areas near poles $|0\rangle, |1\rangle$ where the fractal is not present.

$$\mathscr{D}_2 = 1.563 \pm 0.001 \tag{3.33}$$

Now let us descend to the mixed states, we define function $d(P)$ which for the purity values finds the set of sensitive states and calculate their dimension. For the box-counting we now used only maximal resolution of 5000^2 boxes with 10 randomised positions. This we do to reduce the computational time to less than the maximal allowed time for a doctoral study. From the definition, $d(1) = \mathscr{D}_2$ should hold but with the limited resolution and randomisation, the value can be slightly different. Also, we remind that the box-counting method is very imprecise, namely for determining the number of boxes. We now present one of the crucial results of our work, the plot of $d(P)$.

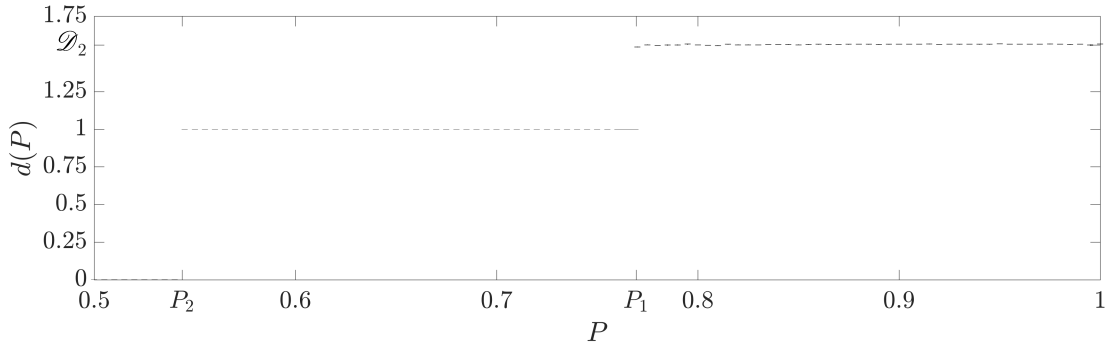

Figure 3.11: Dimension of sensitive states of purity P, $d(P)$. Errorbars expressing the root mean quare error of the linear fit confirm validity of the fit.

The structure seemingly decays with decreasing purity 3.10 and for that reason we had to focus on the structure by selecting such regions of φ, ϑ close to axis $(w, 0, 0)$ where the structure is present; we show an example of the zoomed structure for two reasons. First, to show that in spite of the visual impression from 3.10, the fractal is present for lower values of P. And second, to demonstrate a case where the structure meets computational precision.

Without this zoom the numerical precision would severely impair dimension estimate focusing on regular curves spanning the space while the fractal pattern (scaled down in its absolute size) would be neglected.

Let us draw conclusions from the values of $d(P)$. While the fractal seems at the first sight to decay into a rather regular structure of separate islands, the plot of function $d(P)$, 3.11, proves (numerically) its preservation. The fractalness disappears locally but globally the structure survives keeping its properties (i.e. dimension) until the threshold P_1 is reached. At that point, the structure

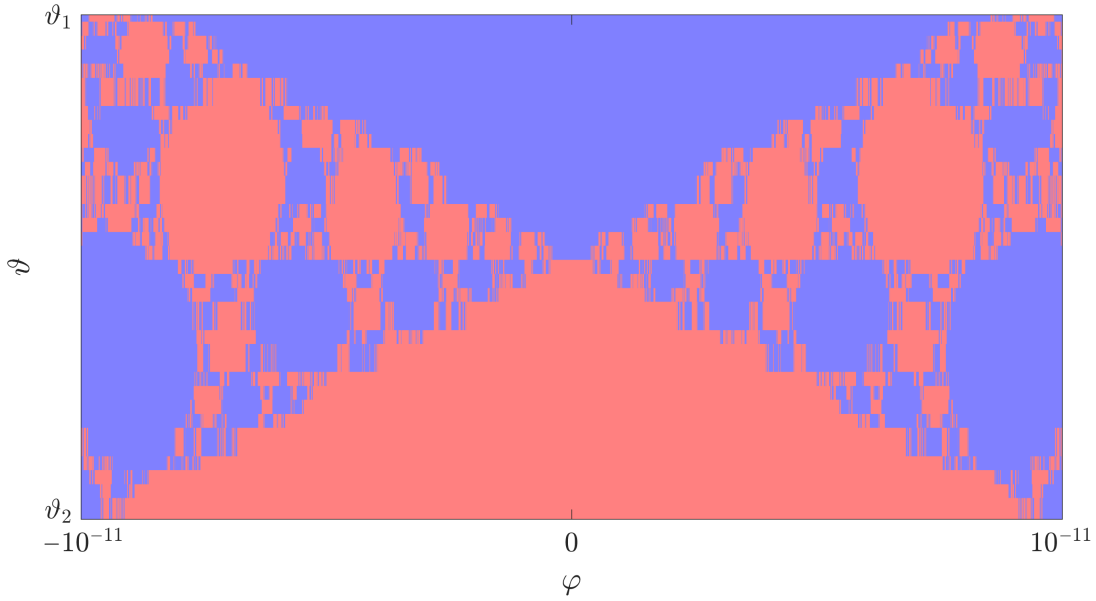

Figure 3.12: A detail of the fractal structure for $P = 0.771$, the range of the spherical angle ϑ is $\vartheta_1 = 1.055788891194002, \vartheta_2 = 1.055788891194010$.

suddenly collapses to a regular group of closed curves that match their visual impression. These curves are retracted to points with lowering P, the points then disappear. At the value of P_2 the last sensitive point of the structure vanishes and all states converge to $\mathbb{1}$. As the structure does not exist, its dimension drops to 0.

The values P_1, P_2 were numerically found to coincide with the purities of the familiar states $(\chi, 1-\chi, 0), (\mu^2, 0, 0)$:

$$\begin{array}{rcl} P_1 & = & \frac{1+\chi^2+(1-\chi)^2}{2} = 1-\chi+\chi^2 \doteq 0.7693 \\ P_2 & = & \frac{1+\mu^4}{2} = \mu \doteq 0.5437 \end{array} \tag{3.34}$$

As a mathematical curiosity, we just drop here a note that while χ is the real root of $x^3 - x^2 + 3x - 1$, P_1 is the real root of $x^3 + 3x^2 + x - 3$ and μ^2 is the real root of $x^3 + x^2 + 3x - 1$. Thanks to these calculations we have found final relation: $1 - 2\chi + 2\chi^2 = \mu$, in physical context of trace distance:

$$t((\chi, 1-\chi, 0), (0, 0, 0)) = \sqrt{\mu}. \tag{3.35}$$

This finding with the rest of our earlier analysis of μ may indicate some more profound mathematical connections of the values P_1 and P_2 that we are unaware of. We rewrite $P_1 = \frac{1+\mu}{2}$. For the moment we just prove the expression for P_2 in previous equation for the people that are not that skilled in modular calculations on the fields of polynomials to immediately see form definition $\mu^3+\mu^2+\mu-1 = 0$ that:

$$1 + \mu^4 = \mu + \mu^2 + \mu^3 + \mu^4 = \mu + \mu(\mu + \mu^2 + \mu^3) = \mu + \mu = 2\mu \tag{3.36}$$

This finding is in agreement with the numerical and analytical findings that these states work as sources for the structure of sensitive points as discussed in the section of inverse iterations and previous paragraph of the chaotic evolution

in previous paragraphs. Actually, this finding suggests a more fundamental hypothesis: while the point $(\mu^2, 0, 0)$ is only connected to the sensitive structure where it acts as a sink, contractive, regular behaviour it relates to the dimension 1. The point $(\chi, 1-\chi, 0)$ is repelling even in the set of sensitive states, in terms of the function of complex variables, this equals to the chaos and the points would be related to the Julia set, which is often fractal. This is associated here with fractal dimension $d(P) \doteq 1.56$ for $P > P_1$.

The fact of a sudden change in the dimension $d(P)$ leads us to the idea of phase transitions. There is a set of sensitive qubits which are in our scope and their structure has a discontinuity with respect to the initial purity. We identify the phase with the quality of the structure of the sensitive states; the quantification is performed via box-counting dimension, which is natural and feasible. The classical analogue of the phase transition in the usual thermodynamic context is e.g. the volume that changes suddenly. The term volume can be related to the dimension thanks to d-dimensional Hadamard measure. The length of the structure for $P < P_2$ is zero, for $P_2 < P < P_1$ the length is finite, though depending on P. For $P_2 < P$ the length is infinite. The length of the curves cannot be well estimated from the attractor maps or other numerical handles, one has also to consider the metric, in spherical representation the lengths are distorted. In the Euclidean metric in the Bloch space the distance is not measured on the sphere - hyperplane of constant purity. For this ambiguity we prefer to analyse the dimension of the structure and identify it with the phase. The dimension is independent of metric and other transformations. The role of the temperature is taken by the purity of the initial states. The critical temperatures P_1, P_2 separate the phase regimes of fractal, regular and empty structure.

Well accepted classification of phase transition was proposed by Ehrenfest, [17], who defined the order of phase transition in terms of derivatives of Gibbs energy based on their discontinuity. Such classification had to be generalised after Onsager found phase transition in Ising model where so called logarithmic divergence occurs [48]. Brief recapitulation on the topic of phase transitions is in [32]. Also the topic of quantum phase transition was introduced specifically for transitions happening at $T = 0$ e.g. where effects of quantum fluctuations influence the spin structure. Our transition does not even match this definition. We deal with a topic that is not directly related to the thermodynamics and Gibbs free energy is not defined for this concept, only entropy. We must not confuse the situation with the experimental realisation of a qubit which is often done with ion traps made of superconducting materials, in this case the thermodynamic potentials are defined on statistical ensembles but these do not connect to our case of investigating of abstract single qubit dynamics. We will return to the topic of phase transition in next section, where another concept will be introduced.

The fact that function $d(P)$ is discontinuous is very interesting for the fact that in the theory of complex functions the Julia set is self-similar and the dimension is the global characteristic, in this case of evolution in three real dimensions the structure of sensitive states does not have a globally unique dimension characteristic but the dimension is a local characteristic with dependence on the purity.

To end with the topic of dimension, we have also tried to estimate the dimension of the fractal on Bloch sphere by the self-similarity concept. While the attractor map in spherical coordinates ϑ, φ or stereographic projection to z, the

areas and lengths of the fractal are distorted; we choose to work in the Bloch sphere (w, u, v) with the physical metric t. We have chosen 10 fractal 'vertices' 3.13 that demarcate self-similar patterns. Because the structure is stretched over sphere, it is scaled unevenly and even our generalised formula cannot give precise results. However we propose to assign each quadrilateral block determined by four vertices $\rho_1, \rho_2, \rho_3, \rho_4$ ordered along circumference its *characteristic length* $n(\rho_1, \rho_2, \rho_3, \rho_4)$ defined as square root of spanned 'area' which we define as a product of the diagonal 'lengths':

$$n(\rho_1, \rho_2, \rho_3, \rho_4) = \sqrt{t(\rho_1, \rho_3) \cdot t(\rho_2, \rho_4)} \tag{3.37}$$

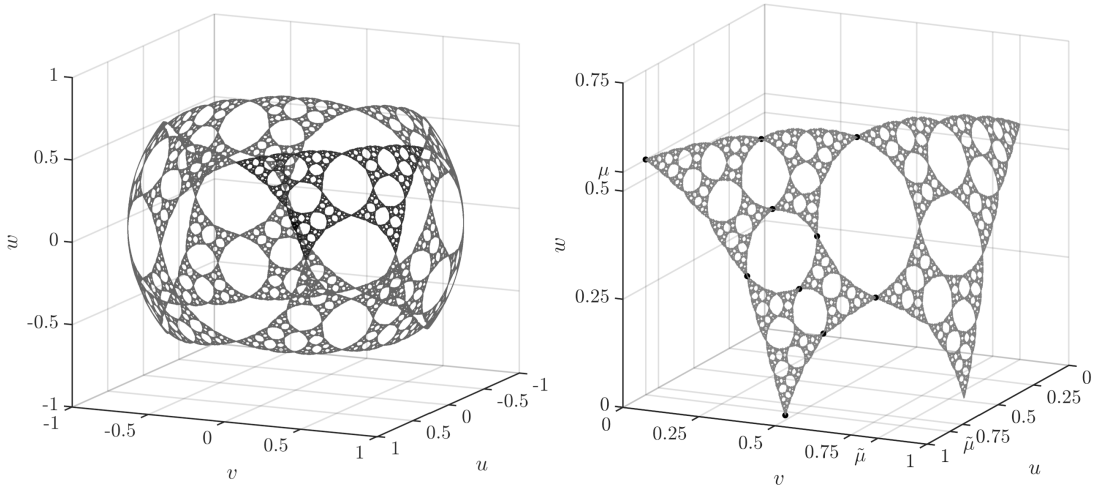

Figure 3.13: *Left*: Chaotic states on Bloch sphere (gray) with a self-similar unit (black). *Right*: 10 particular vertices (black bold points) on zoomed self-similar unit used for calculations of self-similarity dimension.

For the chosen vertices:

$$\begin{aligned}
&\rho_1 \doteq (\mu, \tilde{\mu}, 0),\\
&\rho_2 \doteq (0.594554257, 0.568553091, 0.568553091),\\
&\rho_3 \doteq (0.254269020, 0.683866678, 0.683866678), \quad n(\rho_1, \rho_2, \rho_3, \rho_4) \doteq 0.716490457598,\\
&\rho_4 \doteq (0, 0.878546813, 0.477656255),\\
&\rho_5 \doteq (0.311938205, 0.881788572, 0.353756232), \quad n(\rho_5, \rho_7, \rho_1, \rho_8) \doteq 0.365128662285,\\
&\rho_6 \doteq (0.395388480, 0.754217263, 0.524236846), \quad n(\rho_8, \rho_2, \rho_7, \rho_6) \doteq 0.299843788600,\\
&\rho_7 \doteq (0.599185696, 0.729694405, 0.329427652), \quad n(\rho_6, \rho_{10}, \rho_3, \rho_9) \doteq 0.228035791985,\\
&\rho_8 \doteq (0.455273397, 0.796890304, 0.397104490), \quad n(\rho_9, \rho_4, \rho_{10}, \rho_5) \doteq 0.275436662067,\\
&\rho_9 \doteq (0.283130608, 0.820646402, 0.496363316),\\
&\rho_{10} \doteq (0.182787855, 0.802791723, 0.567550922),
\end{aligned} \tag{3.38}$$

and solving equation provided by our definition of self-similarity dimension 2.53

$$\begin{aligned}
n(\rho_1, \rho_2, \rho_3, \rho_4)^{\mathscr{D}} = \quad & n(\rho_5, \rho_7, \rho_1, \rho_8)^{\mathscr{D}} + n(\rho_8, \rho_2, \rho_7, \rho_6)^{\mathscr{D}} + \\
+ \quad & n(\rho_6, \rho_{10}, \rho_3, \rho_9)^{\mathscr{D}} + n(\rho_9, \rho_4, \rho_{10}, \rho_5)^{\mathscr{D}}
\end{aligned} \tag{3.39}$$

leads numerically to

$$\mathscr{D}_S \doteq 1.559 \tag{3.40}$$

which is in surprisingly precise coincidence with the box-counting approach, in spite of the numerical work. In spit of the fact that the global fractal shape does not have to exhibit self-similarity with acutal fractal shape - the Koch flake is usually constructed upon a triangular substrate but it does not consists of smaller triangles.

To conclude, the fractal dimension of the Julia set has been verified various algorithms realising box-counting approach and self-similarity approach. The value 1.56 is preserved for mixed states until the structure collapses to the single point and vanishes, this transition has signs of phase transition of the second kind compared to the first kind in the exponential growth of basins of attraction of the pure attractor $\mathcal{A}$.

3.5 Purification capabilities an consequences for practical use

Now, as the sensitive states are numerically undetectable because their structure has dimension < 3, we can ask what percentage of states with fixed initial purity converge to which attractor and reliably calculate this quantity numerically. This piece of information is rather indicative because it is impossible to specify which state converges where, although such information is convenient for practical realisation - if the desired attractor would be too close (e.g. in terms of trace distance T, 2.2.11) to the basin of attraction of another attractor, perturbations might cause the protocol to converge to wrong result, to fail.

Because almost all states converge to one of the attractors, pure or maximally mixed, we will speak of purification. Not in terms of the entanglement purification, i.e. increasing concurrence 2.2.7 or the entanglement of formation, but in the sense of decreasing mixedness, statistical uncertainty of the qubit ensemble. In the following text we will always mean the purification in this sense and return to the topic of the entanglement later. We now formulate an important finding based on numerical evidence also visible in 3.10:

Statement 3.5.1. $(\forall \varepsilon > 0)(\exists \rho \ state)(\ Tr\ \rho^2 = 1 - \varepsilon \wedge \rho \to \mathbb{1})$.

We arrive to a serious consequence, the protocol aiming for purifying the state can fail whenever the state is perturbed to a mixed one. However, we will now show that this problem does not impose disproportional experimental limitation. We will now examine the evolution on the spheres of constant purity and will try to give e.g. partition of states of given initial purity that cannot be purified.

Such quantity can be calculated in purely geometric terms of areas on sphere: we can create a grid of points on a sphere, representatives of small areas, find their asymptotic regimes and compare the areas of states with different regimes. But we think it is good to include an additional physical meaning. The pure attractor pure and maximally mixed state are discerned by their entropy. State converges to the pure cycle gains zero entropy, maximally mixed state has entropy 1. In consequence, the partition of states converging to $\mathbb{1}$ also has meaning of average entropy of the asymptotically evolved states of sphere of constant purity. We consider this approach to be more valuable as the average asymptotic entropy

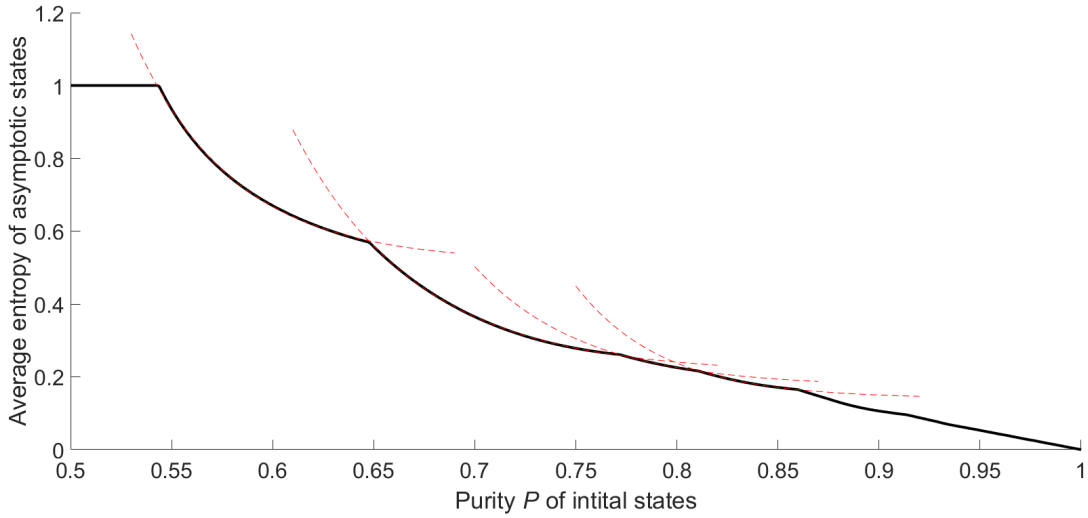

Figure 3.14: Numerical calculation of average entropy $e(P)$ of asymptotic evolution of states of given purity P. Exponential trends determined in 3.2 drawn dashed.

contains information about average purity of the states and could be calculated for a general case where the attractors could be mixed states.

The process was executed in following way: a set of uniformly distributed points on the sphere of radius corresponding to chosen initial purity P was created. These points had been evolved until their asymptotic regime was determined. The entropy of each of the states is calculated and these values are averaged. The uniform distribution of the grid points over a sphere has been implemented using Fibonacci construction, [26], that will be explained later in a more involved case. Following the line of thought of numerical estimation of asymptotic dynamics and attractor maps we can reinterpret the scheme by assigning each point (qubit) of the grid a small area on the sphere in the corresponding Bloch representation. In the attractor map, the pixel (area represented by the point of the grid) can be coloured just as in the corresponding attractor map but the map typically distorts the areas due to transformation to spherical angles or due to stereographic projection. Because the Fibonacci construction using golden ratio guarantees that the points are uniformly distributed, each point has the same weight and we simply calculate the mean value of the found entropies. In this way, we assign to each value of purity of initial states P the mean entropy $e(P)$ of the asymptotic regimes. In our numerical estimates we could write

$$e(P) = \frac{1}{N} \sum_{i=1}^{N} S(\rho_i) \tag{3.41}$$

where ρ_i is the asymptotic output produced from input state with initial purity equal to P. We keep in mind that $e(P)$ also is the probability of the protocol failure on random input with purity P because of the dichotomy that the asymptotic regimes can have only $S = 1$ or $S = 0$.

The graph of the function $e(P)$ is in 3.14 and offers interesting results. First, we confirm the earlier statement that when the purity is taken $P = 1 - \varepsilon$ for arbitrarily small $\varepsilon > 0$ there are states detected to converge to maximally mixed

state, $e(P) > 0$. When we choose purity in range $P \in [0.95; 1]$ the trend seems to be linear and by fitting in Gnuplot software we found that the trend matches

$$e(P) = A \cdot (1 - P), \text{ , where } A = 1.0576 \pm 0.0002. \tag{3.42}$$

Our readers could object that we should use a general linear function $AP + B$, but we obtained the same coefficients (up to a sign) well within the fit error.

The second conclusion to make from the graph of $e(P)$ 3.14 relates to the minimal radius of the immediate basin of attraction of the maximally mixed state. In terms of thepurity the analytic threshold given earlier was 0.5078125, now improved to $P_2 \doteq 0.543689$.

Statement 3.5.2. $(\forall P < P_1 = \mu)(\forall \rho \textit{ state})(\rho \to \mathbb{1})$ *in asymptotic regime.*

But we find a new and very interesting result, $e(P)$ seems to follow exponential trends in P, immediately after the threshold P_2 is exceeded. We have used Gnuplot software to get a numerical fit on few segments, confirming the piecewise exponential trend, results are in 3.2. Only few intervals were fitted, with growing purity the fit is more demanding, it is even possible that the trend gets more complicated. The fact that the number of states that can be purified by the protocol grows exponentially with purity above the threshold P_1 is valuable because it gives a clue about the protocol general purification capabilities. For purity close to 1 the trend is dominated by linear tendency as said.

P range for fit	a	B	C
$[0.5440; 0.6478]$	-20.206 ± 0.051	10.243 ± 0.027	0.5154 ± 0.0005
$[0.6478; 0.7718]$	-16.254 ± 0.023	9.512 ± 0.015	0.2099 ± 0.0003
$[0.7719; 0.8105]$	-18.374 ± 0.034	11.753 ± 0.025	0.1728 ± 0.0002
$[0.8106; 0.8590]$	-23.140 ± 0.068	16.180 ± 0.053	0.1405 ± 0.0002

Table 3.2: Table of exponential fits of $e(P)$. For given intervals of P trend $e^{AP+B} + C$ was used to fit, coefficients found with gnuplot software are written with corresponding errors of the fit.

The fact that the $e(P)$ starting to decrease at P_2 matches the previously found fact that $(\mu^2, 0, 0)$ is the sensitive state with the lowest purity and determines the phase transition. This state is analytically shown to not converge to the maximally mixed state. Surprisingly, the next change of trend is found to happen for value $P \doteq 0.6478$ which is purity of $(0, -\mu, 0)$ where another bubbles of basins of attraction of the pure cycle $\mathcal{A}$ emerge. The next value of trend change also matches with emergence with new bubbles of basins of attraction. But the trend does not change in P_1. The emergence of fractal structure of infinite many bubbles is restricted to spatially negligible areas and probably as this structure is increased, the trend of $e(P)$ becomes more involved.

We can again speak of the phase transition and now we could introduce the concept of the order of transition. We formulate

Conjecture 3.5.3. *The phase transition of the entropy trend at temperatures* $P = \mu, P = \frac{1+\mu^2}{2}, P \doteq 0.7719$ *is fundamentally different from the transition at* $P_1 = \frac{1+\mu}{2}$*. The first kind of transition causes jumps in the average entropy exponent* $e(P) \sim e^{AP}$*. The second kind of the transition introduces continuous change of* $e(P)$*.*

The order of transition is analogous to Ehrenfest classification where first order means jumps in the first derivatives of free energy, in our case jump in the exponent of mean entropy $e(P)$. The second kind has continuous first derivative (and jump in second derivative) which corresponds to changing exponent of $e(P)$.

Following hypotheses are based on numerical observation that new regular curves emerge and such occasion matches the change of the exponent of $e(P)$. Also new sources of fractal structure too, these nests from which the fractal proliferates seem to be created when regular curves touch as the purity increases. First such situation occurs at $\mathcal{R}$ and we come back to our hypothesis of dichotomy of the structure of sensitive states. But we deferred further investigation because of lack of numerical capacities and other goals of this thesis. With this we leave the topic of phase transitions and leave further investigation for professional mathematicians because the dynamics is beyond our current capabilities.

Conjecture 3.5.4. *The both types of transition happen at higher values* P*, transition temperatures of the first kind and both kind have cluster point at* $P = 1$*.*

Conjecture 3.5.5. *The inaccessible points are bound to a structure of dimension* 1 *and emerge with increasing purity marking phase transition of the first order. The accessible points of the structure are bound to the emergence of the fractal structures of dimension* $\mathscr{D} \doteq 1.56$*, the emergence conditioned by increasing purity of initial states forms phase transition of second order.*

We have discussed the chance that protocol fails on random input of purity P, now we want to answer a related question: what partition of all states (regardless of P) converges to the maximally mixed state? What partition converges to the attractive cycle? To which branch in regime of odd/even iterations? To do this, we have to create a certain metric on how we weigh the states. Taking the same number of states for certain purity would result into high density of states near the centre of the Bloch ball. Alternatively, we could assign higher weight to the states that are close to the pure states because we aim at the purification capabilities. We decide to use the Euclidean metric which has the meaning of the trace distance of the quantum states, t, 2.2.11. We create uniformly distributed Cartesian grid of (w, u, v) points, let the states evolve to determine asymptotic behaviour and calculate the fractions of individual dynamical regimes. Due to the symmetries described earlier we can focus on only one octant of the volume of the Bloch ball. We obtained following results: 27.78% of the states converges to the maximally mixed state. Regarding the pure cycle, 48.59% of all states converges to $|0\rangle$ after even number of iterations and the rest 23.64% of states converge to $|0\rangle$ after odd number of iterations.

The partition of states asymptotically converging to the maximally mixed states is also rather statistical marker than an exact limitation for the protocol usage because the fractal nature of the structure of the sensitive states and

bubbles of basins of attraction spread through the ball in a complicated manner. Anyway, this marker will be related to other protocols later, where we will draw conclusions directly related to practical use. At this place, we conclude that in more than two thirds of the cases (in the Cartesian grid of equidistant state distribution) the protocol succeeds in the purification.

As optimistic as this number can seem, it offers no information about the speed of the convergence and purification capabilities for states near $|0\rangle$ whose analogy is important in the two-qubit protocol. We will now answer both questions relevant for practical use. To do so, we have to set a threshold where we are experimentally satisfied with the precision of the convergence. We recall that a mixed state can never become a pure one but can converge to it. In the literature, fidelity of the produced state and the desired state is widely used to measure reliability. But at this place we again choose the trace distance 2.2.11 as a more feasible and illustrative variable. We choose value $t(\rho, |0\rangle) = 10^(-6)$.

We perform following procedure. We choose a value of t which has the meaning of distance of the initial state from $|0\rangle$, $(1, 0, 0)$, the north pole of the Bloch ball. For this value $t \in [0; 2]$ we create an equidistant grid of states using the Fibonacci algorithm with $t = 2T(\rho, |0\rangle\langle 0|)$, [26]. This algorithm is more sophisticated because we want to create grid of 1) precise number of points that 2) are physical states, i.e. belong to the Bloch ball of coordinates all the points have distance t from the north pole and 3) are distributed uniformly on the section of the sphere. Therefore, at this place we present our code to create a set of (`w`, `u`, `v`) coordinates of `N` such points `t` far from the state $|0\rangle$.

```
phi=(1+sqrt(5))/2;
lsp=linspace(0,N-1,N)';
K=1/2-t/4;
w=1-t*cos(acos(1-2*K*lsp/(N+1)));
u=t*cos(2*pi*(lsp/phi-floor(lsp/fi))).*sin(acos(1-2*K*lsp/(N+1)));
v=t*sin(2*pi*(lsp/phi-floor(lsp/fi))).*sin(acos(1-2*K*lsp/(N+1)));
```

When the points are created, we iterate the evolution map. After each iteration we check which states converged successfully, record the number of converged states and delete them from the array of states. For the sake of comprehension we will speak of convergence speed c, it will be the minimal number of iterations required to converge to the state within the set threshold. For each value of the convergence speed, we divide the number of corresponding states by the total number of states to obtain partition $r(c, t) \in [0; 1]$. Naturally, there can be states requiring high number of iterations and there are states that converge to the maximally mixed state, i.e. they never cross the threshold. We fix the number of 50 iteration at this place - if the state does not converge to $|0\rangle$ within this limit, we assign this value of convergence speed to the state. We obtain a set of data $c, t, r(c, t)$ that could be either plotted e.g. as a three-dimensional barplot but for the better comprehensibility we choose a two-dimensional figure with axes c, t and the partition $r \in [0; 1]$ will be coded in greyscale range. Because the partition r is very small, we show a cumulative histogram instead, $R(c, t) = \sum_{c' \leq c} r(c', t)$ which gives the partition of states that converged at latest after c iterations.

The conclusions drawn from the histogram is that the protocol is efficient and there is major part of states that converge to $|0\rangle$ within $\leq$ iterations. The

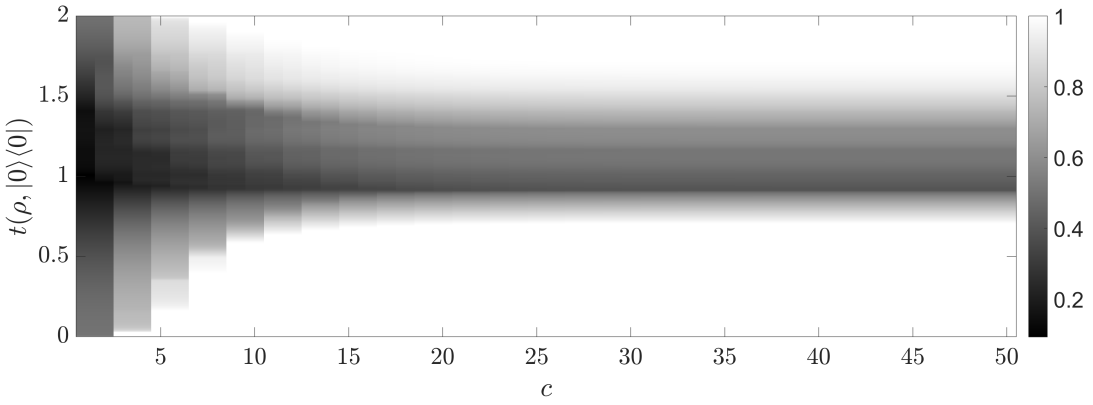

Figure 3.15: Histogram of $R(c,t)$, partition of states that converge to $|0\rangle$ in at most c iterations when in distance t originally. Value $R \in [0;1]$ coded in greyscale colorbar, i.e. white colour means all states have already converged.

exponential converging trends studied two sections earlier are now confirmed as a practical feature of the purification protocol. Now ask the most important question for the protocol practical applicability: what is the closest state in the terms of the trace distance that is not purified towards $|0\rangle$? We have performed numerical evolution on grids of 10^6 states in initial distance of t from the pole and we have found that for

$$t < 1 - \mu^2 \doteq 0.70440226 \tag{3.43}$$

all the states converge to the pure cycle. The nearest state to fail to converge was found to be $(\mu^2, 0, 0)$, its trace distance is exactly. This distance determines the maximal allowed perturbation for which the state is still guaranteed to converge back to the pure cycle. Because of the symmetries, the radius of guaranteed convergence applies to the south pole $|1\rangle$ as well. In consequence, there also is another threshold estimated numerically - states with $t > 1.7993$ are also guaranteed to converge to the pure cycle.

The presented radii are the maximal and minimal limits on the perturbation to guarantee the convergence to the attractor. But there is a significant volume of states outside the limits $0.7044 < t < 1.7993$, as can be seen in 3.15. If the experimental realisation of the qubit cannot guarantee the value of t in prescribed limits, the protocol may suceed but there is also nonzero probability to fail. The worst case value was found at $t \doteq 0.9121$ for which 78.5% of such initial states did not converge to $|0\rangle$ in 50 iterations. Still, the chance of ca 21.5% of purification success is not negligible. Precise probabilities can be given when practical realisation of the experiment is considered because the states with the same t do not necessarily have to be experimentally realisable with the same probabilities. Calculations of such of experimentally influenced probabilities can be executed according to our recipe with considerations of other factors when needed, it is not relevant for the purpose of our thesis. On the other hand, the existence and the value of the minimal radius is an interesting result.

Let us now ask the question on convergence speed from a slightly different point of view. What is the minimal radius of perturbation t from $|0\rangle$ to successfully converge back in at most 2 iterations of the protocol (remember the pairwise flip so we cannot require one iteration only)? When the threshold

on convergence is still set to 10^{-6}, we found numerically that the threshold is $t < 0.0009995 \doteq 10^{-3}$ which is in accordance with analytic approach - we have derived relation for w'' earlier, 3.6. When $u, v \doteq 0$ and $w \doteq 1$ are considered, then

$$w'' \doteq 4\frac{w^2 - 0^2 \cdot 0^2}{(1+1^2)^2 + (0^2 - 0^2)^2} = w^2 \tag{3.44}$$

The numerical calculations that estimated limit $t \doteq 10^{-3}$ basically confirmed that such estimates are sufficiently precise in the sense of Taylor approximation for values as high as $w = 10^{-3} \rightarrow w'' = 10^{-6}$. For the situation of bigger disturbance where the approximations are not small we present another example, when the threshold to say that a state converged to $|0\rangle$ is set to 10^{-3}, the range of perturbed states increases to $t \doteq 0.031138$. Consequently, any state within this limit converges to $|0\rangle$ closer than 10^{-6} in at most 4 protocol iterations. Similarly, all states within radius $t < 0.1633$ require at most 6 iterations to converge, states with $t < 0.3485$ require at most 8 iterations and states with $t < 0.4924$ require at most 10 iterations. Similar thresholds could be found for the case of state initially close to $|1\rangle$.

Current values of t that typically emerge in experimental setups are not known to us as well as standard threshold on fidelity used to realise protocol of quantum teleportation, Shor algorithm etc. The same situation is true for trace distance - we have no knowledge of a widely accepted value of distance to deem two states experimentally indistinguishable. Such threshold must be merely a convention, not a physical quantity. But the fact that an error in terms of $t \sim 10^{-2}$ can be corrected with at most four iterations proves very good purification capabilities of the protocol.

At this place we only mention that two protocol iterations require 4 copies of the qubit, four iterations require 16 copies of qubit , 2^n qubits for n iterations. That price for the purification is paid exponentially to the iterations required. The convergence speed is therefore of high importance. We will return to this topic in the fifth chapter where generalised protocols are introduced. For now, we conclude e.g. that arbitrary state ρ such that $t(\rho, |0\rangle\langle 0|) < 0.03$ at most 16 copies must be sent through the channel and 4 protocol iterations performed to guarantee succesful purification, that is $t(\rho^{(4)}, |0\rangle\langle 0|) < 10^{-6}$.

The fact that there is a threshold 3.43 and other specific thresholds can be found depending on experimental realisation, this means that the protocol is robust. One could naively expect that the mixedness as an expression of statistical uncertainty will be amplified by nonlinear protocol, but the converse is true. The protocol is capable of purifying mixed states. This conclusion is the dedicated to the protocol [36] and before we proceed on, let us make a short resume.

3.6 Summary

Before we proceed to more general model of the purification protocol, let us summarise important findings so far. One of the reasons to study the protocol [1] is its practical purpose to purify entanglement, namely repair Bell state that suffers from decoherence that is inevitable during transmission in realistic channels. We have proposed a toy model of CNOT based protocol which allows studying interesting dynamics of mixed states. Our model can be represented in

three-dimensional space equipped with Euclidean-like metric. The role of the Bell state Φ^+ is taken by $|1\rangle$ and the analogy will be discussed in the sixth chapter. Previous research [35, 36] showed that this state of interest is a part of attractor length 2 cycle, i.e. the purification protocol works as expected. But only when restricted to a particular subset of the pure states which is a serious practical limitation. a state typically evolves to a mixed one due to the decoherence. Our result is much stronger, we claim that the attractor cycle is attractive for the mixed states as well, i.e. the protocol can be reliably used to purify (for the single qubit protocol the purification is meant in the terms of mixedness) even mixed states. *The protocol is robust.* We have also given a threshold in terms of the trace distance on the convergence speed and cost of input states. We also gave probabilities of the protocol failure when random state of given purity is used as the input. The question that remains unanswered is whether the original protocol is robust in the regime of the two-qubit dynamics which is even more complicated, we will study two-qubit protocol later.

For the first time, we have studied nonlinear evolution of mixed states, evolution equations were derived and analysed both analytically and numerically. We have dedicated our effort to evolution trends and found that the exponential trends are the dominant feature of the evolution. We have found all attractors and cycles and derived their stability. Next, we have introduced the concept of Lyapunov exponents and calculated some of them in addition to usual stability characterisation via Jacobi matrices. We have found a peculiar value μ which proliferates into basically all relevant characteristics. I even used the letter μ to accent that it has been MY favourite number ever since I started studying it. It's mine. My precious.

The most interesting finding is the existence of the fractal structure of sensitive states - their asymptotic evolution is affected by the smallest perturbations. We have shown that this structure is repelling and possesses also other fundamental properties known for the Julia sets, i.e. fractal structure. This result in multidimensional analogue is highly nontrivial. The preimages of the sensitive states exhibit unusual evolution that led us to state hypotheses on fundamental dichotomy. There are true chaotic states in analogue to the Julia sets which are fully invariant on backward iterations. And there is a set of sensitive points that cannot be accessed by backward iterations. This feature is crucial difference to the Julia sets. This structure probably is regular. The dimension of the structure has been calculated in the Bloch ball with result $\mathscr{D}_3 \doteq 2.17$ and the fractal slices on spheres of constant purity have $\mathscr{D}_2 \doteq 1.56$, the values have been verified by multiple approaches, the box-counting and self-similarity.

We have also described the distribution of the fractal structure of sensitive states in the Bloch ball. We arrived to phase transition which is the main result of this chapter. The fractal dimension is constant and drops suddenly when purity is decreased under threshold P_1. The phase transition was put into coincidence with emergence of new curves and fractal nests of sensitive states with increasing purity. The order of phase transition was introduced when mean entropy $e(P)$ was introduced, marking whether regular or fractal structure emerges and demonstrated. $e(P)$ also has physical meaning of probability of failure of the protocol on random initial state of purity P. Other experimentally relevant characteristics were discussed, including speed of convergence.

4. Protocols with twirling gates

4.1 Twirling operators

After analysing the protocol equipped with the modified Hadamard gate H_2 we propose to change this operator, called *twirling operator*; its purpose is to modify the dynamics. In the most general case it can be any unitary operator U.

A general unitary matrix can be expressed in parametrisation of four angles. For example as

$$U = e^{i\alpha} \begin{pmatrix} \cos x e^{i\beta} & \sin x e^{-i\gamma} \\ -\sin x e^{i\gamma} & \cos x e^{-i\beta}. \end{pmatrix} \tag{4.1}$$

For any operator U, by modification with an arbitrary constant to $U' = e^{i\alpha}U$ we obtain a different unitary operator. Yet, the evolution of the state $U\rho U^\dagger = U'\rho U'^\dagger$. Therefore, we state that such global phase is irrelevant for the physical application and we sort all unitary operators to classes of equivalence when they differ in the global phase only. Taking this into account, we can parameterise all classes of unitary operators in following way which is convenient for further physical context. The operators depend only on three parameters, angles.

$$U = TR, \text{where}$$

$$T_\tau = \begin{pmatrix} 1 & 0 \\ 0 & e^{-i\tau} \end{pmatrix}, \; R_{x,\psi} = \begin{pmatrix} \cos x & \sin x e^{-i\psi} \\ -\sin x e^{i\psi} & \cos x \end{pmatrix} \tag{4.2}$$

Our motivation to exclude the matrix T lies in time evolution of a free qubit. If the two levels $|0\rangle, |1\rangle$ of the qubit are separated by energy gap of ΔE, then they gain a relative phase when the qubit is treated as a free particle for a time period Δt, as follows from Schrödinger equation:

$$\alpha|0\rangle + \beta|1\rangle \to \alpha|0\rangle + e^{-\frac{i}{h}\Delta E \Delta t}\beta|1\rangle \tag{4.3}$$

when pure states are considered for the simplicity at the moment. Calling $\tau = \frac{i}{h}\Delta E \Delta t$ we can write the evolution of the free qubit in the matrix form

$$|\psi\rangle = \begin{pmatrix} \alpha \\ \beta \end{pmatrix} \to |\psi'\rangle = T_\tau \cdot |\psi\rangle = \begin{pmatrix} \alpha \\ e^{-i\tau}\beta \end{pmatrix} \tag{4.4}$$

Please note that the last chapter was dedicated to a special case of protocol with twirling gate H_2 determined by $x = \frac{\pi}{4}, \psi = \tau = 0$.

We will use the TR decomposition to introduce new notation. One iteration of the protocol executed on state ρ will be marked by brackets (representing the nonlinear action imposed by CNOT gate) and the twirling operators decomposed to TR product; additionally equipped with index n to symbolise n iterations or the infinity symbol to mark the state of asymptotic evolution.

$$\rho' = \frac{TR(\rho \odot \rho)R^\dagger T^\dagger}{\mathrm{Tr}(TR(\rho \odot \rho)R^\dagger T^\dagger)} \equiv TR[\rho] \tag{4.5}$$

$$\rho'' \equiv TR[TR[\rho]] \equiv TR[\rho]^2, \ldots, TR[\rho]^\infty \equiv TR[TR[\ldots TR[\rho]\ldots]] \tag{4.6}$$

4.2 Twirled protocol action

The general recipe 3.2 remains and the calculations of the state evolution $\rho' = TR[\rho]$ in terms of Bloch coordinates can be summed up to new three-dimensional map:

$$
\begin{aligned}
w' &= \left\{ \frac{W}{N}\cos 2x + \right. \\
&\qquad + \frac{U}{N}\sin 2x\cos\psi + \\
&\qquad \left. + \frac{V}{N}\sin 2x\sin\psi \right. \\
u' &= \left\{ -\frac{W}{N}\sin 2x\cos(\psi-\tau) + \right. \\
&\qquad + \frac{U}{N}\left[\cos 2x\cos\psi\cos(\psi-\tau) + \sin\psi\sin(\psi-\tau)\right] + \\
&\qquad \left. + \frac{V}{N}\left[\cos 2x\sin\psi\cos(\psi-\tau) - \cos\psi\sin(\psi-\tau)\right] \right. \\
v' &= \left\{ -\frac{W}{N}\sin 2x\sin(\psi-\tau) + \right. \\
&\qquad + \frac{U}{N}\left[\cos 2x\cos\psi\sin(\psi-\tau) - \sin\psi\cos(\psi-\tau)\right] + \\
&\qquad \left. + \frac{V}{N}\left[\cos 2x\sin\psi\sin(\psi-\tau) + \cos\psi\cos(\psi-\tau)\right] \right.
\end{aligned}
\tag{4.7}
$$

where we introduced polynomial factors

$$
N = 1 + w^2, W = 2w, U = u^2 - v^2, V = 2uv. \tag{4.8}
$$

The factors are determined by the elementwise matrix product induced by the CNOT gate, i.e. measurement based modification. Their nonlinearity is the key element to the chaotic features. The rest of the formula combining these nonlinear factors represents linear transformation fully encoded in $U = TR$. The fact that the unitary operator follows the measurement based selection allows separating the two parts - nonlinear and geometrical - of the formula. The consequence follows that the twirling can be viewed strictly geometrically in the Bloch representation as rotations and other isometries. The nonlinear factors stir up the ball of the initial states inducing whirls and various scaling when trajectories of states are tracked under protocol iterations. Naturally, when the protocol is iterated, both nonlinear and unitary parts alternate in each iteration. Even similar twirlings can result into very different asymptotic dynamics.

4.3 Symmetries

Previous formulas seem to be complicated but numerical calculations can help to understand the evolution. Thanks to the created attractor maps, we have discovered various symmetries which are now to be described. Such symmetries are very important for further analysis as they reduce all possible situations of both input quantum states and applied purification protocols to far smaller sets and cases.

First, we discuss the input states. As the evolution equations contain quadratic terms, we can expect some form of singularity. Checking the action closer, we can uncover the map is two-fold, always mapping two states onto a single one. This is true regardless of the twirling parameters because the nonlinearity is the consequence of the CNOT gate. Of course, the protocol parameters determine the preimage $\rightarrow$ image but the two preimages of a single image are connected by a bond independent of the protocol parameters, lets look at the factors U, V. Substituting $u \rightarrow -u, v \rightarrow -v$ simultaneously gives the same U, V and thus the same image.

Yes, we have observed this property earlier for H_2, now we see it is more fundamental property of the protocol. We exploit this feature by only considering half of the Bloch ball of all possible input states, we restrict the spherical coordinates of the state 2.39 to $\varphi \in [0; \pi)$, in other words $v \geq 0$. The domain is reduced to a half in size. Alternatively, we could set $u \geq 0$ but we made the choice of v because numerically the states tend to $v = 0$ for the H_2 protocol and also for other reason that the state $u = 1, w = v = 0$ plays and will play an important role in later chapters, it is also suitable for the reason that in spherical coordinates it has $\varphi = 0$. To give a hint now for the symmetries of the future chapters, we remind that if the state is rotated around the w axis by $\varphi \rightarrow \varphi + \pi$ the substitution $u, v \rightarrow -u, -v$ is performed. We can say there is two-fold axial symmetry around w-axis.

On contrary, the central symmetry $(w, u, v) \leftrightarrow (-w, -u, -v)$ is lost, such states can evolve differently. The restriction of the state parameters to $\varphi, \vartheta \in [0; \pi]$ is the narrowest possible.

The first note to take regarding the protocol parameters, concerns the rotation angle x which is always doubled in the map 4.7, therefore choosing any of values $x, x + \pi$ results into the same evolution equations, i.e. the same protocols. Therefore, we can restrict ourselves to $x \in [0; \pi)$.

Another symmetries are found, let us take a protocol with x, ψ, τ yields (w', u', v') when cast upon input state (w, u, v). Protocol with $\pi - x, \psi, \tau$ cast upon input state $(-w, u, v)$ yields $(-w', u', v')$. That is, the Bloch sphere can be reflected across plane $w = 0$, evolved with protocol alternated by $x \rightarrow \pi - x$ and then the outputs reflected back afterwards; we obtain the same state as if the first protocol would be used straight. These two protocols are not identical, we might rather use a word conjugate, similarly to 2.3.2. Still, we will also and equivalently speak of symmetry for following reason. When the attractor maps for these two protocols are created in spherical coordinates φ, ϑ, the reflection of input states manifests as an upside-down flip of the map. The reflection of the output state changes the colour scheme of the map. When RGB code 2.5 is used, the blue component is inverted for the mentioned protocols.

Another conjugation is found: protocol with $x, \psi, \pi - \tau$ cast upon $(w, u, -v)$ yields $(w', u', -v')$ and when cast upon $(w, -u, v)$ we get $(w', -u', v')$. And last, protocol with $x, \psi, \tau + \pi$ applied to (w, u, v) (or $(w, -u, -v)$) gives $(w', -u', -v')$. It follows straight from the goniometric functions of $\psi - \tau$ in 4.7. Together with aforementioned symmetry $\varphi \rightarrow \varphi + \frac{\pi}{2}$ we conclude the dynamics is equivalent for both protocols.

As the output states of conjugate protocols after on iteration are connected, the whole evolution with asymptotic dynamics is. Namely, the fractal structures

can be mapped one onto another by symmetries. Also, the convergence speed and other dynamical features are equivalent though not visible in attractor maps. In [39] we have introduced the concept of equivalence, although for pure states only. It was represented by special matrices S such that $S \odot S$ was a permutation matrix. The action of S on a qubit changed the evolution scheme in a simple way modifying the input states and output regimes by permutation of Bloch coordinates and eventually reverting orientation of the axes. Simply told in the visualisation, the attractor maps of two different protocols were the same up to a flip in left-right, up-down and/or diagonal direction and the colour code was also inverted in corresponding way. Now, we see that such concept is valid even for mixed states. We could generalise it not only to e.g. arbitrary unitary transformations of the Bloch coordinate of the input and output states. But the last symmetry in $\tau \leftrightarrow \pi - \tau$ is found to possess even stronger property. For that reason, we introduce and formalise a new concept of our own - *asymptotic equivalence* - as follows.

Definition 4.3.1. *Two protocols represented by twirling operators R_1, T_1 and R_2, T_2 are* asymptotically equivalent *whenever there are two unitary operators $U_1^{-1} = U_1^\dagger, U_2^{-1} = U_2^\dagger$ such that for all ρ states*

$$T_1 R_1[U_1 \rho U_1^\dagger]^\infty = U_2 (T_2 R_2[\rho]^\infty) U_2^\dagger. \tag{4.9}$$

Let us now discuss the consequences of this definition. When evolution of certain initial state is performed in a desired way to be purified to a specific output with one protocol, we can also use a unitary gate and iterate the other asymptotically equivalent protocol and apply another unitary gate to obtain the same result. The meaning of the input is the physical qubit, not its geometrical representation like for symmetries above. Such symmetries may be only purely abstract concepts without direct physical realisation. Recalling the symmetry of protocols with $\tau \leftrightarrow \pi + \tau$ yielding $(w, u', v'); (w, -u', -v')$ on the same input state, such case is an example of asymptotically equivalent protocols, the unitary operators are $U_1 = \sigma_0, U_2 = \sigma_3$. On the other hand, reflection $(w, u, -v) \to (w, u, -v)$ for protocols $\tau \leftrightarrow \pi - \tau$ cannot be realised by unitary evolution of qubit ρ.

This concept motivated by physical purposes is of a crucial practical importance because, even naively, some gates can be prepared more easily than others. Iterating the more feasible gates can be executed with higher precision. Therefore, the whole quantum communication process can have higher probability of success.

As for the visual interpretation in the Bloch space, resp. the attractor maps, the structures of the equivalent protocols are related in a unitary manner. Also, the colour code of the attractors is changed and could be understood as a unitary transformation in RGB space if represented in a clever way. We conclude that all the shapes can be shifted, reflected and rotated and gain different colours in the attractor maps, but in a form determined by properties of unitary operators. We remind that all unitary operations are isometric and for this reason the (Hausdorff) dimension of an object cannot change when mapped by an isometric map. This fact comes from the definition using the diameters of optimal coverings 2.3.35. These values do not change under the unitary transformations. Our

interest in fractal structures, that are characterised by their dimension, is therefore not affected by considering such transformations. In our case, the choice of a particular member of the class of asymptotically equivalent protocols is not relevant and the investigation of asymptotic properties and fractal structures gives information about the whole class of protocols.

We conclude that the symmetries and equivalences form classes of protocols that significantly reduce parameter combinations of protocols to be studied. For now, we have restricted the values of input states to half of the original range $\varphi \in [0;\pi), \vartheta \in [0;\pi]$ and the protocol parameters to 1/16 of the original range: $x, \tau \in [0;\frac{\pi}{2}]$.

There are also symmetries in ψ. Namely, protocol with $x, \psi + \pi, \tau$ yields $(-w', u', v')$ when acting on $(-w, u, v)$ and protocol with $x, \pi - \psi, \tau$ transforms $(-w, u, -v)$ into $(-w', u', -v')$. But we will see right next that these can be related to the symmetries of τ after we present one of the most important result of the chapter. The next symmetry reduces the parameter space by a whole degree of freedom.

4.4 Manipulation of time relaxation

The reason to introduce the concept of asymptotic equivalence lies mainly in the fact that there are symmetries that combine the action on states with the protocol parameters. We can now focus on the angular factors of ψ, τ which seem in 4.7 to take form similar to goniometrical identities.

Consider now two protocols with the same angle x and different angles ψ_1, τ_1 and ψ_2, τ_2. We set up a question whether two protocols can induce the same dynamics with different pairs of the angles. The answer to this is negative when one desires each state to evolve to identical output, identical asymptotic regime regardless of the protocol. However, we can ask only for the asymptotic equivalence of the protocols as such protocols share the same dynamical attributes. In this case, we surprisingly succeed as following figures suggest.

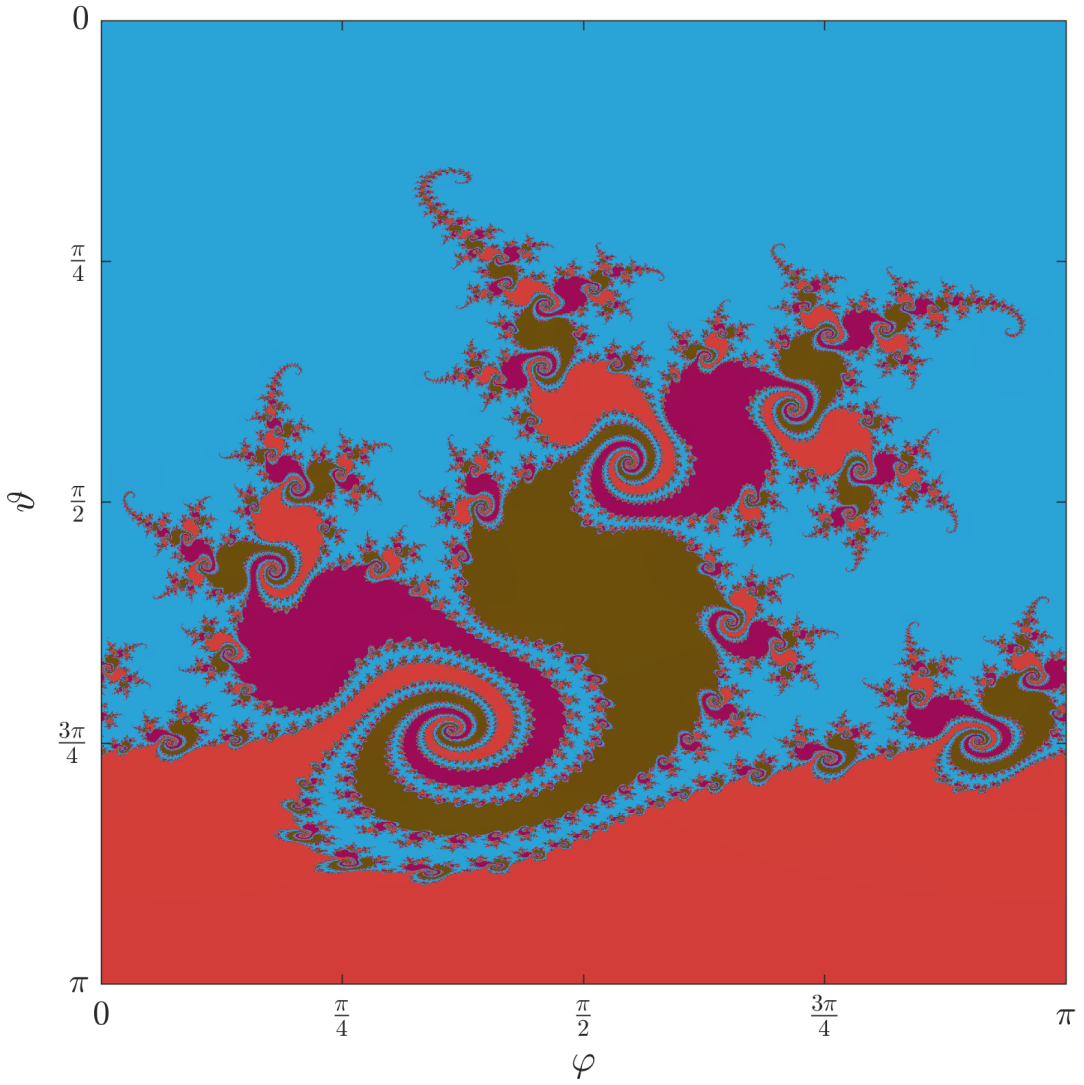

Figure 4.1: Attractor map of a protocol with $x = 30°, \psi = 0°, \tau = 137°$. Spherical angles capture $v \geq 0$ hemisphere, the map is repeated to $\varphi \to \varphi + \pi$ thanks to symmetries. Note that north pole $|0\rangle$ is represented by the top of the figure, $\vartheta = 0$, while the south pole $\vartheta = \frac{\pi}{2}$, the bottom line of the figure, represents $|1\rangle$.

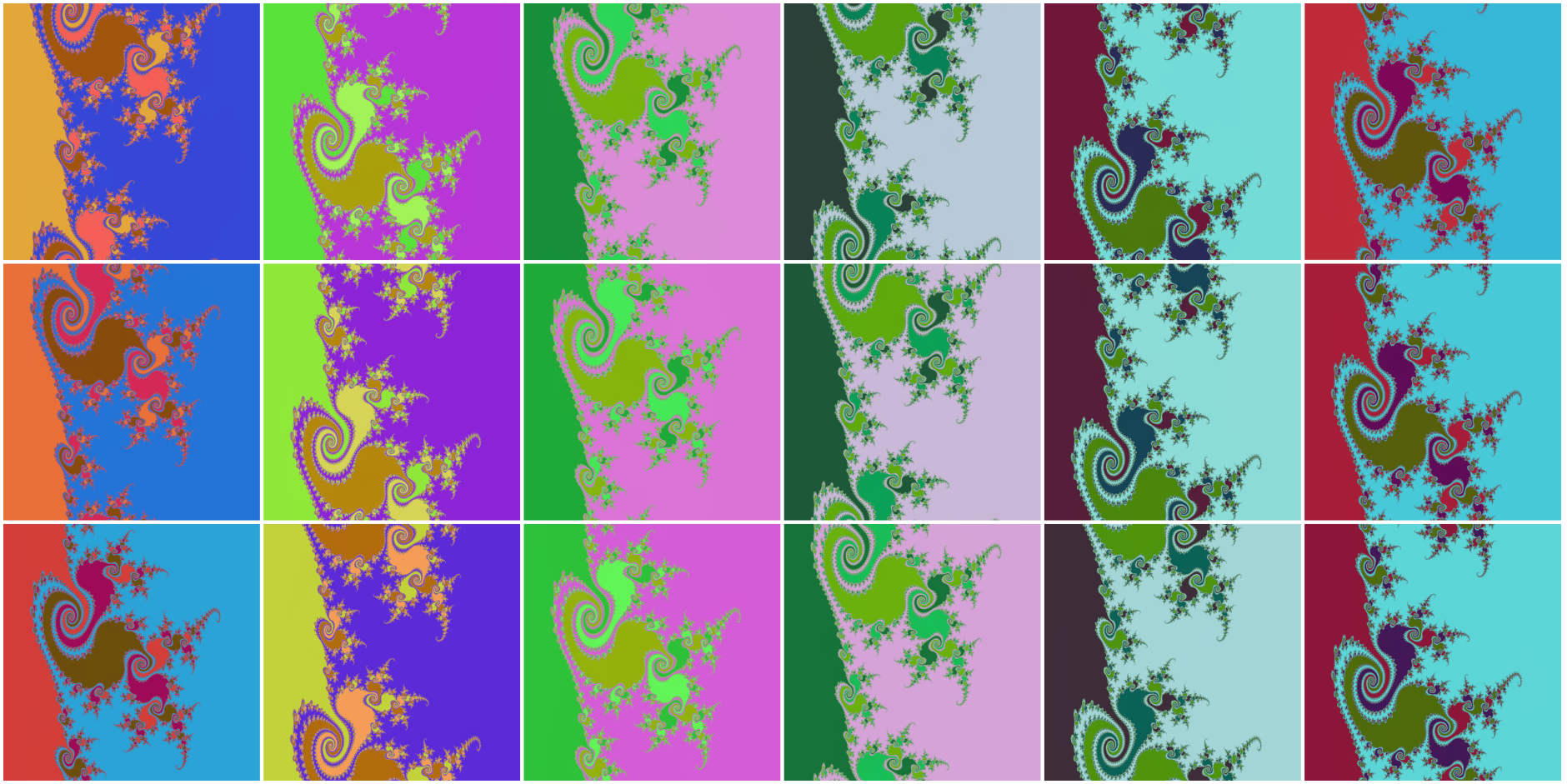

Figure 4.2: Attractor maps of protocols asymptotically equivalent with x=30°, ψ=0°, τ=137°. ψ is set to following values when ordered from *left to right*, then *from top to bottom*: 30°, 60°, 90°, 120°, 150°, 180°, 210°, 240°, 270°, 300°, 330°, 360°, 420°, 480°, 540°, 600°, 660°, 720°. $\tau = \frac{\psi}{2} + 137°$ always. Axial system is the same for all figures as in previous 4.1.

To prove the relation that will be precisely formulated below, we start with goniometry. The evolution equations 4.7 can be alternatively rewritten using identities of goniometric functions valid for all angles:

$$\begin{aligned}
\cos^2 x\cos\tau + \sin^2 x\cos(2\psi{-}\tau) &= \cos(2x)\sin\psi\sin(\psi{-}\tau) + \cos\psi\cos(\psi{-}\tau)\\
\cos^2 x\cos\tau - \sin^2 x\cos(2\psi{-}\tau) &= \cos(2x)\cos\psi\cos(\psi{-}\tau) + \sin\psi\sin(\psi{-}\tau)\\
\cos^2 x\sin\tau + \sin^2 x\sin(2\psi{-}\tau) &= -\cos(2x)\cos\psi\sin(\psi{-}\tau) + \sin\psi\cos(\psi{-}\tau)\\
\cos^2 x\sin\tau - \sin^2 x\sin(2\psi{-}\tau) &= \cos(2x)\sin\psi\cos(\psi{-}\tau) - \cos\psi\sin(\psi{-}\tau)
\end{aligned} \tag{4.10}$$

We have never encountered such equations and we consider them to be pretty (and) nontrivial, so we decide to accompany them with a proof. Hopefully, our readers will excuse us if they are not fans of such relations. We show the proof for only one case, e.g. the last equation, the other cases can be processed analogically. Tricky expansions are marked in gray. First, we express the left side in the terms of products of sole cosine/sine factors.

$$\begin{gathered}
\cos^2 x\sin\tau - \sin^2 x\sin(2\psi-\tau) =\\
= \cos^2 x\sin\tau\underbrace{(\cos^2\psi + \sin^2\psi)} - 2\sin^2 x\sin\psi\cos\psi\cos\tau +\\
+\underline{\sin^2 x\cos^2\psi\sin\tau}\underbrace{-\sin^2 x\sin^2\psi\sin\tau}
\end{gathered}$$

Combining factors marked with corresponding underlining we obtain

$$\underbrace{\cos 2x\sin^2\psi\sin\tau} - 2\sin^2 x\sin\psi\cos\psi\cos\tau + \underline{\cos^2\psi\sin\tau}$$

where we expand the middle member to

$$\begin{gathered}
-\sin^2 x\sin\psi\cos\psi\cos\tau + \cos^2 x\sin\psi\cos\psi\cos\tau -\\
-\cos^2 x\sin\psi\cos\psi\cos\tau - \sin^2 x\sin\psi\cos\psi\cos\tau
\end{gathered}$$

recognising goniometrical identities again to put back together into

$$\begin{gathered}
\cos 2x\sin\psi\sin\psi\sin\tau + \cos 2x\sin\psi\cos\psi\cos\tau +\\
+\cos\psi\cos\psi\sin\tau - \cos\psi\sin\psi\cos\tau =\\
= \cos(2x)\sin\psi\cos(\psi-\tau) - \cos\psi\sin(\psi-\tau)
\end{gathered}$$

To come back to the protocols, we can suspect now there is some kind of self-symmetry. One can elaborate with the help of the figure 4.2 and previous identities that two protocols with $\psi_1, \tau_1, \psi_2, \tau_2$ satisfying $\psi_1 - 2\tau_1 = \psi_2 - 2\tau_2$ will share the characteristic dynamics. The evolution of initially same qubits outlined by equations 4.7 is different but we discover they share a strong connection that forms one of the most important results of our work.

Theorem 4.4.1. *Two purification protocols $T_1R_1[.], T_2R_2[.]$ with parameters x_1, ψ_1, τ_1 and x_2, ψ_2, τ_2 are asymptotically equivalent when*

$$x_1 = x_2, \psi_1 - 2\tau_1 = \psi_2 - 2\tau_2. \tag{4.11}$$

Defining $\tau_0 \equiv \tau_1 - \tau_2$ and $T_0 = \begin{pmatrix} 1 & 0 \\ 0 & e^{-i\tau_0} \end{pmatrix}$, following equation holds.

$$T_0 \cdot T_1R_1[\rho] \cdot T_0^\dagger = T_2R_2[T_0 \cdot \rho \cdot T_0^\dagger] \tag{4.12}$$

Proof. The proof is direct yet subtle because the manipulation of the expressions is demanding even for computer. Examining directly the action of operator T_0, for the moment with unknown phase τ_0, upon the state $\rho = \frac{1}{2}\begin{pmatrix} 1+w & u-iv \\ u+iv & 1-w \end{pmatrix}$ we get $T_0\rho T_0^\dagger = \frac{1}{2}\begin{pmatrix} 1+w & (u-iv)e^{i\tau_0} \\ (u+iv)e^{-i\tau_0} & 1-w \end{pmatrix}$. If such modified state is taken as the input for the iteration of the protocol, it is sufficient to substitute $u \to u\cos\tau_0 + v\sin\tau_0, v \to -u\sin\tau_0 + v\cos\tau$ into the evolution equations. Because the coordinate w remains unaffected, quadratic factors N, W, U, V change to $N, W, U\cos(2\tau_0)+V\sin(2\tau_0), -U\sin(2\tau_0)+V\cos(2\tau_0)$. The fact that U, V change the same way as u, v, only the angle gets doubled, is the base pillar of this proof.

To continue, we have to compare the states obtained at both sides (left L, right R) of the equation of the equation 5.15. To show that they are identical, we have to show all their Bloch coordinates are identical. For simplicity, we start with w' coordinate. Since the operator T_0 does not modify w coordinate we can write straightforwardly the result w'_L using angles x_1, ψ_1, τ_1 and for the right side one has to use the angles x_2, ψ_2, τ_2 and modify factors U, V because of the prior operation of T_0 to get coordinate w'_R:

$$w'_R = \begin{cases} \frac{W}{N}\cos 2x_2 + \\ + \left(\frac{U}{N}\cos 2\tau_0 + \frac{V}{N}\sin 2\tau_0\right)\sin 2x_2\cos\psi_2 + \\ + \left(-\frac{U}{N}\sin 2\tau_0 + \frac{V}{N}\cos 2\tau_0\right)\sin 2x_2\sin\psi_2 \end{cases} \tag{4.13}$$

When we want to prove $w'_L = w'_R$, we have to confirm in addition to equality of x_1, x_2 also

$$\begin{aligned} \cos(2\tau_0)\cos\psi_2 - \sin(2\tau_0)\sin\psi_2 &= \cos\psi_1 \\ \sin(2\tau_0)\cos\psi_2 + \cos(2\tau_0)\sin\psi_2 &= \sin\psi_1 \end{aligned} \tag{4.14}$$

which is trivial because

$$\cos(2\tau_0)\cos\psi_2 - \sin(2\tau_0)\sin\psi_2 = \cos(\psi_2 + 2\tau_0) \tag{4.15}$$

and we sum up

$$\begin{aligned} w'_L &= \frac{W}{N}\cos 2x_1 + \frac{U}{N}\sin 2x_1\cos\psi_1 + \frac{V}{N}\sin 2x_1\sin\psi_1 \\ w'_R &= \frac{W}{N}\cos 2x_2 + \frac{U}{N}\sin 2x_2\cos(\psi_2+2\tau_0) + \frac{V}{N}\sin 2x_2\sin(\psi_2+2\tau_0) \end{aligned} \tag{4.16}$$

The equality holds (for all input states, i.e. for all w, u, v) if and only if $x_1 = x_2 \equiv x$, we write this explicitly to accent that different $x_{1,2}$ values cannot give the same equations. For the sake of simplicity, we will from now on write only the unique x. The other angles must satisfy $2\tau_0 = \psi_1 - \psi_2$. We took the value τ_0 for unknown, but we have just obtained a restriction for it.

Calculations of the other Bloch coordinates are technically demanding but as

they are carried out in the same way as before we write only the results:

$$
\begin{aligned}
u'_L &= \begin{cases} -\frac{W}{N}\sin 2x\cos(\psi_1-\tau_1-\tau_0)+ \\ +\frac{U}{N}\left[\cos 2x\cos(\psi_1-\tau_1-\tau_0)\cos\psi_1+\sin(\psi_1-\tau_1-\tau_0)\sin\psi_1\right]+ \\ +\frac{V}{N}\left[\cos 2x\cos(\psi_1-\tau_1-\tau_0)\sin\psi_1-\sin(\psi_1-\tau_1-\tau_0)\cos\psi_1\right] \end{cases} \\
u'_R &= \begin{cases} -\frac{W}{N}\sin 2x\cos(\psi_2-\tau_2)+ \\ +\frac{U}{N}\left[\cos 2x\cos(\psi_2-\tau_2)\cos(\psi_2+2\tau_0)+\sin(\psi_2-\tau_2)\sin(\psi_2+2\tau_0)\right]+ \\ +\frac{V}{N}\left[\cos 2x\cos(\psi_2-\tau_2)\sin(\psi_2+2\tau_0)-\sin(\psi_2-\tau_2)\cos(\psi_2+2\tau_0)\right] \end{cases} \\
v'_L &= \begin{cases} -\frac{W}{N}\sin 2x\sin(\psi_1-\tau_1-\tau_0)+ \\ +\frac{U}{N}\left[\cos 2x\sin(\psi_1-\tau_1-\tau_0)\cos\psi_1-\cos(\psi_1-\tau_1-\tau_0)\sin\psi_1\right]+ \\ +\frac{V}{N}\left[\cos 2x\sin(\psi_1-\tau_1-\tau_0)\sin\psi_1+\cos(\psi_1-\tau_1-\tau_0)\cos\psi_1\right] \end{cases} \\
v'_R &= \begin{cases} -\frac{W}{N}\sin 2x\sin(\psi_2-\tau_2)+ \\ +\frac{U}{N}\left[\cos 2x\sin(\psi_2-\tau_2)\cos(\psi_2+2\tau_0)-\cos(\psi_2-\tau_2)\sin(\psi_2+2\tau_0)\right]+ \\ +\frac{V}{N}\left[\cos 2x\sin(\psi_2-\tau_2)\sin(\psi_2+2\tau_0)+\cos(\psi_2-\tau_2)\cos(\psi_2+2\tau_0)\right] \end{cases}
\end{aligned}
\tag{4.17}
$$

Both of the equalities are satisfied simultaneously when the already known restriction $2\tau_0 = \psi_1 - \psi_2$ is satisfied and in addition, another restriction emerges: $\psi_2 - \tau_2 = \psi_1 - \tau_1 - \tau_0$. These equations can be used to eliminate unknown τ_0 to obtain restriction solely on $\psi_{1,2}, \tau_{1,2}$ and then to express unknown parameter τ_0 that fits demanded equations:

$$\psi_1 - 2\tau_1 = \psi_2 - 2\tau_2 \tag{4.18}$$

$$\tau_0 = \frac{\psi_1 - \psi_2}{2} = \tau_1 - \tau_2 \tag{4.19}$$

This completes the proof of equation 5.15, now we rearrange

$$T_1 R_1[\rho] = T_0^\dagger \cdot T_2 R_2[T_0 \cdot \rho \cdot T_0^\dagger] \cdot T_0 \tag{4.20}$$

to realise that for arbitrary $n \in \mathbb{N}$ we can inductively follow:

$$
\begin{aligned}
T_2 R_2[T_0 \cdot \rho \cdot T_0^\dagger]^n &= T_2 R_2[T_2 R_2[T_0 \cdot \rho \cdot T_0^\dagger]]^{n-1} = \\
&= T_2 R_2[T_0 T_0^\dagger \cdot T_2 R_2[T_0 \cdot \rho \cdot T_0^\dagger] \cdot T_0^\dagger T_0]^{n-1} = T_2 R_2[T_0 \cdot T_1 R_1[\rho] \cdot T_0^\dagger]^{n-1} \\
&= T_2 R_2[T_0 \cdot T_1 R_1[\rho]^2 \cdot T_0^\dagger]^{n-2} = \cdots = T_0 \cdot T_1 R_1[\rho]^n \cdot T_0^\dagger
\end{aligned}
\tag{4.21}
$$

In the limit $n \to \infty$ we obtain the statement about asymptotic equivalency of the protocols and so complete the proof.

$$T_2 R_2[T_0 \cdot \rho \cdot T_0^\dagger]^\infty = T_0 \cdot T_1 R_1[\rho]^\infty \cdot T_0^\dagger \tag{4.22}$$

□

There is a natural consequence following from the proof. The equivalence of the protocols is not true for only asymptotic regime but for arbitrary number of iterations $k \in \mathbb{N}$, just as we have seen for other symmetries.

$$T_0^\dagger \cdot T_1 R_1[\rho]^k \cdot T_0 = T_2 R_2[T_0 \cdot \rho \cdot T_0^\dagger]^k \tag{4.23}$$

However, this fact is not of much importance because we focus on the asymptotic evolution, fractal structures etc. We could have proposed a theorem with single iteration and derive the asymptotic equivalence from it, but we wanted to accent the asymptotic dynamics. The important knowledge of relation between unitary gates of the asymptotically equivalent protocols in 4.3.1, $U_1 = U_2 = T_0$, is relevant for experimental application. And it also gives relation between corresponding fractal structures.

We now discuss various ideas that accompany and accent the importance of this theorem. Let us start with a word *commutation*. This can come into one's mind when seeing relation 4.20. The fact that such equation holds is highly nontrivial, it is nontrivial even for linear operators A, B where $TA\rho A^\dagger T^\dagger \neq BT\rho T^\dagger B^\dagger$ generally. Especially if $A = B$ we come to the commutation relation $AT = TA$ and the existence and properties of operator T can fill the books on their own. For unitary operators A, B, T there must be relation of similarity, $B = TAT^\dagger$ satisfied to validate $TA\rho A^\dagger T^\dagger = BT\rho T^\dagger B^\dagger$ for all input states ρ. The fact that a similar relation is valid for nonlinear operator based on the CNOT gate (here represented by brackets [.]) is very interesting, even more for the fact that the T_0 is of the form of the free time evolution operator. The discovery of the exact relation amongst the angles is the culmination of our general result.

Let us now explain the theorem in the geometrical representation in the Bloch space. The action of T_0 upon a qubit makes it rotate around w-axis by angle τ_0. This prominent role of the w-axis is the reason why we use the notation (w, u, v). The equation 4.20 is interpreted in following way now. When we take two protocols satisfying theorem conditions and we apply the first one on the whole Bloch sphere of initial states, we obtain the same results as if we would first rotate the ball by the angle $\tau_0 = \tau_1 - \tau_2$ around the w-axis, apply the second protocol and then rotate back, i.e. by $-\tau_0$ around the w-axis. Furthermore, this geometrical representation works not only for a single iteration but also for any number of iterations, as the proof showed. Of course, in this geometric point of view, the rotation there and back that is performed between two iterations act together simply as the identity.

Ultimately, in the asymptotic regime we arrive to the attractor maps that for these two equivalent protocols are connected in following way. In spherical angles φ, ϑ for fixed P, we will see that the pattern corresponding to the first protocol is shifted by angle $\tau_0 = \tau_1 - \tau_2$ to the left, i.e. $\varphi \to \varphi + \tau_0$ compared to the pattern in the map of the second protocol. In other words, when parameter τ is increased by τ_0 while keeping $\psi - 2\tau$, the image is shifted to the right by τ_0. This is the result of the T_0 action on the initial state ρ. The final rotation of the $T_2 R_2[T_0 \cdot \rho \cdot T_0^\dagger]$ imposed by $T_0^\dagger$ transforms the output state which is represented by colour. This means that the patterns in the attractor maps will have modified colours. When the colour coding would be determined as a function of the spherical coordinates, let us symbolically write the RGB coding as $R_1 = R(P, \varphi, \vartheta), G_1 = G(P, \varphi, \vartheta), B_1 = B(P, \varphi, \vartheta)$, one can see that this scheme

is also shifted to $R_2 = R(P, \varphi - \tau_0, \vartheta), G_2 = G(P, \varphi - \tau_0, \vartheta), B_2 = B(P, \varphi - \tau_0, \vartheta)$.

Geometrically, one could suggest that the natural coordinates for this protocol are the cylindrical $\sqrt{u^2 + v^2}, \varphi, w$. However, our analysis showed that the evolution equations do not simplify in a manner that would offer an advantage. While the purity as a spherical radius is physically more relevant parameter, we keep the spherical coordinates. Still, the cylindrical symmetry is important and we have to be aware of it.

The strictly abstract representation above is also important for another reason - the physical understanding of the situation. The action of T_0, seen as a rotation in the Bloch space in fact is the free time evolution of the qubit 4.4, that was our motivation to decompose the twirling operator $U = TR$. We now interpret the equation 4.20 in the context of experimental execution of the protocol. Taking the two equivalent protocols with $x, \psi_1, \tau_1; x, \psi_2, \tau_2$ according to the theorem again, we can execute the first protocol with x, ψ_1, τ_1 and than leave the state evolve freely for the period corresponding to the relative phase $\tau_0 = \tau_1 - \tau_2$ or we can first let the state evolve freely for τ_0 and then execute the other protocol with x, ψ_2, τ_2. We obtain the same results in both cases. The same conclusion is valid for arbitrary number of iterations.

Now we have discovered the reason why the theorem has such significant importance. We are given a guide to realise the protocol experimentally. So far, the idea of the use of the protocol did not take into account that the qubit is sent across the universe and it evolves (for this moment let us say) freely. The protocol also is assumed to be performed multiple times to guarantee that the state is purified sufficiently. The single iteration steps cannot be executed instantaneously and by practical limitations are separated by short time gaps when the qubit evolves freely. If we are to apply the protocol then, the initial state is changed which can affect the convergence etc. However, now, we can use another protocol to eliminate the effect of the free time evolution. By changing the twirling gate angles ψ, τ in a manner preserving value $\psi - 2\tau$, the time gap is virtually manipulated.

Before we analyse this thought in detail, let us make one more point on the importance of the theorem 5.15. When the subsequent iterations of the protocol application are performed, each iteration with different twirling - $T_i R_i$ for i-th iteration - but all these operators satisfy $\psi_i - 2\tau_i = const.$ for the same constant, the time evolution operators T_i can be commuted out of the iterations. The whole series of iteration can be executed by certain time evolution on the input state, a series of iterations with modified rotations and a final time evolution of the output state.

Let us write down basic consequences of 4.20 to obtain and interpret some practical results. First of all, as we have already mentioned, the time gap τ can be manipulated at the cost of alteration of ψ, we now list exact prescriptions to elementary situations of protocol applications.

- *Adding the time relaxation to the protocol.*

  $$R_1[R_1[R_1[\dots R_1[\rho]\dots]]] \to T \cdot (TR_2[TR_2[TR_2[\dots TR_2[T^\dagger \cdot \rho \cdot T]\dots]]]) \cdot T^\dagger \tag{4.24}$$

  If the protocol iterations are executed immediately but we need certain time evolution, resp. the phase τ to take place, we can implement it without

actually leaving the system to evolve freely. The required time for protocol implementation can dramatically decrease. Gate R_2 must be chosen with $\psi_2 = \psi_1 + 2\tau$.

- *Eliminating the time relaxation from the protocol.*

  $$TR_1[TR_1[TR_1[\dots TR_1[\rho]\dots]]] \to T^\dagger \cdot (R_2[R_2[R_2[\dots R_2[T \cdot \rho \cdot T^\dagger]\dots]]]) \cdot T \tag{4.25}$$

  On contrary, if the protocol iterations are separated by time evolution (for example due to transmission of state or due to technological realisation) we can modify the protocol to undo this unwanted phase τ with setting $\psi_2 = \psi_1 - 2\tau$.

- *Changing the time relaxation of the protocol from τ_1 to τ_2.*

  The most general case has the same equation 4.25, with the meaning that the time delay between protocol iterations can be lengthened or shortened at will by premodification of the input state and postmodification of the output state with the time relaxations by $\tau = \tau_1 - \tau_2$ and change $\psi_2 = \psi_1 + 2\tau_2 - 2\tau_1$

All these options are still considering one particularly desired protocol, but we can turn the thinking another way around. Let us assume we have a protocol with a known attractor (w, u, v) but we desire experimentally to achieve another attractor. Now, we claim that any attractor

$$(w, u\cos\tau_0 - v\sin\tau_0, u\sin\tau_0 + v\cos\tau_0) \tag{4.26}$$

is achievable by some another protocol obtained by setting corresponding angles ψ, τ. Proof is obvious from 4.20. Or, in case we have only limited experimental possibilities to prepare input state, we can use another protocol with suitable ψ, τ to simulate another input state. The possibilities are the same as listed above but there is a limitation, the states must share common coordinate w. At this moment it is not clear, whether there can be protocol found to have an attractor of specific w; we will resolve this problem later.

We conclude that the symmetry has crucial experimental significance. The relation $\psi_2 - \psi_1 = 2(\tau_2 - \tau_1)$ is key ingredient to transfer the protocol from theory to practical use which is burdened with certain time relaxation between the protocol iterations. We are aware of the fact that the evolution between the iterations is not typically free as considered in our text. However, when the perturbations are small, the purification capabilities of the protocol together with the manipulation of time relaxation are very promising for experimental success of the protocol. Or at least much more promising than so far.

Let us now finish the topic of symmetries started in previous section. For the purpose of our work of exploring chaotic features of the protocols, we draw following conclusions. The symmetries of the initial states allow to take only $P \in [\frac{1}{2}; 1], \varphi \in [0; \pi), \vartheta \in [0; \pi]$ and protocols with $x \in [0; \frac{\pi}{2}], \psi = 0, \tau \in [0; \frac{\pi}{2}]$. All the other protocols with $\psi \neq 0$ can be transformed using the symmetries or the

theorem 5.15 to case $\psi \to 0, \tau \to \tau - \frac{\psi}{2}$. The evolution equations 4.7 reduce to

$$\begin{array}{rcccccccc} w' = & +\dfrac{W}{N} & \cos 2x & +\dfrac{U}{N} & \sin 2x & + & 0 & & \\ u' = & -\dfrac{W}{N} & \sin 2x \cos\tau & +\dfrac{U}{N} & \cos 2x \cos\tau & + & \dfrac{V}{N} & \sin\tau & \\ v' = & +\dfrac{W}{N} & \sin 2x \sin\tau & -\dfrac{U}{N} & \cos 2x \sin\tau & + & \dfrac{V}{N} & \cos\tau & \end{array} \tag{4.27}$$

which are significantly simplified compared to the original equations.

Another alternative to setting $\psi = 0$ could be made based on equations written in 4.10, we could set $\psi \to 2\tau - \psi \leftarrow \tau$. Such protocol would induce evolution equations

$$\begin{array}{rcccccccc} w' = & & \dfrac{W}{N}\cos 2x & +\dfrac{U}{N} & \sin 2x \cos\psi & +\dfrac{V}{N} & \sin 2x \sin\psi & & \\ u' = & - & \dfrac{W}{N}\sin 2x & +\dfrac{U}{N} & \cos 2x \cos\psi & +\dfrac{V}{N} & \cos 2x \sin\psi & & \\ v' = & & 0 & -\dfrac{U}{N} & \sin\psi & +\dfrac{V}{N} & \cos\psi & & \end{array} \tag{4.28}$$

These equations may seem more simple, in particular for $\psi = 0$ where the Bloch coordinate evolution is separated in U, V, W, N factors. However, these factors contain all the coordinates, so even in this case, deriving some statements e.g. about convergence in $v \to 0$ would be highly nontrivial. For the reason of the physical interpretation of τ as the time we prefer the protocol setting with $\psi = 0$.

Another easy and reasonable option to rewrite the equations is obtained for transforming $\psi \to \frac{1}{3}(2\tau - \psi) \wedge \tau \to \frac{2}{3}(2\tau - \psi)$ to guarantee property $2\psi - \tau = 0$ for the protocol angles which simplifies equations, it may be better seen in the identities 4.10 we have proven. In this case, the evolution equations are

$$\begin{aligned} w' &= \begin{cases} \dfrac{W}{N}\cos 2x + \\ \qquad + \dfrac{U}{N}\sin 2x \cos\psi + \dfrac{V}{N}\sin 2x \sin\psi \end{cases} \\ u' &= \begin{cases} -\dfrac{W}{N}\sin 2x \cos\psi + \\ \qquad + \dfrac{U}{N}\left[\cos^2 x \cos 2\psi - \sin^2 x\right] + \dfrac{V}{N}\cos^2 x \sin 2\psi \end{cases} \\ v' &= \begin{cases} +\dfrac{W}{N}\sin 2x \sin\psi + \\ \qquad - \dfrac{U}{N}\cos^2 x \sin 2\psi + \dfrac{V}{N}\left[\cos^2 x \cos 2\psi + \sin^2 x\right] \end{cases} \end{aligned} \tag{4.29}$$

but these have shape very similar to 4.27. The relation $\tau = 2\psi$ also is of no importance to physics, therefore we stick to the variant where $\tau = 0$ is set.

The very last option we list is to set $\tau \to 0, \psi \to \psi - 2\tau$, we obtain equations

$$\begin{aligned}
w' = &\left\{ \begin{array}{l} \frac{W}{N}\cos 2x + \\ \qquad + \frac{U}{N}\sin 2x \cos\psi + \\ \qquad + \frac{V}{N}\sin 2x \sin\psi \end{array} \right. \\
u' = &\left\{ \begin{array}{l} -\frac{W}{N}\sin 2x \cos\psi + \\ \qquad + \frac{U}{N}\left[\cos 2x \cos\psi \cos\psi + \sin\psi \sin\psi\right] + \\ \qquad + \frac{V}{N}\left[\cos 2x \sin\psi \cos\psi - \cos\psi \sin\psi\right] \end{array} \right. \\
v' = &\left\{ \begin{array}{l} -\frac{W}{N}\sin 2x \sin\psi + \\ \qquad + \frac{U}{N}\left[\cos 2x \cos\psi \sin\psi - \sin\psi \cos\psi\right] + \\ \qquad + \frac{V}{N}\left[\cos 2x \sin\psi \sin\psi + \cos\psi \cos\psi\right] \end{array} \right.
\end{aligned} \tag{4.30}$$

It would be similarly good to take these instead of 4.27 but we prefer the first variant for the context of time evolution; also, other equations will be more simple in next text due to one nullified factor in w'.

Let us conclude that there is an equivalence class on the purification protocols characterised by $\psi - 2\tau = const.$ For further purposes of fractal analysis the equivalence brings significant reduction of protocol parameters. The degree of freedom in the choice of parameters is reduced from 3 to 2. It is enough to analyse the asymptotic dynamics for one representative of the class, all other cases can be converted to such representative by prescribed formulas, no dynamical regimes will be missed in our research.

4.5 Inverse iterations, stability, invariant sets

Let us proceed to backward iterations which can be used to detect fractal structures. Even though we have found the inaccessible states in last chapter, backward iterations still may be an important tool helping to approximate the fractals. For pure states, the backward iterations still are perfectly valid instrument of Julia set detection regardless of the twirling parameters. We split the deriving of the equations into two parts. First, multiplying and adding/subtracting equations 4.7 we get relations

$$\begin{aligned}
u'\sin(\psi{-}\tau) - v'\cos(\psi{-}\tau) = &\quad \tfrac{U}{N}\sin\psi - \tfrac{V}{N}\cos\psi, \\
u'\cos(\psi{-}\tau) + v'\sin(\psi{-}\tau) = &\quad \left(\tfrac{U}{N}\cos\psi + \tfrac{V}{N}\sin\psi\right)\cos 2x - \tfrac{W}{N}\sin 2x.
\end{aligned} \tag{4.31}$$

continuing with multiplying these equations and equation for w' with factors $\cos(\psi-\tau)$ etc. we can enjoy surprising fun[1] coming to

$$\begin{aligned}
\frac{W}{N} &= \begin{cases} w'\cos 2x - \\ \qquad -u'\sin 2x\cos(\psi-\tau) - \\ \qquad -v'\sin 2x\sin(\psi-\tau) \end{cases} \\
\frac{U}{N} &= \begin{cases} w'\sin 2x\cos\psi + \\ \qquad +u'\left[\cos 2x\cos(\psi-\tau)\cos\psi+\sin(\psi-\tau)\sin\psi\right] + \\ \qquad +v'\left[\cos 2x\sin(\psi-\tau)\cos\psi-\cos(\psi-\tau)\sin\psi\right] \end{cases} \\
\frac{V}{N} &= \begin{cases} w'\sin 2x\sin\psi + \\ \qquad +u'\left[\cos 2x\cos(\psi-\tau)\sin\psi-\sin(\psi-\tau)\cos\psi\right] + \\ \qquad +v'\left[\cos 2x\sin(\psi-\tau)\sin\psi+\cos(\psi-\tau)\cos\psi\right] \end{cases}
\end{aligned} \tag{4.32}$$

which can be also derived by application of $(TR)^{-1}$ twirling operator to the ρ'.

With the factors $\frac{W}{N}, \frac{U}{N}, \frac{V}{N}$ we invert them using their definitions 4.8. Again like in the previous chapter we start with w which is determined solely by $\frac{W}{N}$. The inverse function is surprisingly

$$w = \frac{\sqrt{1+\frac{W}{N}}-\sqrt{1-\frac{W}{N}}}{\sqrt{1+\frac{W}{N}}+\sqrt{1-\frac{W}{N}}} \tag{4.33}$$

which allows to express N and U, V right after. Realising that in complexification $U+IV{=}(u+iv)^2$, we finish

$$u = Re(\sqrt{U+IV}),\ u = Im(\sqrt{U+IV}) \tag{4.34}$$

Let us follow the case for H_2 from the last chapter and first study the pure states. It is reasonable because

Proposition 4.5.1. *Pure states remain pure under iteration of any protocol, i.e. with arbitrary x, ψ, τ.*

Proof. For any protocol we use trace cyclic property $Tr(TR(\rho\odot\rho)R^\dagger T^\dagger) = Tr([\rho]) = Tr(H_2(\rho\odot\rho)H_2^\dagger)$ which in other words is the known fact that the unitary gate does not change the purity. We have proven the purity of evolved state $H_2(\rho\odot\rho)H_2^\dagger$ in previous chapter; now we add that the unitary twirling cannot change the purity of the evolved state. □

In this case, we can perform the identification of the Bloch sphere with Riemann sphere again. Evolution function $z' = f_{x,\psi,\tau}(z)$ can be derived from the mixed states or more easily straight from the definition $\begin{pmatrix}1\\z'\end{pmatrix} = \frac{1}{\nu}TR\cdot\begin{pmatrix}1\\z^2\end{pmatrix}$ where norm ν is physically irrelevant. We state that evolution function of the twirled protocol is

$$f_{x,\psi,\tau}(z) = e^{-i\tau}\frac{z^2\cos x - e^{i\psi}\sin x}{\cos x + z^2 e^{-i\psi}\sin x} \tag{4.35}$$

$$f^{-1}_{x,\psi,\tau}(z) = \sqrt{-\frac{ze^{i\tau}\cos x + e^{i\sin\psi}\sin x}{ze^{-i(\tau+\psi)}\sin x - \cos x}} \tag{4.36}$$

[1] No sarcasm intended.

We recall the asymptotic equivalence and at this place we set $\psi = 0$ to simplify notation with

$$f_{x,0,\tau} \equiv f_{x,\tau}. \tag{4.37}$$

Complete characterisation of asymptotic dynamics can be easily performed for particular angles $x = 0$ and $x = \frac{\pi}{2}$ for which the functions reduce to

$$f_{0,\tau}(z) = e^{-i\tau} z^2, \quad f_{\frac{\pi}{2},\tau}(z) = -e^{i(-\tau)} \frac{1}{z^2} \tag{4.38}$$

In the case of $x = 0$: all states with $|z| < 1$ converge to 0, all states with $|z| > 1$ converge to ∞. These states are attractors. The states on the unit circle belong to the Julia set and exhibit chaos with number $e^{i\tau}$ belonging to it as a parabolic state. The case of $x = \frac{\pi}{2}$ has attractive cycle $0 \leftrightarrow \infty$ attracting all states except for the unit circle which is the Julia set again.

But for the case $x = 0$ we can easily stretch the analysis to the mixed states where we afford to write evolution equations into a compact matrix form embracing rotation by angle τ around w-axis:

$$w' = \frac{W}{N}, \begin{pmatrix} u' \\ v' \end{pmatrix} = \begin{pmatrix} \cos\tau & \sin\tau \\ -\sin\tau & \cos\tau \end{pmatrix} \cdot \begin{pmatrix} \frac{U}{N} \\ \frac{V}{N} \end{pmatrix}. \tag{4.39}$$

First, $w' = \frac{2w}{1+w^2}$ is solely function of w, with following property: $w' = w \Leftrightarrow w \in \{-1, 0, 1\}$ while $|w'| > |w| \wedge \mathrm{sgn}(w)=\mathrm{sgn}(w')$ for other w values. States with $w = \pm 1$ are $|0\rangle, resp. |1\rangle$ and serve as attractive for all states with $w > 0, w < 0$ respectively. Mixed states of equatorial plane $w = 0$ are attracted to maximally mixed state because $u'^2 + v'^2 = \frac{U^2+V^2}{N^2} = \left(\frac{u^2+v^2}{1+w^2}\right)^2 < u^2 + v^2$ which follows from mixedness condition $u^2 + v^2 < 1 - w^2$. Also, stability analysis by Jacobi matrix confirms that the equatorial plane is repelling, $\mathbb{1}$ is a saddle point and we for the first time encounter situation when (mathematically) almost all states are purified, equator $u^2 + v^2 = 1 \wedge w = 0$ contains chaos and the rest of equatorial plane is attracted in the plane to a single state yet repelled from the plane to the poles. Because experimentally $w = 0$ can never be sustained precisely, any state would eventually converge to either $|0\rangle$ or $|1\rangle$ which are represented by $z = \infty, z = 0$ in the complex representation of the pure states.

We have mentioned the Jacobi matrix - it can be calculated not only for $x = 0 \vee x = \frac{\pi}{2}$ but generally for protocol with any x, τ at any point (w, u, v):

$$\mathbb{J} = 2 \begin{pmatrix} \mathbb{J}_{11} & \mathbb{J}_{12} & \mathbb{J}_{13} \\ \mathbb{J}_{21} & \mathbb{J}_{22} & \mathbb{J}_{23} \\ \mathbb{J}_{31} & \mathbb{J}_{32} & \mathbb{J}_{33} \end{pmatrix} \tag{4.40}$$

$$\mathbb{J}_{11} = \frac{(1-w^2)\cos 2x - w\,(u^2 - v^2)\sin 2x}{(1+w^2)^2}$$

$$\mathbb{J}_{12} = \frac{u \sin 2x}{1+w^2}, \ \mathbb{J}_{13} = -\frac{v \sin 2x}{1+w^2}$$

$$\mathbb{J}_{21} = -\frac{\cos\tau\,((1-w^2)\sin 2x + w\,(u^2 - v^2)\cos 2x) + 2uvw\sin\tau}{(1+w^2)^2}$$

$$\mathbb{J}_{22} = \frac{u\cos\tau\cos 2x + v\sin\tau}{1+w^2}, \ \mathbb{J}_{23} = \frac{u\sin\tau - v\cos\tau\cos 2x}{1+w^2}$$

$$\mathbb{J}_{31} = \frac{\sin\tau\left((1-w^2)\sin 2x + w\left(u^2-v^2\right)\cos 2x\right) - 2uvw\cos\tau}{\left(1+w^2\right)^2}$$

$$\mathbb{J}_{32} = \frac{v\cos\tau - u\sin\tau\cos 2x}{1+w^2},\ \mathbb{J}_{33} = \frac{u\cos\tau + v\sin\tau\cos 2x}{1+w^2}$$

together with its eigenvalues and eigenvectors that can be expressed analytically as radices of multivariable polynomials (in Bloch coordinates) of degree 8.

To start with more general case let us set $\tau = 0$, which is also very convenient because equations 4.27 reduce this time to

$$\begin{pmatrix} w' \\ u' \end{pmatrix} = \begin{pmatrix} \cos 2x & \sin 2x \\ -\sin 2x & \cos 2x \end{pmatrix} \cdot \begin{pmatrix} \frac{W}{N} \\ \frac{U}{N} \end{pmatrix}, v' = \frac{V}{N}. \tag{4.41}$$

where evolution of v is partially separated and as a consequence, circle K, i.e. physical states in the plane $v = 0$, form an invariant set. When we realise that pure states are also invariant, we have just proven

Proposition 4.5.2. *Purification protocol with $\tau(=\psi) = 0$ and arbitrary x has invariant sets K and ∂K.*

This property was present in case $x = \frac{\pi}{4}$ studied earlier, now it is more general. When we restrict to the pure states in this plane, i.e. $w^2 + u^2 = 1 \wedge v = 0$, the main meridian of the Bloch sphere, we could introduce a polar coordinate on this circle ∂K but we can also realise that these states are the set of real numbers in the approach of complex functions where states are represented by $z \in \mathbb{C}$. Therefore, we can have the evolution function

$$f_{x,0}(z) = \frac{z^2\cos x - \sin x}{\cos x + z^2\sin x} \tag{4.42}$$

restricted to the real domain. Existence of invariant sets $K, \partial K$ is reason why protocols with $\psi = \tau = 0$ deserve particular care and their own section. But before, we wish to illustrate various types of evolution induced by these evolution functions. We will now plot orbits of state $|0\rangle$, i.e. $z = 0$. This state has no particular importance in general, though it is a member of the attractor cycle for $x = \frac{\pi}{4}, \tau = 0$. The state can converge to a fixed state or a cycle of some period (not necessarily 2). Or it can be a part of the Julia set yielding chaotic evolution. We have also detected quasi-periodic behaviour which probably occurs near the transition between the chaotic and regular evolution. In following figures we let the state evolve for 1000 iterations to settle down the initial evolution and settle towards the asymptotic regime. Then, another 1000 iterations are performed. Because the state described as $f^n_{x,\tau}(z) \in \mathbb{C}$ can be understood as a discrete time signal, we can perform its Fourier transformation to find the lengths of the cycles from the frequency spectrum. The spectrum for $x = \frac{\pi}{4}, \tau = 0$ where the state oscillates between two states $z = 0 \leftrightarrow 1$ would have a single peak at frequency $\frac{1}{2}$ marking cycle of length 2; the length of the cycle is the period, the reciprocal value of the frequency. Multiple frequencies present in the spectrum mean that the cycle is composed of multiple subcycles. We can illustrate this in an analogy of moons orbiting planets orbiting stars orbiting galaxies... with various periods. For chaotic evolution, the spectrum contains all frequencies.

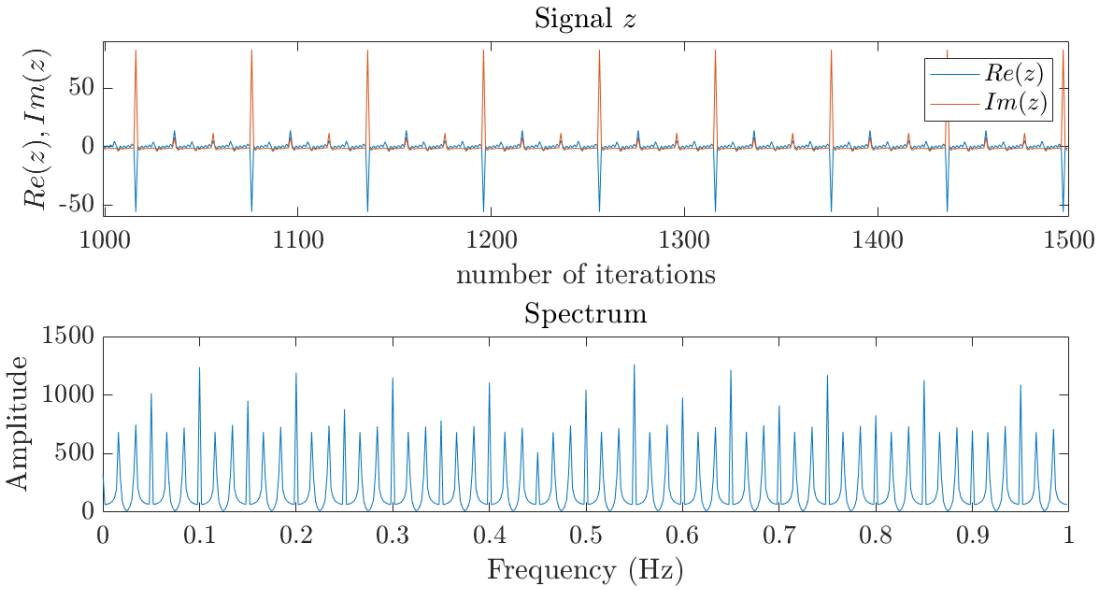

Figure 4.3: A sequence from the orbit of $z = 0$ for protocol with $x = 34°, \tau = 76°$. The state converges to cycle of period 60; the cycle consists of distinct triplets of close points.

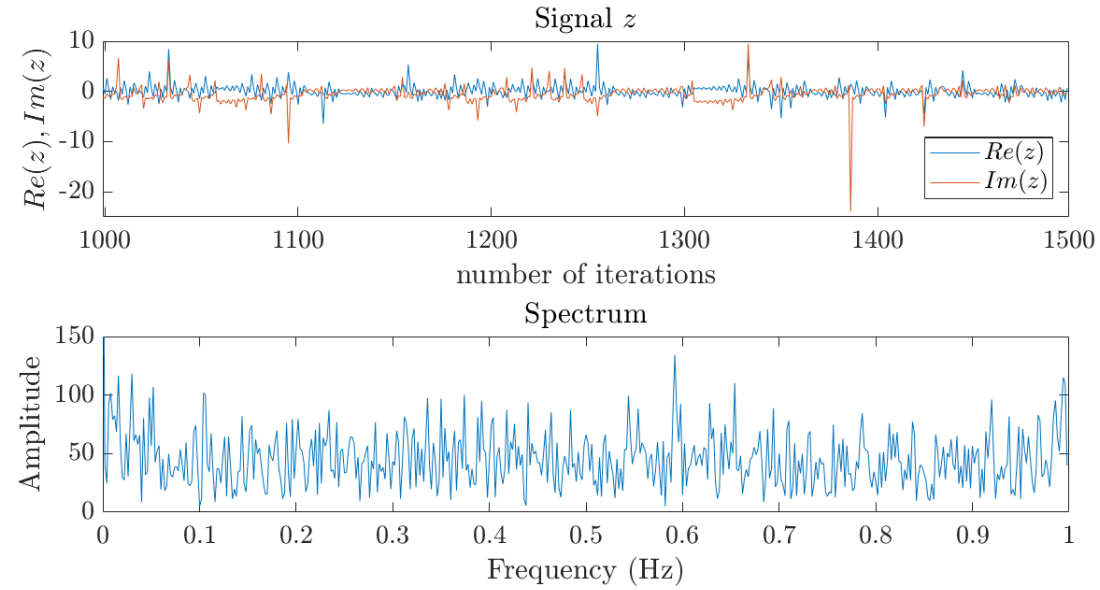

Figure 4.4: A sequence from the orbit of $z = 0$ for protocol with $x = 34°, \tau = 76°$. The state chaotically jumps across the whole Bloch sphere but not uniformly, many points of the orbit concentrate into several clusters.

4.6 Universality

We remind that we consider only $x \in [0; \frac{\pi}{2}]$. Case of $x \to \pi - x$ is conjugate to protocol with x when $w \to -w$ is also transformed. In the complexification, such transformation reads $z \to z^{-1}$. For all protocols with $\psi = \tau = 0$ we can compute the fixed points resp. 2-cycles amongst pure states. The polynomial equation $f_{x,0}(z) = z$ resp. $f^2_{x,0}(z) = z$ is of degree 3 resp. 5. The case of fixed point is therefore analytically solvable, either all fixed points are real or

there is 1 real and 2 complex conjugate. It is in principle possible to express the fixed points in radicals - they are solutions of a cubic equation, but they have similar shape to value of μ, 3.10, of course enhanced with general parameter x. We do not present exact form because it is too complicated and can be easily determined in mathematical software, we used Mathematica. The case of 2-cycles is much more interesting because with the knowledge of fixed points we can reduce the degree 5 polynomial equation to quadratic equation of states that satisfy $f_{x,0}(z) \neq z \wedge f_{x,0}^2(z) = z$, these states will be determined precisely and play crucial role later.

Before we present the overview of the fixed points and 2-cycles, we present two critical values of x:

$$\begin{aligned} x_b &= \operatorname{acos}\tfrac{1}{2}\sqrt{3(3-\sqrt{3})} \doteq 0.223297 \doteq 12.8^\circ \\ x_c &= \operatorname{atan}\sqrt{-3+2\sqrt{3}} \doteq 0.598031 \doteq 34.4^\circ \end{aligned} \tag{4.43}$$

These determine whether the states are real and also if they are attractive. For fixed states:

- $0 \leq x < x_b$

  There are three distinct real fixed points $f(z) = z \in \mathbb{R}$

- $x_b < x < \frac{\pi}{2}$

  There is a single real fixed point and two complex conjugate fixed points.

- $x = x_b$

  There is one fixed point and one double degenerate fixed point, all real. For x_b it is

  $$z_1 \doteq -0.189591,\ z_2 = z_3 \doteq 2.296630 \tag{4.44}$$

Recall that symmetry $x \to \pi - x$ must change $z \to z^{-1}$. The case $x = \pi - x_b$ would induce fixed point and degenerate dublet

$$z_1^{-1} \doteq -5.274511,\ z_2^{-1} = z_3^{-1} \doteq 0.435421. \tag{4.45}$$

We have succeeded to determine that numbers $-z_2, z_2^{-1}$ are the real roots of polynomial $z^4 + 2z^3 + 2z + 1$, namely $-z_2^{-1} = \frac{1}{2}(-1 - \sqrt{3} + \sqrt[4]{12})$ is important. Now, searching for 2-cycles:

- $0 \leq x < x_c$

  There is an imaginary 2-cycle.

- $x_c < x < \frac{\pi}{2}$

  There is a real 2-cycle.

- $x = x_c$

  The 2-cycle degenerates towards the real fixed point. There is triple degenerate fixed point $-z_2^{-1}$.

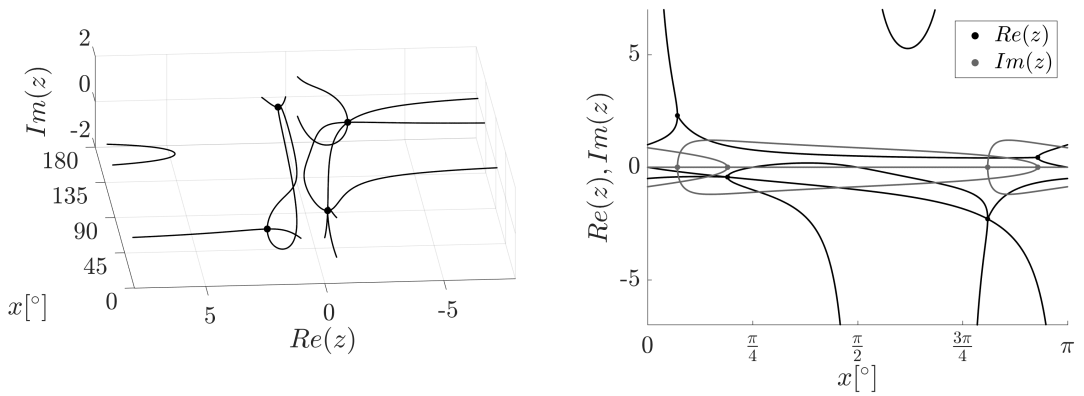

Figure 4.5: *Left:* All 5 states satisfying $f^2_{x,0}(z) = z$ regardless of attractive/repelling character, depending on x of the protocol with $\psi = \tau = 0$. Degenerate radices highlighted with bold points. *Right:* Separate plots of the real and imaginary parts of the solutions. Nodes highlighted in both the real and imaginary parts for given x belong to single complex numbers $z_{1,2}, z^{-1}_{1,2}$.

Regarding the stability of the solutions, let us note that the derivatives may be positive, negative and also imaginary; we have found they always have absolute value ≤ 4. In consequence, the points can be attractive, repelling and also work as a focus. For practical purposes, we now list the attractive cases:

- $x = 0$

  Superattractive states $z = 0$ and $z = \infty$.

- $x = \frac{\pi}{2}$

  Superattractive cycle $z = 0 \leftrightarrow \infty$.

- $0 < x < x_b$

  Two (real) fixed points satisfying $z < 0 \vee z > z_2$.

- $x_b < x < x_c$

  Single attractor, the fixed point satisfying $z < 0$.

- $x_c < x < \frac{\pi}{2}$

  The (real) cycle. Superattractive for $x = \frac{\pi}{4}$, the known protocol from previous chapter.

By exact calculations of the derivatives in Mathematica we have just arrived to an important piece of information: all attractors are real. The proof of following proposition is then obvious if we realise from 2.39 that case of $z \in \mathbb{R}$ is equivalent to $v = 0$.

Proposition 4.6.1. *For arbitrary $x \in \left[0; \frac{\pi}{2}\right]$, any protocol with parameters $\psi = \tau = 0$ has pure attractors only in invariant plane $v = 0$, i.e. in the circle ∂K.*

Another observation is that the 2-cycle is real if and only if it is attractive. This is convenient because surprisingly, for x the cycle is determined by simple equations

$$\frac{-1 + \sqrt{-2\cos 2x - \cos 4x}}{1 + \cos 2x + \sin 2x} \leftrightarrow \frac{-1 - \sqrt{-2\cos 2x - \cos 4x}}{1 + \cos 2x + \sin 2x}. \tag{4.46}$$

Such simple formula cannot be given for the fixed points; the solution is analytic though because a cubic equation is solved. We leave the formula to be calculated in mathematical software if one needs to. Let us now look at the situation from another point of view. We now ask not what z is fixed for given x but we ask if/what x can be chosen so that given $z \in \mathbb{R}$ is attractor. We find and conclude the answer is positive in following cases of the fixed states.

- $z \in (-z_2^{-1}; 0]$

  Value $x \in [0; x_c)$ can be found that $f(z) = z$ is attractive.

- $z \in (z_2; \infty)$

  Value $x \in [0; x_b)$ can be found.

While for 2-cycles we have possibilities:

- $z < 0$ except for $z = -z_2^{-1}$

  $x \in \left[x_c; \frac{\pi}{2}\right]$ exists such that z is part of a 2-cycle.

- $z \in [0; -z_1)$

  There are two values in $x \in [\frac{\pi}{4}; \frac{\pi}{2}]$ such that z is a member of 2-cycle.

- $z = z_1$

  z is 2-cycle member for unique value $x = \text{atan}\,\sqrt{3 + 2\sqrt{3}} \doteq 1.196062$.

The intervals of z typically are not closed because at the border points the derivatives have absolute value equal to 1 marking indifferent points. The particular case of protocol with $x = x_c$ is to discussion. There is the triple degenerate fixed point $z = -z_2^{-1}$ which is the reason why it is excluded from previous list with $z < 0$. Let us recall the transformation from complex to spherical coordinates of the qubit 2.38 Whenever z is real, the Bloch coordinates of pure states are simple to calculate: $w(z) = \frac{1-z^2}{1+z^2}, u(z) = \frac{2z}{1+z^2}, v = 0$. For this reason, we find special value $w_c = w(z_2^{-1}), -w_c = w(z_2)$, these numbers are the real roots of polynomial $w^4 + 6w^2 - 3$ and can be expressed analytically.

$$w_c = \sqrt{-3 + 2\sqrt{3}} \doteq 0.681250 \tag{4.47}$$

Let us appreciate that we find relation $x_c = \text{atan}\, w_c$ and also $z_2^{-1} = \sqrt{\frac{1-w_c}{1+w_c}}$.

The triple degenerate fixed point in Bloch coordinates reads $(w_c, -\sqrt{1 - w_c^2}, 0)$ where $-\sqrt{1 - w^2} = -\sqrt{4 - 2\sqrt{3}}$ and this state can be put into Jacobi matrix 4.40. Obtained eigenvalues are

$$\begin{array}{lll} \lambda_{1,2} = -1 & \text{with eigenvectors} & (0,0,1), (\sqrt{\frac{2}{\sqrt{3}}}, 1, 0) \\ \lambda_3 = \frac{1}{2} & \text{with eigenvector} & (-\sqrt{1 + \frac{2}{\sqrt{3}}}, 1, 0) \end{array} \tag{4.48}$$

The state is indifferent in the pure states with eigenvalues -1. The same result is obtained via multiplicator $f'_{x_c,0}(z_2^{-1}) = -1$. For the first time we detect indifferent behaviour in our chaotic model of quantum dynamics. And we state that the protocol is not capable of convergence to the critical point in pure states. However,

the state is attractive in direction towards mixed states, this can be understood as certain purification. But in experimental realisation the exact evolution can be undeniably influenced by perturbations and lead to undesired evolution. But besides this exceptional value, we have demonstrated the attractivity for all other cases, the last parsing of attractors is a key to prove next proposition.

Proposition 4.6.2. *For arbitrary value $w \in [-1;1]$ except w_c there can be found $x \in [0;\frac{\pi}{2}]$ such that there is pure state $(w,\sqrt{1-w^2},0)$ or $(w,-\sqrt{1-w^2},0)$ which is an attractor of the purification protocol with parameters $x, \psi = \tau = 0$. x value can always be chosen so that the state is a member of attractive length-2 cycle. For $w \in [-1;-w_c)\cup(w_c;1]$ there exists such x that $(w,-\sqrt{1-w^2},0)$ is attractive and fixed, for $w \in [-w_c;w_c]$ no x can be found that state with Bloch coordinate w is attractive and fixed.*

Proof. First lets discuss case of $w = \pm 1$ for which we can choose $x = 0$ for $z = 0, z = \infty$ fixed and $x = \frac{\pi}{2}$ for cycle $z = 0 \leftrightarrow 1$ which match $w = \pm 1$.

Considering $|w| < 1$, we put the mosaic together. We have relation of $z(x) \in \mathbb{R}$ determining attractive cycle for $x \in (x_c;\frac{\pi}{2})$, we also have coordinate transformation 2.38, namely $z(w) = \pm\sqrt{\frac{1-w}{1+w}} \in \mathbb{R}$. For given w let us choose the negative z. For arbitrary $z \leq 0$ except $-z_2^{-1}$ (which corresponds to excluded w_c), a protocol can be found such that z is a member of its attractive 2-cycle. The reason is in 4.46 which can be inverted at cost of high effort. For $z < -z_2^{-1}$ (i.e. $w < w_c$), inverting branch $z = \frac{-1-\sqrt{-2\cos 2x-\cos 4x}}{1+\cos 2x+\sin 2x}$ we obtain

$$x = \operatorname{atan}\frac{1-z^2-\sqrt{1-4z-6z^2-4z^3+z^4}}{2z} \tag{4.49}$$

while for $z_2^{-1} < z$ one has to take

$$x = \operatorname{atan}\frac{1-z^2+\sqrt{1-4z-6z^2-4z^3+z^4}}{2z}. \tag{4.50}$$

With $z > 0$ one could even take x from both branches. But for our cause, we restrict to $z \leq 0$. Combining $x(z(w))$ we can find value x for the protocol which has a state with w for a member of attractive 2-cycle. Because the state is pure by construction and previous finding 4.6.1, one can either use transformation $u(z) = \frac{2z}{1+z^2}$ or relation $w^2 + u^2 = 1$ to verify $u = \pm\sqrt{1-w^2}$ at the same time. Because of the evolution equations 4.27 and the combination of square roots and tangens function, the attractor is $(w,-\sqrt{1-w^2},0)$ when $x \in [0;\frac{\pi}{4}]$ while $(w,\sqrt{1-w^2},0)$ is the attractor for $x \in [\frac{\pi}{4};\frac{\pi}{2}]$. For $x = \frac{\pi}{4}$ the u component is zero. Universal value $v = 0$ is the consequence of the restriction to real z.

Because exact prescription for $x(z(w))$ is of utter bitterness, we do not write it but present its graph 4.6.

If we desire z to be the fixed state and not only a member of 2-cycle, z can be chosen from $(-z_2^{-1};0]\cup(z_2,\infty)$ only. We do not present inverted function $x(z)$ for its extreme complexity, but it exists because it is based on solving a cubic equation. Realising that value w is determined only by z^2 (or $|z|$ if one desires), there are values of w that correspond to $z \in [z_2;z_2^{-1}]$ that cannot be reached. These values satisfy $w \in [-w_c;w_c]$. □

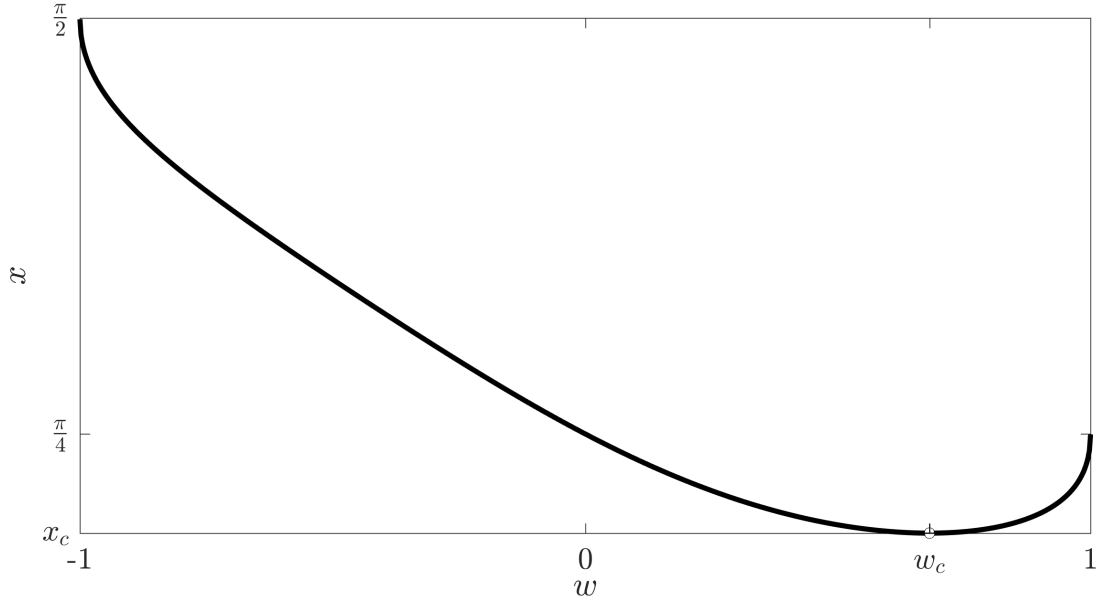

Figure 4.6: Graph of composition function $x(z(w))$ that assigns to coordinate w corresponding protocol parameter x such that one of states $(w, \pm\sqrt{1-w^2}, 0)$ is attractor.

We have now shown that there is a range of states with $|w| < w_c$ for which protocol cannot be found so that an attractive pure state with w and $v = 0$ exists. While the condition $v = 0$ could be seen restrictive, we recall we have determined by derivative analysis that only fixed states and 2-cycles in plane $v = 0$ can be attractive. Therefore, the following is proved.

Proposition 4.6.3. *For all $w \in [-w_c, w_c]$ there is no protocol with $x, \psi = \tau = 0$ such that an attractive fixed state with (w, u, v) exists for some u, v.*

But in spite of this inconvenience we are able to construct a protocol with arbitrary state $(w, -\sqrt{1-w^2}, 0)$ except for $w = w_c$ being the attractor, at the cost of pairwise iterations at worst. The attractive 2-cycles play prominent role in the protocol dynamics.

In the previous section dedicated to the manipulation of the time relaxation we mentioned that viewed physically, the attractor can be changed at cost of change parameters while $\psi - 2\tau$ and x are preserved. These two pieces of information together form a strong statement, one of the most important results of our work.

Theorem 4.6.4 (Protocol universality theorem)**.** *For arbitrary pure state (w, u, v) with $w \neq w_c$, protocol with x, τ, ψ can be found such that the state is attractive.*

Proof. For given state we have to discern case of $w = \pm 1$ for which we can choose $\tau = \psi = 0$ and $x = 0 \vee x = \frac{\pi}{2}$.

In case $|w| < 1$, from previous 4.6 we can find protocol with $x, \psi = \tau = 0$ and attractive cycle $(w, -\sqrt{1-w^2}, 0)$. Recalling the asymptotic equivalence 5.15, we introduce protocol with $x, \psi = 2\tau, \tau$ which is equivalent because $\psi - 2\tau = 0$ for any choice of τ. The attractors of such protocol are modified 4.26 by $\tau_0 = -\tau$ to

$$(w, \pm\sqrt{1-w^2}\cos\tau, \pm\sqrt{1-w^2}\sin\tau). \tag{4.51}$$

When the angle τ is set so

$$\tau = \text{acos}\ \frac{\pm u}{\sqrt{1-w^2}} \tag{4.52}$$

then we have protocol with $x, \psi = 2\text{acos}\ \frac{\pm u}{\sqrt{1-w^2}}, \tau = \text{acos}\ \frac{\pm u}{\sqrt{1-w^2}}$ which has (w, u, v) for attractor. □

The advantage of the proof is that it is constructive. We add a note that the construction may not be unique because there can be other values x yielding the same w and with the principle of asymptotic equivalence other protocols may be found, even such that (w, u, v) is fixed. On the other hand, if one wished for a protocol such that (w, u, v) would be a pure repelling state, there is no such fixed state or cycle with $|z| > z_2$. For this reason, states with $w < -w_c$ cannot be repelling for any protocol.

One could object that the protocol is not universal, we cannot find any x to have (w_c, u, v) for an attractor. But we have to recall that the protocol has another degree of freedom in τ where we can search for a suitable protocol. But another option will be presented in next chapter; therefore, we do not inspect this possibility in detail.

Instead, we can ask ourselves a question, how the fixed states (regardless of the attractive/repelling regimes) of the protocol depend on the twirling parameters. We focus only on mixed states and now present the mixed fixed points for range $x, \tau \in [0; \frac{\pi}{2}]$, we detected them in Mathematica software by solving numerically the fixed state equations $w' = w \wedge u' = u \wedge v' = v$. For the other values of the angles, the points can be found from the symmetries. We have found out that the points lie on approximately but not exactly a conic surface, see 4.7. We have succeeded to determine by fitting numerically obtained coordinates w, u, v of the fixed points that they satisfy relation

$$u^2 + v^2 = w^4 + 3w^2. \tag{4.53}$$

Although we do not have an analytic proof, even to numerically find such relation for the fixed states in a three-dimensional nonlinear dynamics, that is a surprising success. Based on this, we believe that this equation can be obtained by a clever manipulation of the fixed state equations. However, it is too much effort at the moment, without a practical potential. We drop the topic for mathematicians.

The fact that the number of attractors changes when x is changed is another well-known effect of nonlinear dynamics. We illustrate it with a plot of w=$w(x)$ and $u = u(x)$ coordinates of attractors when x is varied.

Now, we turn to another fact that is tightly bound to chaos. For the first time we encounter the effect of bifurcation, well known for example in logistic map, [43] that was first introduced in population models by Verhulst [63, 64]. The bifurcation points are exactly x_b, x_c where the attractivity of the fixed states or 2-cycles changes to indifferent character. Numerically, for $x \doteq x_c$ it can be seen that the all states $z \in \mathbb{C}$ evolve towards a cluster in the vicinity of the state $(w_c, -\sqrt{1-w_c^2}, 0)$ where they stop converging, probably due to numerical precision, and orbit indifferently in the neighbourhood of the fixed point/cycle.

We will discuss the bifurcations in the next chapter where they will become a more prominent phenomenon. At this place, we only warn that this single

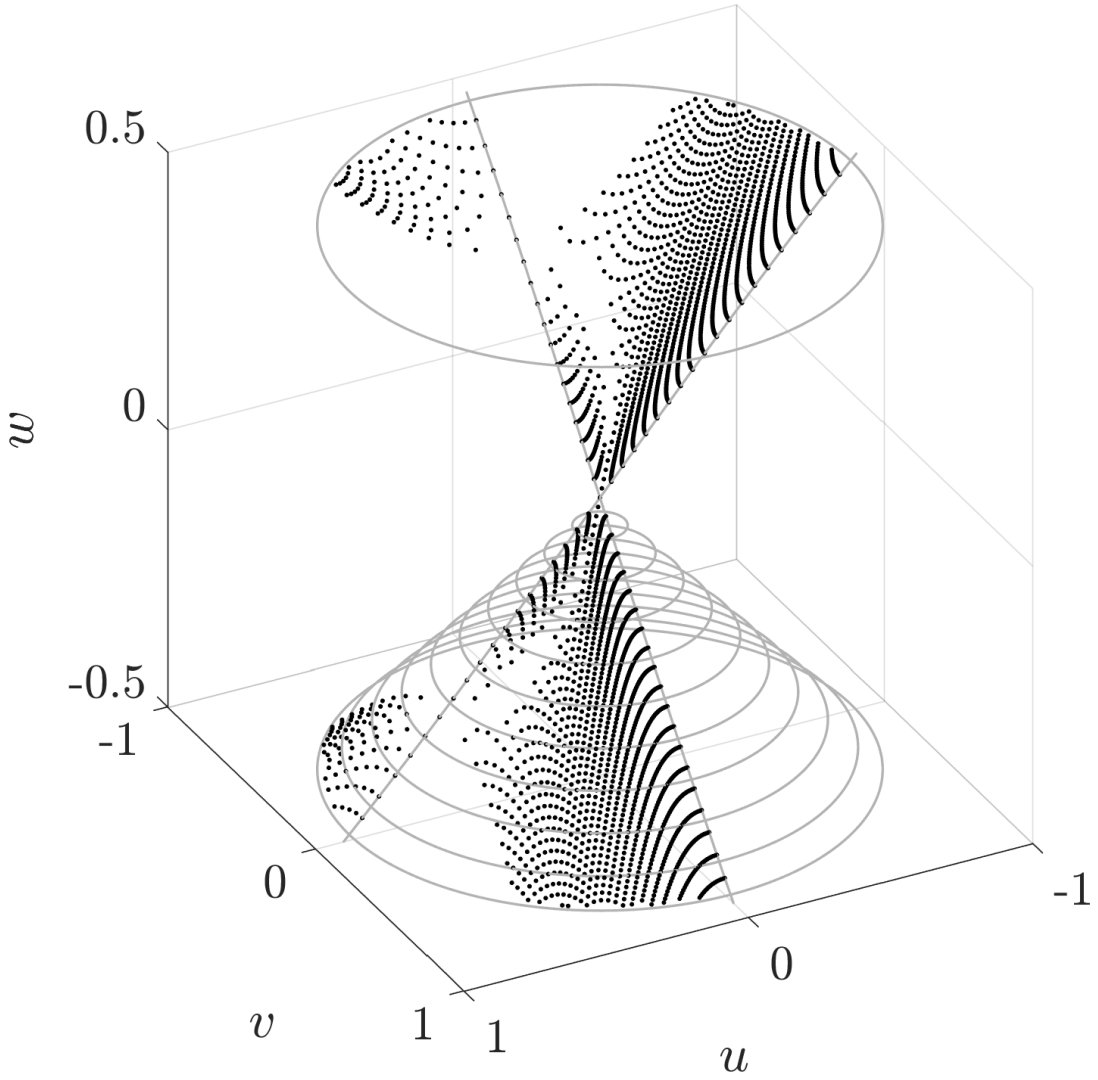

Figure 4.7: The mixed fixed states (in *black*) of all the protocols lie on a conic-like surface $u^2+v^2 = w^4+3w^2$ (sketched in *grey*). States for only $x, \tau \in [0; \frac{\pi}{2}]$ plotted. If plotted for all possible angles, they would stretch over the whole surface.

example of bifurcation is shown when $\tau = \psi = 0$ is taken. When τ is changed, the bifurcation will not only happen at different x but will also lead to different attractor regimes with cycles of various lengths.

We touch now the topic of convergence speed. While the universality theorem claims almost all pure states (truly in Lebesgue style, w_c is a parallel on the Bloch sphere) can be attractive, it does not offer any information about the radius of the basin of attraction, i.e. affordable perturbation that can be corrected by the protocol, and the speed of convergence. For the moment, we just claim that the multiplicator of fixed state or cycle is close to 1 when x to near x_c are used. We can therefore understand the situation in the way that the convergence speed diminishes when attractor with w closer to w_c is required.

Also, the stability is guaranteed in the pure states, it is not guaranteed that the state is attractive for mixed states too. We will answer partially this question in following sections dedicated to dimension and phase transition.

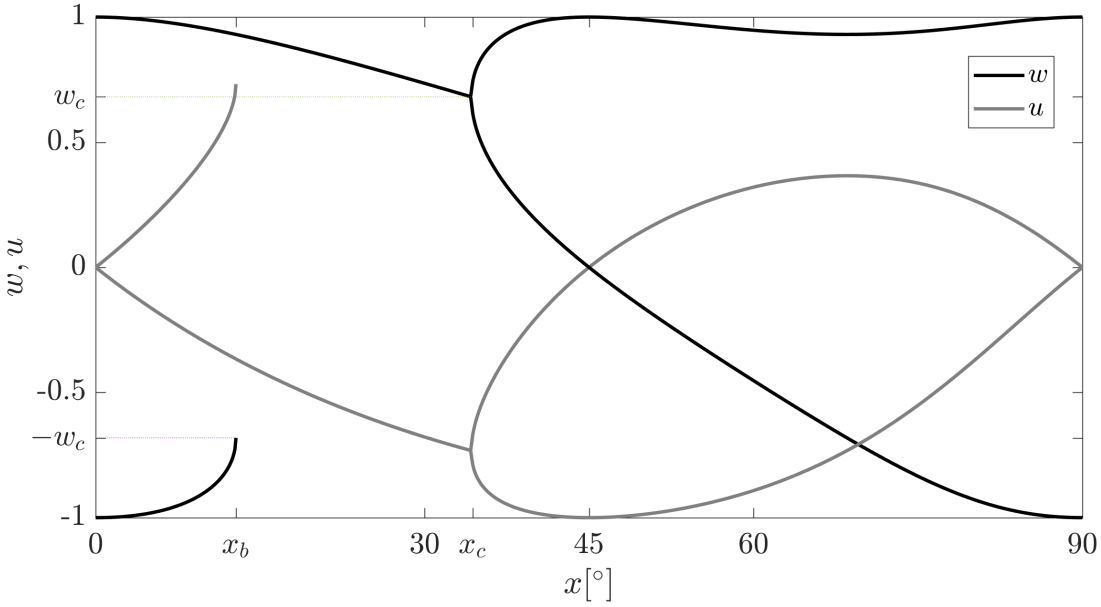

Figure 4.8: Bifurcation of attractors of protocols with $\tau = 0$. Bloch coordinates w, u plotted depending on x. One of the fixed attractor suddenly disappears, the other is split into a cycle.

4.7 Julia set dimension

In the previous chapter we have seen that the evolution function $f_{\pi/4,0,0}$ in pure states has fractal shaped Julia set with dimension $\mathscr{D} \doteq 1.56$, this structure persisted in the dynamics of the mixed states. Now, we would like to know what Julia sets are generated by protocol with general twirling operators. We follow the same approach - we create the attractor maps of Bloch sphere for parameters in range $x, \tau \in [0; \frac{\pi}{2}], \psi = 0$. We detect the Julia set as the border of basins of attraction and apply the box-counting algorithm. For the sake of computational time, we only perform one box randomisation and maximal covering of 5000^2 boxes. In this way we obtain a function $d(x, \tau)$. When an estimate > 2 is obtained (highest value was a single value ca 2.2, other values were typically below 2.05), we treat it as a numerical artefact of the box-counting algorithm and set it to value 2 exactly. Because of the two variables, we code the dimension with colour in the x, τ plane. Results which can be found in the next figure form one of the biggest discoveries of our work.

The first observation is that there is another symmetry. Yes, it emerges only when $\psi = 0$, for that reason we did not mention it earlier. Now, let a protocol with $x, \psi = 0, \tau$ act on state (w, u, v) to get (w', u', v'). When we take protocol with $x, \psi = 0, \frac{\pi}{2} - \tau$ and let it act on state $(-w, v, u)$, we obtain $(-w', v', u')$. The proof is based on fact that permutation $u \leftrightarrow v$ and sign change $w \to -w$ causes $U \to -U, W \to -W$ but $V \to V, N \to N$. At the same time the change $\tau \to \frac{\pi}{2} - \tau$ causes $\sin\tau \leftrightarrow \cos\tau$. All these changes put into equations 4.27 give the sign change of w and swap u with v. When one would like to improve this symmetry to general ψ, they could compose this symmetry with the time relaxation manipulation - after setting $\psi = 0$, than using this symmetry and then use the time relaxation again to restore ψ. But, although the fractal structure

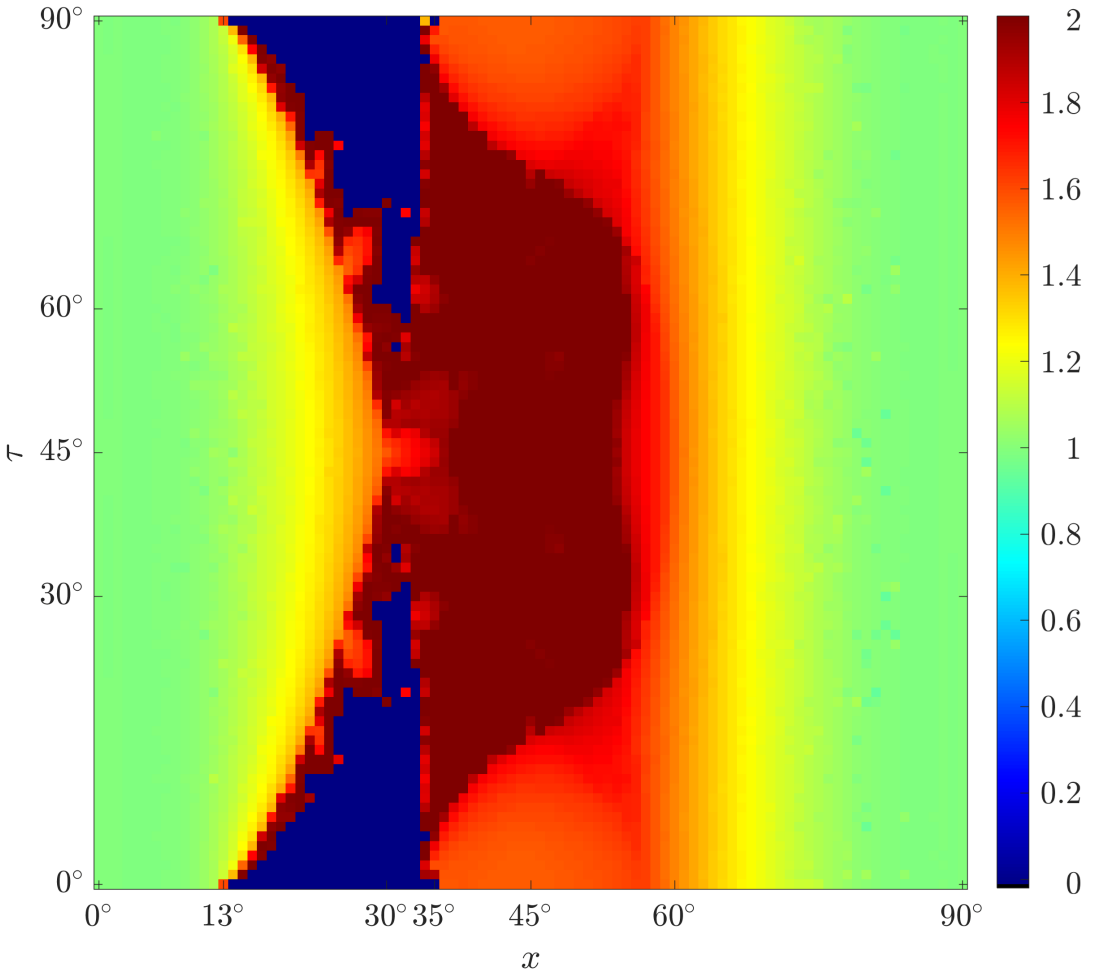

Figure 4.9: Dimension $d(x, \tau)$ of Julia set for protocols with arbitrary x, τ coded in colour. Generalised Mandelbrot set consists of points with $d(x, \tau) \geq 1$, that is, pixels of red - yellow - green tones. Dark blue pixels stand for protocols where no structure was detected by the box-counting algorithm.

would be the same, the executed time changes induce a shift in the input/output states. I.e. the attractor maps of such conjugate protocols are flipped upside down, flipped left to right and shifted by some φ and also the colours are shifted, this transformation is not obvious, at least not at the first sight. But we can exploit this last symmetry to reduce parameter range to $\tau \in [0; \frac{\pi}{4}]$.

Even more interesting observation in 4.9 is that there is a metastructure, the function $d(x, \tau)$ seems to create fractal shape on itself. This is similar to existence of Mandelbrot set, 2.47. The Mandelbrot set is based on dichotomy of Julia sets that are connected/totally disconnected which is equivalent to bound/unbound evolution of critical point 0, 2.3.33. We are unable to give similar proposition for rational polynomial functions of our case. But instead, we have another observation. In 4.9 there is an area where no structure is detected. This is not because the Julia set would be empty - for functions of degree ≥ 2 the Julia set is nonvacuous, 2.3.17. But we now testify that our approach based on the edge detection of the fractal structure A has critical disadvantage. While it works well to find fractal structures which are connected, or at least behave as connected

when handled numerically, we encounter problems when Julia set is discontinuous, when it is Cantor dust [40] - chaotic states cannot be detected by our approach because the Julia set is numerically unstable on (forward) iterations. This can lead to wrong dimension estimate $d(x, \tau) = 0$. On the other hand, it has its advantage because parameters for which the Julia set numerically behaves as totally disconnected are automatically highlighted in the plot of $d(x, \tau)$.

Because all the dimension estimates obtained in 4.9 (whenever a structure was detected) were either ≥ 1 or were very close to this value and visual control suggested that the lower value was only a numerical artefact of imperfect box-counting method, we decided to perform following refactorisation: the points with dimension estimate < 1 were set to 1 precisely, points where no structure was detected were assigned black colour. In this way we have reduced the colour range to $d(x, \tau) \in [1; 2]$ which allows to visually perceive better details of the fractal metastructure, see 4.10.

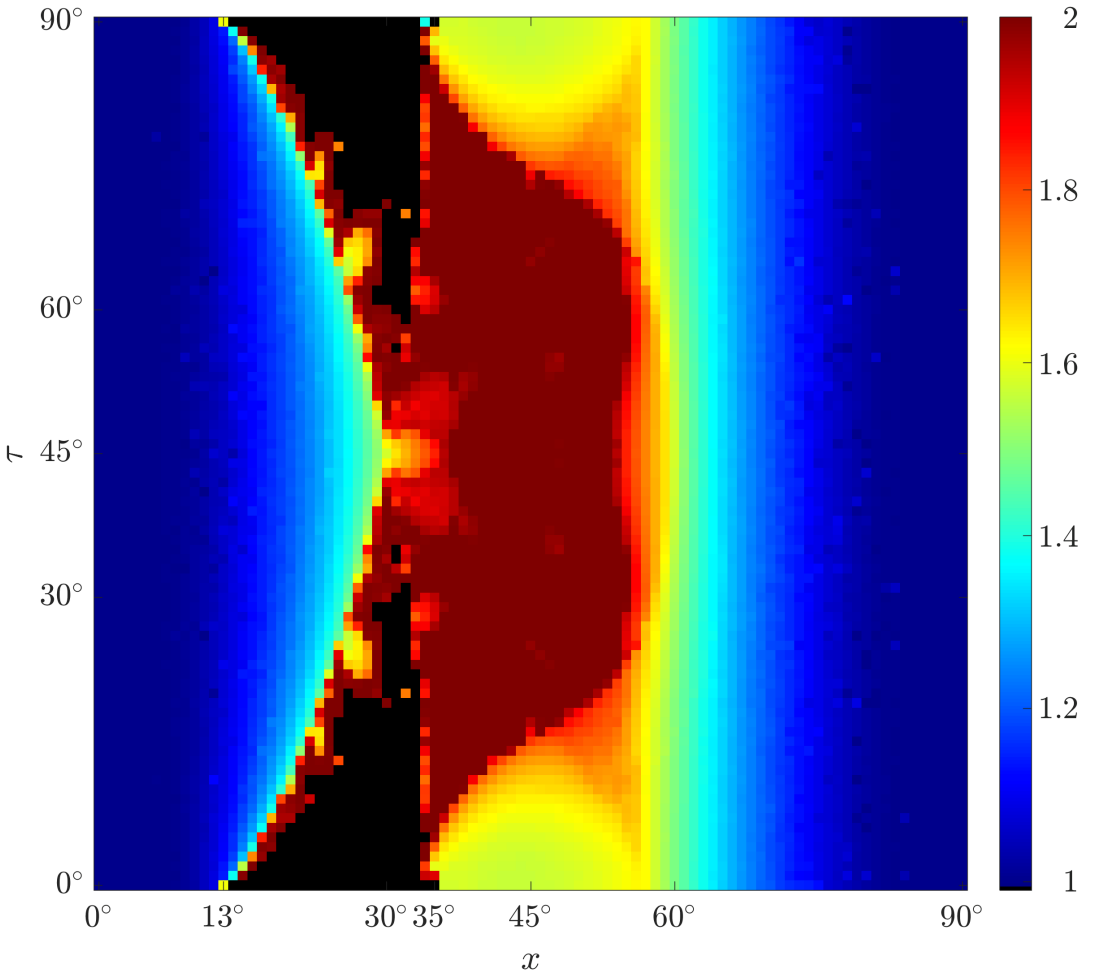

Figure 4.10: Dimension $d(x, \tau)$ with refinement of colours to highlight fine structure. All values $d < 1$ were artificially set to 1.

The Mandelbrot set is defined for quadratic functions as a set of parameters for which the Julia set is connected. We now propose its generalisation for our evolution maps 4.35. Our theoretical instruments are limited, we restrict ourselves to numerical analysis, therefore we will build next definition on the second box-

counting approach from A.

$$\widetilde{\mathcal{M}}=\left\{(x,\tau)\in\left[0;\frac{\pi}{2}\right]^{\times 2}\middle|\,\mathcal{J}(f_{x,\tau})\text{ has box-counting dimension estimate}\geq 1\right\} \tag{4.54}$$

Let us take the protocols with $\tau = 0$ and $x \in (x_b; x_c)$. These have a single attractor, fixed state. Working numerically, all states will be found to converge to the attractor which leads us to $\{(x,0)|x_b < x < x_c\} \not\subset \widetilde{\mathcal{M}}$. As soon as there are two attractive points or a cycle with two disjoint parts of Fatou set separated by (therefore connected) Julia set, the connectedness requires dimension ≥ 1. Therefore, $\{(x,0)|x < x_b \vee x > x_c\} \subset \widetilde{\mathcal{M}}$. More general situation for $\tau \neq 0$ has not been analysed in detail and is left to numerical calculations. It is suggested to us in analogy to Mandelbrot set:

Conjecture 4.7.1. *$\widetilde{\mathcal{M}}$ is compact, $\partial\,\widetilde{\mathcal{M}}$ is fractal.*

At the moment we do not have instruments to proceed with this conjecture and we propose it to be a subject to further studies. Our finding that such structure exists is already very interesting, let us look at another properties.

We can see from 4.9 that there are regions of very similar colours. This signalises that the dimension of the corresponding fractal does not change suddenly. Such situation happens e.g. near $x = \frac{\pi}{4}, \tau = 0$ which is the known case related to entanglement purification. But then there are sudden changes to the structure, i.e. when $\tau \doteq 12°, x \doteq 20°$ is changes slightly. We could again speak of a phase transition but we have found that there is already a concept called *J-stability*, [42, 24]. In this concept families of functions are studied depending on parameters. J-stability means that the Julia set is deformed in a continuous manner when the parameters are changed. We observe such behaviour. However, the change of the Julia set is related to conjugation of functions in the sense 2.3.2, we have not found such conjugation map so far.

4.8 Protocol robustness

The fact that Julia set is typically J-stable when x, τ are changed is vital for practical realisation of the protocol. The stability of the Julia set implies that the protocol is resistant to imprecision in physical realisation of the gates. So far, we have discussed only perturbations to the input states but the gates are also physical objects realised only with certain fidelity. We want to claim

Statement 4.8.1. *Purification protocol with $x = \frac{\pi}{4}, (\psi =)\tau = 0$ is robust to perturbation of gates, i.e.*

$$(\exists\varepsilon_0, \delta_0 > 0)(\forall\varepsilon < \varepsilon_0)(\exists\delta \geq \delta_0)(||U - H_2|| < \varepsilon \Rightarrow t(U[\rho]^\infty, |0\rangle) < \delta) \tag{4.55}$$

Of course, this statement has limitations, therefore we do not dare to call it a proposition. We rather want to suggest the idea fo the would-be proposition. First, we do not give precise relation between ε and δ and boundaries on maximal ε_0, δ_0. Exact proof of mathematical style needs to consider some operator norm $||.||$ which probably could be chosen convenientely. And also a detailed analysis

of dynamics in mixed states, like we did in previous chapter. We substitute this approach with numerical instead. But before we do so, we mention more general case. In realistic physical scenario, the gate can be perturbed differently in each step of the protocol iteration. Therefore we come up with stronger statement:

Statement 4.8.2. *Purification protocol with H_2, i.e. $x = \frac{\pi}{4}, (\psi =)\tau = 0$ is robust to time-dependent perturbation of gates. Let us mark U_i the twirling gate of i-th iteration.*

$$(\exists \varepsilon_0, \delta_0 > 0)(\forall \varepsilon_i < \varepsilon_0)(\exists \delta_i \geq \delta_0) \tag{4.56}$$
$$((\forall i \in \mathbb{N})(||U_i - H_2|| < \varepsilon) \Rightarrow t(\dots U_i[\dots U_1[\rho]\dots]\dots, \mathcal{A}) < \delta)$$

We remind that $\mathcal{A}$ is the pure attractive cycle $|0\rangle \leftrightarrow |0\rangle - |1\rangle$, the distance is meant in the sense of the closest distance to any member of the cycle. We support the statement with following numerical observations. For easier orientation, we express x, τ in degrees.

- When $x \in [35°; 55°], \tau \in [-10°; 10°]$ was uniformly and independently chosen for each iteration, all pure states converge to one of two possible regimes, analogue of parity 2-cycle that evolves chaotically in time.
- When $x \in [30°; 60°], \tau \in [-15°; 15°]$ was uniformly and independently chosen for each iteration, all pure states converge to a single unique regime (cycle, with different parity regimes), this analogue of fixed point evolves chaotically in time. This is probably caused by the fact that at some point, a protocol is chosen with a single fixed attractor, that is the area marked in 4.10 with the black colour to be $\not\subset \widetilde{\mathcal{M}}$.

Thanks to this observation we limit ourselves to watch only orbit of e.g. $|0\rangle$. We introduce parameter Δ to characterise random twirling: x is chosen uniformly and independently from interval $45° \pm \frac{\Delta}{2}$, τ from $0° \pm \frac{\Delta}{2}$ and we restrict to $\Delta \leq 10$ to guarantee $x > x_c$, so the dynamics would globally evolve to a 2-cycle. We conclude that under these conditions the orbit behaves similarly to the cycle $|0\rangle \leftrightarrow |0\rangle - |1\rangle$. The points jump across approximately rectangular areas on the Bloch sphere, see 4.11. We aim at describing maximal deviation of the state from $|0\rangle$ for given Δ. For that we perform 10^6 iterations and from the even parity branch (when the state is close to $|0\rangle$) we calculate trace distance of the orbit point ρ_n from the initial state (and desired attractor), $t(\rho_n, |0\rangle\langle 0|)$. Maximal value obtained for all even $n \in \cdot 10^6$ is assigned to value Δ. The following figure represents a certain form of numerical stochastic proof to previous statements. Although, the norm, distance between operators is not defined in a traditional way and is left to rather easy than reasonable concept of changing parameters x, τ. The conclusion from the numerical results can be made as already said, the protocol with H_2 is robust not only to perturbation of the initial pure state but also to the perturbation in the twirling gate realisation.

We recall that the concept of J-stability tells that there are regions in the Mandelbrot set where the Julia set is continuously changing. The same effect seems to manifest here; it results into bounds on the state evolution. When a threshold of 'small' deviation in the twirling gate is exceeded, the rectangular shaped areas not only dissolve but the attractor regimes and fractal structures change suddenly which results into random evolution over all the Bloch sphere.

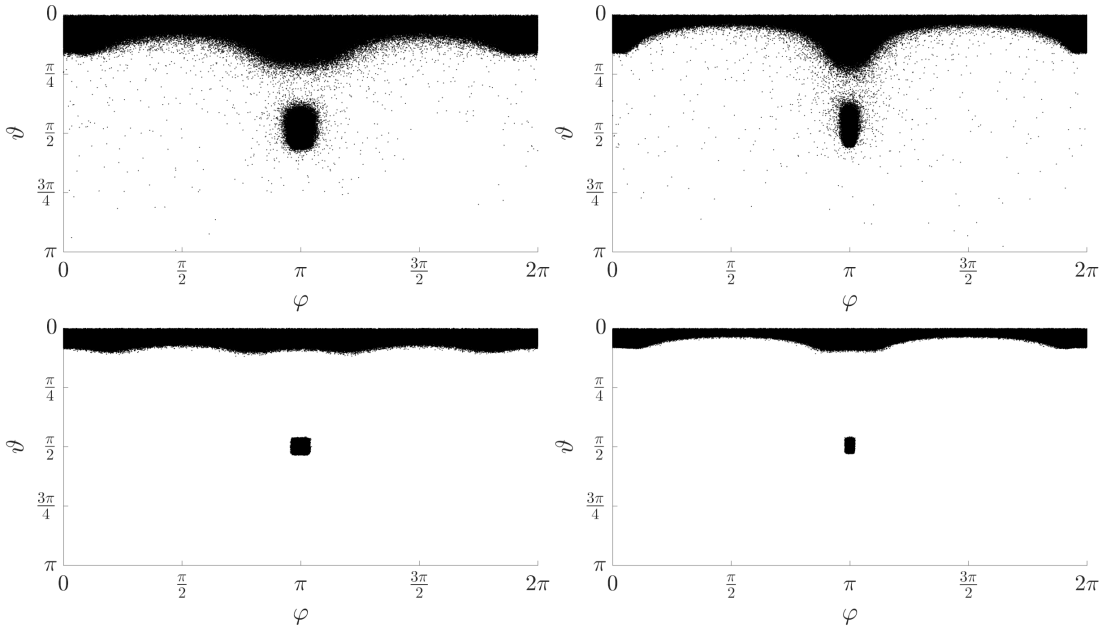

Figure 4.11: Range of x, τ sets limits on scattering of state's evolution. 10^6 iterations of $|0\rangle$ plotted on the Bloch sphere, in spherical coordinates 2.38. *Left top* $x \in [35°; 55°], \tau \in [-10°; 10°]$, *right top* $x \in [35°; 55°], \tau \in [-5°; 5°]$, *left bottom* $x \in [40°; 50°], \tau \in [-10°; 10°]$, *right bottom* $x \in [40°; 50°], \tau \in [-5°; 5°]$.

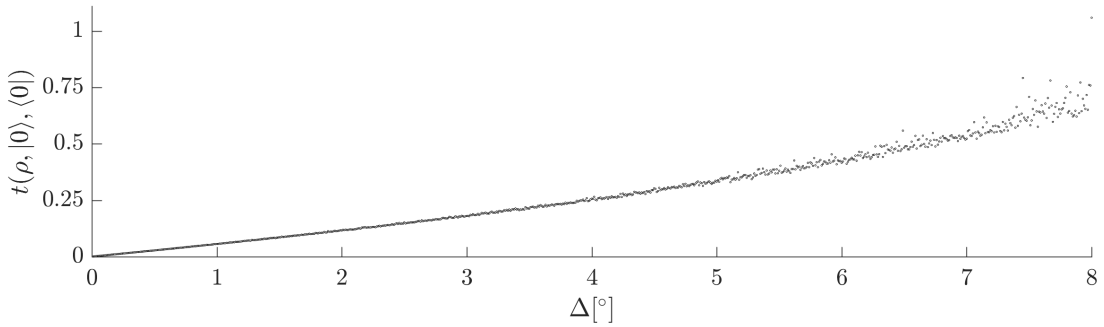

Figure 4.12: Maximal distance of $5 \cdot 10^5$ pairs of iteration of state $|0\rangle$ with random twirling with $x \in [45° - \frac{\Delta}{2}; 45° + \frac{\Delta}{2}]$, $\tau[-\frac{\Delta}{2}; \frac{\Delta}{2}]$.

Still, the orbit typically seems to form clusters near the unperturbed attractor. It is probably no surprise that twirling chosen with arbitrary random parameters x, τ make the state evolve chaotically over the Bloch sphere. Such a case is of no practical importance unless we wish to create a random state generator. But of course, to guarantee that the twirling gates are chosen randomly enough, that is probably even more difficult than to prepare a random state.

We have not yet explicitly spoken of the mixed states. The pure states remain pure, the unitary twirling regardless of the perturbation also preserves the purity. It could be possible that the mixed states could be driven towards the maximally mixed state. When we remember we estimated radius of basin of attraction, it is probably not surprising that numerical calculations confirmed that when the twirling is close to the original gate in the sense of close values of x, τ, the same behaviour - converging to chaotically evolving pure cycle - was verified even for mixed states from vicinity of $|0\rangle$.

We conclude based on numerical evidence:

Statement 4.8.3. *The protocol with $x = \frac{\pi}{4}, \psi = \tau = 0$ is robust to perturbations both of the state and the twirling gate.*

4.9 Atlas of attractor maps

In figure 4.9 there are also other clear areas of similar fractal dimension than the neighbourhood of H_2. These correspond to fundamentally different fractal structures induced by other protocols. We now offer a very brief excerpt from an atlas, a selection of attractor maps, typical representatives of fractal structures so that readers get some impression of what structures can be encountered. All maps are for pure states, Bloch sphere.

We discern five basic types of structures. The first is similar to the case of $x = \psi = \tau = 0$ - in this case the sensitive states form an equator on the Bloch sphere, a one-dimensional object. For increasing x the shape of the set seems to be continuously deformed. The sensitive structure probably remains connected and separates two basins of attraction. We cannot confirm visually whether the object is indeed a fractal or a one-dimensional object, though very deformed. The dimension estimate is very close to 1 but that can be both because the shape is fractal and because of numerical artefacts of the box-counting algorithm.

The next type of typical structure is the disconnected Cantor dust which we already acknowledged. This structure emerges e.g. for $x \in (x_b; x_c), \tau = \psi = 0$. All pixels in the attractor maps converge to the unique dynamical regime of the map and while points of the Julia set cannot be numerically captured. Because the box-counting algorithm based on edge detection cannot succeed, we used the approach with inverse iterations to verify and estimate the dimension. Choosing $x = \frac{\pi}{6}, \tau = 0$ we calculated backward iterations by un-twirling

$$\sin 2x\, w' + \cos 2x\, u' = \frac{u^2 - v^2}{1 + w^2}, \sin 2x\, u' - \cos 2x\, w' = \frac{-2w}{1 + w^2} \tag{4.57}$$

and then using the inverse map that has already been found 3.24, 3.25. After we had chosen a point on the Bloch sphere, we calculated 10 backward iterations, from these points we chose randomly only a quarter of them and iterated these

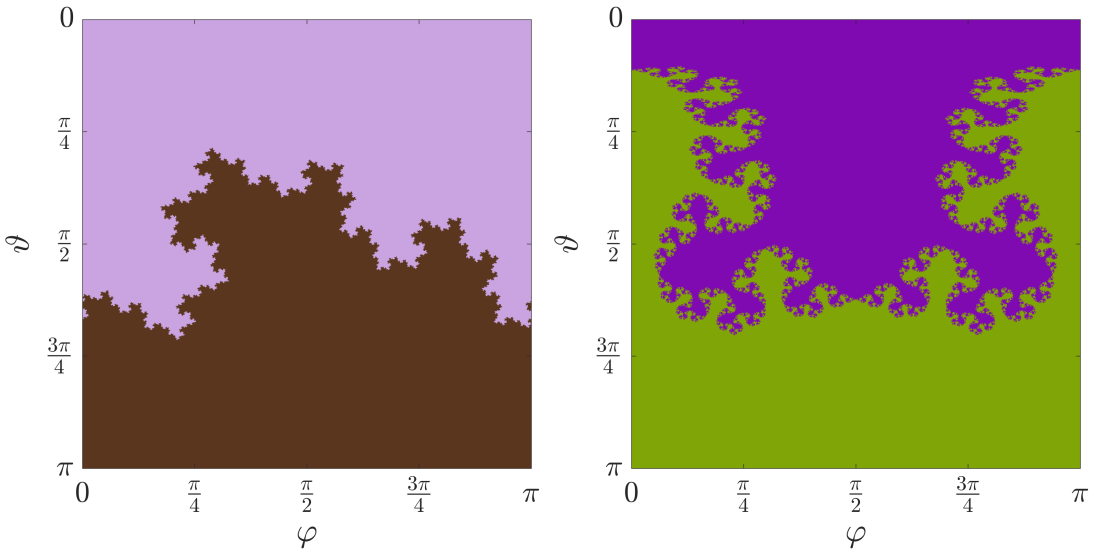

Figure 4.13: Attractor maps of fractals separating two regions. *Left*: $x = 24°, \tau = 45°$, *right*: $x = 56°, \tau = 90°$.

backwards 22 more times. Ca $4 \cdot 10^6$ obtained points were processed with the third box-counting algorithm based on rounding. The result $d(\frac{\pi}{6}, 0) = 1.408 \pm 0.004$. This result is very interesting because the structure which is visually disconnected and also shattered beyond the resolution of one of our box-counting approach; yet the structure is so complicated that its dimension exceeds 1. This means that the fractal proliferates through the pure states so that it is more complicated than a line. It is structurally much closer to the fractal studied earlier for H_2 than to any ordinary curve. The calculated dimension estimate is probably valid for the whole region, similarly to the case of J-stability near H_2 where value $\mathscr{D} \doteq 1.56$ changed only slightly.

At this place we arrive to a very troubling conclusion. There are fractals that cannot be captured and estimated by our box-counting algorithm based on the `edge` command. It is for the reason that a disconnected repelling structure cannot be numerically reached. The alternative and the usual way to obtain the Julia set cannot generally be used for the analysis inside the Bloch ball of mixed states. We have discovered inaccessible states earlier for the protocol H_2, 3.4.1. It is highly probable that the structure of sensitive states cannot be captured by any numerical means. We decided to use backward iterations for input state $(0.01, 0.01, 0.01)$ and we converged close to the Bloch sphere, to purity values $P > 0.87$ after 30 iterations. Although this finding imposes severe limitations to future numerical research, we will find out later in the section about the phase transition that even for the Cantor dust in pure states the box-counting is able to detect the fractal structure in the mixed states where fractal shaped islands form that are basin of attraction of the mixed attractor. In this point of view, the case of pure states may be viewed as an exceptional. But still, the numerical results must be accepted only as approximative and possibly burdened with computational artefacts.

The third type of structure is in a sharp contrast to the Cantor dust, the basins of attraction entangle into each other in a complicated way and their borders grow through the space. They can fill a majority of the attractor map, this results into

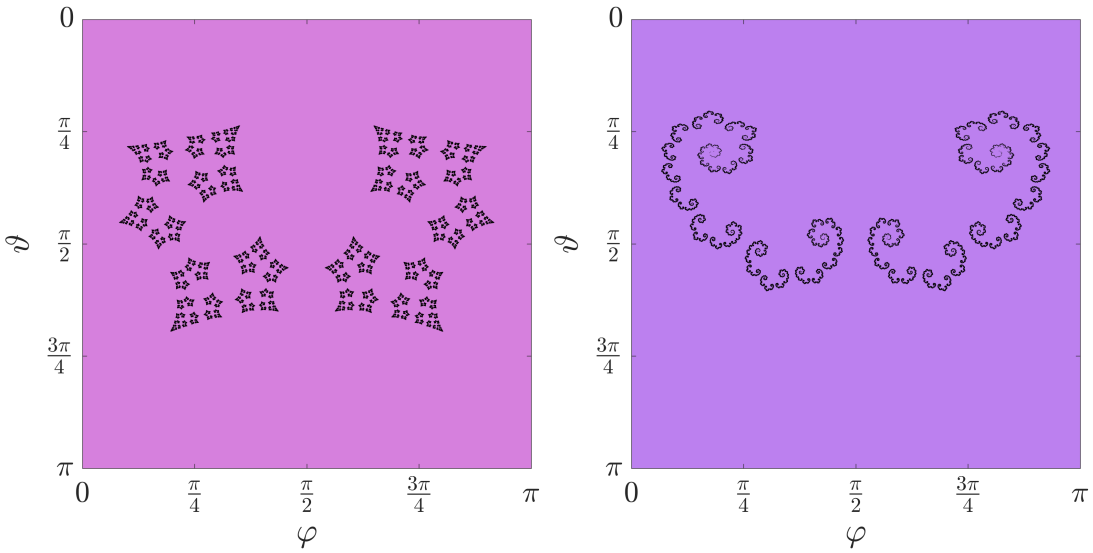

Figure 4.14: Attractor maps with Cantor dust. The Julia set points obtained by backward iterations marked in black. *Left*: $x = 30°, \tau = 0°$, *right*: $x = 18°, \tau = 0°$.

resemblance of white noise. The concept of white noise would be obtained if each point would evolve randomly, i.e. each state is sensitive. The corresponding structure fills the space completely and so has Hausdorff dimension equal to 2. Such structure is an extremal case to all structures in two-dimensional space. The structure does not have to be connected or possess any other convenient properties but can be formally assigned area. An example of two-dimensional disconnected structure are pairs of rational numbers, $\mathbb{Q}^2$. During writing of our thesis, a paper was published,[25], where a particular case of $x = \frac{\pi}{4}, \psi = \frac{3\pi}{2}, \tau = 0$ and pure states is shown in framework of Latté maps. The action of map

$$f_{\pi/4,3\pi/2,0}(z) = \frac{z^2 + i}{iz^2 + 1}, \tag{4.58}$$

induces dynamics that is exponentially sensitive at any point of the Riemann sphere $z \in \mathbb{C}$ which results into white noise, $\mathcal{J}(f_{\pi/4,3\pi/2,0}) = \mathcal{C}$. Figure 4.15 suggests that similar effect can be present to not only the single choice of parameters. However, the proof in [25] relies on conjugation of functions which is extremely difficult in general cases. Our work intends to focus more on the dimension of the structure, therefore we leave this topic to future research. At this place, we only comment that our numerical approach based on the box-counting idea must be taken precautiously. It is also possible that the dynamics is so diverging in the vicinity of the Julia set that the points are significantly deviated by computational precision. Or it may be also possible that the Cantor dust structure spreads through the space that it seems to turn to the white noise case.

As a special case of these seemingly white noise maps we present a map in 4.15 that seem to consist of lakes of white noise and islands of stability. In spite that visual appearance suggests such possibility, it is forbidden by proposition 2.3.28. The Julia set cannot have both regions of stability and regions of chaos. In this case the shape of the Julia set is very complicated so numerical calculations cannot capture it but the Julia set must be composed of fractal curves or Cantor

dust only.

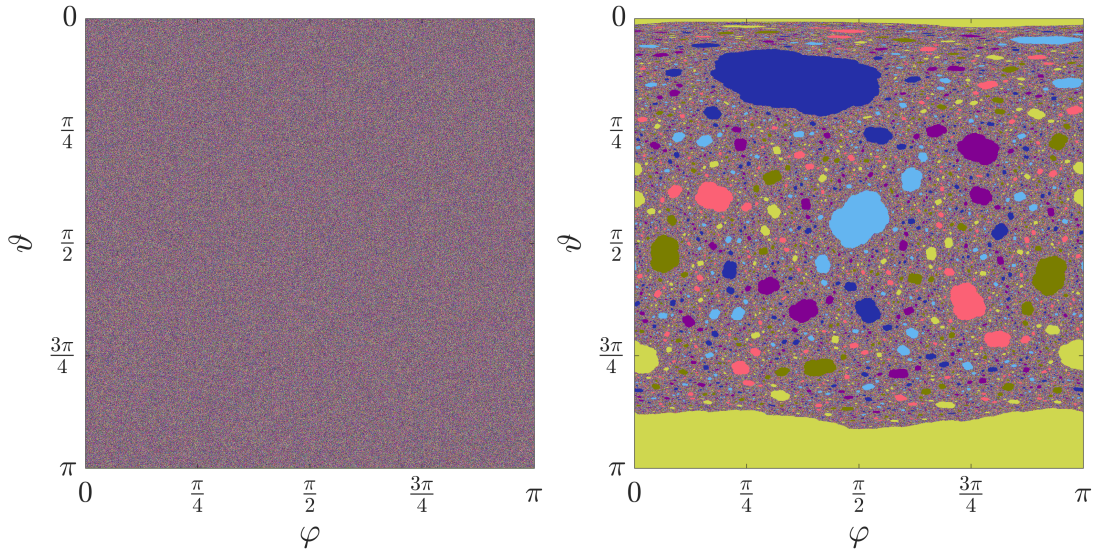

Figure 4.15: Attractor maps resembling white noise. *Left*: $x = 45°, \tau = 30°$, *right*: $x = 54°, \tau = 41.5°$.

The fourth type of structure can be represented e.g. by the known case $x = \frac{\pi}{4}, \tau = 0$. The fractal forms borders between recurring islands of basins of attraction (corresponding to regimes of even-odd convergence). These islands can be deformed and twisted, but their structure is preserved in certain range of parameters.

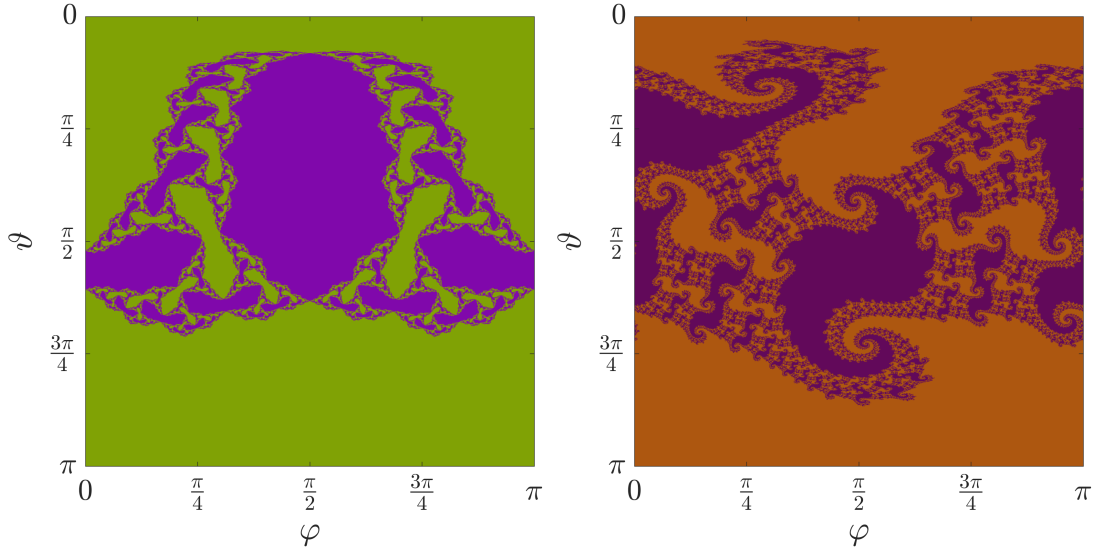

Figure 4.16: Attractor maps with recurring islands of basins of attraction. *Left*: $x = 56°, \tau = 90°$, *right*: $x = 36°, \tau = 84°$.

The last and probably the most appealing type of structures are the most complicated. These are transitions amongst previous cases. Typical features of this type are spiral-shaped whirls. The spiral arms can be different in number and size. The transition from one type of the structure to another happens by distortion of the structure type, the shape is suddenly twisted and stretched to

spiralling objects which proliferate across the Bloch ball. Then they dismantle into Cantor dust or refactor to regular islands again. The orientation of the spiral whirl changes often in the transition.

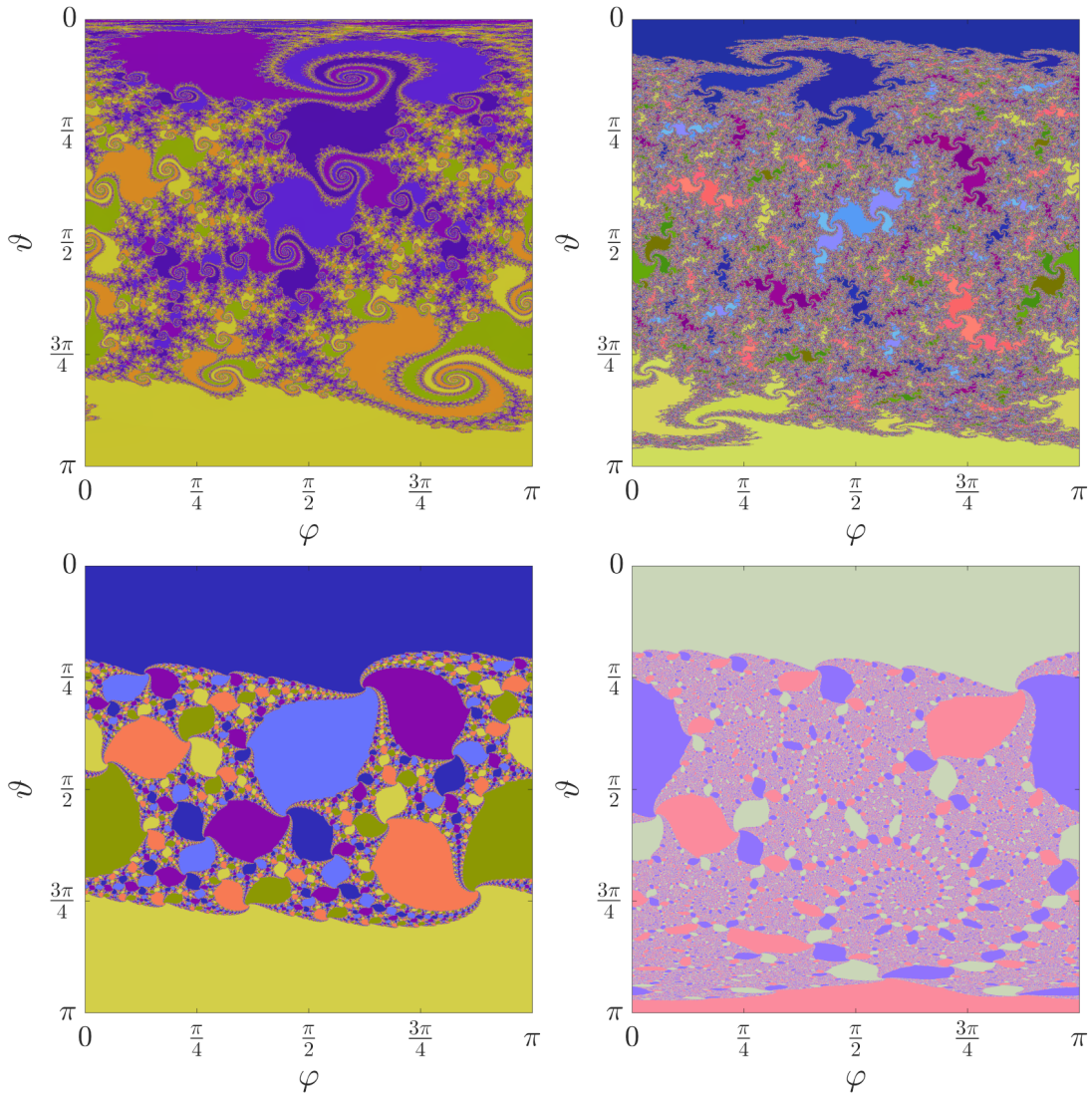

Figure 4.17: Fractal structure suddenly changes, switching amongst previous types. *Left top*: $x = 56°, \tau = 64.75°$, *right top*: $x = 54°, \tau = 45°$, *left bottom*: $x = 58°, \tau = 45°$, *right top*: $x = 32°, \tau = 48.5°$.

From the numerical analysis, we find out that the transition matches with ocurrence of the bifurcations. During the transitions, a cycle of certain period can split into cycles of longer/shorter periods. The spirals change their number of arms in these bifurcations. After the spirals disentangle, islands of a wide variety of colours can remain, the length of the attractive cycles is not in principle restricted. There is an effect called period-doubling well known for the logistic map, [43] during which the cycle splits to new cycles with double period. We find its analogue in our protocols now, although the lengths of the cycles can vary significantly. In figure 4.18 we show such bifurcating transition from cycle with period 7 and one fixed point for protocol with $x = 28°, \tau = 34.15°$ to a cycle with period 17 and single fixed point for protocol with $x = 28°, \tau = 35.55°$. It is possible that a dominant effect of bifurcation is that one member of

the cycle is split in two but it is possible that the splitting may be much more involved. The evolution near the bifurcation angles is very involved and we do not dare to specify some patterns in it. But the presence of bifurcations is a very interesting phenomenon on its own. The structure-shattering effect accompanying the bifurcations also seem to separate regions we connected to the concept of J-stability a while ago, the transition amongst the stable regions is very violent and sudden with a typical feature of slow convergence of the evolution requiring thousands of iterations to determine the asymptotic evolution reliably.

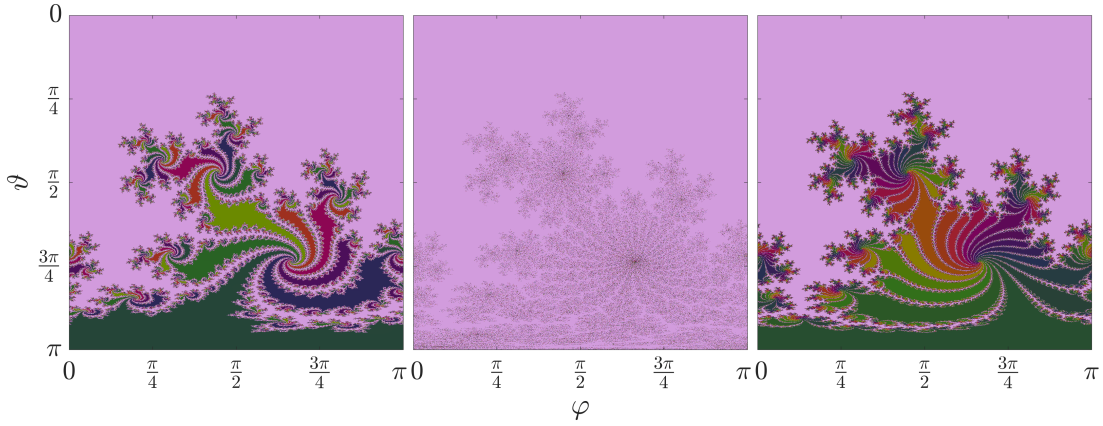

Figure 4.18: Fractal structure is shattered to reconstitute into a cycle of different period. All attractor maps with same axial system taken for $x = 28°$. *Left*: $\tau = 34.15°$, *centre*: $\tau = 35°$, *left*: $\tau = 35.55°$.

4.10 Phase transition

New protocols and new fractal structures bring a new question - was the phase transition - i.e. the sudden drop of the fractal dimension with decreasing purity - an unique phenomenon for the particular twirling gate H_2 or is its ocurrence a general feature of chaotic dynamics in purification protocols? We have seen that not only dimension $d(P)$ - which now can be straightforwardly extended to $d(P; x, \tau)$ to respect parameters of the new protocols - exhibits interesting behaviour. We recall the mean entropy 3.41 which now can be also extended to $e(P; x, \tau)$ for protocols with corresponding twirling gates. We focused mainly on protocols with $\tau = 0$, therefore we only consider now on $e(P; x, 0)$, when we code the value e with colour plotted in axes x, P. We remind that thevalue of ψ is not important because this degree of freedom is eliminated by the asymptotic equivalence 5.15. Let us first look at the $e(P; x, \tau)$ restricting ourselves to $\tau = 0$. Then, being a two-variable function, we can code its value with colour in the x, P plane.

We have argued that for $x = \psi = \tau = 0$ the two attractors attract all states except for plane $v = 0$. In other words, all states were numerically (and in consequence also must be experimentally) purified. To our big surprise this behaviour is quite common; there is a wide range of x (with $\tau = 0$) bordered with values approximately equal to $21.85°, 60°$ in which the transition of exponential trends of $e(P)$ occurs. Also, in other words, the protocols can fail to purify certain

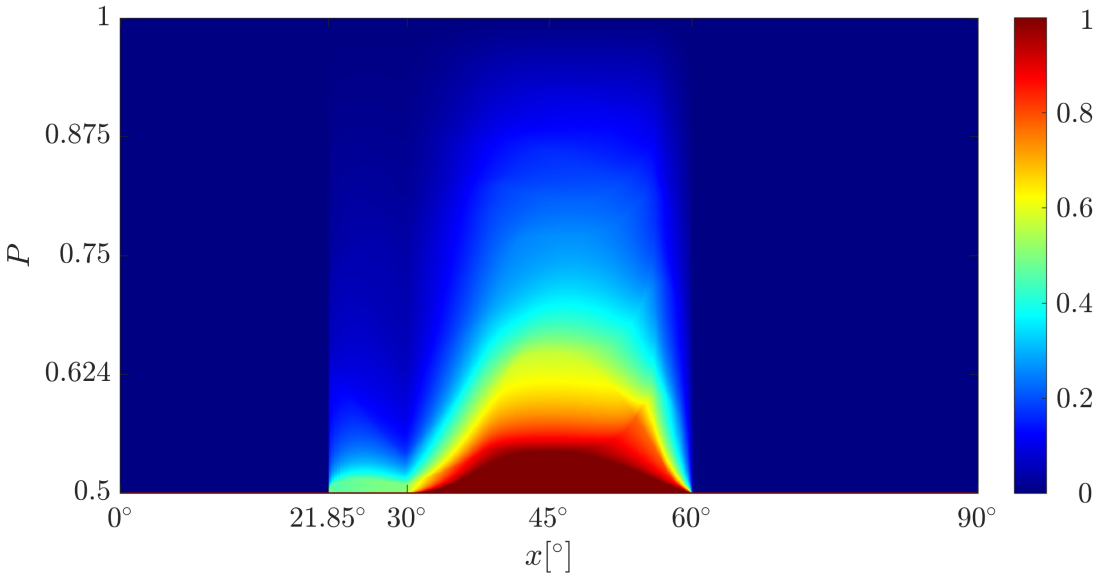

Figure 4.19: $e(P; x, 0)$, coded in colour.

initial states when $21.85° \doteq x_k \leq x \leq 60°$ while outside this interval it is capable of experimentally purifying all states except for $\mathbb{1}$. We now present for better comprehensibility a plot in style of the previous case of $x = \frac{\pi}{4}$ to demonstrate the piecewise exponential trends of $e(P)$ which are generally present.

Inside the interval $x \in [21.85°; 60°]$ where the protocol can fail, there seems to be one exceptional value $x \doteq 30°$. When we realise that the fixed state must be repelling to be numerically unstable, we raise a question about its stability. We can recall the Jacobi matrix 4.40. In case of $(\psi =)\tau = 0$ and evaluated at the maximally mixed state $w = u = v = 0$ we find surprisingly simple eigenvalues and eigenvectors:

$$\lambda_1 = 2\cos 2x \text{ with } (-2\frac{\cos 2x}{\sin 2x}, 1, 0);\ \lambda_{2,3} = 0 \text{ with } (0,0,1), (0,1,0) \tag{4.59}$$

The maximally mixed state is therefore superattracting in the $w = 0$ plane directions for all x. However, the superattractivity is granted in the last direction only when $x = \frac{\pi}{4}$. Solving the equation $|2\cos 2x| = 1$ to find indifferent states, we arrive to following conclusion:

- $x = \frac{\pi}{6} \vee x = \frac{\pi}{3}$

  $\mathbb{1}$ is indifferent.

- $x < \frac{\pi}{6} \vee x > \frac{\pi}{3}$

  $\mathbb{1}$ is repelling. It belongs to the structure of sensitive states.

- $\frac{\pi}{6} < x < \frac{\pi}{3}$

  $\mathbb{1}$ is attractive.

Because in interval $x \in \left(x_k, \frac{\pi}{6}\right)$ the protocol can fail as can be seen from $e(P; x, 0) > 0$ in 4.19, there are states that do converge neither to pure states nor to $\mathbb{1}$. We have just discovered an exciting fact.

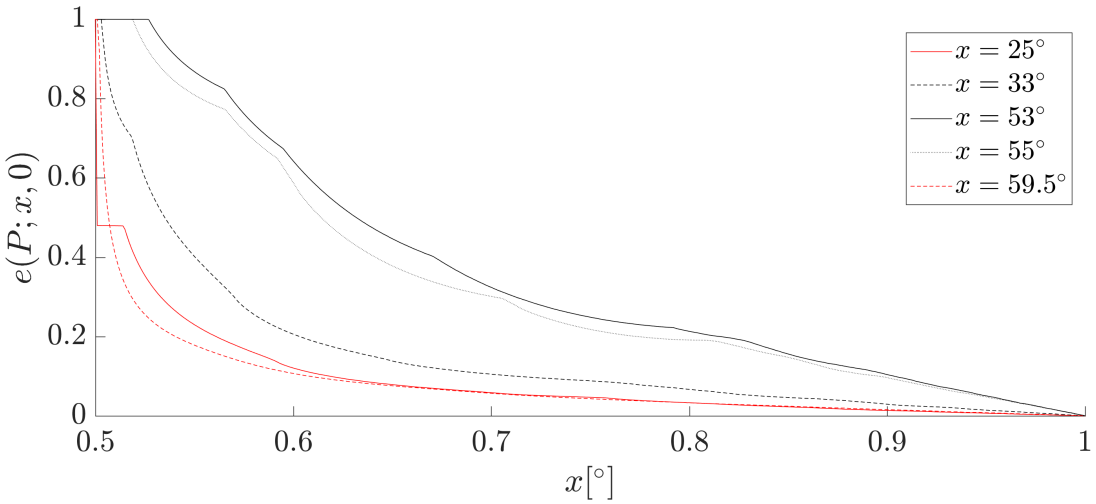

Figure 4.20: $e(P;x,0)$ for specific values of x. Exponential trends remain characteristic.

Theorem 4.10.1. *There are protocols with mixed attractors, different from* $\mathbb{1}$.

Proof. We show an example. Choosing $x = 27^\circ, \tau = 0^\circ$ we have found fixed state $w \doteq -0.07011936, u \doteq 0.12167875, v = 0$ which has two complex conjugate eigenvalues with magnitude $\doteq 0.690817$ and one real with value $\doteq 0.242164$. This makes it an attractive focus. The maximally mixed state has eigenvalues $0, \sqrt{\frac{1}{2}(5-\sqrt{5})} > 0$ which makes it a saddle point. □

We have detected mixed attractors only for protocols in specific parts of range $x_k < x < 60^\circ$ and we have also detected saddle states able to numerically attract significant amount of states. That is a surprising property. For choice $x = 0 = \tau$ we have found there are three mixed fixed states (besides $\mathbb{1}$), two of them repelling, one of them attracting in one direction and unstable focus in another plane determined by complex eigenvectors. In spite of the instability of the focus, the numerical iteration converged to a very good proximity of the state. However, maximal vigilance is needed with numerical calculations in spite of this example of successful convergence to a focus.

The information that there can be nontrivial mixed attractive states is important mainly for experimental realisation. When the state converges to the maximally mixed state, results of its measurement are random. Different attractive mixed state would show bias in measurements. Because such mixed state ρ has entropy $0 < S(\rho) < 1$, the mean entropy $e(P;x,\tau)$ looses its meaning of probability, now $1 - e(P)$ is not the chance that a random state of initial purity P converges to a pure attractor, at least on interval $(x_k, 30^\circ)$. But it remains an interesting indicator of the statistical uncertainty of the output of the protocol.

Coming back to the topic of dimension, now we present $d(P;x,\tau)$ for few pairs of selected parameters. We have numerically confirmed that in the vicinity of the $x = \frac{\pi}{4}, \tau = 0$ case the phase transition is preserved, only the temperatures change slightly; we are unable to give a formula though. The fractal dimension also seem to deviate but we cannot distinguish with our computation precision and methods whether it is not only a numerical artefact. Then, we have focused

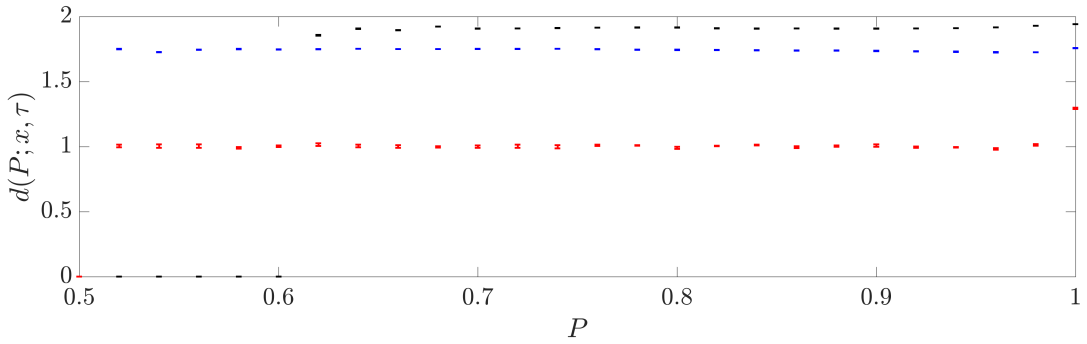

Figure 4.21: $d(P;x,0)$ for specific values of x. Piecewise trend is characteristic. *Black*: $x = 54°, \tau = 45°$, *blue*: $x = 36°, \tau = 84°$, *red*: $x = 24°, \tau = 45°$

on other, new types of fractal structures. For these, the phase transition is also clearly observable.

Although we have not enough sources to check each combination even numerically, we conjecture the following proposition:

Conjecture 4.10.2. *For arbitrary $x, \tau, (\psi,)$ the function $d(P;x,\tau)$ is piecewise constant.*

The special cases where the temperature of the phase transition is very near values $P = 1$ or $P = \frac{1}{2}$ are presented, this is a new observation. We have seen in $e(P)$ that all states can be purified except for $\mathbb{1}$, in this case the transition probably occurs exactly at 0, an example is the case $x = 24°, \tau = 45°$. Also, the two temperatures for transitions fractal $\to$ regular $\to$ empty can possibly merge together to a single transition fractal $\to$ empty; we see this for $x = 54°, \tau = 45°$. This might be connected to nonexistence of the inaccessible points which we found earlier, 3.4.1. But we have not supported this idea yet even numerically and leave this question to future research. It is questionable whether we should keep speaking of phase transition even in these degenerate cases. Any structure must collapse to a single point at $P = \frac{1}{2}$ because the sphere of constant purity actually is a single point. One should not forget, that the original case of two transitions is still present for large set of parameters. We also tried to understand what happens to the fractal (more precisely, its slice on the sphere of constant purity) with decreasing purity. We have confirmed that the fractals decay in a similar way to the prototypical case of $x = \frac{\pi}{4}, \tau = 0$, small islands of convergence to $\mathbb{1}$ (or another mixed attractor) appear suddenly and grow. These islands then merge together until they consume the whole sphere of constant purity. For those x for which $\mathbb{1}$ is not the attractor, the basin of attraction of the pure attractor can surround the maximally mixed state and therefore, the structure of sensitive states disappears for low values of P. We have seen this in case of H_2 protocol, but at that case the $\mathbb{1}$ was the attractor.

We conclude that the phase transition is not a unique phenomenon bound to a singlet of parameters. The sudden change of the dimension is probably a fundamental characteristic of the evolution maps 4.7. Let us accent now another important observation, that the dimension never increases when the purity is decreased, the fractals can only decay and there are probably "sources" of the fractal structure, similarly to fixed state $\mathcal{R}$ in previous chapter.

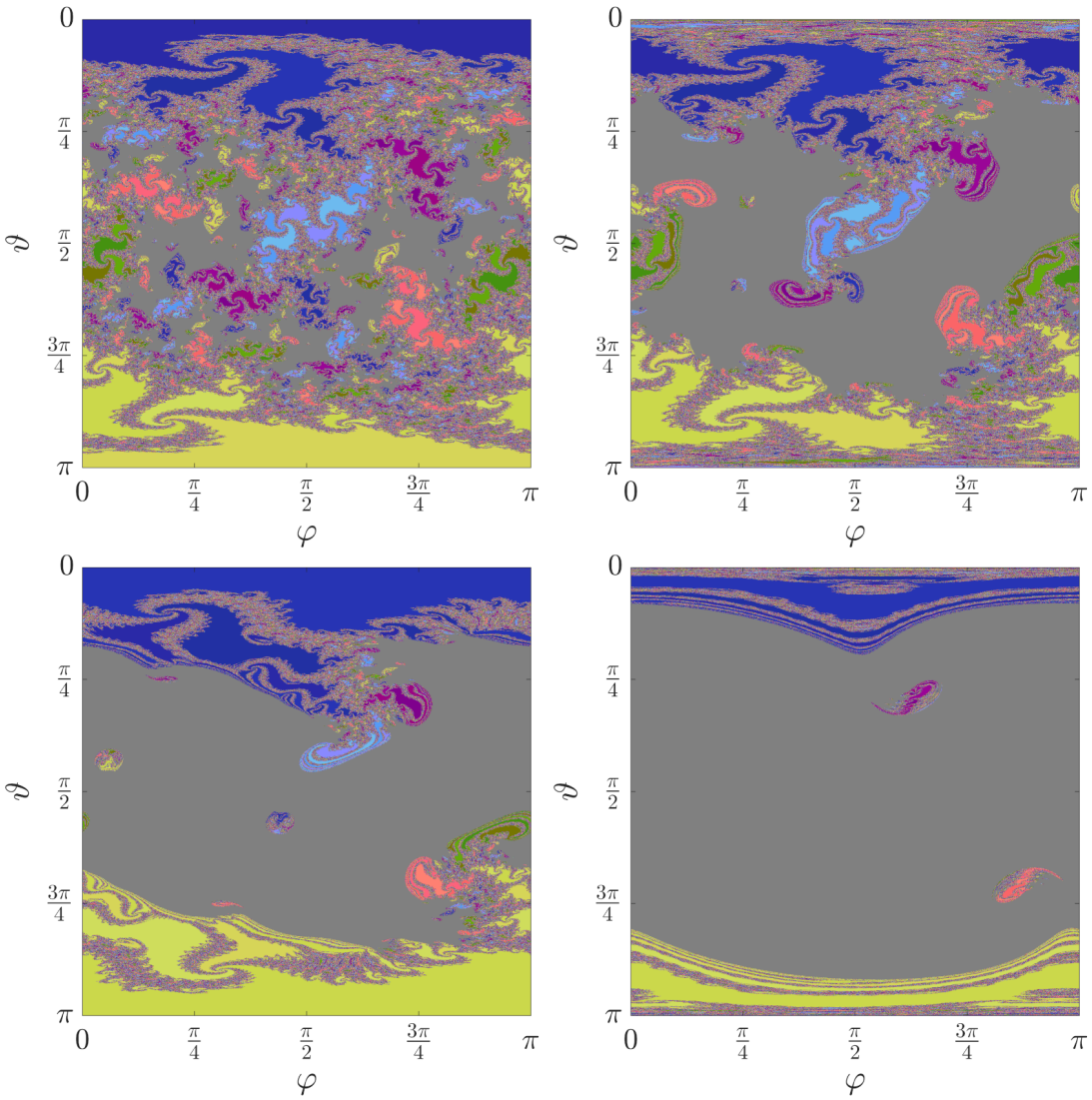

Figure 4.22: The purity dependent decay of the fractal structure for protocol with $x = 54°, \tau = 45°$. Case $P = 1$ shown in 4.17. The gray colour stands for convergence to $\mathbb{1}$. *Left top*: $P = 0.9$, *right top*: $P = 0.8$, *left bottom*: $P = 0.72$, *right bottom*: $P = 0.62$

Conjecture 4.10.3. *For arbitrary $x, \tau, (\psi,)$ the function $d(P; x, \tau)$ is non-decreasing with increasing P.*

We support this with figure 4.23where $d(P; x, \tau)$ is again plotted as in 4.10; but this time the initial states are mixed, taken from the sphere of constant purity. We see now how the Mandelbrot set analogue changes when we decrease the purity. Actually, we did not define the set for mixed states and we do not mean to for following reason. The concept is bound to the Julia set which is not defined in three-dimensional dynamics. Also, the original idea of the Mandelbrot set is built upon the connectedness. When the fractal structure is elevated into the third dimension, it may automatically become connected even though the Julia set for the pure states is totally disconnected. And at last, in the following figure the would-be analogue to the Mandelbrot set seems to stretch to the whole plane x, τ. This happens because for $P < 1$ we detect basins of attraction belonging to

the mixed attractor. These may be connected to the inaccessible points with no chaotic behaviour and may be connected; that would interfere with the original purpose of definition of $\widetilde{\mathcal{M}}$.

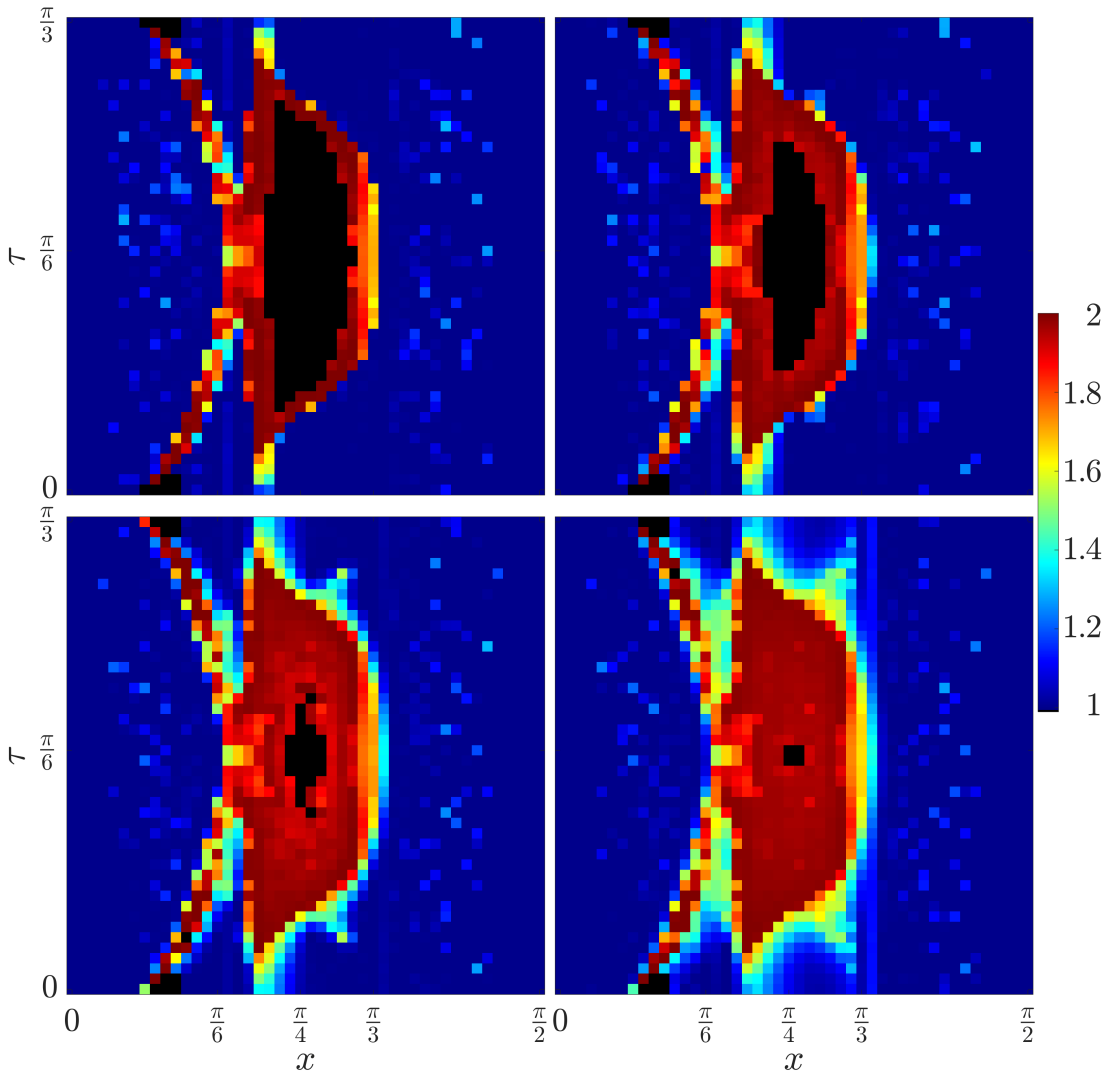

Figure 4.23: $d(P; x, \tau)$ for specific values of P. Cases with no detected structure in black. *Left top*: P=0.9, *right top*: P=0.8, *Left bottom*: P=0.7, *right bottom*: P=0.6.

We kindly remind that these conjectures are based on numerical calculations and would deserve also other forms of verification; hopefully an analytic approach will be also available in the future. Let us conclude that the phase transition of the fractal structure is an interesting phenomenon which significantly deepens our understanding not only in the field of the chaotic dynamics but mainly in quantum physics. Such regimes have not yet been observed and the existence of metastructure in the plot of $d(P; x, \tau)$ 4.9 is one of few physical models that is capable to join theory of chaos and Mandelbrot set to a real physical setting. We have searched only to find a specific temperature complexification to analyse phase transitions in Ising model, [50], and specifically designed circuits to realise coupled logistic maps, [31]. The case of Ising model is rather a mathematical trick, our twirling protocols are a dynamical model to which the (generalised)

Mandlebrot set belongs as its integral part. Let us summarise this chapter with particular focus on the experimental view of our discoveries.

4.11 Practical use of generalised protocols

We have brought three main experimental results in this chapter. First important theorem 5.15 allows us to modify the time gap between the protocol iterations at cost of additional unitary transformation of the input and output state, this modification is executed by free time evolution. This is crucial for realistic implementation where the iterations cannot be implemented instantaneously.

Also, an attractor of some protocol can be modified in certain way by changing the twirling parameters. The next fundamental theorem states that a protocol can be designed so that an arbitrary prescribed state is its attractor. There is a single exception of family of states with $w = w_c$, these exceptional states can be reached by other protocols and will be treated in next chapter. Therefore, our protocol is universal for purification purposes.

The last result of significant experimental importance was based on numerical evidence where both the input state and the protocol twirling gates could be perturbed. We have shown that the protocol is robust, i.e. the output is deviated only in a restricted way under certain assumptions.

5. Protocols of higher degrees

We have just seen that the protocol based on the CNOT gate could be enhanced with twirling operators; we focused on the symmetries attractors, fractal structures, also convergence speed. All of them were determined by parameters of the twirling gates. There were protocols found, namely with $\tau = \psi = 0, x \doteq x_c$ where the convergence was slow, even changed to indifferent character of fixed points/cycles. We now come to idea whether the convergence speed can be altered so that the protocol would converge faster to its attractor. The CNOT gate manifested as Hadamard elementwise product and in consequence it induced map of type $z \to z^2$. Can we realise polynomial functions of higher degree?

5.1 Protocol setting

We propose now to use generalised gate cluster defined on a multiplet of qubits. The scheme of the protocol is below; its purpose is, physically said, to use more copies of a state to repair its another copy.

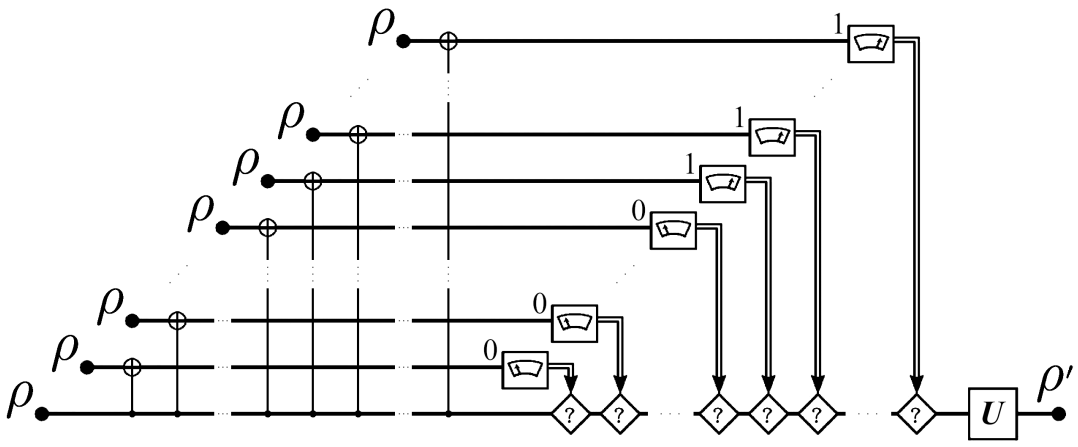

Figure 5.1: Scheme of the n qubit protocol based on CNOT gates.

Also, the protocol as designed in [1] allowed for two basic possibilities, projection onto $|0\rangle$ or onto $|1\rangle$. The protocol that we have studied so far used the first option. Let us study the results when the other base state is used. At first, for the sake of simplicity, consider only two qubit case - let us simplify the basis of the composed system $\mathbb{C}^2_c \otimes \mathbb{C}^2_t$ and use notation as suggested in theoretical chapter **??** In this case, the measurement based selection with the projection onto $|1\rangle_t$ transforms the input control state ρ to (in Bloch representation):

$$\rho' = \frac{1}{\nu} \begin{pmatrix} (1+w)(1-w) & (u-iv)(u+iv) \\ (u+iv)(u-iv) & (1-w)(1+w) \end{pmatrix}. \tag{5.1}$$

where norm ν guarantees Tr $\rho = 1$. When we adopt the X matrix representation of NOT matrix as we wrote earlier 2.27, we find out we can write

$$\rho' = \rho \odot (X\rho X). \tag{5.2}$$

When multiple qubits are used as the target qubits, each measured qubit implements the post-selection, mathematically as the elementwise product, either with ρ for the case of projection onto $|0\rangle$, or with $X\rho X$ in case of projection onto $|1\rangle$. The fact that projections onto orthogonal subspaces (subsystems) are commutative (independent) and the tracing over measured subsystems is independent too, 2.16, goes hand in hand with the observation that the elementwise product is commutative, the output state does not depend on order of the performed measurements. The elementwise product can be thus shortened to powers - in case that protocol uses 1 control qubit, m target qubits with projection onto $|0\rangle$ and n onto $|1\rangle$, the output state is

$$\rho' = \frac{\rho^{\odot m+1} \odot (X\rho X)^{\odot n}}{\mathrm{Tr}\ \rho^{\odot m+1} \odot (X\rho X)^{\odot n}} \tag{5.3}$$

To make the text more comprehensible and give a simple clue to what protocol we are dealing with, let us introduce a new notation inspired by another often used convention of qubit notation, $|+\rangle, |-\rangle$, let us think of *P*ositive and *N*egative. Protocol with this number of qubits - 1 control, m and n target with projections onto $|0\rangle$ and $|1\rangle$ will be called Pm+1Nn. Because we will focus on the case of projections onto $|0\rangle$, we will briefly write Pk instead of PkN0 and also Nk instead of $P1Nk$. The original protocol from the third chapter is therefore $P2$ as it uses 1 qubit to repair another. The parameterisation of the twirling operator (which is the single unitary gate applied after the nonlinear part) will be again used, the same as in the previous chapter, i.e. decomposition with parameters x, ψ, τ. To mark that the nonlinear operation is based on measurements of $m+n$ qubits modifying +1 qubit, we will use brackets with indices; again in case $n = 0$ it will be omitted:

$$\rho \to U[\rho]_{m+1,n} \tag{5.4}$$

The fact that projections act independently gives trivial consequences:

Lemma 1. *Consider protocol equipped with arbitrary twirling operator U and protocol with no twirling, i.e. identity in place of the unitary gate $\mathbb{1}$. Then*

$$U[\rho]_{k,k} = U[\mathbb{1}[\rho]_{1,1}]_{k,0} = U[\mathbb{1}[\rho]_{k,0}]_{1,1}. \tag{5.5}$$

More generally, if $m+1, n$ have common divisor q, $m+1 = q\tilde{m}, n = q\tilde{n}$, it can be put into relation instead of 1. We may write

$$U[\rho]_{q\tilde{m},q\tilde{n}} = U[\mathbb{1}[\rho]_{\tilde{m},\tilde{n}}]_{q,0} = U[\mathbb{1}[\rho]_{q,0}]_{\tilde{m},\tilde{n}}. \tag{5.6}$$

Proof. The proof comes from associativity and commutativity of the elementwise product, which is trivial for arbitrary matrices $\mathbb{A}, \mathbb{B}$ of the same size. For any integers p, q, r:

$$(\mathbb{A} \odot \mathbb{B})^{\odot p} = \mathbb{A}^{\odot p} \odot \mathbb{B}^{\odot p},\ (\mathbb{A}^{\odot q})^{\odot r} = \mathbb{A}^{\odot q+r} \tag{5.7}$$

□

This fact is relevant experimentally because the order of measurements is irrelevant. Of course, we have a silent and non-physical assumption of instantaneous protocol application. It is only natural that the measurements can be executed

at any order when they are performed at the same time. But also, this lemma gives computational advantage. The evolution equations can be split into two successive iterations which can be computationally more convenient, i.e. equations for $P8$ with polynomials of degree 8 can be reduced to triple iterations of only quadratic equations for protocol $P2$.

5.2 Protocol N_1

When the simplest protocol with alternative projection $N1$ with trivial twirling $U = \mathbb{1}$ is taken, we see from 5.1 that the evolution equation in terms of Bloch coordinates are very dull.

$$w' = v' = 0,\ u' = \frac{u^2 + v^2}{2(1 - w^2)};\ w'' = v'' = 0,\ u'' = \frac{u'^2}{2} \tag{5.8}$$

From the second iteration on, the evolution drags any mixed state along u axis to the maximally mixed state with function of type $z \to z^2$. All the pure states are mapped onto state $u = 1, w = v = 0$ which is a representation of $|0\rangle + |1\rangle$ and remain there fixed. All mixed states are converging to the maximally mixed state.

For this reason, such protocol has no purification potential. The only use can be to homogenise the input states; this reduces experimental utilisability of the protocol for purification. Because any protocol $PmNn$ with $n \geq 1$ induces at least partially such homogenisation, we defer to study these protocols and focus on protocols Pm only. This does not mean that nonlinear dynamics and chaos are not present in such protocols but we keep in mind the physical motivation lying primarily in the purification properties.

5.3 Multiple qubit protocols Pn

Because the protocol manifests as the elementwise product on the density matrices, we can suspect that the evolution equations of Pn will contain higher powers of the Bloch coordinates. Because of this, we will speak of n as of the *degree* of the protocol. After we present the new evolution equations which also include twirling operators, we follow the line of thought from previous chapters.

5.4 Action and symmetries of Pn

The elementwise product of n qubits density matrices gives (without renormalisation)

$$\rho^{\odot n} = \begin{pmatrix} (1+w)^n & (u-iv)^n \\ (u+iv)^n & (1-w)^n \end{pmatrix}, \tag{5.9}$$

this lead us to define generalised version of polynomial factors:

$$\begin{aligned} W_n &= \tfrac{1}{2}((1+w)^n - (1-w)^n) = \sum_{\text{odd } k=1}^{n} \binom{n}{k} w^k, \\ N_n &= \tfrac{1}{2}((1+w)^n + (1-w)^n) = \sum_{\text{even } k=0}^{n} \binom{n}{k} w^k \\ U_n &= Re\,(u+iv)^n = \sum_{\text{even } k=0}^{n} \binom{n}{k} u^k v^{n-k} (-1)^{\frac{k}{2}} \\ V_n &= Im\,(u+iv)^n = \sum_{\text{odd } k=1}^{n} \binom{n}{k} u^k v^{n-k} (-1)^{\frac{k-1}{2}} \end{aligned} \tag{5.10}$$

Note that $W_n + N_n = (1+w)^n, U_n + iV_n = (u+iv)^n$ The factors $\frac{W_n}{N_n}, \frac{U_n}{N_n}, \frac{V_n}{N_n}$ are then combined with geometrical factors induced by the twirling operator. This geometrical part of the protocol is for each n identical to the previous case $n = 2$, only with general polynomial factors, 4.7.

Let us write now a special case of $n = 3, x = \frac{\pi}{4}, \tau = \psi = 0$ which will be studied more extensively.

$$\begin{aligned} w' &= \frac{u^3 - uv^2}{1+3w^2} \\ u' &= -\frac{3w + w^3}{1+3w^2} \\ v' &= -\frac{3u^2 v - v^3}{1+3w^2} \end{aligned} \tag{5.11}$$

We write it to make an observation, the degree of the polynomials in the numerators and denominators are at most but not necessarily equal to n - the denominator N_n for odd n has degree $n-1$ only. This affects number of fixed points etc.

First, let us again write down maybe trivial but very important fact

Proposition 5.4.1. $\mathbb{1}$ *is a fixed state for arbitrary protocol.*

Proof. It is probably not necessary to explain that elementwise product of arbitrary number of identity matrices gives the identity matrix just like the post-modification with unitary matrix according to time evolution 2.13. □

Let us search now for the symmetries in the input states.

Theorem 5.4.2. *Protocol Pn induces n-fold rotational symmetry around the w-axis in the Bloch space of input states.*

Proof. When $u \to \tilde{u} = \cos\frac{2\pi}{n}u + \sin\frac{2\pi}{n}v$ and $v \to \tilde{v} = -\sin\frac{2\pi}{n}u + \cos\frac{2\pi}{n}v$ are simultaneously substituted in the input state, than

$$\begin{aligned} (\tilde{u} + i\tilde{v})^n &= ((\cos\tfrac{2\pi}{n} - i\sin\tfrac{2\pi}{n})u + (i\cos\tfrac{2\pi}{n} + \sin\tfrac{2\pi}{n})v)^n = \\ &= (\cos\tfrac{2\pi}{n} - i\sin\tfrac{2\pi}{n})^n (u+iv)^n = \\ &= \left(e^{-i\frac{2\pi}{n}}\right)^n (u+iv)^n = (u+iv)^n \end{aligned} \tag{5.12}$$

Therefore, the values U_n, V_n are the same for both inputs. Because w was not modified, w', u', v' must be identical for both inputs (w, u, v) and $(w, \tilde{u}, \tilde{v})$. □

Let us appreciate for the moment that thanks to this proposition, we can restrict the studied input states to a spherical section $\varphi \in [0; \frac{2\pi}{n})$. Now it is obvious that the coordinate w has unique role in all considered protocols and that was the reason why we highlight it from the beginning of our work.

Regarding the symmetries in terms of the protocol parameters, we again find the symmetry in $x \to \pi + x$ which is direct consequence of the geometrical action of twirling and represents the same protocol without any conjugation. Then we recall the symmetry in $x \to \pi - x$. It is also valid, but not so trivially. When the parameter is changed then $\cos 2x \to \cos 2x$ while $\sin 2x \to -\sin 2x$. This effect in the evolution equations for u', v' can be undone by transforming $\frac{W_n}{N_n} \to -\frac{W_n}{N_n}$. Therefore, the equation for w' will be then kept when $w \to -w$ additionally. These two conditions are valid thanks to the definition of the factors W_n, N_n. We have purposely written them in 5.10 to show that W_n has only odd powers of w while N_n has only even powers. From this fact we deduce

$$w \to -w \Rightarrow \frac{W_n}{N_n} \to -\frac{W_n}{N_n}. \tag{5.13}$$

and the symmetry is proved - when protocol with x, ψ, τ gives (w', u', v') from the input (w, u, v), then protocol with $\pi - x, \psi, \tau$ acting on $(-w, u, v)$ gives $(-w', u', v')$ for the output.

Next symmetries could be also studied be we will derive them later. At this moment, we are very curious what happens with the time relaxation symmetry, 5.15. We can confirm that the theorem remains valid when it is modified to suit general n.

Theorem 5.4.3. *Two protocols Pn with parameters $x_1, \psi_1, \tau_1, x_2, \psi_2, \tau_2$ are asymptotically equivalent when*

$$x_1 = x_2 \wedge (n-1)\psi_1 - n\tau_1 = (n-1)\psi_2 - n\tau_2 \tag{5.14}$$

Defining $\tau_0 \equiv \frac{\tau_1 - \tau_2}{n-1}$ and $T_0 = \begin{pmatrix} 1 & 0 \\ 0 & e^{-i\tau_0} \end{pmatrix}$, following equation holds.

$$T_0 \cdot T_1 R_1[\rho]_n \cdot T_0^\dagger = T_2 R_2[T_0 \cdot \rho \cdot T_0^\dagger]_n \tag{5.15}$$

Proof. Just like in case of $n = 2$ we need to realise that when protocol is applied to evolve the ansatz state $T_0 \rho T_0^\dagger$, now the rotation in the Bloch ball is powered by n in contrast to factor 2 in 4.13. Identical rotation was argued a while before in the proof of the n-fold symmetry, 5.12. When we follow the proof and compare the w' coordinates for both sides, we now come to

$$x_1 = x_2 \wedge \psi_1 = \psi_2 + n\tau_0 \tag{5.16}$$

Comparing u', v' we obtain the same condition as before

$$\psi_2 - \tau_2 = \psi_1 - \tau_1 - \tau_0 \tag{5.17}$$

The two conditions together make the statement

$$\tau_0 = \frac{\tau_1 - \tau_2}{n} \wedge (n-1)\psi_1 - n\tau_1 = (n-1)\psi_2 - n\tau_2 \tag{5.18}$$

which completes the proof. Because the equation holds for one iteration, again, it inductively holds for any number of iterations and also the asymptotic regime. □

We believe that there is a synergy in the proof and reformulation of the same theorem for pure states in the complex representation which will make further text more comprehensible. Also, we will later verify that the pure states form an invariant set for arbitrary protocol.

Proof. Considering pure state z, the action of the time evolution with parameter τ shifts it to $e^{-i\tau}z$. Let us naturally introduce $f_{n;x,\psi,\tau}$ for the evolution function corresponding to the Pn protocol with parameters x, ψ, τ. Therefore, the theorem can be reformulated to

$$e^{-i\tau_0} f_{n;x_1,\psi_1,\tau_1}(z) = f_{n;x_2,\psi_2,\tau_2}(e^{-i\tau_0}z) \tag{5.19}$$

When we derive from $TR(\begin{pmatrix}1\\z\end{pmatrix} \odot \begin{pmatrix}1\\z\end{pmatrix})$ the evolution function generally:

$$f_{n;x,\psi,\tau}(z) = e^{-i\tau}\frac{z^n \cos x - e^{i\psi}\sin x}{\cos x + z^n e^{-i\psi}\sin x} \tag{5.20}$$

From this we can already see that to identify $x_1 = x_2 \equiv x$ is necessary; the left side of the theorem is

$$e^{-i\tau_0} \cdot e^{-i\tau_1}\frac{z^n \cos x - e^{i\psi_1}\sin x}{\cos x + z^n e^{-i\psi_1}\sin x} \tag{5.21}$$

and the right side is

$$e^{-i\tau_2}\frac{z^n e^{-in\tau_0}\cos x - e^{i\psi_1}\sin x}{\cos x + z^n e^{-in\tau_0}e^{-i\psi_1}\sin x} = e^{-i(\tau_2+n\tau_0)}\frac{z^n \cos x - e^{i(\psi_2+n\tau_0)}}{\cos x + z^n e^{-i(\psi_2+n\tau_0)}\sin x} \tag{5.22}$$

Comparing both sides, one obviously gets $\psi_1 = \psi_2 + n\tau_0$ and the exponential factor requires $\tau_0 + \tau_1 = \tau_2 + n\tau_0$. These two equations form the statement. □

The consequences of the theorem are the same as for the case $n = 2$, therefore we do not repeat them again here. Let us rather ask about the other symmetry of the protocol in τ. We will use the previous theorem to choose $\psi_2 = \psi_1 + 2\pi$. This formal choice translates into next equation when the equivalence principle is used.

$$\tau_1 - \tau_2 = 2\pi\frac{n-1}{n} = 2\pi - \frac{2\pi}{n} \tag{5.23}$$

This means that two protocols with the same x and τ must give the same output for the same input when $\tau \to \tau + \frac{2\pi}{n}$. Of course, we could use any multiple $2k\pi$, so all the k protocols $\tau \to \tau + \frac{2k\pi}{n}$ are equivalent. The symmetry is now also n-fold, we could say in this sense. Similarly, one could find symmetry in ψ, but we will again set $\psi = 0$ in the rest of the chapter.

The last and most complicated symmetry we found in the last chapter allowed to choose $\tau \to \frac{\pi}{2} - \tau$, now for general n the situation is more complicated.

Theorem 5.4.4. *Two protocols with common $x, \psi = 0$ and $\tau, \tilde{\tau} = \frac{\pi}{n} - \tau$ are conjugate if and only if n is even.*

Proof. We must distinguish four cases, the reason for this is in the essential property $i^0 = i^4 = 1, i^1 = i, i^2 = -1, i^3 = -i$. But for any of following cases we remember that whenever $w \to -w$ is changed, than $W_n \to -W_n, N_n \to N_n$ is true.

1. $n \equiv 2 \bmod 4$:

   In this case, when $v \leftrightarrow u$ is substituted, let us write $\tilde{u} = v, \tilde{v} = u$, in the input state (this case we discussed earlier), we find that generally the corresponding nonlinear factors will be

$$\tilde{U} + i\tilde{V} = (\tilde{u} + i\tilde{v})^n = (v + iu)^n \tag{5.24}$$

   while for the first protocol on the first input state it is $U + iV = (u + iv)^n$. When we use the binomial theorem, we can compare both variants. Because $n = 4k + 2$ for some $k \in \mathbb{N}$, we get

$$\begin{aligned}
(u+iv)^{4k+2} = \;& u^{4k+2} + i\binom{4k+2}{1}u^{4k+1}v - \binom{4k+2}{2}u^{4k}v^2 - \dots \\
& \cdots + \binom{4k+2}{1}u^1 v^{4k+1} - v^{4k+2} \\
(v+iu)^{4k+2} = \;& v^{4k+2} + i\binom{4k+2}{1}v^{4k+1}u - \binom{4k+2}{2}v^{4k}u^2 - \dots \\
& \cdots + \binom{4k+2}{1}v^1 u^{4k+1} - u^{4k+2}
\end{aligned} \tag{5.25}$$

   Comparing the real and imaginary parts we see that $\tilde{U} = -U$ and $\tilde{V} = V$. Recalling the evolution equations

$$\begin{aligned}
w' &= \tfrac{W_n}{N_n}\cos 2x + \tfrac{U_n}{N_n}\sin 2x \\
u' &= -\tfrac{W_n}{N_n}\sin 2x\cos\tau + \tfrac{U_n}{N_n}\cos 2x\cos\tau + \tfrac{V_n}{N_n}\sin\tau \\
v' &= \tfrac{W_n}{N_n}\sin 2x\sin\tau - \tfrac{U_n}{N_n}\cos 2x\sin\tau + \tfrac{V_n}{N_n}\cos\tau
\end{aligned} \tag{5.26}$$

   and for the other protocol we use $\tilde{U}_n = -U_n$ and $\tilde{W}_n = -W_n$:

$$\begin{aligned}
\tilde{w}' &= -\tfrac{W_n}{N_n}\cos 2x - \tfrac{U_n}{N_n}\sin 2x \\
\tilde{u}' &= \tfrac{W_n}{N_n}\sin 2x\cos\tilde{\tau} - \tfrac{U_n}{N_n}\cos 2x\cos\tilde{\tau} + \tfrac{V_n}{N_n}\sin\tilde{\tau} \\
\tilde{v}' &= -\tfrac{W_n}{N_n}\sin 2x\sin\tilde{\tau} + \tfrac{U_n}{N_n}\cos 2x\sin\tilde{\tau} + \tfrac{V_n}{N_n}\cos\tilde{\tau}
\end{aligned} \tag{5.27}$$

   While the equation for w shows that the substitution $w \to -w$ in the input state goes well with $\tilde{w}' = -w'$, the other coordinates must be handled. If we try to identify $\tilde{u}' \stackrel{?}{=} -u'\cos\alpha + v'\sin\alpha, \tilde{v}' \stackrel{?}{=} u'\sin\alpha + v'\cos\alpha$ we find another nice opportunity to use goniometric relations.

$$\begin{aligned}
\tilde{u}' &\stackrel{?}{=} (\tfrac{W_n}{N_n}\sin 2x - \tfrac{U_n}{N_n}\cos 2x)\cos(\alpha-\tau) + \tfrac{V_n}{N_n}\sin(\alpha-\tau) \\
\tilde{v}' &\stackrel{?}{=} -(\tfrac{W_n}{N_n}\sin 2x + \tfrac{U_n}{N_n}\cos 2x)\sin(\alpha-\tau) + \tfrac{V_n}{N_n}\cos(\alpha-\tau)
\end{aligned} \tag{5.28}$$

   The identification matches for $\alpha - \tau = \tilde{\tau} = \frac{\pi}{n} - \tau$, i.e. $\alpha = \frac{\pi}{n}$.

   We finish concluding: when protocol with $x, \psi = 0, \tau$ acts on input state (w, u, v) yielding (w', u', v') then protocol with $x, \psi = 0, \frac{\pi}{n} - \tau$ acting on $(-w, v, u)$ yields $(-w', -u'\cos\frac{\pi}{n} + v'\sin\frac{\pi}{n}, u'\sin\frac{\pi}{n} + v'\cos\frac{\pi}{n})$. One can easily see that this formula reduces to previously studied for $n = 2$.

2. $n \equiv 0 \bmod 4$:

When we take $\tilde{u} = v\cos\frac{\pi}{n} - u\sin\frac{\pi}{n}, \tilde{v} = v\sin\frac{\pi}{n} + u\cos\frac{\pi}{n}$ then

$$\begin{aligned}(\tilde{u}+i\tilde{v})^n &= (v\cos\tfrac{\pi}{n} - u\sin\tfrac{\pi}{n} + iv\sin\tfrac{\pi}{n} + iu\cos\tfrac{\pi}{n})^n = \\ &= (v(\cos\tfrac{\pi}{n} + i\sin\tfrac{\pi}{n}) + iu(\cos\tfrac{\pi}{n} + i\sin\tfrac{\pi}{n}))^n = \\ &= (e^{i\frac{\pi}{n}})^n(v+iu)^n = -(v+iu)^n\end{aligned} \tag{5.29}$$

At this time we can write $n = 4k$ for some $k \in \mathbb{N}$, therefore

$$\begin{aligned}(u+iv)^{4k} = \;& u^{4k} + i\binom{4k}{1}u^{4k-1}v - \binom{4k}{2}u^{4k-2}v^2 - \dots \\ & \cdots - i\binom{4k}{1}u^1v^{4k-1} + v^{4k} \\ (v+iu)^{4k} = \;& v^{4k} + i\binom{4k}{1}v^{4k-1}u - \binom{4k}{2}v^{4k-2}u^2 - \dots \\ & \cdots - i\binom{4k}{1}v^1u^{4k-1} + u^{4k}\end{aligned} \tag{5.30}$$

Without the previous transformation 5.29 this would mean $\tilde{U} = U, \tilde{V} = -V$ but adding minus sign by the additional transformation we have $\frac{\tilde{U}_n}{\tilde{N}_n} = -\frac{U_n}{N_n}, \frac{\tilde{V}_n}{\tilde{N}_n} = \frac{V_n}{N_n}$, taking $\tilde{w} = -w$ we again have $\frac{\tilde{W}_n}{\tilde{N}_n} = -\frac{W_n}{N_n}$. The rest of the proof is the same as for the previous case. We conclude that if protocol with $x, \psi = 0, \tau$ acting on (w, u, v) yields (w', u', v') then protocol with $x, \psi = 0, \frac{\pi}{n} - \tau$ acting on $-w, v\cos\frac{\pi}{n} - u\sin\frac{\pi}{n}, v\sin\frac{\pi}{n} + u\cos\frac{\pi}{n}$ yields $(-w', -u'\cos\frac{\pi}{n} + v'\sin\frac{\pi}{n}, u'\sin\frac{\pi}{n} + v'\cos\frac{\pi}{n})$.

3. $n \equiv 1 \bmod 4 \vee n \equiv 3 \bmod 4$:

   In this case, $(v+iu)^n$ gives $\tilde{U}_n = \pm V_n, \tilde{V}_n = \pm U_n$. No transformation can disentangle this cross-connection. Therefore, we get to compare

$$w' = \frac{W_n}{N_n}\cos 2x + \frac{U_n}{N_n} \stackrel{?}{=} \frac{W_n}{N_n}\cos 2x \pm \frac{V_n}{N_n} = \tilde{w}' \tag{5.31}$$

   which can never be satisfied. Therefore, such symmetry does not exist.

□

We should highlight that this theorem discovers one fundamental difference between protocols with odd versus even degree n. We conclude that the restrictions can be now made:

$$\begin{aligned}x \in [0;\pi), \psi = 0, \tau \in [0;\tfrac{\pi}{n}), \varphi \in [0;\tfrac{2\pi}{n}), \vartheta \in [0;\pi] \text{ for } n \text{ odd} \\ x \in [0;\pi), \psi = 0, \tau \in [0;\tfrac{\pi}{2n}), \varphi \in [0;\tfrac{2\pi}{n}), \vartheta \in [0;\pi] \text{ for } n \text{ even}\end{aligned} \tag{5.32}$$

and all the dynamical features will be explored.

We might also want to elaborate inverse map formulas to apply backward iterations to determine the Julia set. We have already argued the inversion of the geometrical part 4.32, therefore we just derive the inversion formulas for the nonlinear factors here. From w', u', v' one obtains $\frac{W_n}{N_n}, \frac{U_n}{N_n}, \frac{V_n}{N_n}$. The first factor is only function of w and one can easily check it is bijection it is a bijection on $[0;1]$

for arbitrary n. Therefore, it can be inverted immediately. We have found that the function is surprisingly dual:

$$w = \frac{\sqrt[n]{1+\frac{W_n}{N_n}}}{\sqrt[n]{1+\frac{W_n}{N_n}}} \tag{5.33}$$

Let us make a short note that through our thesis we are often encountering functions of type

$$z \to \frac{1-z^n}{1+z^n} \tag{5.34}$$

which especially for $n = 1$ is the well-known Möbius transform which is equal to its own inverse function. a similar pattern now rules the inverse map which was also found earlier 4.33. The case $n = 2$ drives the evolution in the original protocol applied to the pure states. One can check, that for arbitrary n,

$$f_{n;\frac{\pi}{4},0,0}(z) = \frac{1-z^n}{1+z^n} \tag{5.35}$$

which is a remarkable fact.

Back to the inverting formulas, with w in our hands, we can express solely U_n, V_n and compose them formally into $U_n + iV_n$. From definition formula 5.10 we get

$$u = Re(\sqrt{U_n + iV_n}),\ v = Im(\sqrt{U_n + iV_n}). \tag{5.36}$$

Note that because $w \to \frac{W_n}{N_n}$ is a bijection, there is only a single solution for w when looking for preimages. The complex number $U_n + iV_n$ can be formally multiplied by unit $e^{2\pi i}$ before taking the n-th square root; in this way we obtain n preimages. These naturally belong to sphere sections which were found when discussing the n-fold symmetry. We mention this not only because the preimages are distributed symmetrically in the Bloch sphere but to stress that there are exactly n preimages. Purely mathematically, solving 3 equations with multivariate rational polynomials factors leads to many other solutions but those are non-physical as they are outside the Bloch ball.

5.5 Asymptotic regimes of general protocols

Our readers are now probably curious whether the properties of protocol with $n = 2$ are preserved for higher degrees. Yes, they are. We have promised to show

Proposition 5.5.1. *Pure states form the invariant set for any protocol P_n with arbitrary twirling x, ψ, τ.*

Proof.

$$\begin{aligned} w'^2 + u'^2 + v'^2 = & \ \frac{((1+w)^n-(1-w)^n)^2+|2(u+iv)^n|^2}{((1+w)^n+(1-w)^n)^2} = \\ & = \frac{(1+w)^{2n}-2(1-w^2)^n+(1-w)^{2n}+4(u^2+v^2)^n}{(1+w)^n+(1-w)^n} = \\ & = \frac{(1+w)^{2n}+2(1-w^2)^n+(1-w)^{2n}}{((1+w)^n+(1-w)^n)^2} = 1 \end{aligned} \tag{5.37}$$

where we used definition $U_n + iV_n = (u+iv)^n$ with realising $|u+iv|^2 = u^2+v^2 = 1-w^2$ because of the purity condition $w^2+u^2+v^2 = 1$. □

And a trivial observation is that, again, the maximally mixed state $\mathbb{1}$ is fixed state of any protocol. But we do not say anything about its stability

Now let us demonstrate the protocol action for some trivial cases. Let us start with the simplest case, $x = 0$. In this case, $w' = \frac{W_n}{N_n}$. Because difference $w' - w > 0$ is true for all $w > 0$ while $w' - w < 0$ when $w < 0$, one does not have problems to realise that all state except for the equatorial plane $w = 0$ converge to the poles depending on the hemisphere they belong to. Case with $x = \frac{\pi}{2}$ turns the poles into a cycle again. The equator is the Julia set for both these trivial protocols. All other states, i.e. those in the equatorial plane with $w = 0, u^2 + v^2 < 1$ converge to the maximally mixed state.

We can also see that when $\tau = 0$ is set (additionally to $\psi = 0$), equations 4.27 again separate the evolution of v component which again makes circle K (in plane $v = 0$) and its border ∂K invariant sets, this information will be straight used in following.

The protocol with H_2 was a prominent protocol because it allowed to purify towards state $|0\rangle$. Let us take a closer look at the dynamics of protocol of higher degree with this twirling gate. While our readers might be scared that another extensive chapter with detailed analysis similar to chapter 3 would follow, we can calm them. The evolution equations of higher degrees cease to be solvable eariler than one would hope for. Software Mathematica which we use to solve equations cannot give neither analytical nor even numerical answers. Furthermore, the Jacobi matrices of longer cycles are also not manageable. Therefore, we typically restrict to numerical evolution to obtain attractor maps and we identify the attractors this way.

Now specifically for $n = 3$: besides $\mathbb{1}$ stable fixed state there are four other fixed states, all of them unstable, pure with $v \neq 0$. When looking for length 2 cycles we find two composed of four additional states conjugate to previous fixed points by specific sign changes. There is also a cycle $(0, 0, 1) \leftrightarrow (0, 0, -1)$, all of them repelling. One could expect that aprotocol with $n = 3$ could have attractive length 3 cycle, possibly containing $|0\rangle$, but such expectation is wrong. There are many 3-cycles, none of them attractive but we finally find the single and only pure attractor:

$$\mathcal{C}' \equiv (1, 0, 0) \to (0, -1, 0) \to (-1, 0, 0) \to (0, 1, 0) \circlearrowleft \tag{5.38}$$

Physically, when norms are omitted:

$$\mathcal{C}' \equiv |0\rangle \to |0\rangle - |1\rangle \to |1\rangle \to |0\rangle + |1\rangle \circlearrowleft \tag{5.39}$$

Theorem 5.5.2. *For protocols Pn with $x = \frac{\pi}{4}, \psi = \tau = 0$, cycle $\mathcal{C}$ is pure attractor for arbitrary n even, $\mathcal{C}'$ is pure attractor for n odd.*

Proof. The density matrices corresponding to members of the cycles are

$$\rho \in \left\{ \frac{1}{2}(\sigma_0 \pm \sigma_2), \pm\sigma_1 \right\}. \tag{5.40}$$

For all of these matrices we can easily verify $\rho^{\odot 3} = \rho$. Therefore, $\rho^{\odot n} = \rho = \rho^{\odot 3}$ for arbitrary n odd and $\rho^{\odot n} = \rho^{\odot 2}$ for n pure. The output of the nonlinear parts of the protocol is the same for all even cases and the same for all odd cases

(but different for odd versus even). The twirling is also the same for arbitrary protocols, whence the output states are the same for all the odd/even degree protocols.

Regarding the attractivity, the Jacobi matrix of the state $|0\rangle$ can be estimated to give the result. Because the function u' is always a function of w only (this is the result of particular twirling leading to $u' = -\frac{W_n}{N_n}$), the Jacobi matrix must have $(\mathbb{J}_{21}, 0, 0)$ in the second row. The member in the first column can be found for general n as

$$\mathbb{J}_{21} = -n\frac{(1-w^2)^{n-1}}{N_n^2} \tag{5.41}$$

and when we consider we are evaluating the matrix at $w = 1$, we find $\mathbb{J}_{21} = 0$, the second row guarantees one zero eigenvalue, i.e. superattractivity in one direction. The other directions are similar - because the nominators U_n, V_n are polynomials where each member is of degree n formed solely of u, v, then the derivatives contain also such polynomials, only a degree lower. But because we want to determine the Jacobi matrix at $u = v = 0$, all these polynomials yield 0; no matter what other factors appear thanks to derivatives of the denominator, the first and last row of the Jacobi matrix must contain only zeros.

To conclude, the Jacobi matrix belonging to $|0\rangle$ is zero and for any cycle containing this state, the Jacobi matrix of the cycle is by the chain rule 2.45

$$\mathbb{J} = \mathbb{J}_1 \cdot \ldots \cdot \begin{pmatrix} 0 & 0 & 0 \\ 0 & 0 & 0 \\ 0 & 0 & 0 \end{pmatrix} \cdot \ldots = \begin{pmatrix} 0 & 0 & 0 \\ 0 & 0 & 0 \\ 0 & 0 & 0 \end{pmatrix}. \tag{5.42}$$

This means that the cycle is superattractive regardless of n. □

Theorem 5.5.3. *$\mathbb{1}$ is mixed attractor for arbitrary protocol Pn with $x = \frac{\pi}{4}, \psi = \tau = 0$.*

Proof. As before, demanding $u = v = 0$ results into zeros in the first and last row of the Jacobi matrix. The second row contains again $(\mathbb{J}_{21}, 0, 0)$ but for this case $w = 0$ the Jacobi matrix is

$$\mathbb{J} = \begin{pmatrix} 0 & 0 & 0 \\ -n & 0 & 0 \\ 0 & 0 & 0 \end{pmatrix} \tag{5.43}$$

which again makes all eigenvalues zero, meaning the state is superattractive. □

What we cannot proof at the moment and remains supported by only numerical calculations is

Statement 5.5.4. *There are no other attractors besides $\mathbb{1}, \mathcal{C}$, resp. $\mathbb{1}, \mathcal{C}'$ for all protocols P_n with n even, resp. odd and twirling parameters $x = \frac{\pi}{4}, \psi = \tau = 0$.*

Let us now show the evolution in the invariant plane $v = 0$ for $n = 3$. Because of the attractor cycle which goes hand in hand with sign changing during protocol iteration, we cannot now restrict the analysis to only one quarter, e.g. $w \geq 0, u \leq 0$ like for $n = 2$.

The attractor map in the circle K is - regarding the structure although not exact proportions - identical to the case of $n = 2$, only now the basins of attraction

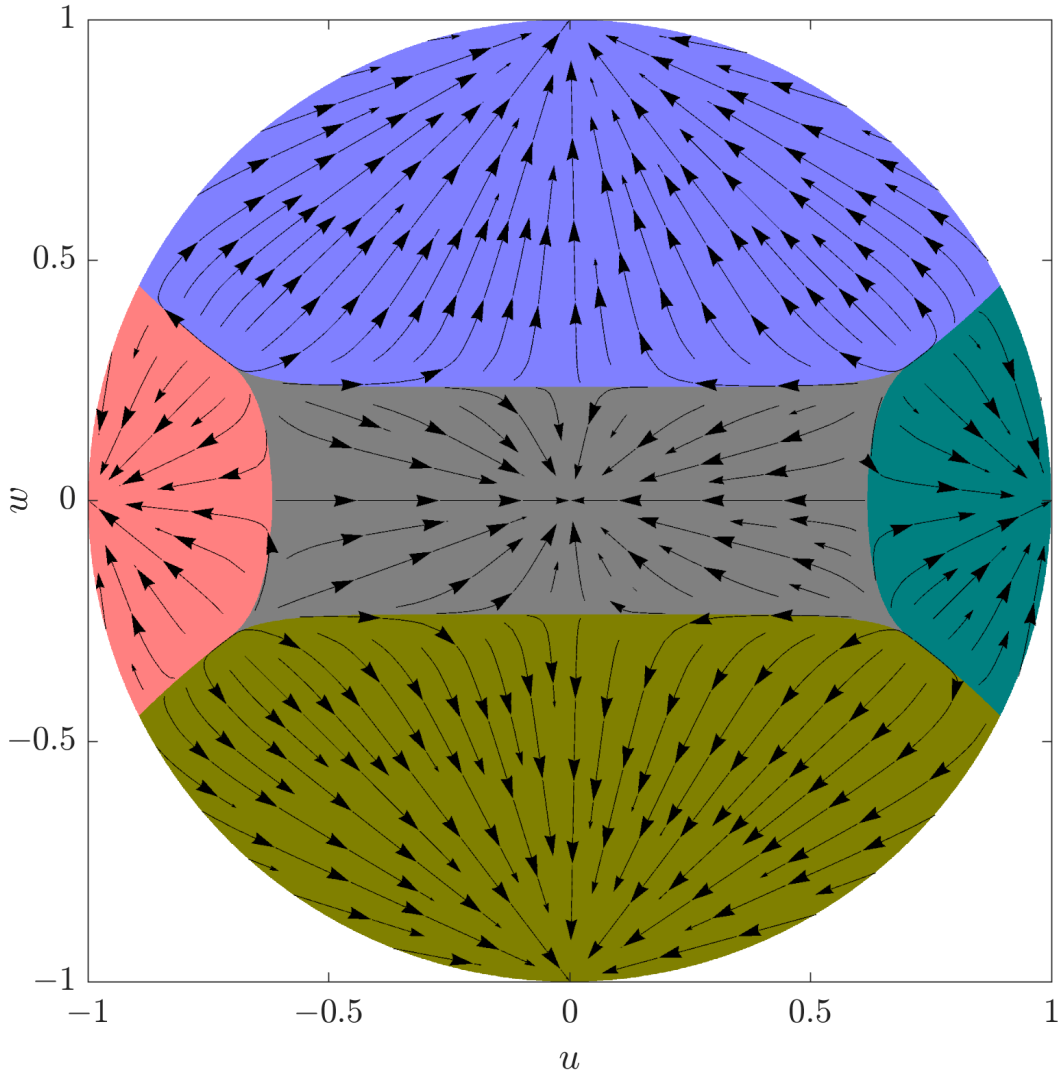

Figure 5.2: Attractor map of $P3$ protocol with H_2 twirling gate. Flow of points after four consecutive iterations is illustrated with arrows. White points are non-physical states outside the Bloch balls.

must be composed of four parts because of the 4-cycle. The members of the cycle are 'the apices', the intersections of the u, w axes and the circumference ∂K. Then there are four peculiar states. Being in the circle ∂K which in the complex representation of pure states means $z \in \mathbb{R}$, we can recall the evolution function 5.35 and find these states form a length four cycle. There are 72 complex solutions to $f^4_{3;\frac{\pi}{4},0,0}(z) = z$, then solution $z = \pm i$ forming the mentioned length two cycle, and of course cycle $\mathcal{C}'$ with $z = (0, -1, \infty, 1)$. But the reason why we are speaking of the 4-cycles is the newly found

$$\Phi \equiv \phi \to \phi - 1 \to -\phi \to -\phi + 1 \circlearrowleft \tag{5.44}$$

where ϕ is the golden ratio, satisfying $\phi^{-1} = \phi - 1$. This fact is very interesting, although probably only as a mathematical curiosity. When we would consider

higher values of n and we repeat this process, we find for low values of n that

$$\begin{aligned} &f_{n;\frac{\pi}{4},0,0}(z) = z \text{ leads to single real root of } z^{n+1} - z^n + z + 1 \text{ for } n \text{ even,} \\ &f^4_{n;\frac{\pi}{4},0,0}(z) = z \text{ leads to } \left\{ \begin{array}{c} \text{2 real roots of } -z^{n+1} + z^n + z + 1 \\ \text{and 2 real roots of } z^{n+1} + z^n + z - 1 \end{array} \right\} \text{ for } n \text{ odd.} \end{aligned} \tag{5.45}$$

The four roots for n odd form a 4-cycle. The structure of the roots belong rather to mathematical research, and so we leave the deeper connections that could be found in this topic for other research.

Let us come back to the invariant sets. There were invariant subsets of K in the $n = 2$ case, namely line segments L_2. These have to be extended for odd n to the whole axed range

$$L_2^{\pm} = \{(w, 0, 0)|w \in [-1; 1]\} \cup \{(0, u, 0)|u \in [-1; 1]\} \tag{5.46}$$

but not necessarily for even n. There is again the flip between the w, u axes, regardless of n. While for n even only the positive w semiaxis is mapped onto negative u semiaxis and vice versa, for n odd the semiaxes are jumped across, in the counterclockwise sense. When we take state $(0, u, 0)$, after two iterations it is brought to $(0, u'', 0)$, where

$$u'' = \frac{(1-u^n)^n - (1+u^n)^n}{(1-u^n)^n + (1+u^n)^n} =: l_{2,n}(u) \tag{5.47}$$

where it is obvious that $l_{2,n}(-u) = l_{2,n}(u)$ for n even and $l_{2,n}(-u) = -l_{2,n}(u)$ for n odd. Plots of these functions for a few values of n are below in 5.3 and suggest the idea we pursued when defining the protocols with higher degrees, that the convergence may be faster. These plots prove it, although for a very special set of all possible mixed states. With increasing n the u coordinate is drawn significantly closer to the attractive values $0, 1$ after only a pair of protocol iterations.

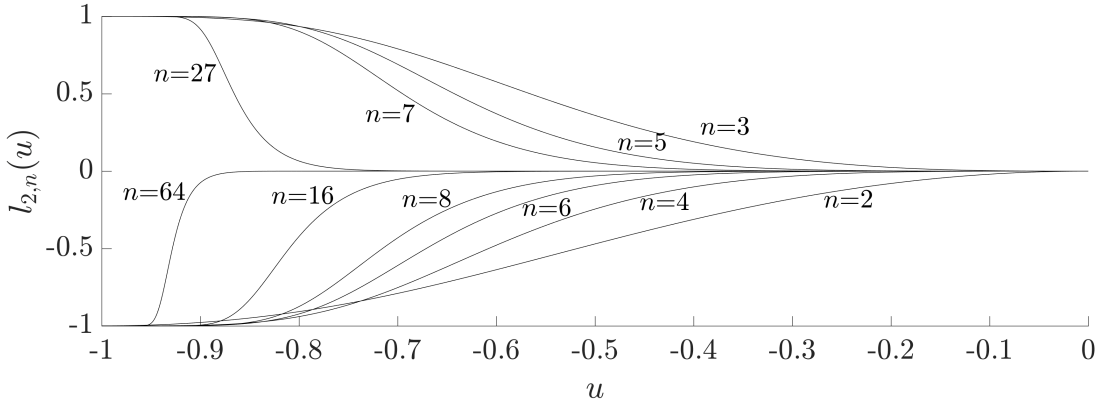

Figure 5.3: Functions $l_{2,n}$ restricted to negative u semiaxis. The odd n degree shows the flip to positive semiaxis.

Much bigger surprise is found when we try with L_1 set. We cannot avoid now writing evolution equations in K from which also $l_{2,n}$ was derived:

$$w' = \frac{2u^n}{(1+w)^n + (1-w)^n},\ u' = -\frac{(1+w)^n - (1-w)^n}{(1+w)^n + (1-w)^n} \tag{5.48}$$

The L_1 set was defined by condition $w = 1+u$. Let us study whether $w' = 1+u'$. That is equivalent to

$$2u^n = -(1+w)^n + (1-w)^n + (1+w)^n + (1-w)^n = 2(1-w)^n \tag{5.49}$$

When n is even, then inserting $1-w = -u$ satisfies the equation. However, not for n odd. The reason is the sign change which causes the state to jump across different quadrants during evolution; more precisely, in the u, w axes and maps like 5.2, the state rotates counterclockwise: with $w, u > 0$ the state evolves to $w' > 0, u' < 0$, then $w'', u'' < 0$, after third iteration $w''' < 0, u''' > 0$ and cycle ends in $w'''', u'''' > 0$ again. With this idea we can prove that the line segment $w = 1+u$ is mapped onto segment $w = -1-u$, then to $w = -1+u$ and to $w = 1-u$ before the cycle starts to repeat. Therefore, in case of odd n one has to extend L_1 to

$$L_1^{\pm} = \left\{ (w,u,0) | w,u \in [-1;1] \wedge \left(\begin{array}{c} w = 1+u \ \vee \ w = 1-u \vee \\ \vee \, w = -1+u \ \vee \ w = -1-u \end{array} \right) \right\}. \tag{5.50}$$

The actual convergence is not influenced by the particular quadrant, the evolution is symmetrical in reflection around the w, u axes. The importance of these subsets is that we are unable to look for mixed cycles or fixed states because of the limited computational possibilities in three-dimensional space. But the calculations suggest that the only cycles and fixed points belong to these one-dimensional subsets where the evolution is (more) solvable.

Also, we can look for a fixed state without considering four iterations to repeat the cycle. Setting the input state to $(w, 1-w, 0)$ that has $w > 0$ and is the member of the cycle, then it must be mapped onto $(w, w-1, 0)$. In this way we derive evolution function

$$l_{1,n}(w) := \frac{2(1-w)^n}{(1+w)^n + (1-w)^n} \tag{5.51}$$

which determines the fixed points when $l_{1,n}(w_1) = w_1$ is solved; $w_1 > 0$ is gained in this procedure. The invariant cycle is then

$$(w_1, w_1 - 1, 0) \to (-w_1, w_1 - 1, 0) \to (-w_1, 1 - w_1, 0) \to (w_1, 1 - w_1) \circlearrowleft \tag{5.52}$$

for n odd; for n even this cycle is reduced to a single fixed state

$$(w_1, w_1 - 1, 0). \tag{5.53}$$

Although the values of fixed points for each n can be given in terms of roots of exact polynomials, such solution cannot be given in radicals as soon as $n = 5$, this is a well known situation from algebra. Therefore, we present a table of the states for given n, also with their purity calculated as $P = 1 - w_1 + w_1^2$.

Note that function $l_{1,n}$ does not describe the evolution properly, artificially constructed above only one branch of $L_1^{\pm}$ it is not defined on $[-1;0)$ and must be reevaluated for other quadrants. The function $l_{1,n}$ changes with degree n in a manner similar to $l_{2,n}$. When increases, the convergence towards attractors determined is faster and the value of the fixed point w_1 separating the points converging to the two dynamical regimes tends to 0. That means that the convergence is faster but the analogue to the basin of attraction of $|0\rangle - |1\rangle$ shrinks

n	w_1	$w_1 - 1$	P
2	$\chi \doteq 0.361103$	$\chi - 1 \doteq -0.638897$	$1 - \chi + \chi^2 \doteq 0.769292$
3	0.288392	−0.711608	0.794778
4	0.242592	−0.757408	0.816259
5	0.210707	−0.789293	0.833691
6	0.187050	−0.812950	0.847938
7	0.168703	−0.831297	0.859758
8	0.154003	−0.845997	0.869714
9	0.141924	−0.858076	0.878218
16	0.093829	−0.906171	0.914975
32	0.055509	−0.944491	0.947572

Table 5.1: Table of cycles in $L_1^{\pm}$ for Pn protocols with H_2 twirling.

n	w_2	P	$-u_2$	P
2	$\mu^2 \doteq 0.295598$	$\mu \doteq 0.543689$	$\mu \doteq 0.543689$	$\frac{1+\mu^2}{2} \doteq 0.647799$
3	$\sqrt{5}-2 \doteq 0.2361$	$5-2\sqrt{5} \doteq 0.5279$	$\phi^{-1} \doteq 0.6180$	$\frac{5-\sqrt{5}}{4} \doteq 0.6910$
4	0.199069	0.519814	0.667961	0.723086
5	0.173428	0.515039	0.704408	0.748095
6	0.154425	0.511924	0.732464	0.768252
7	0.139681	0.509755	0.754878	0.784920
8	0.127852	0.508173	0.773283	0.798983
9	0.118117	0.506976	0.788721	0.811041
16	0.079112	0.503129	0.853376	0.864125
32	0.047556	0.501131	0.909207	0.913328

Table 5.2: Table of cycles in $L_2^{\pm}$ for Pn protocols with H_2 twirling.

while the basin of attraction of $|0\rangle$ grows. The same trend is found from 5.3 - basin of attraction of the maximally mixed state (in $L_2^{\pm}$ determined by $u = 0$), i.e. interval of u converging to 0 is growing, determined by $(u_2; 0]$, the values are given below in table 5.2. The fixed points determined by $l_{2,n}(u) = \pm u$ that separates the two asymptotic regimes tend to 1 with growing n. This means that the convergence is faster but the basin of attraction of the pure attractor shrinks.

On the other hand, the evolution on subset $(w, 0, 0)$ of $L_2^{\pm}$ is also faster and the basin of attraction of the pure attractor grows with growing n. We are also interested in the invariant states in the L_2 set, the states $(w_2, 0, 0)$ mapped onto itself after four iterations (onto itself or $(-w_2, 0, 0)$ after two iterations depending on parity of n). We present the w_2 values in a table below, together with the purity values of corresponding states $P = \frac{1+w_2^2}{2}$. We also decide to accompany these states with the states from the other branch, we will write coordinates of states $(0, u_2, 0)$ that are mapped onto themselves after four iterations, for analogy to protocol $P2$ or other even n we write $w \geq 0, u \leq 0$. Note that there are also states $(\pm 1, 0, 0), (0, \pm 1, 0), (0, 0, 0)$ as the solutions to corresponding equations. As a kind of a trivial solution, we do not present them.

We have probably given enough clues to guess the general evolution in K for higher n. To support readers' intuition and sketch the change for increasing n, we present the attractor maps in a quadrant of K.

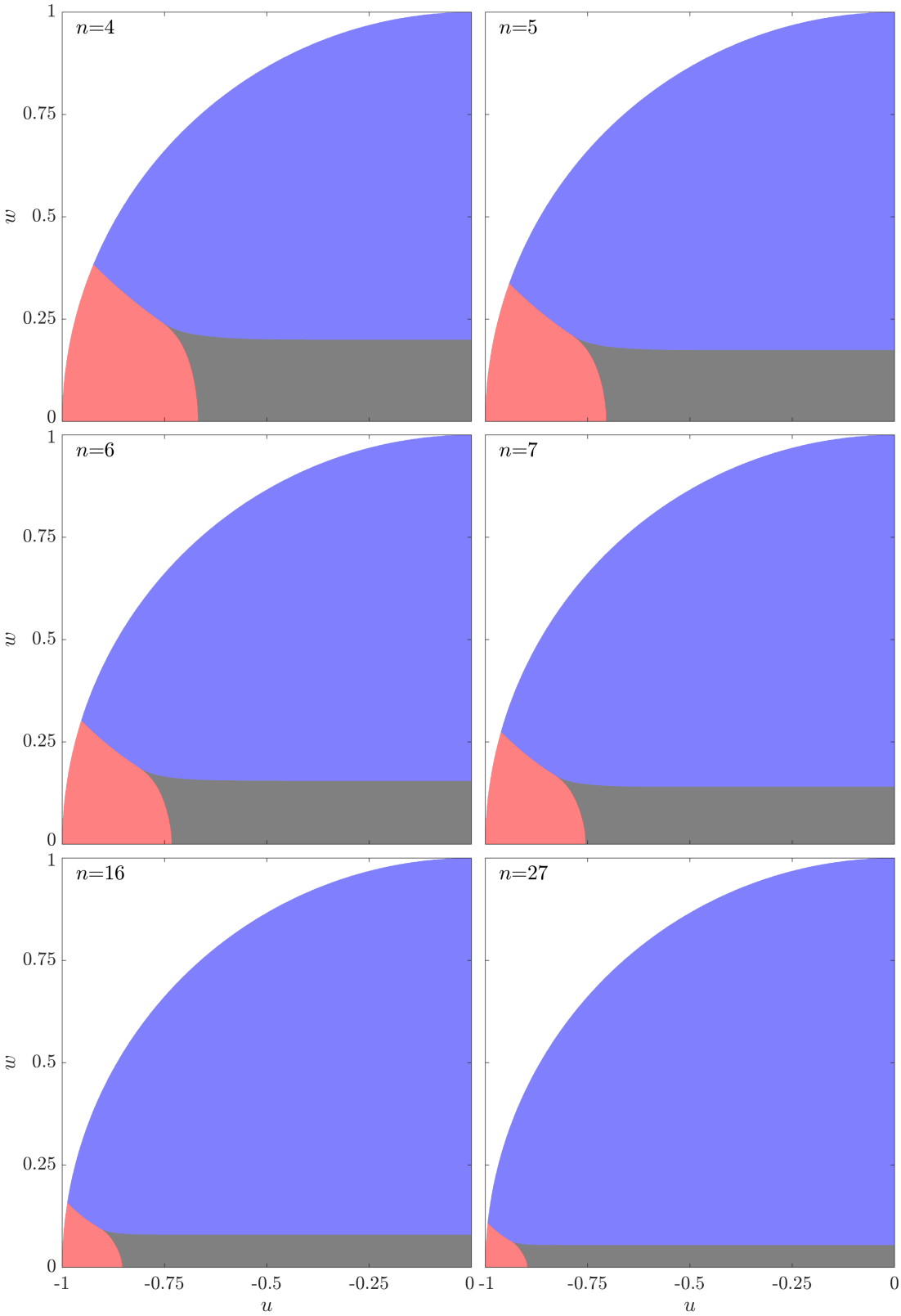

Figure 5.4: Attractor maps of Pn protocols in quadrants of $v = 0$ plane. Other quadrants can be added symmetrically with respect to parity of n; for odd n the map in the whole range $w, u \in [-1; 1]$ is analogous to 5.2. Speed of convergence increases with n. Immediate basins of attraction of $|0\rangle$ and $|1\rangle$ grow, immediate basins of attraction of $|0\rangle \pm |1\rangle$ shrink, invariant points/cycles tend to the maximally mixed states or the pure attractors.

5.6 Universality of Pn protocols

While the case $x = \frac{\pi}{4}, \psi = \tau = 0$ is well documented now, we recall that when changing x in $n = 2$ case one could find attractors with other values of w, except for a single value w_c. We will not give exact prescriptions for what attractive states and cycles are available when x is chosen. Instead, we give a statement without a general proof, only numerical evidence.

Statement 5.6.1. *P_n protocols with n even and $\psi = 0$ are universal, i.e. for each except one value of $w = w_{c,n}$ depending on n, for arbitrary state (w, u, v), parameters x, τ can be found such that (w, u, v) is a member of attractive 2-cycle of the protocol. For values w such that $w_{c,n} < |w| \leq 1$, x, τ can be found for state (w, u, v) so it is fixed attractive state.*

The critical values $w_{c,n}$ decrease towards 0 with increasing degree n. Also, the corresponding parameters $x_{c,n}$ - where the bifurcation occurs - tend to grow to $\frac{\pi}{4}$. Let us present the attractors of protocols with $x, \psi = \tau = 0$ like we already have - with the plot of their w and u coordinates. To make the plots clear, we separate the coordinates.

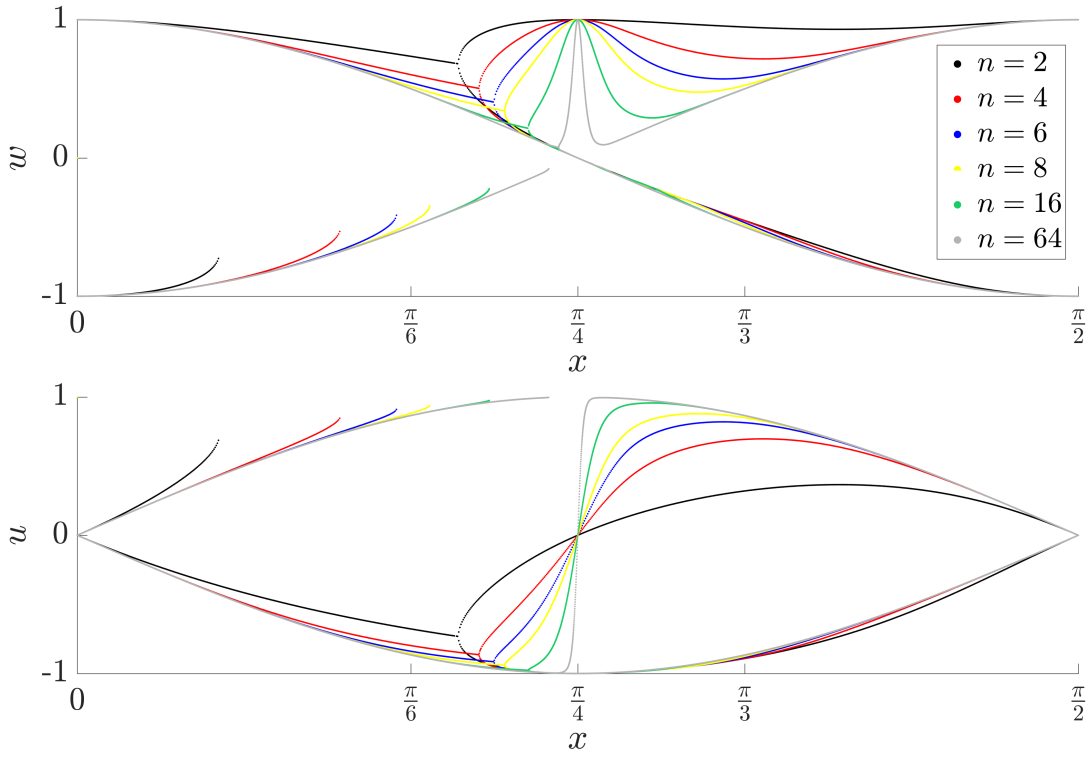

Figure 5.5: The bifurcation of attractors Pn with n even according to legend, w, u coordinates of attractors drawn separately. Critical angles where bifurcation occurs tend to $x = \frac{\pi}{4}$ with increasing n.

There is an observation that emerged to us after more detailed calculations.

Conjecture 5.6.2. *With $n \to \infty$, the state $(w, -\sqrt{1-w^2}, 0)$ can be made attractive fixed state of the protocol when x is chosen so that $\frac{acos\,|w|}{2} = x < \frac{\pi}{4}$. For the same x, state $(-w, \sqrt{1-w^2}, 0)$ is a fixed attractor too. State $(w, \sqrt{1-w^2}, 0)$*

can be made a member of attractive 2-cycle when $\frac{acos\,|w|}{2} = x > \frac{\pi}{4}$. *In this case, the other member of the cycle is* $(-w, -\sqrt{1-w^2}, 0)$.

This proposal does not distinguish parity of n because in the limit of high n the behaviour coincides, except for certain vicinity of $x \doteq \frac{\pi}{4}$.

Now, we want to discuss the case of low odd n. These protocols are fundamentally different to those with n even. Not only because of the 4-cycles, but also in the bifurcation when the attractors depending on x are plotted. The bifurcation is obviously more dramatical for $n = 3$ and the same trend holds for greater values of n odd. With n growing, the region where the bifurcations occur is more and more restricted towards $x = \frac{\pi}{4}$.

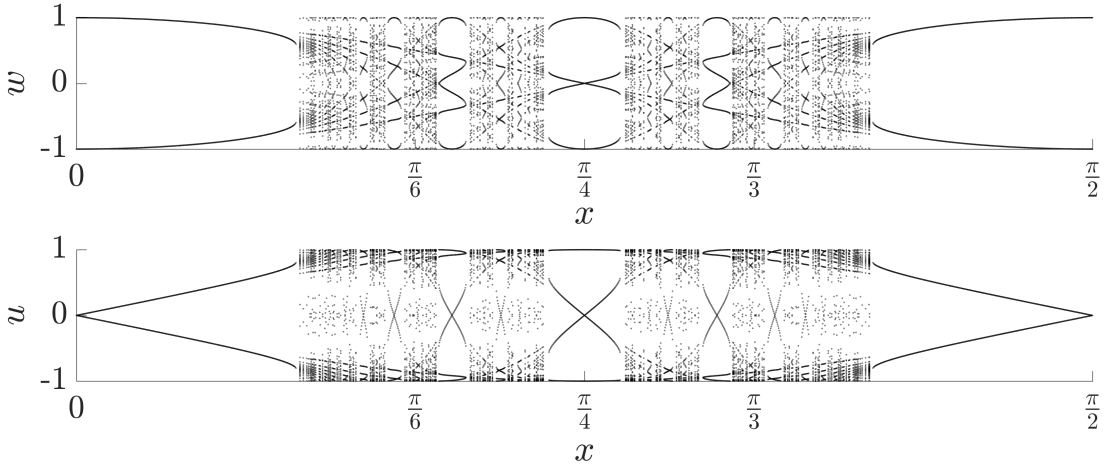

Figure 5.6: Bifurcation of attractors in protocols $P3$ with $\tau = 0$. w, u coordinates drawn separately, $v = 0$ always. For higher n the bifurcations are restricted closer to $x = \frac{\pi}{4}$, the curves tend to $\pm\sin 2x, \pm\cos 2x$

These plots remind very well of logistic function. In our context, we will try to connect them to the change of fractal structures. it is the best time to uncover what fractal structures are offered by general protocols.

5.7 Fractal structures and phase transition in Pn protocols

Because the pure states in the complex number representation again evolve with rational polynomial functions, now with degree n, we are guaranteed to have non-vacuous Julia sets in the pure states. We will again use the box-counting method to estimate its dimension, we will use notation $d(n; x, \tau)$ for the dimension estimate of the Julia set induced by protocol Pn with twirling gate parameters x, τ. For the rest of the chapter we assume $\psi = 0$.

First, for $n = 3$ we show the dimension estimate $d(3; x, \tau)$ again in plane coded with colour similarly to 4.9. This time for the sake of computational time we have chosen only one randomisation box to average over, the results are therefore burdened with higher error which leads to increased individual variation in the pixels. The maximal box resolution remains 5000^2. We have (similarily to the case $n = 2$) seldom points with $d < 1$ as random errors, we have them rounded

to 1. Only 36 of these error points were below $\in (0.98, 0.916)$ and a single value dropped to ca 0.885; 2256 values were in interval $[0.98; 1.02]$. We believe that this is a very convincing result in favour of our box-counting algorithm even when the statistical approach with random boxing was not implemented; it justifies us to consider the corrected points being random errors.

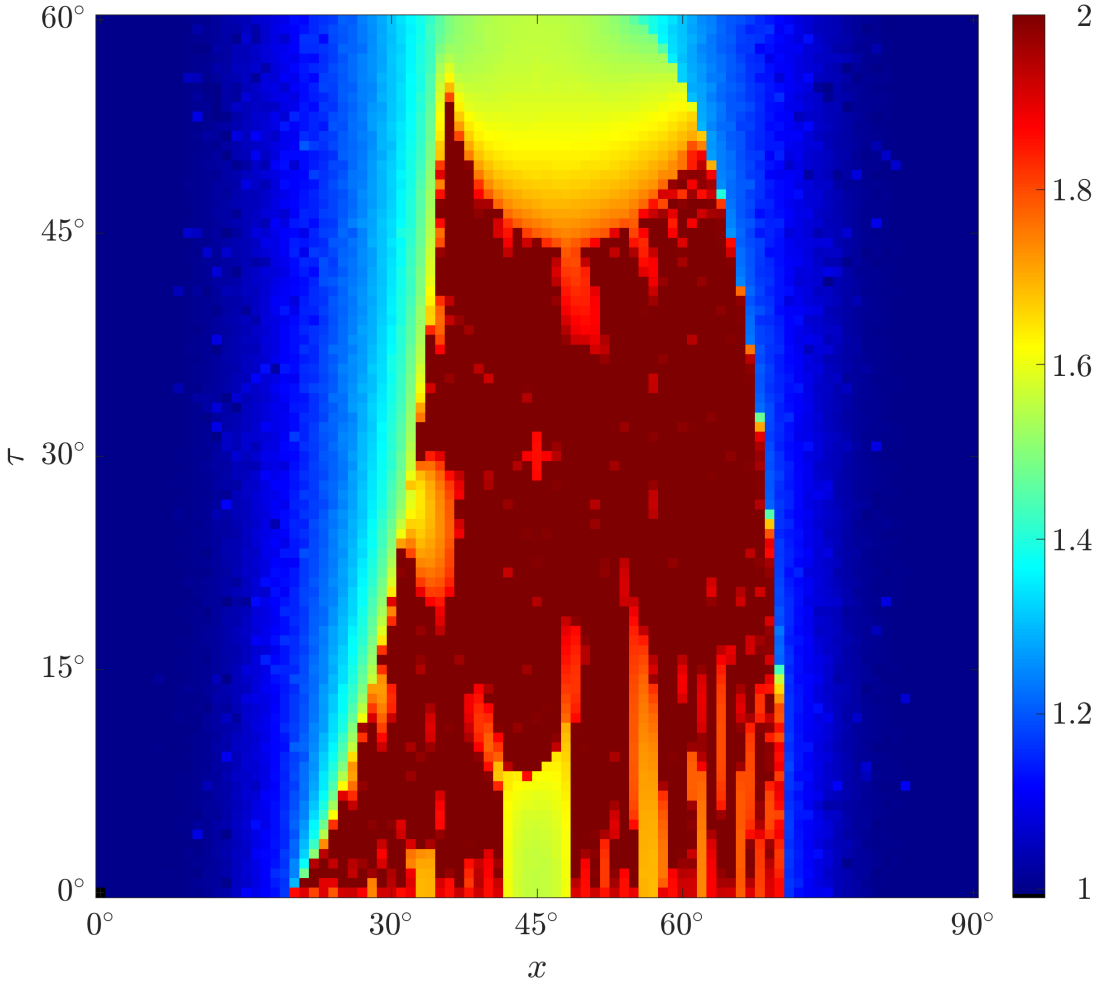

Figure 5.7: Dimension $d(3; x, \tau)$ represented by colour in plane x, τ.

This case has one big difference to case $n = 2$, the generalised Mandelbrot set - let us naturally index it with the degree $n = 3$ - $\widetilde{\mathcal{M}}_3$ seems now to be equal to the whole parameter space $x \in [0; \frac{\pi}{2}], \tau \in [0; \frac{\pi}{6}]$. This means that the totally disconnected structure, Cantor dust as in 4.10, 4.14 has not been identified for any pair of parameters x, τ. We will see in a moment, this is another canonical difference between protocols with odd and even n. We formulate a conjecture.

Conjecture 5.7.1. *$\partial\, \widetilde{\mathcal{M}}_3 = \emptyset$ for protocols $P3$.*

When we check the fractal structures visually, we can now discern all the previously identified types (save for the Cantor dust), i.e.

1. single fractal curve separating two immediate basins of attraction,
2. recurring islands of multiple basins of attraction, now with resemblance of symmetries of higher orders,

3. shattered structure resembling white noise and islands of regular evolution in regions of white noise,

4. island of stability surrounded by white noise,

5. transient structures exhibiting complicated morphology of spiral shaped recurring islands. These structures typically combine multiple features of the previous and usually shatter across the attractor map.

Compared to the case $n = 2$, there is a feature often visible of pairs of whirls rotating in opposite directions. These whirls seem to shatter across the Bloch sphere in bifurcation and can create also structures resembling dendrites. Let us now present a short excerpt of the atlas of $P3$ maps that speaks for itself.

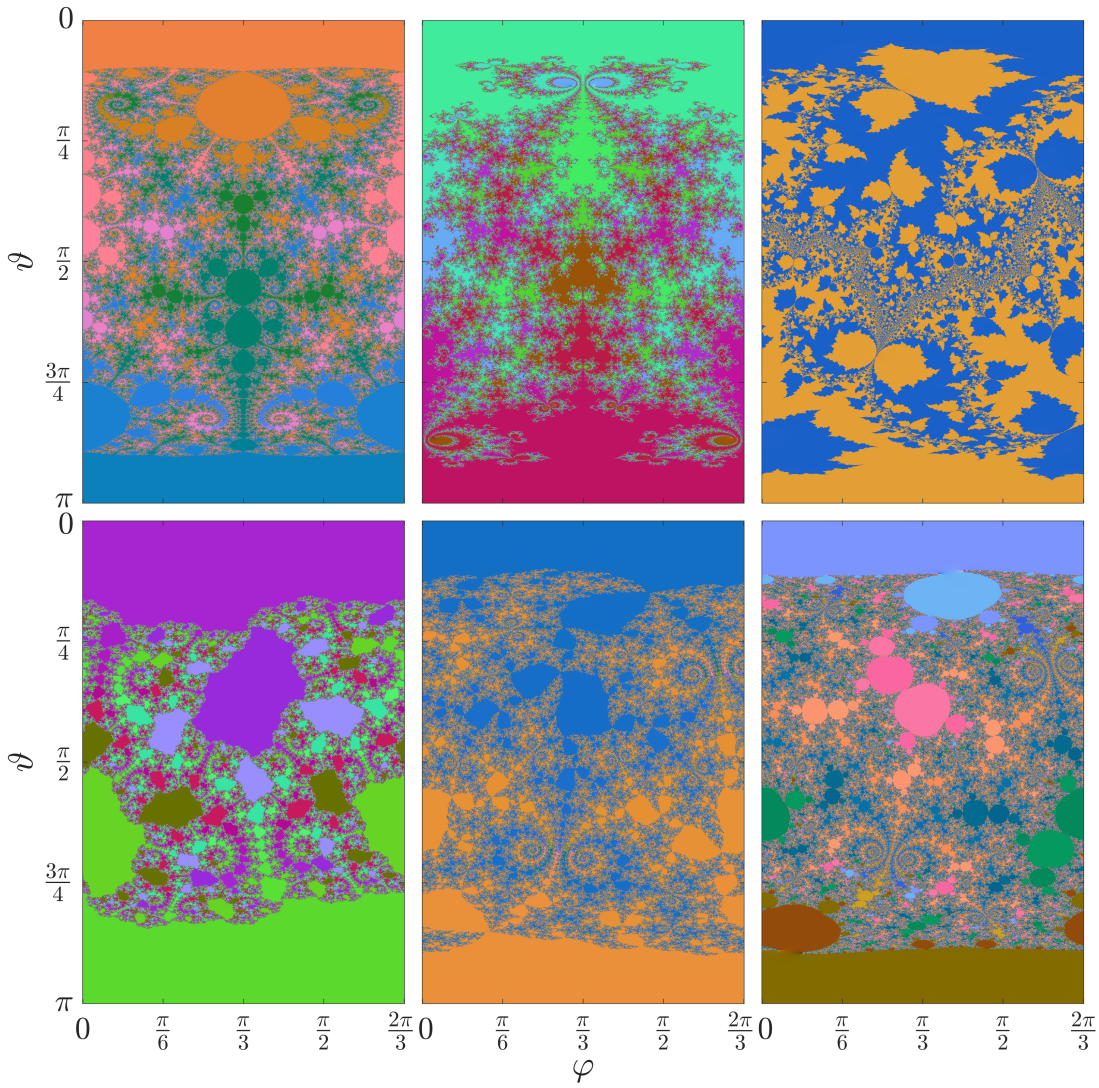

Figure 5.8: Fractal structures for $P3$ protocols often contain pairs of whirls. *Top left:* $x = 32°, \tau = 0°$, *top centre:* $x = 38°, \tau = 120°$, *top right:* $x = 68°, \tau = 32.\bar{6}°$, *bottom left:* $x = 68°, \tau = 106.\bar{6}°$, *bottom centre:* $x = 69°, \tau = 18.\bar{6}°$, *bottom right:* $x = 69°, \tau = 23.\bar{3}°$.

Now, for more general n, our readers will probably be disappointed, but no new features are discovered. We state based on numerical evidence an important conclusion.

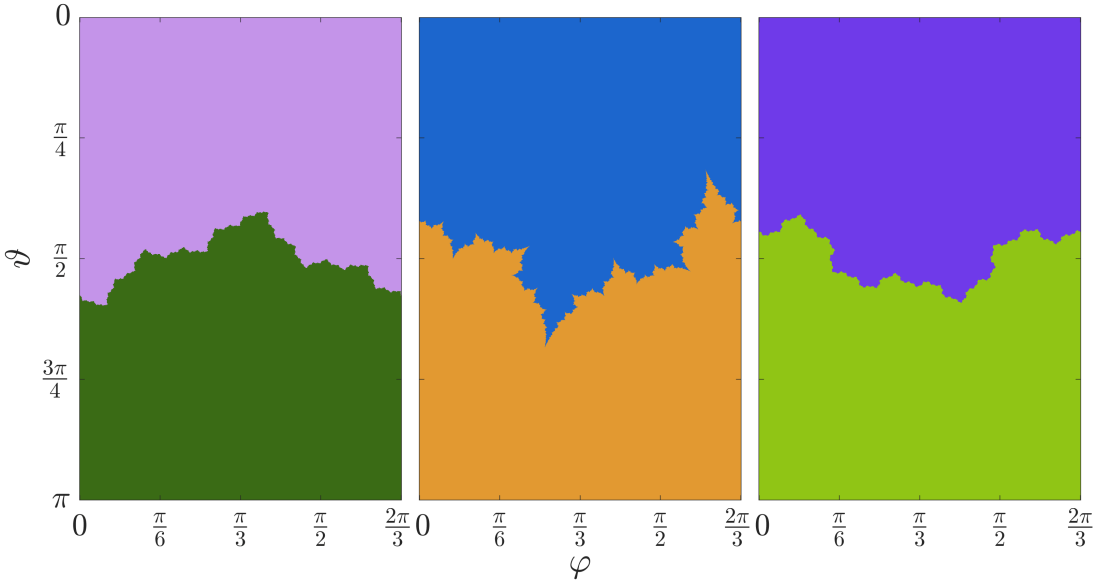

Figure 5.9: Fractal structures for x close to 0 or $\frac{\pi}{2}$ separate attractor basins of two fixed states or regimes of attractive cycles. *Left:* $x = 16°, \tau = 12°$, *centre:* $x = 69°, \tau = 26.\bar{6}°$, *right:* $x = 72°, \tau = 72°$.

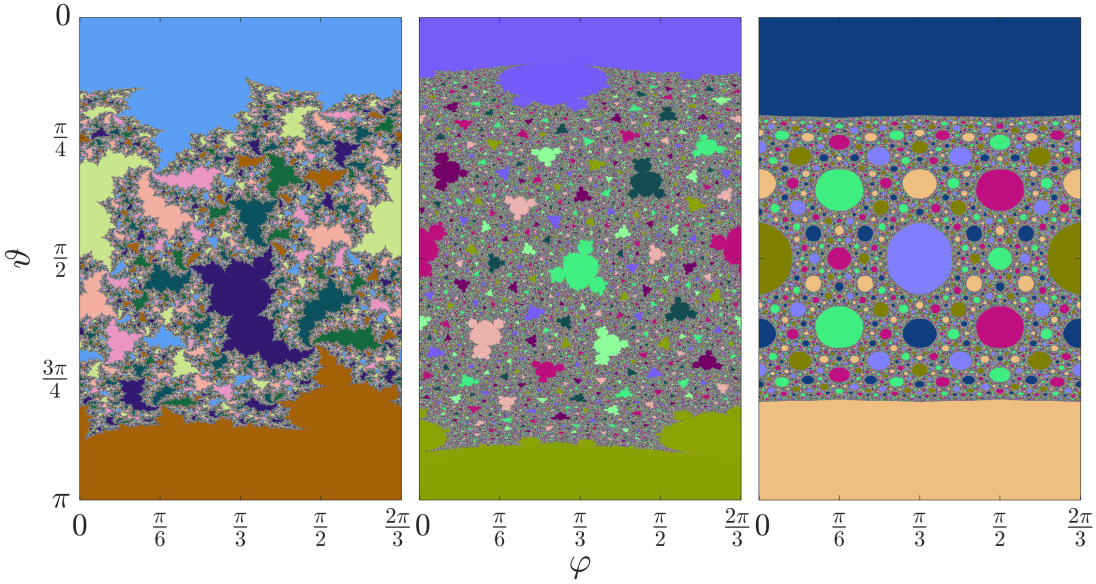

Figure 5.10: A common type of structure resembles regular islands in a sea of white noise. But these are only complicated recurring islands of basins of attraction. Some of the islands may resemble structure of the Mandelbrot set, 2.2. *Left:* $x = 29°, \tau = 10.\bar{6}°$, *centre:* $x = 39°, \tau = 84°$, *right:* $x = 45°, \tau = 30°$.

Statement 5.7.2. *All protocols Pn with n even are canonically similar to case P2. All protocols Pn with n odd are canonically similar to case P3.*

We lack any apparatus that could compare the generalised Mandelbrot sets $\widetilde{\mathcal{M}}_n$. Therefore, we do not dare to speak of some continuous transformations or to use any mathematical concepts. Not even to mention that the fractal structures can oppose the concept of continuity. While we tried to be precise and analytical, or at least well established numerically, now we must condemn that

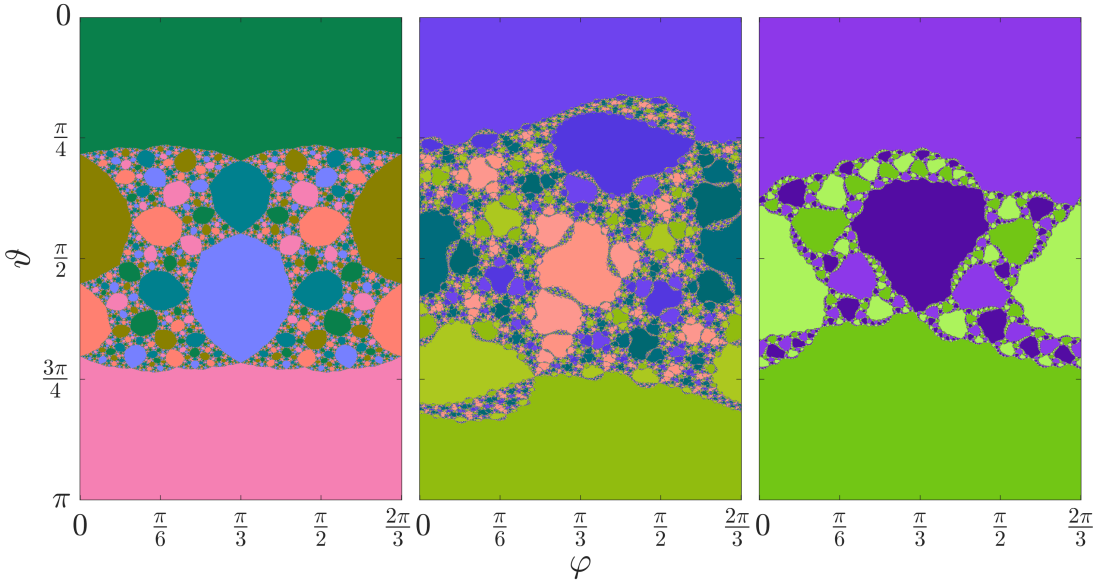

Figure 5.11: Fractal structures often consist of recurring islands similarly to the case of the original protocol $P2$ with H_2. *Left:* $x = 33°, \tau = 0°$, *centre:* $x = 41°, \tau = 9.\bar{3}°$, *right:* $x = 54°, \tau = 66°$.

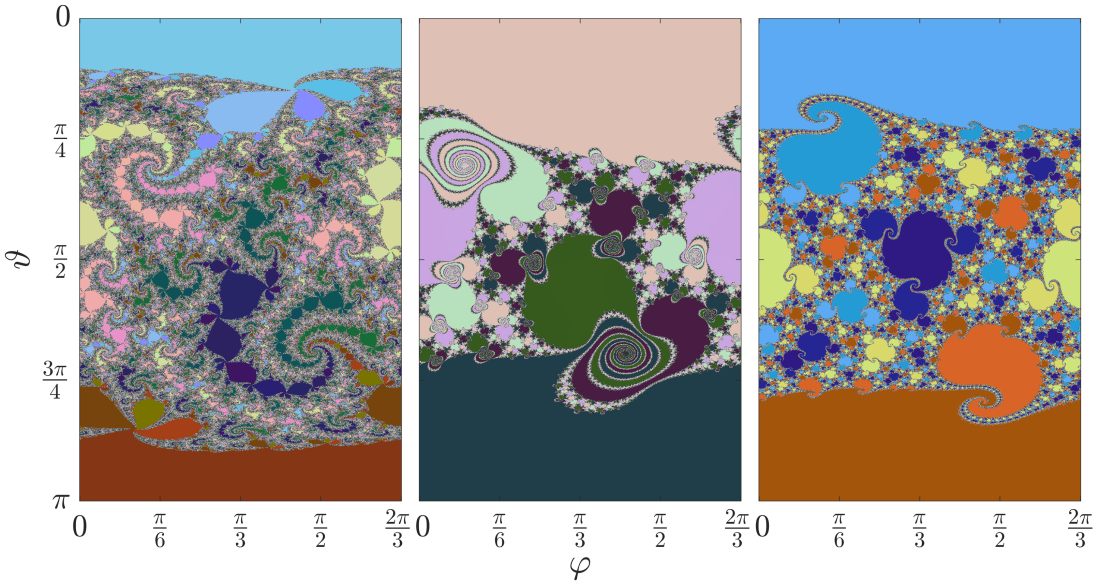

Figure 5.12: Spiral shaped fractals often appear as a transition between different types of structure. *Left:* $x = 28°, \tau = 12°$, *centre:* $x = 32°, \tau = 28°$, *right:* $x = 49°, \tau = 44°$.

the conclusions on the topic of the metastructure can be done only vaguely and rather in a popular and not an academic manner of speech. Hopefully our readers will forgive us using simply the word 'similar' to compare the Mandelbrot sets. Let the readers judge themselves.

However, we believe that new discoveries can rather inspire future research that will settle down the terminology, mathematical formalism and build a stable and precise background. We would certainly support any future research on the topic of the multivariate rational polynomial functions and the chaos they

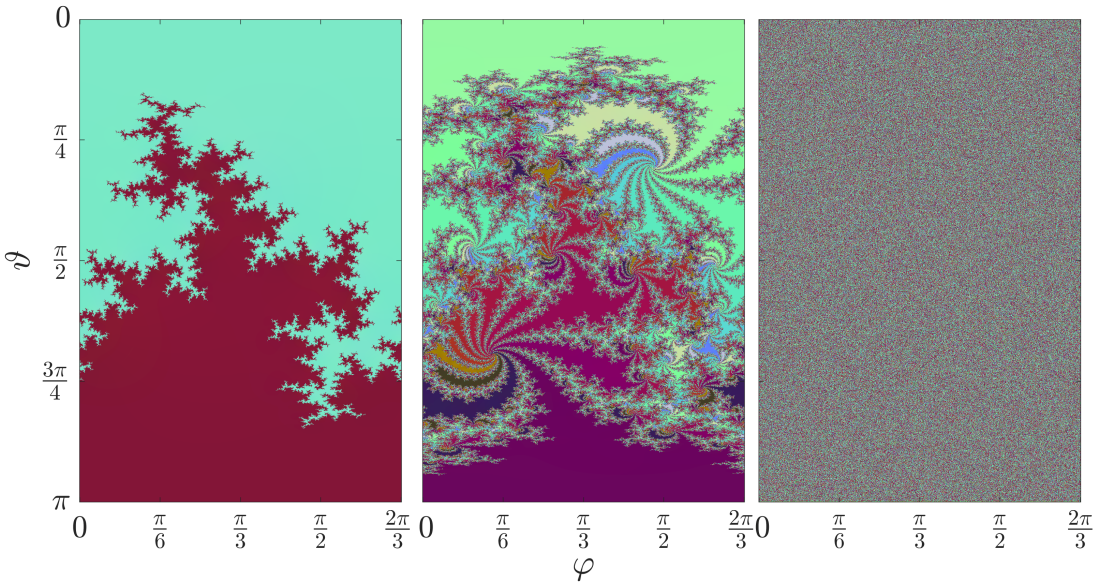

Figure 5.13: Bifurcations in $P3$ protocols dramatically influence fractal structures. *Left:* $x = 25°, \tau = 112.\bar{6}°$, *centre:* $x = 25°, \tau = 113.\bar{3}°$, *right:* $x = 25°, \tau = 114°$.

induce. Most examples of studied chaos concern continuous time evolution, e.g. weather, stock exchange and resulted later into few important concepts, let us mention strange attractor [55] as an example. We believe that this new field tightly bound to quantum physics opens a whole new branch of science.

Let us satiate our curiosity on new fractal shapes induced by protocols with higher degrees, overview is presented in 5.16-5.22.

While it could seem from this overview that such complicated patterns are the characteristic, the opposite is true. We submit that the majority of protocols for high n generates simpler structures resembling Koch flakes, 2.3, their symmetry obviously reflects the degree of the protocol. In the overview, we highlighted the interesting representatives. The fact that exotic fractals are restricted closer to $x = \frac{\pi}{4}$ is observable in 5.14, 5.15 and also in 5.5, although only $\tau = 0$ is considered there, just like in a figure 5.26 presented later.

The new fractal structures are just one of two main questions we would like to answer in this section. The other touches the mixed states again; we seek whether the phase transition is also present in case of $n > 2$ and what similarities or differences can be found. We will now deeply study the popular case of $x = \frac{\pi}{4}$ with various n. First, we tried to determine the box-counting dimension of the whole structure of the sensitive states in the three-dimensional space. We used again the third approach from appendix A based on rounding just like in the third chapter. Because the structure is distributed near the Bloch sphere for higher n, we have determined the sensitive points in 2000^3 boxes grid of interval $[0; 1]^{\times 3}$ from which only those with $0.5 \leq w^2 + u^2 + v^2 \leq 1$ were kept. After performing the box-counting fit with $\lambda \in [100; 250]$, we obtained:

The slight decrease of the result is most probably induced by the fact that the structure is more spatially restricted for higher n which effectively reduces the resolution that is key to the box-counting estimate. Now, let us proceed to employ the second approach of box-counting based on `edge` command to estimate

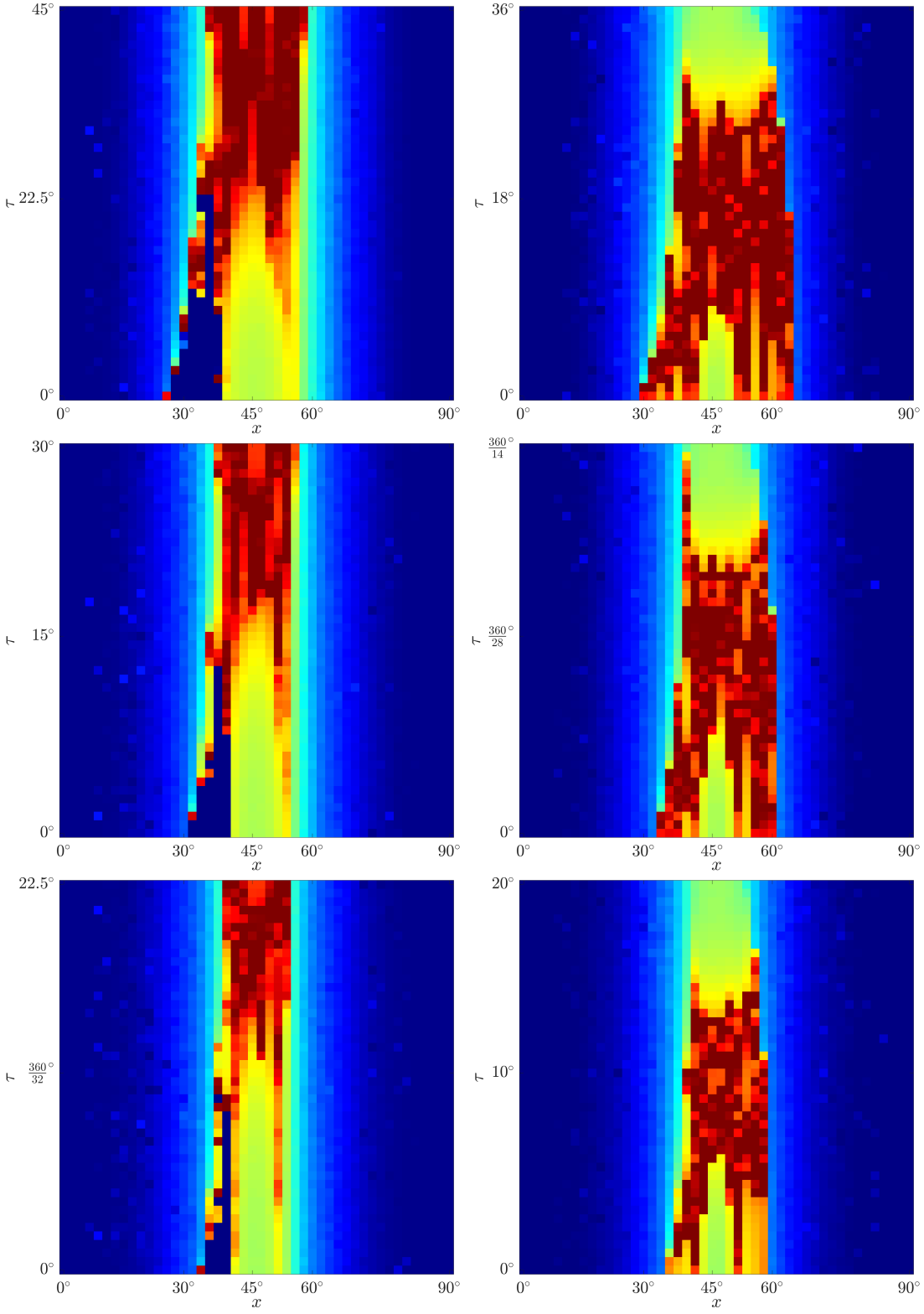

Figure 5.14: Generalised Mandelbrot sets for Pn protocols. *Left column from top*: $n = 4, 6, 8$, *right column from top*: $n = 5, 7, 9$.

the dimension of the fractal slices on the hyperspheres of constant purity aiming to verify the presence of the phase transition. We plot the function of the dimension estimates $d(P; n; \frac{\pi}{4}, 0)$ for various n.

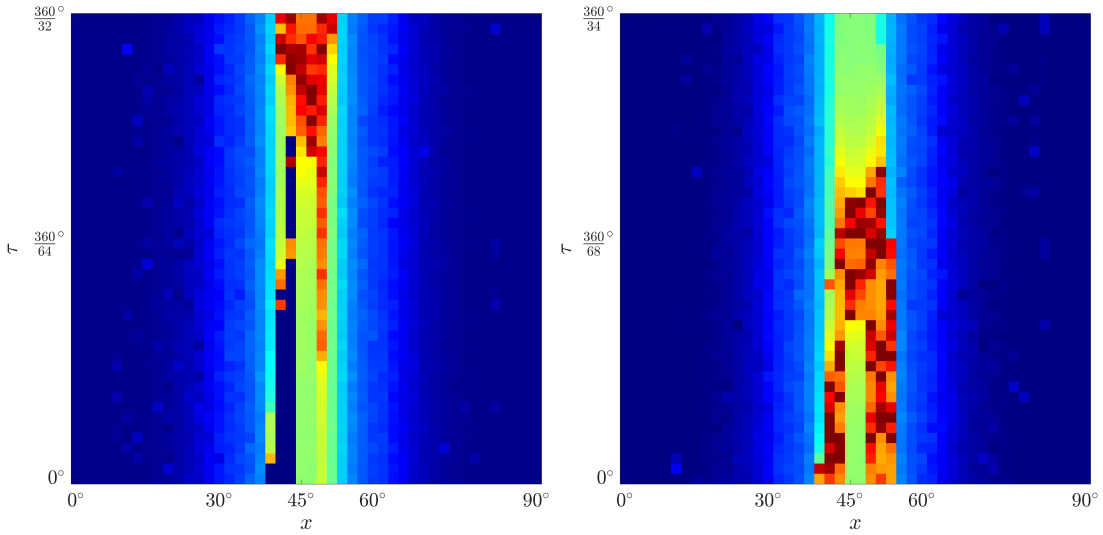

Figure 5.15: Generalised Mandelbrot sets for Pn protocols with higher n keep their shape. *Left*: $n = 16$, *right column from top*: $n = 17$.

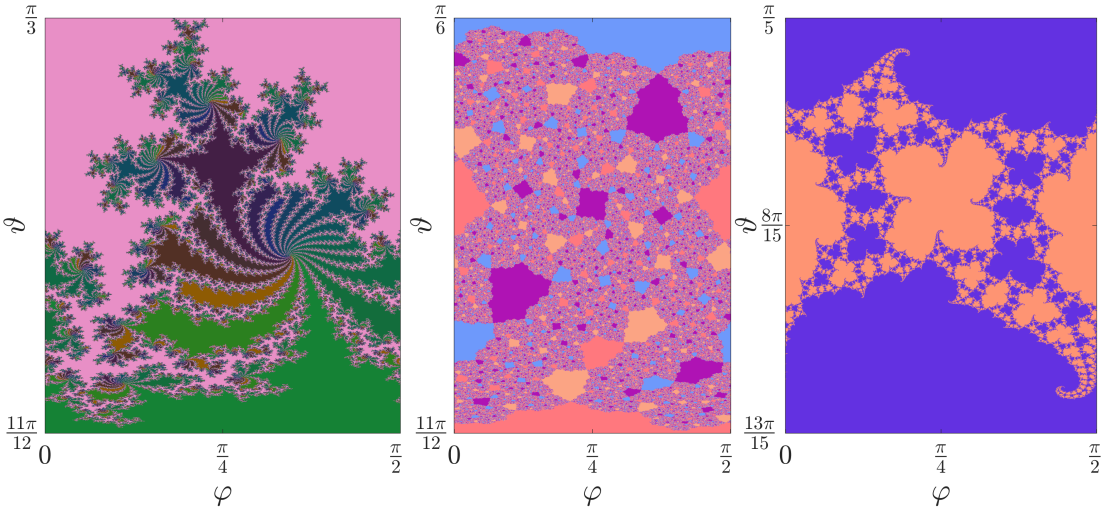

Figure 5.16: Fractal patterns generated by $P4$ protocols. *From left to right:* $x = 32°, \tau = 14.5°$; $x = 44°, \tau = 16.5°$; $x = 48°, \tau = 7.5°$.

n	3D box-counting dimension
2	2.206 ± 0.002
4	2.198 ± 0.002
6	2.191 ± 0.002
8	2.186 ± 0.002

n	3D box-counting dimension
3	2.202 ± 0.002
5	2.192 ± 0.002
7	2.187 ± 0.002
16	2.178 ± 0.003

Table 5.3: Table of dimension estimates of the fractal structures in the Bloch space, generated by protocols Pn with H_2 twirling.

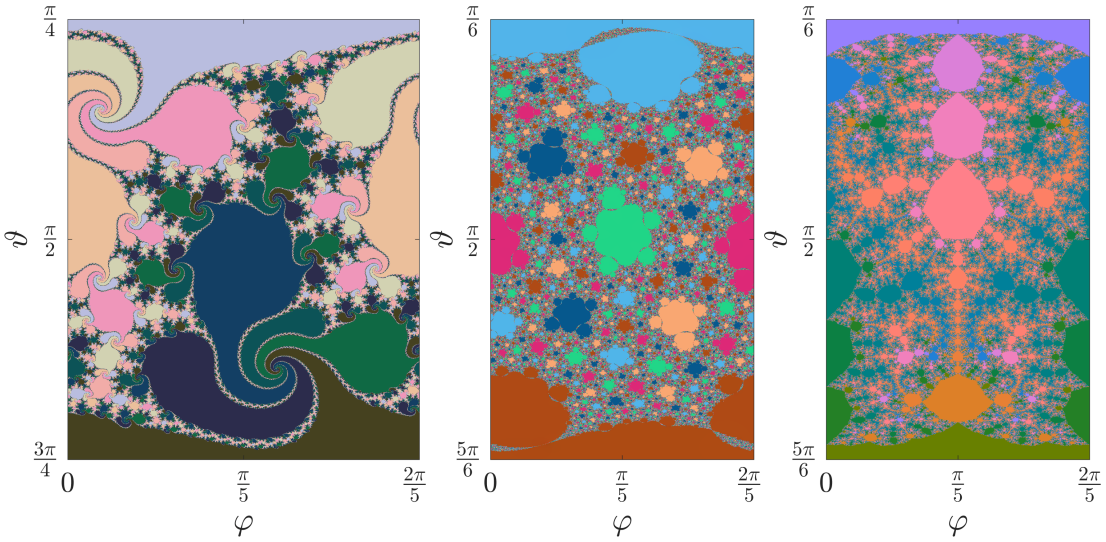

Figure 5.17: Fractal patterns generated by $P5$ protocols. *From left to right:* $x = 36°, \tau = 22.4°$; $x = 48°, \tau = 18.4°$; $x = 62°, \tau = 0°$.

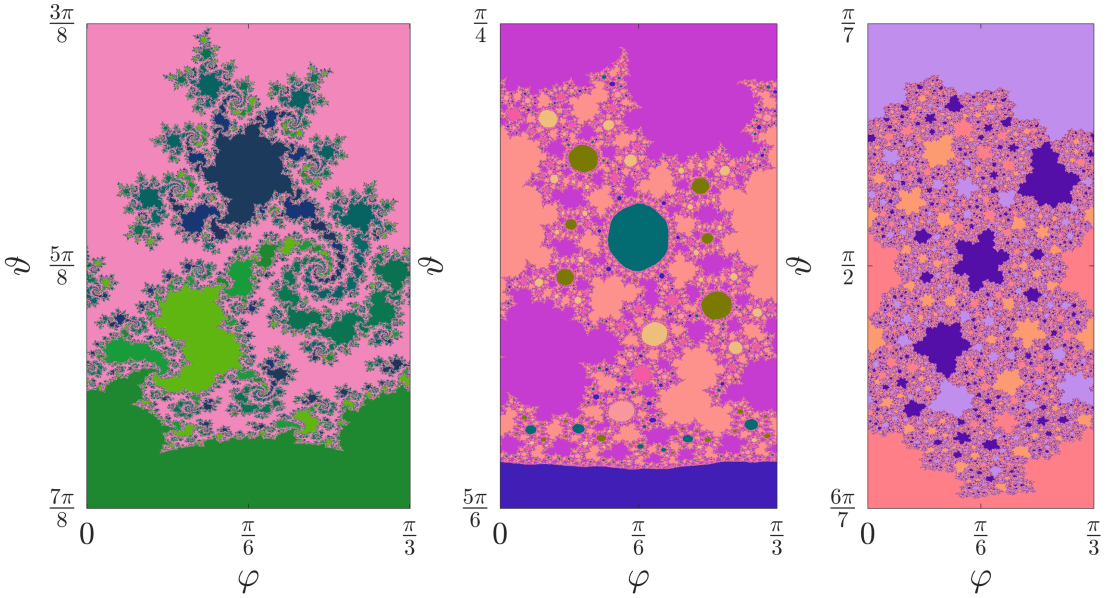

Figure 5.18: Fractal patterns generated by $P6$ protocols. *From left to right:* $x = 34°, \tau = 6.\bar{6}°$; $x = 42°, \tau = 9°$; $x = 48°, \tau = 12°$.

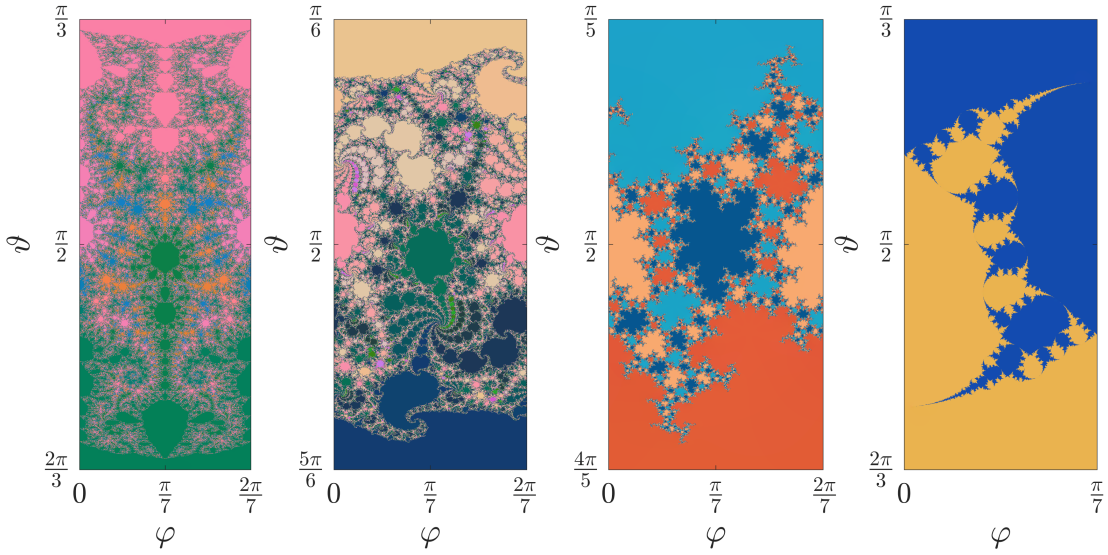

Figure 5.19: Fractal patterns generated by $P7$ protocols. *From left to right:* $x = 34°, \tau = 0°$; $x = 38°, \tau = \frac{144}{7}°$; $x = 48°, \tau = \frac{128}{7}°$; $x = 52°, \tau = \frac{176}{7}°$.

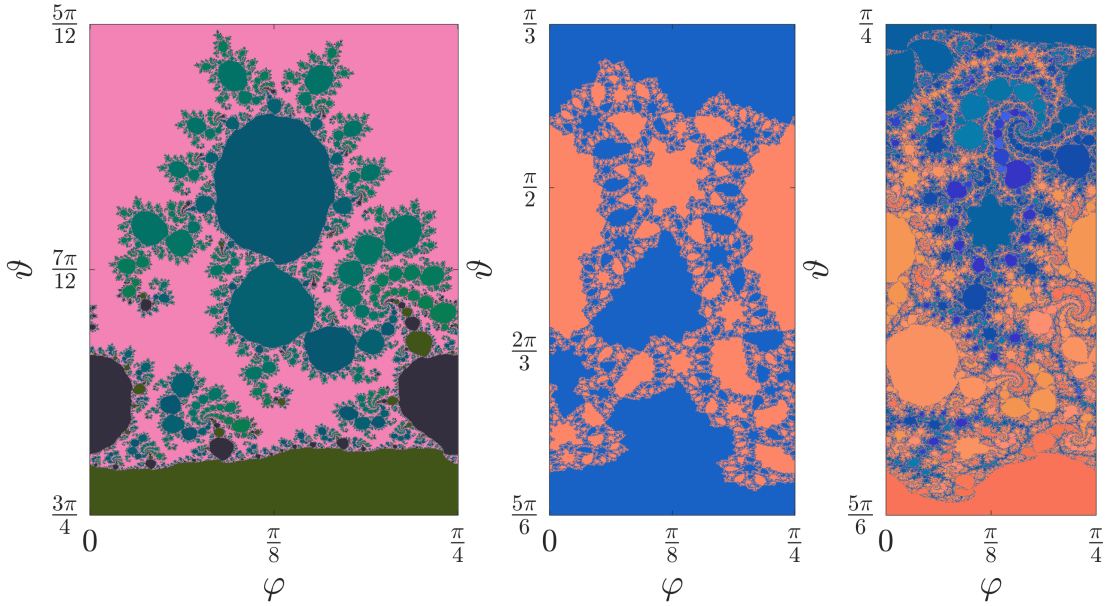

Figure 5.20: Fractal patterns generated by $P8$ protocols. *Left:* $x = 34°, \tau = 1.5°$, *centre:* $x = 50°, \tau = 3.75°$, *right:* $x = 52°, \tau = 8.25°$.

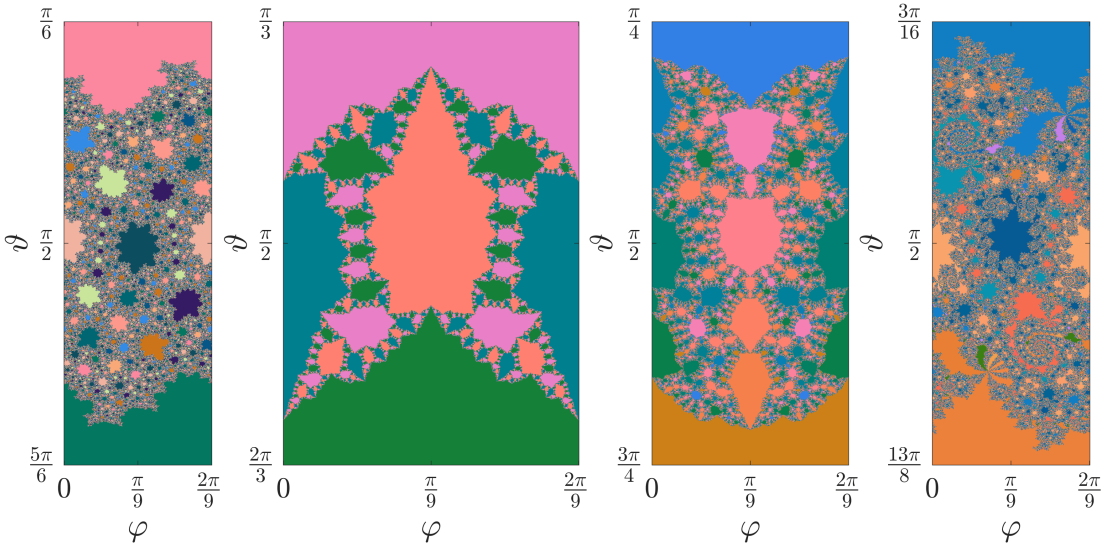

Figure 5.21: Fractal patterns generated by $P9$ protocols. *From left to right:* $x = 42°, \tau = 11.\bar{3}°$; $x = 48°, \tau = 0°$; $x = 50°, \tau = 0°$; $x = 50°, \tau = 13.\bar{3}°$.

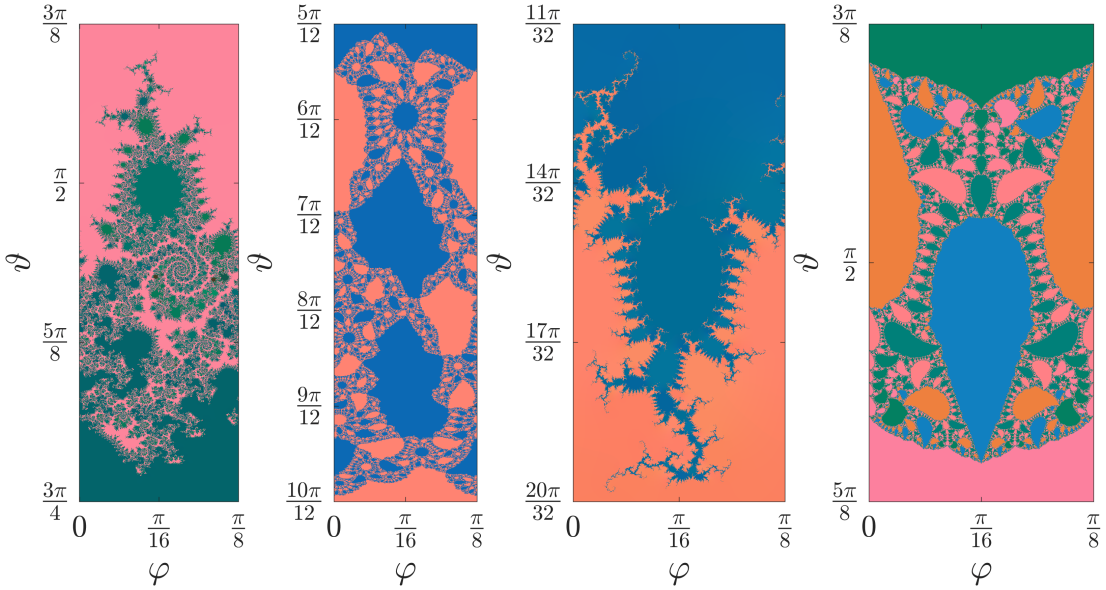

Figure 5.22: Three fractal patterns generated by $P16$ protocols. *From left to right:* $x = 42°, \tau = 11.\bar{3}°$; $x = 48°, \tau = 0°$; $x = 50°, \tau = 0°$; $x = 50°, \tau = 13.\bar{3}°$. *Right:* Fractal pattern for $P17$, $x = 38°, \tau = 0°$.

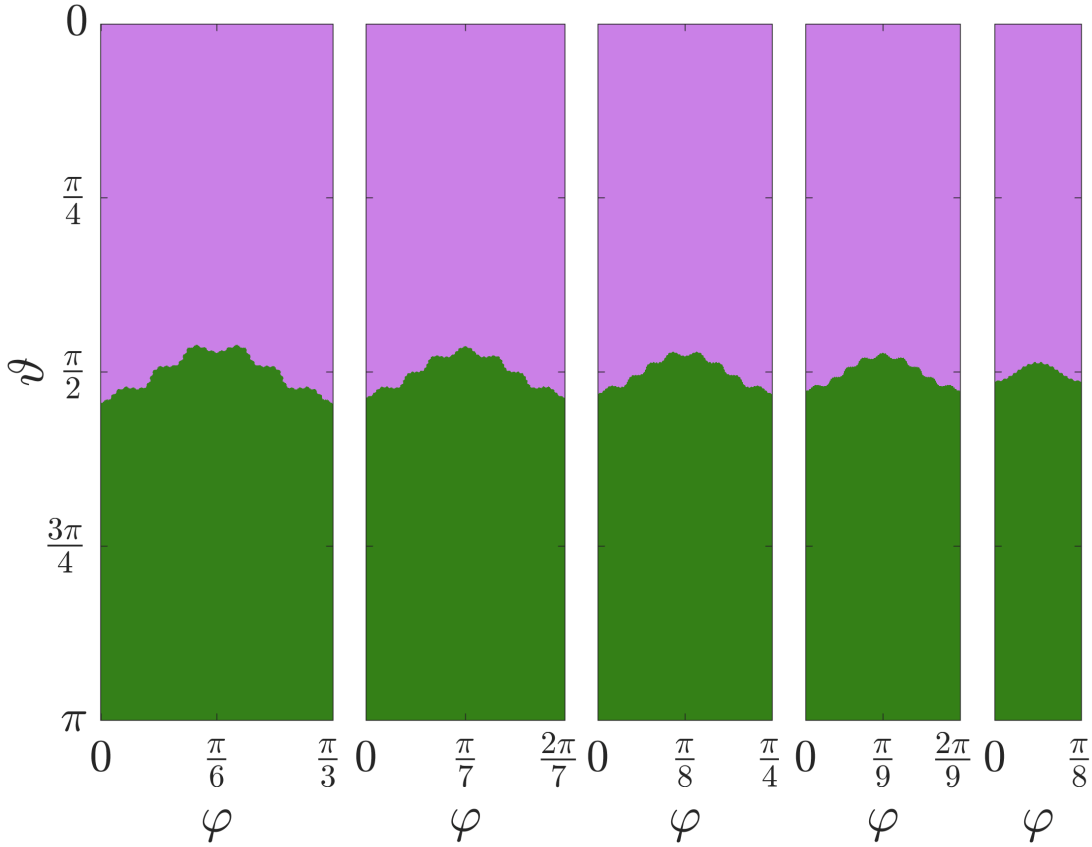

Figure 5.23: Three fractal patterns generated by Pn protocols with $x = 18°, \tau = 0°$. *From left to right*: $n = 6, n = 7, n = 8, n = 9, n = 16$.

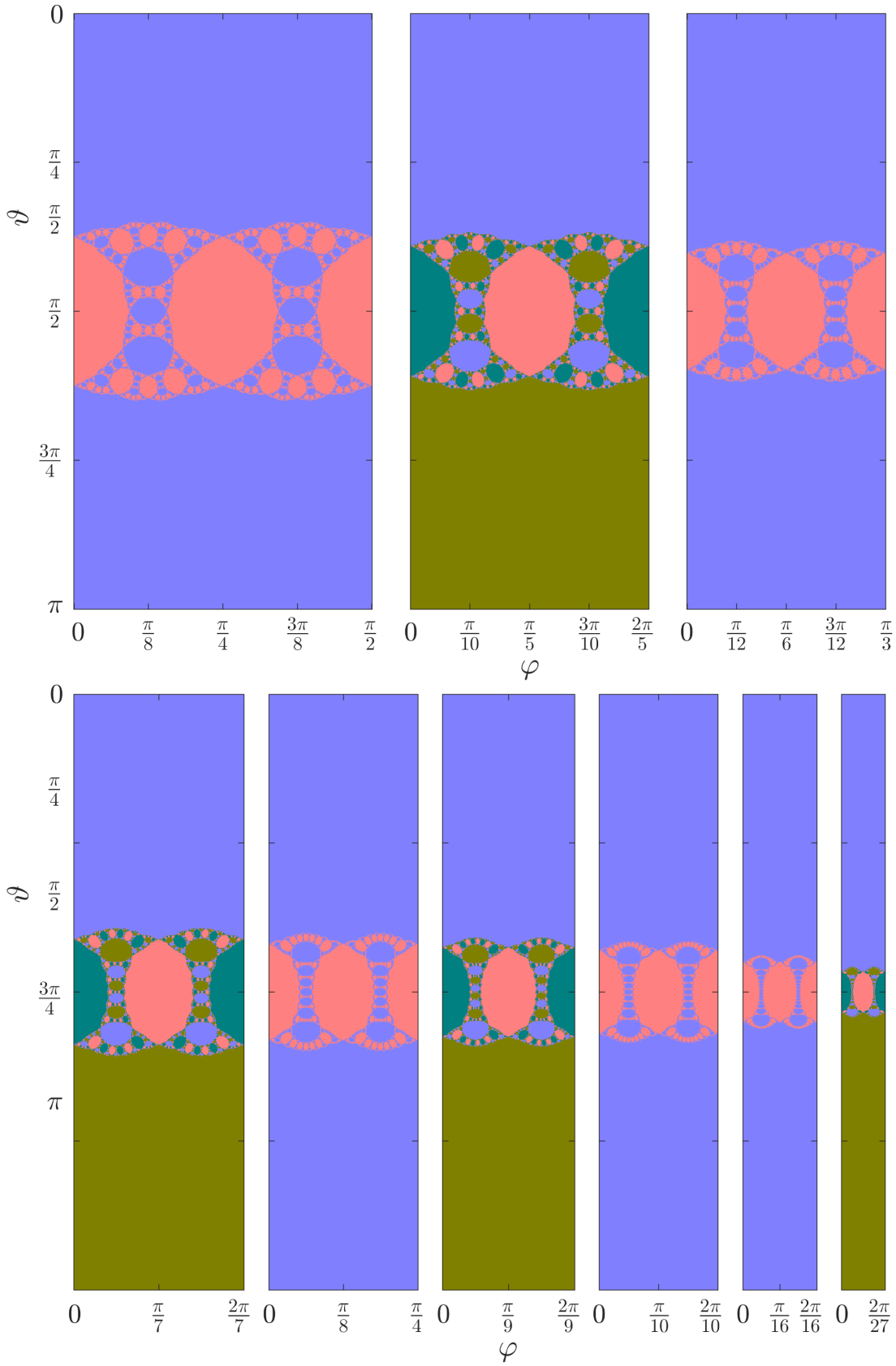

Figure 5.24: The attractor maps and Julia sets of the protocols Pn with H_2 twirling gate. *Top from left to right:* $n = 4, 5, 6$. *Bottom from left to right:* $n = 7, 8, 9, 10, 16, 27$.

The conclusion is unquestionable and leads us to formulation:

Conjecture 5.7.3. *The dimension of the sensitive states for protocols Pn with $x = \frac{\pi}{4}, \psi = \tau = 0$ is the same regardless of n with value ca $\mathscr{D} \doteq 2.21$. The dimension of the Julia set of functions*

$$f_{n,\frac{\pi}{4},0,0}(z) \tag{5.54}$$

is equal to $\mathscr{D} \doteq 1.56$ regardless of the degree n. The phase transition in the terms of quality structure changing its phase fractal $\rightarrow$ regular $\rightarrow$ empty is present for all degrees n and the temperatures exhibit monotonic tendency - increasing to $P = 1$ for the transition fractal $\rightarrow$ regular and decreasing to $P = \frac{1}{2}$ for transition regular $\rightarrow$ empty.

Let us also show how the pattern of the Mandelbrot metastructure changes when the dimension is determined on spheres of lower initial purity.

The phase transition temperature matches again the purity of the prominent states - the fixed repelling states $(w_1, w_1 - 1, 0)$ in $L_1^{\pm}$ seem to be the points of the lowest purity where the fractal structure emerges from, transition fractal $\rightarrow$ regular occurs at the purity of these points, the values are noted in table5.1. The transition regular $\rightarrow$ empty again seems to occur at the states $(w_2, 0, 0)$ in the $L_2^{\pm}$ invariant set, this is the sensitive state of the least purity. The temperatures of the transition being the purity of these states are already presented in table 5.2.

We want to stress now that the transition where the structure of sensitive states is emptied means again that all states with purity smaller than the transition temperature belong to the attractor basin of $\mathbb{1}$. The fact that this transition temperature decreases with growing n implies that the protocol may be more efficient to purify states. More precisely, the probability of failure on a random input of purity P may be smaller. We recall we defined the average entropy function, now enhanced with the degree $e(P; n; x, \tau)$, we recall the results for $n = 2$ are in 4.19, which has the meaning of the protocol failure when the attractors are only either pure or maximally mixed for the protocols of arbitrary degrees. The mixed attractive states can be found for higher n; this prevents us from setting formal conlcusions from 5.26.

We now show plots of $e(P; n; x, 0)$ to confirm our suspicion, again we choose $\tau = 0$ to visualise the results.

Based on this numerical evidence, we can confirm that the protocols Pn are not only capable of repairing more damage states, i.e. the transition temperature is lower, but also offer higher probability of success. Of course, this probability takes the assumption of random input of given purity. We now want to give information more relevant for experimental application, but that deserves a new section. For this moment, let us remind that the exponential trends in $e(P; n)$ are also present for higher n, just like we have shown in 4.20.

We are now ought to finish the topic of phase transition. We have now discussed a special case of $x = \frac{\pi}{4}, \tau = 0$. It is impossible to check all possible degrees n, all possible parameters x, τ but we will give now one stand-for-all example to support our last conjecture.

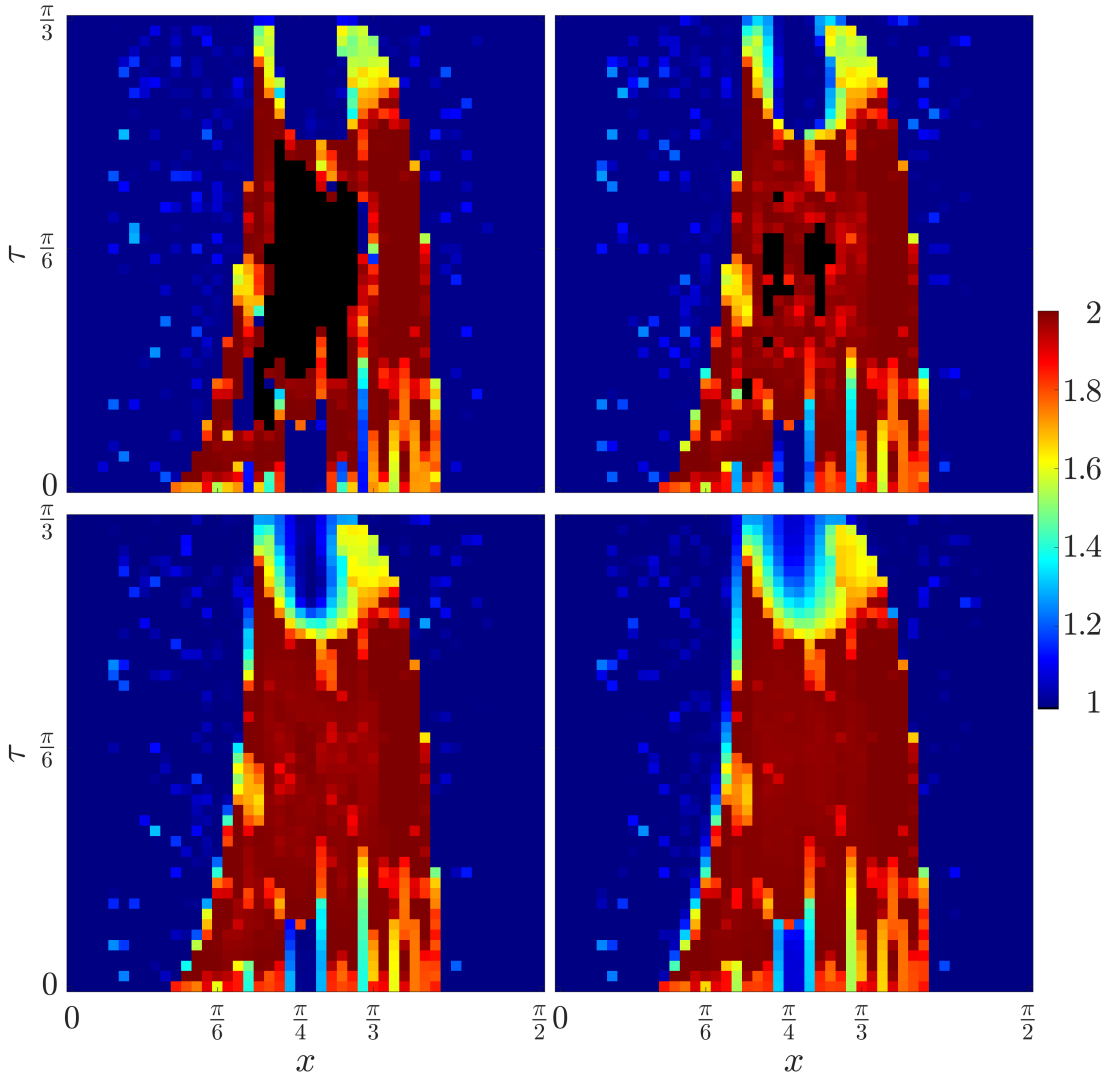

Figure 5.25: The fractal structures generally decay with decreasing P. The metastructure changes, giving rise to regions in black (not present for pure states) which stand for protocols where no sensitive states are detected on given purity sphere. Dimension estimate coded in colorbar.

Conjecture 5.7.4. *The phase transition is a common feature to all protocols Pn with all twirling gates determined by x, ψ, τ. The dimension can only decrease with decreasing purity.*

Again, we do not specify exactly what 'common' means. The case $x = \psi = \tau = 0$ always induce exactly a circle on a sphere of constant purity. Therefore, the $d(P; n; 0, 0) = 1$ for all $P > \frac{1}{2}$. Because the fractal is no fractal but regular curve, we can take it as a special case of fractal with dimension 1 and assign the transition to $P = 1$, the transition at $P = \frac{1}{2}$ is only the consequence of the sphere of constant purity collapsing to a point; we can speak again of the transition. But these cases are merely an issue of terminology, not the phase transition. For this reason, we do not aspire to give a precise classification for these marginal cases. The common situation of $0 < x < \frac{\pi}{2}$ suits the concept of the phase transition well.

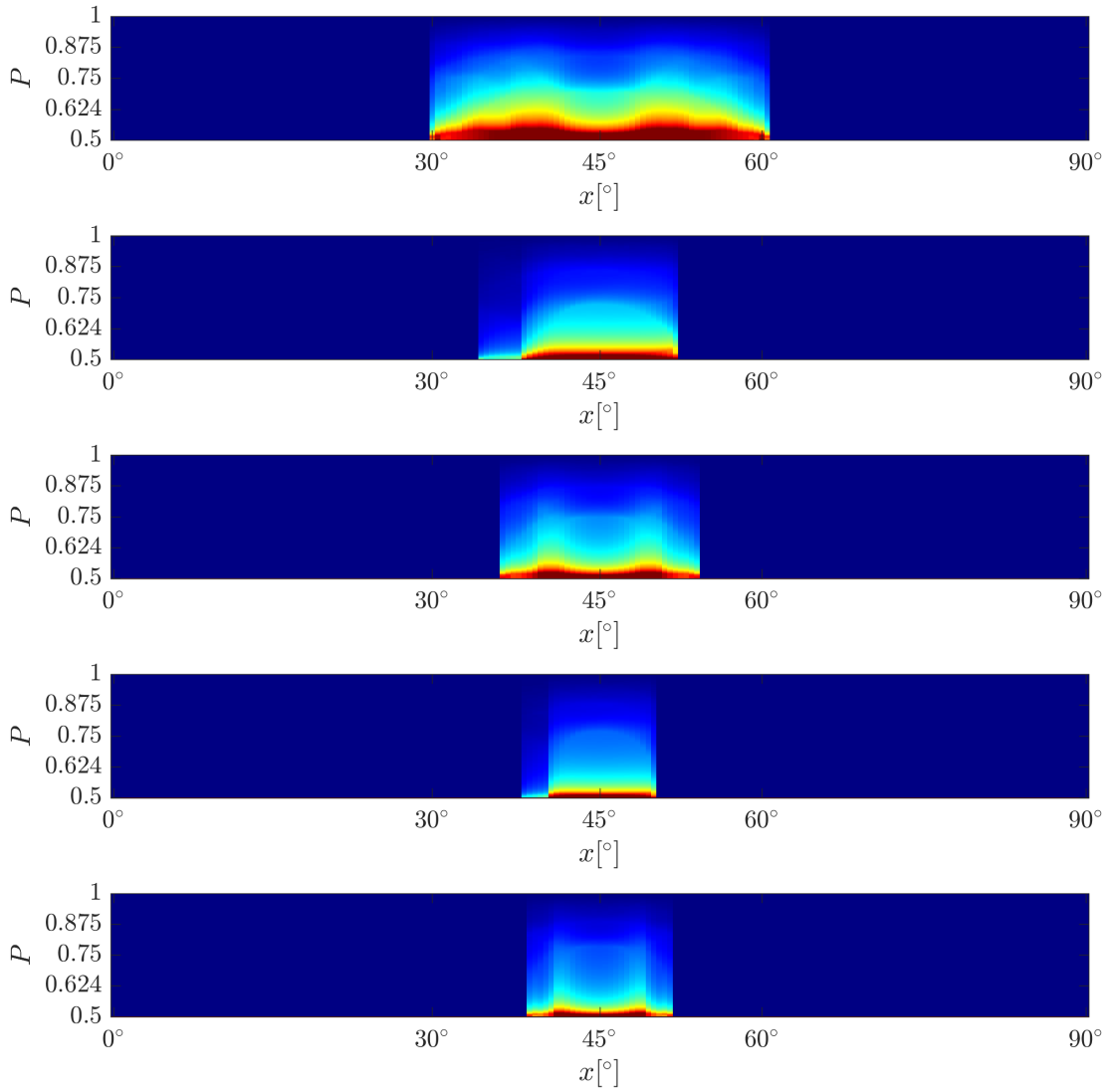

Figure 5.26: $e(P; n; x, 0)$ for values $n = 3, n = 4, n = 5, n = 6, n = 7$, ordered from the top to bottom.

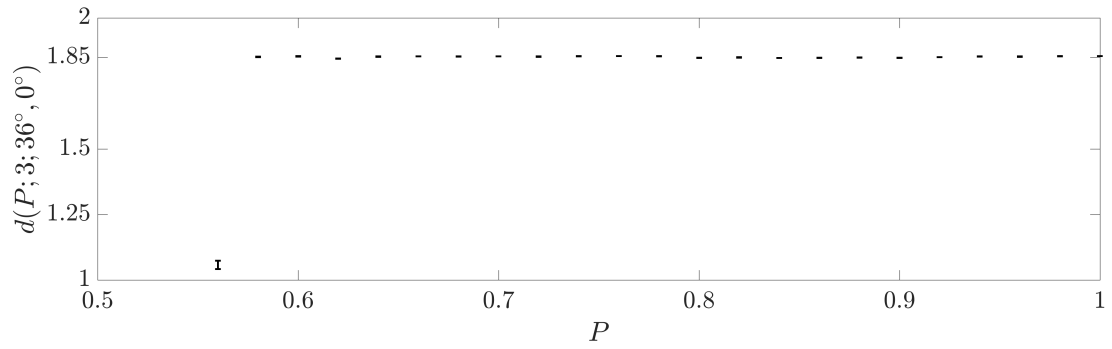

Figure 5.27: The phase transition is a generally present feature of the protocol dynamics. The case of $n = 3$, $x = 36°, \tau = 0°$; we do not show dimension values below 1 that correspond to the fact that no structure was detected.

5.8 Convergence speed and practical use of Pn protocols

Our purification is proposed to repair a state damaged by decoherence. The physical motivation is to send through a communication channel state, thath is an attractor, for simplicity we again choose $|0\rangle$. Therefore, we again try to find the maximal trace distance t of the input from $|0\rangle$ for which the purification must be successful. Just like in the third chapter we now can answer this question together with analysis of convergence speed. We ask the readers to remind themselves the histogram 3.15 that described $R(c,t)$ percentage of states with initial trace distance t converge within precision $t < 10^{-6}$ after at most c iterations. Now, we present the same histograms for higher degrees, $R(n;c,t)$.

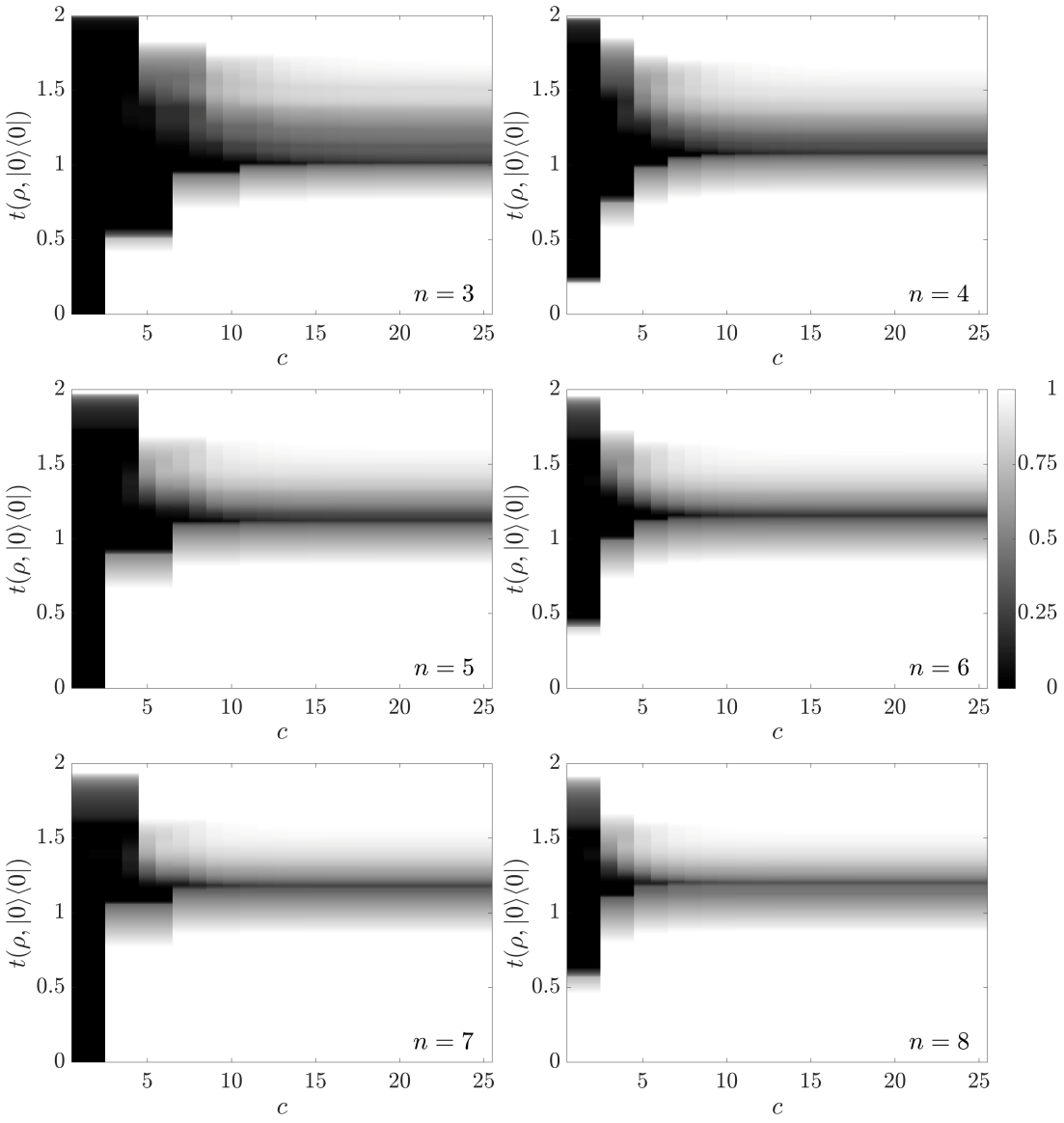

Figure 5.28: Histograms of number of partition of all states R (coded with colour) with initial distance t from $|0\rangle$ that converge to this state in at most c iterations. Cases for protocols Pn with degree as inscribed in plots.

It is obvious from the figures that the protocols are more efficient with in-

creasing n. Again, we were numerically convinced that the closest state (to $|0\rangle$ in terms of t) is the $(w, 0, 0)$ member of the mixed 2-cycle for even n, resp. 4-cycle for odd n, which belongs to L_2 resp. L_2^- invariant subset, the one with $w > 0$. We have identified these states in this chapter in table 5.2 with values w_2. Translated to the trace distance, we conclude that maximal perturbations to $|0\rangle$ that can be successfully corrected by the protocol are basically already noted in the table 5.2 as $t = 1 - w_2$. We remind that this result is again based on numerical calculations.

Also, the convergence speed is improved. Of course, the effect of 4-cycles impedes the utilisability of the odd-n protocols. For this reason, it is more suitable to use e.g. $n = 4$ instead of $n = 3$ when two iterations are sufficient instead of four. With this we come to the last and possibly the most important question. What is the price of the purification? When we realise that Pn protocol requires n copies of qubit to produce a single copy of repaired state, the cost is exponential with number of iterations n^c. The trivial example of two iterations for $n = 4$ and four iterations for $n = 3$ require $4^2 = 16$ and $3^4 = 81$ copies. While this seems to favour the higher degrees n, it is vital to realise that the histograms $R(n; c, t)$ do not offer significant improvement for states with small t. In this case, comparing e.g. 4 iterations of $P2$ and 2 iterations of $P8$ means $2^4 = 16$ versus $8^2 = 64$ copies. The base of the exponential plays a crucial role for small number of iterations. We must conclude that the exponential cost is such a drawback that protocol $P2$ seems to be the most suitable for the practical use.

The use of higher degree Pn protocols can be suitable when state with high perturbation t must be treated. We can of course combine protocols and therefore we suggest for the cases of high t to first use protocol with high n and then protocol $P2$ to finish the converging trend at lower costs.

The cost of qubit copies might not be a problem for situations e.g. in photonic signals where we could generate large amount of input states. However, we must remember that the CNOT operators are burdened with experimental imprecision. The lower amount of these operations the better. Final compromise must be chosen with respect to experimental setup, expectations and relevance that is required from purity of the state etc. But $P2$ can be generally recommended as an interesting protocol well capable of purification of mixed states.

6. Entanglement purification

So far, we were studying, modifying and improving a toy model with a single qubit that could be modified to increase its purity, in other word mixedness, the statistical uncertainty. Although such purification showed interesting results, the aim of the original proposition of the protocol was in purification of entanglement. Being the important source for quantum information and communication, we now return to the topic of the entanglement purification and come back to protocols defined on qubit pairs. We can straightforwardly merge our definition of the twirling modified Pn protocol 5.1 with the original proposition 2.4. Our scheme from previous chapter is simply taken twice - with one part identified as the target and the other as the control subsystem.

The reason why we studied the protocols Pn extensively with the focus on case $x = \frac{\pi}{4}, \tau$ will now be revealed to derive conclusions to the two-qubit dynamics form the previous single-qubit case. Let us recall that the original protocol used the Hadamard gate 2.28 for the twirling. However, the name of Hadamard is used for a whole class of matrices.

Definition 6.0.1. *We say* $\mathbb{A} \in \mathbb{R}^{n,n}$ *is Hadamard matrix when*

1. $(\forall i, j \in \hat{n})(\mathbb{A}_i j = \pm 1)$
2. $\mathbb{A}\mathbb{A}^T = n\mathbb{1}$

In spite of the requirement on the entries of Hadamard matrices to be real, we can consider redefining them on complex numbers and take them as unitary, for this we have to renormalise the matrix by factor $\frac{1}{\sqrt{n}}$. When such matrix is to be used for the evolution operator we can omit the norm and renormalise the density matrix later, we will use this to make the expressions more condense and comprehensive. We now designate four particular cases in $\mathbb{R}^{2,2}$ (up to the norm $\frac{1}{\sqrt{2}}$):

These unitary matrices can act as the single qubit gates.

If we consider the action of the single qubit protocol $P2$ with H_2 twirling on the qubit in the Bloch parameterisation, we realise we are in the thirdd chapter of our thesis, to accent the similarities and differences, we write the output after one and two protocol iterations:

$$\rho = \begin{pmatrix} 1+w & u-iv \\ u+iv & 1-w \end{pmatrix} \to \rho' = \begin{pmatrix} 1+w^2+u^2-v^2 & -2(w+iuv) \\ -2(w-iuv) & 1+w^2-u^2+v^2 \end{pmatrix} \to \quad (6.1)$$

$$\to \rho'' = \begin{pmatrix} 1+6w^2+w^4+u^4-6u^2v^2+v^4 & -2(1+w^2)(u^2-v^2)+8iuvw \\ -2(1+w^2)(u^2-v^2)-8iuvw & 1-2w^2+w^4+u^4+2u^2v^2+v^4 \end{pmatrix}$$

If we use H_1 instead, we obtain

$$\rho = \begin{pmatrix} 1+w & u-iv \\ u+iv & 1-w \end{pmatrix} \to \rho' = \begin{pmatrix} 1+w^2+u^2-v^2 & +2(w+iuv) \\ +2(w-iuv) & 1+w^2-u^2+v^2 \end{pmatrix} \to \quad (6.2)$$

$$\to \rho'' = \begin{pmatrix} 1+6w^2+w^4+u^4-6u^2v^2+v^4 & 2(1+w^2)(u^2-v^2)-8iuvw \\ 2(1+w^2)(u^2-v^2)+8iuvw & 1-2w^2+w^4+u^4+2u^2v^2+v^4 \end{pmatrix}$$

From these we discover following conjugacy of the two protocols. When protocol with H_1 is used on input (w, u, v) to obtain (w', u', v'), protocols with H_2 used on $(w, -u, -v)$ gives $(w', -u', -v')$. For the visualisation in the attractor maps, the two maps are symmetrical. They contain two identical blocks in $\varphi \in [0; \pi)$ and $\varphi \in [\pi; 2\pi)$ when working in spherical coordinates 2.38 again. The analogous situation is valid for any pair H_i, H_j. This symmetry is a key ingredient to findings that follow. For simplicity, we will now introduce new notation that will serve mainly to capture the structure of the matrix. We shortcut the Bloch coordinate formulas to capital letters. For the case of protocol with H_1 we write

$$\rho = \frac{1}{2}\begin{pmatrix} 1+w & u-iv \\ u+iv & 1-w \end{pmatrix} =: \begin{pmatrix} A & \bar{Z} \\ Z & \bar{A} \end{pmatrix} \to \rho' =: \begin{pmatrix} A' & \bar{Z}' \\ Z' & \bar{A}' \end{pmatrix} \to \rho'' =: \begin{pmatrix} A'' & \bar{Z}'' \\ Z'' & \bar{A}'' \end{pmatrix} \tag{6.3}$$

Heading towards the entanglement, we now consider the two-qubit situation. Our physically motivated request is for the protocol to be LOCC, i.e. the two-qubit gate should be a tensor product of single-qubit gates. Thanks to this, the operation can be performed separately on the subsystems. Therefore, we now construct

$$H_{ij} = H_i \otimes H_j \tag{6.4}$$

Proposition 6.0.2. *Taking identical notation as in 6.3, the two-qubit protocol with H_{11} acting on the state*

$$\rho = \begin{pmatrix} A & 0 & 0 & \bar{Z} \\ 0 & 0 & 0 & 0 \\ 0 & 0 & 0 & 0 \\ Z & 0 & 0 & \bar{A} \end{pmatrix} \tag{6.5}$$

yields after one and two iterations:

$$\begin{pmatrix} A' & \bar{Z}' & \bar{Z}' & A' \\ Z' & \bar{A}' & \bar{A}' & Z' \\ Z' & \bar{A}' & \bar{A}' & Z' \\ A' & \bar{Z}' & \bar{Z}' & A' \end{pmatrix}, \begin{pmatrix} A'' & 0 & 0 & \bar{Z}'' \\ 0 & 0 & 0 & 0 \\ 0 & 0 & 0 & 0 \\ Z'' & 0 & 0 & \bar{A}'' \end{pmatrix} \tag{6.6}$$

Proof. The proof can be mechanically performed by direct calculation. The main ingredient is the combination of plus and minus signs in the Hadamard matrices. □

The consequences of this proposition are very important: the nonlinear dynamics studied for the single qubit case is now directly translated to a particular invariant subset of the two-qubit states. The attractor maps, convergences etc., all results from the third chapter are now valid (under the symmetry $u \to -u, v \to -v$) for the subset of two-qubit mixed states

$$\mathcal{X}_1 = \left\{ \frac{1}{2}\begin{pmatrix} 1+w & 0 & 0 & u-iv \\ 0 & 0 & 0 & 0 \\ 0 & 0 & 0 & 0 \\ u+iv & 0 & 0 & 1-w \end{pmatrix} \middle| w, u, v \in \mathbb{R}, w^2+u^2+v^2 \leq 1 \right\} \tag{6.7}$$

Let us now study the evolution when more general H_{ij} is used as the twirling gate. We will list only few examples and will focus on the structural shape of the density matrices

$$
\begin{aligned}
H_{12}: \quad \rho' &= \begin{pmatrix} A' & -\bar{Z}' & \bar{Z}' & -A' \\ -Z' & \bar{A}' & -\bar{A}' & Z' \\ Z' & -\bar{A}' & \bar{A}' & -Z' \\ -A' & \bar{Z}' & -\bar{Z}' & A' \end{pmatrix}, \quad \rho'' = \begin{pmatrix} A'' & 0 & 0 & -\bar{Z}'' \\ 0 & 0 & 0 & 0 \\ 0 & 0 & 0 & 0 \\ -Z'' & 0 & 0 & \bar{A}'' \end{pmatrix} \\
H_{13}: \qquad \rho' &= \begin{pmatrix} \bar{A}' & Z' & Z' & \bar{A}' \\ \bar{Z}' & A' & A' & \bar{Z}' \\ \bar{Z}' & A' & A' & \bar{Z}' \\ \bar{A}' & Z' & Z' & \bar{A}' \end{pmatrix}, \qquad \rho'' = \begin{pmatrix} 0 & 0 & 0 & 0 \\ 0 & A'' & -\bar{Z}'' & 0 \\ 0 & -Z'' & \bar{A}'' & 0 \\ 0 & 0 & 0 & 0 \end{pmatrix} \\
H_{14}: \quad \rho' &= \begin{pmatrix} \bar{A}' & -Z' & Z' & -\bar{A}' \\ -\bar{Z}' & A' & -A' & \bar{Z}' \\ \bar{Z}' & -A' & A' & -\bar{Z}' \\ -\bar{A}' & Z' & -Z' & \bar{A}' \end{pmatrix}, \quad \rho'' = \begin{pmatrix} 0 & 0 & 0 & 0 \\ 0 & A'' & \bar{Z}'' & 0 \\ 0 & Z'' & \bar{A}'' & 0 \\ 0 & 0 & 0 & 0 \end{pmatrix} \\
H_{21}: \quad \rho' &= \begin{pmatrix} A' & \bar{Z}' & -\bar{Z}' & -A' \\ Z' & \bar{A}' & -\bar{A}' & -Z' \\ -Z' & -\bar{A}' & \bar{A}' & Z' \\ -A' & -\bar{Z}' & \bar{Z}' & A' \end{pmatrix}, \quad \rho'' = \begin{pmatrix} 0 & 0 & 0 & 0 \\ 0 & A'' & \bar{Z}'' & 0 \\ 0 & Z'' & \bar{A}'' & 0 \\ 0 & 0 & 0 & 0 \end{pmatrix} \\
H_{22}: \quad \rho' &= \begin{pmatrix} \bar{A}' & \bar{Z}' & \bar{Z}' & A' \\ -Z' & -\bar{A}' & -\bar{A}' & -Z' \\ -Z' & -\bar{A}' & -\bar{A}' & -Z' \\ A' & \bar{Z}' & \bar{Z}' & A' \end{pmatrix}, \quad \rho'' = \begin{pmatrix} \bar{Z}'' & 0 & 0 & A'' \\ 0 & 0 & 0 & 0 \\ 0 & 0 & 0 & 0 \\ \bar{A}'' & 0 & 0 & Z'' \end{pmatrix} \\
\vdots \qquad & \qquad \vdots \qquad \qquad \vdots
\end{aligned}
\tag{6.8}
$$

We see that the evolution is very similar and creates specific structures in the density matrices. The sign changes are irrelevant for asymptotic evolution because the elementwise product $\rho \odot \rho$ is not changed by any sign change in any matrix element. We introduce

$$
\mathcal{X}_2 = \left\{ \frac{1}{2} \begin{pmatrix} 0 & 0 & 0 & 0 \\ 0 & 1+w & u-iv & 0 \\ 0 & u+iv & 1-w & 0 \\ 0 & 0 & 0 & 0 \end{pmatrix} \middle| \, w,u,v \in \mathbb{R}, w^2+u^2+v^2 \leq 1 \right\} \tag{6.9}
$$

and while $\mathcal{X}_1 \cup \mathcal{X}_2$ form matrices with element sturcture

$$
\mathcal{X} = \left\{ \begin{pmatrix} \bullet & 0 & 0 & \bullet \\ 0 & \bullet & \bullet & 0 \\ 0 & \bullet & \bullet & 0 \\ \bullet & 0 & 0 & \bullet \end{pmatrix} \right\} \tag{6.10}
$$

we add dual matrix structures, now without direct physical meaning of the density matrices

$$
\mathcal{O} = \left\{ \begin{pmatrix} 0 & \bullet & \bullet & 0 \\ \bullet & 0 & 0 & \bullet \\ \bullet & 0 & 0 & \bullet \\ 0 & \bullet & \bullet & 0 \end{pmatrix} \right\} \tag{6.11}
$$

It is possible to show explicitly following statement but the proof will not be presented in full, it is easy and straightforward, just too long. We have verified in Mathematica following:

Proposition 6.0.3. *Protocol $P2$ with arbitrary H_{ij} evolves a density matrix which is a convex combination of arbitrary matrices from $\mathcal{X}_1$ and $\mathcal{X}_2$ to a linear combination of $\mathcal{X}$ and $\mathcal{O}$ structures and then back to $\mathcal{X}$ with next iteration. That is, density matrices with $\mathcal{X}$ structure are invariant on two iterations.*

We have given exact relations between the structures in [39] and we have also shown there that more structures can be introduced with similar behaviour. Various combinations of Hadamard and Pauli matrices create a complicated system of sets that are mapped one onto another and invariant on two iterations. In this thesis, we focus on chaotic features, whence we will not further analyse all the possibilities and only refer to [39] leaving the detailed description of connections and symmetries for future work; we will now restrict ourselves only to the interpretation of our results from this thesis for the two-qubit case.

What we also will not discuss in detail (but is interesting) is the exact action of the protocol on the convex combination of two density matrices, not only from $\mathcal{X}_1$ and $\mathcal{X}_2$ but also of two matrices from the same set. The reason is simple, transformation $z \to z^2$ changes $\lambda\rho_1 + (1-\lambda)\rho_2$ to $\lambda^2\rho_1^{\odot 2} + 2\lambda(1-\lambda)\rho_1^{\odot}\rho_2 + (1-\lambda)^2\rho_2^{\odot 2}$. The output is not a convex combination of the component outputs; the formulas become extremely difficult to handle even after a single iteration.

We will now focus on the protocols leading to the Bell states - these belong to the $\mathcal{X}$ structures; therefore, we leave the other structures aside.

The observation about the invariance of $\mathcal{X}$ structure can be now generalised to arbitrary protocol Pn wiht H_{ij} twirling. The reason is that the invariance is a consequence of the Hadamard property of the twirling gates, not the elementwise product (note it is also called Hadamard product, that is rather confusing coincidence at this moment). Higher order of the protocol can influence the convergence speed, attractor maps but not the structure $\mathcal{X}$. In case of the odd n four iterations are needed but 4 is even number and the $\mathcal{X}$ is invariant on even number of iterations.

Because all considered two-qubit protocols are equivalent (even H_{11} and H_{22} induce the same evolution equations without any sign changes) to the single qubit version with H_2, we will interpret previous results to the current protocols acting on states from $\mathcal{X}_1$, resp. $\mathcal{X}_2$. We translate now the Bloch parameterisation for $\mathcal{X}_1$:

$$\begin{gathered} |0\rangle \to w = 1, u = v = 0 \to |00\rangle \\ |1\rangle \to w = -1, u = v = 0 \to |11\rangle \\ |0\rangle + |1\rangle \to u = 1, w = v = 0 \to |00\rangle + |11\rangle \equiv \Phi^+ \\ |0\rangle - |1\rangle \to u = -1, w = v = 0 \to |00\rangle - |11\rangle \equiv \Phi^- \end{gathered} \tag{6.12}$$

and for $\mathcal{X}_2$:

$$\begin{gathered} |0\rangle \to w = 1, u = v = 0 \to |01\rangle \\ |1\rangle \to w = -1, u = v = 0 \to |10\rangle \\ |0\rangle + |1\rangle \to u = 1, w = v = 0 \to |01\rangle + |10\rangle \equiv \Psi^+ \\ |0\rangle - |1\rangle \to u = -1, w = v = 0 \to |01\rangle - |10\rangle \equiv \Psi^- \end{gathered} \tag{6.13}$$

In this correspondence we have arrived to situation where the Bell states are attractors, they form 2-cycles:

$$\Phi^+ \leftrightarrow |00\rangle,\ \Psi^+ \leftrightarrow |01\rangle \tag{6.14}$$

In the last chapters we focused on $|0\rangle$, the role of w coordinate was prominent, and we showed the convergence rates towards this state. However now, the other member of the attractor cycle is physically important to us. We can cheat with performing one iteration of the protocol and transform the Bell state to the separable state and apply the previous results for this case. But we also decide to offer another approach. We must be aware that the shrinking basin of attraction can cause us to take the perturbed inital state from the immediate basin of attraction of the separable member of the cycle and although we would converge to the cycle, ti would be in the wrong parity regime, we would obtain its separable member i.e. $|00\rangle$.

To describe the maximal allowed perturbation, we would like to change the approach and recall the concurrence, 2.2.7. For states ρ in $\mathcal{X}_{1,2}$ it can be precisely expressed in terms of (w, u, v) because we have calculated the eigenvalues of $\rho(\sigma_2 \otimes \sigma_2)\bar{\rho}(\sigma_2 \otimes \sigma_2)$:

$$\begin{gathered}\lambda_{1,2} = \tfrac{1}{2}\left(\sqrt{1-w^2} \pm \sqrt{u^2+v^2}\right) > 0 \\ \lambda_{3,4} = 0\end{gathered} \tag{6.15}$$

The concurrence is then

$$C(w, u, v) = \sqrt{u^2 + w^2} \tag{6.16}$$

which means that the surfaces of constant concurrence and therefore also surfaces of constant entanglement of formation are coaxial cylinders with axis coinciding with w-axis. The concurrence has straightforward geometrical meaning of the distance from w-axis. Therefore, we will not further process it to the entanglement of formation which lacks such geometrical interpretation.

However, this means that we cannot use concurrence to give a threshold on purification capabilities, e.g. like that the states with concurrence higher than certain value are always purified to the Bell state. State with $(0, \frac{1}{\sqrt{2}}, \frac{1}{\sqrt{2}})$ evolves towards $|00\rangle$ after even number of iterations, state $(0, 1, 0)$ after odd (when protocol with n even is chosen); both states have concurrence 1, thus are maximally entangled but belong to different asymptotic regime. We will therefore use the trace distance again so we can at least estimate average improvement of the concurrence. Consider state ρ at distance t from the attractive Bell state. We calculate its concurrence $C(\rho)$ and concurrence after two iterations $C(\rho'')$ and determine the difference caused by the evolution $C(\rho) - C(\rho'')$. When we calculate this difference for an ensemble of such initial points, we can evaluate average improvement of concurrence, let us call it $\Gamma(n; t)$; it is naturally not only the function of the initial trace distance from the Bell state but also the order of the protocol. Because some states could be purified while others could be made more separable, that means the protocol fails, we will set $\Gamma(n; t) = 0$ whenever a state (with t) is detected with $C(\rho) - C(\rho'') < 0$.

The conclusion to take from these plots for various n is following. The Pn protocols provide slightly better purification capabilities with higher order n.

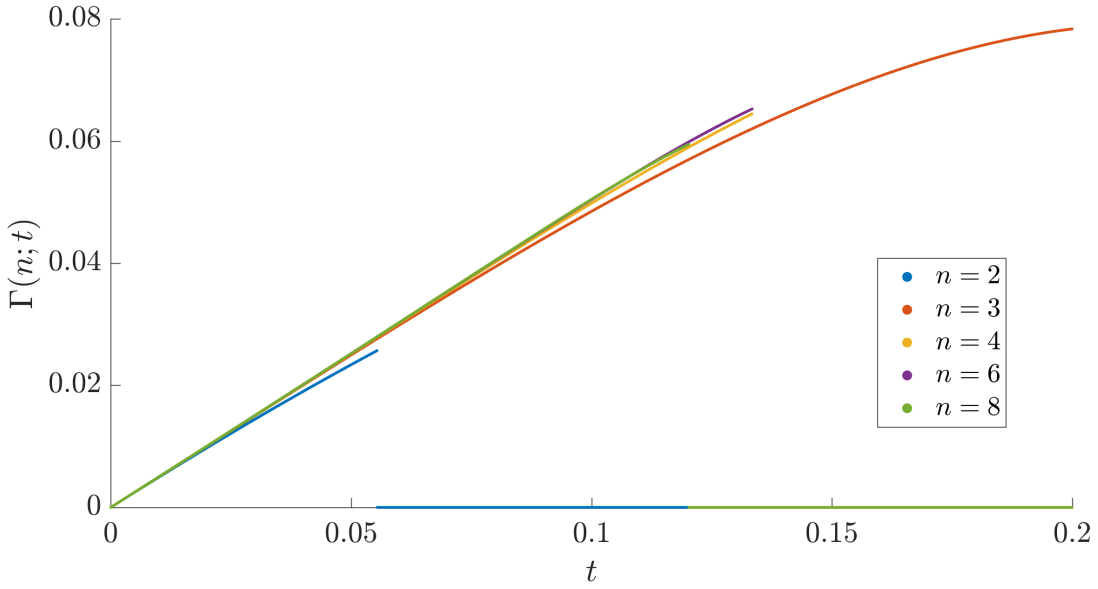

Figure 6.1: Average improvement of concurrence for protocols Pn with Hadamard twirling.

However, the difference is negligible when t is small. Soon, the effect of shrinking basins of attraction causes that the high order protocols are not capable of purifying most of the states (even with small t) because they belong to the other parity branch of the cycle or even to the basin of attraction of the analogue to the maximally mixed attractor.

We have not yet mentioned the role of this analogue of $\mathbb{1}$. Depending on the set $\mathcal{X}_{1,2}$ it is either $|00\rangle\langle 00| + |11\rangle\langle 11|$ or $|01\rangle\langle 01| + |10\rangle\langle 10|$. These are indeed mixed; with purity $\frac{1}{2}$ they are the most mixed in the sets $\mathcal{X}_{1,2}$ but not the maximally mixed state of all two-qubit space.

As an optimal degree of the protocol we can recommend values $n = 2, n = 3, n = 4$ based on the plots 6.1. These values offer good improvement of the concurrence which must be also balanced with respect to the costs. We once again stress that the price is exponential in the number of copies of the state, now the Bell pair. Therefore, we must be able to produce tens of copies to be able to iterate the protocol repeatedly. The exact choice must be made based on specific experimental setting and capabilities but the choice of $n = 2$ seems to be a good compromise.

While we now cared for the protocols with Hadamard gates, one could raise a question on protocols with different twirling operatorss. Unfortunately, general twirling gate does not invoke similar structures, invariant sets. The evolution, although restricted to initial state determined by three parameters w, u, v is now affected by another, structural mixing of the density matrix elements which turn the evolution to happen in the whole 15-dimensional state space of qubit pairs. This causes that we are unable to give general evolution formulas. We have proven that the Bell states are attractors for a significantly wider classes of states than was previously known; we have even described the fractal structures, determined its dimension and found the phase transition. But he most important question that is still to be answered, is the character of dynamics in the 15-dimensional space. The multidimensional perturbations might discover that the Bell state is

sensitive to certain perturbations, we have seen that saddle states can exist. It is also possible that the dynamics would be sensitive to defects of experimental realisation of the gates. Nevertheless, current progress in the chaotic dynamics and fractal structures in quantum physics is very inspiring and hopefully will encourage future research in this field.

7. Resume

Chaos and quantum information have a surprising overlap. Our models of the purification protocols have no analogue in classical physics, and therefore we find a new manifestation of chaos in the quantum laws of the Universe. The motivation in quantum information processing and quantum communication, nowadays very promising branches, gives our research priority. The chaotic dynamics can have both detrimental and improving effects for practical applications, and therefore it is vital to understand this highly nontrivial area.

After introduction, in the theoretical chapter, we put together the elementary knowledge needed for our cause. Because the intersection of the involved disciplines may be not familiar to some readers, we focused mainly on the comprehensibility and illustrative approach allowing the readers to follow our lines of thought even when their knowledge is limited in some advanced areas.

Now let us summarise the main results of our research. The second chapter studied for the first time a chaotic model of mixed state dynamics. This model of single qubit dynamics corresponds to previously known case of the pure state evolution. The protocol is based on measurement-based selection and modification which manifests as nonlinear evolution in the open quantum system. Our main contribution lies in the detailed and analytic description of the mixed state evolution. Besides the peculiar geometrical and algerbaic properties of the fixed states and cycles that were found, we focused on the character of the dynamics, i.e., we identified attractors and for the first time we identified saddle states and foci in the purely quantum system.

We have introduced a concept of sensitive states that serves as an analogue of the Julia set, the set of chaotic states known from the theory of complex functions. The sensitive structure was characterised by its dimension which was estimated and checked by various approaches; the main accent was put on the box-counting method. The dimension approximately equals to ca 2.20 proved the existence of the fractal shaped structure in the mixed states. A very peculiar statement was constructed based on numerical evidence - the fractal structure changes its quality, i.e. dimension, in the three-dimensional space. When sliced into surfaces according to spheres of states of constant initial purity, we found that the slices also form fractal structures and their dimension is piece-wise constant function of the purity. The specific dependence, when the structure quality is unchanged until suddenly changed from fractal (with dimension ca 1.56) to regular (with dimension 1) and to empty (with dimension 0) when certain thresholds are crossed, is highly nontrivial and can be understood as a phase transition; that is our first fundamental result. The phase in this interpretation is the structure described by its dimension. The role of the temperature is played by the initial purity.

We attempted to classify the phase transition, we used the concept of entropy to introduce the mean entropy function. Based on numerical evidence, we argued that this function has two; modes of sudden changes, these can be assigned to the transitions of the first and second kind. Because these transitions in the mean entropy function can be related to the transition of the structure, the classification can also be used in the context of the structure transition, although it does not have a direct physical - standard - form and application.

The exponential trends identified in the mean entropy function also allowed us to interpret the purification capabilites of the protocol; these were also described using the concept of trace distance. We have calculated thresholds representing practical limitations of the protocol. We have also described the efficiency of the protocol by describing convergence speed in a certain sense. With this, the complete analysis of the protocol was finished.

Next chapter introduced generalisations to the previous mode; we used the twirling operators to enhance the dynamical regimes and to offer a whole new field to study. We have focused on symmetries which allowed us to radically reduce the set of studied protocols. Only one represenant of whole classes of equivalent protocols is enough to fully describe nonlinear dynamics, fractal structures etc. One of the symmetries has stronger, physics related properties which led us to establish a concept of asymptotic equivalency more formally, this equivalency connects fractal structures induced by equivalent protocols; this allowed us to reduce a whole degree of freedom in the choice of the twirling parameters. This symmetry was interpreted in terms of time evolution and allowed to introduce, change, or eliminate time relaxation between iterations of the protocol. This equivalency is our second fundamental result. At the same time, the theorem allows for modifying protocol parameters in order to modify the attractors in a desired way. Formulas for the processes are presented and also interpreted in the geometrical representation.

The next fundamental result of our work is that our protocol is universal, i.e. the setting of the twirling operator can be done in a way to set arbitrary state (with a singular exception) to be the attractor of the protocol. Protocol for the exceptional case was offered in next chapter. Exact prescription was given to find protocolar parameters x, ψ, τ from the state parameters w, u, v.

We also presented changes to the fractal structure corresponding to new protocols. We have found that there are regions in the protocol parameter space x, τ where the induced fractal structure seems to be qualitatively the same or very close, as far as the numerical estimates allow. These regions seem to fit the concept of J-stability. Sudden and dramatic changes to the fractal structure have also been detected; these are known from the J-stability concept as well. We have also introduced the concept of the Mandelbrot set to our evolution functions to highlight the analogy of our physically motivated research to the abstract analysis of very simple complex functions. The fact that there is a fractal metastructure above the fractal structures corresponding to various protocols is highly nontrivial and very interesting.

We have classified the fractal structures into basic groups and have demonstrated their shapes. All possible variants of the Julia set were encountered, from Cantor dust to white noise. The phase transition was shown to be a common feature of the fractal structures for arbitrary twirling. Because the topic is very new and the multidimensional dynamics is a demanding and complicated field, we have raised many new questions for future research; our observations were often presented as conjectures. We believe that future research in this field may be fruitful and can open a whole new door to human knowledge.

Among the questions or conjectures that deserve to be put on a more solid ground, we have put forward:

- What are the properties of the metastructure we described as the generalised

Mandelbrot sets, $\widetilde{\mathcal{M}}_n$?

- What relationship is there amongst these sets for various n? Is there some link amongst the fractal structures of protocols with different n? In the special case of $x = \frac{\pi}{4}, \psi = \tau = 0$ the fractals seem to have the same structure (i.e. dimension) regardless of n.

- Is there a way to decide whether the Julia set of a rational polynomial function is connected/disconnected? Is there an analogue to the Mandelbrot theorem?

- Is it possible to characterise symmetries that can be seen in the fractal structures, at least for some particular fractal shapes?

- Is it possible to give a better proof than numerical estimates on an ensemble of chosen protocols, that the phase transition, i.e., sudden change of the structure of the sensitive states with the purity, is a general feature of the protocols? Is the function of dimension $d(P; n; x, \tau)$ non-decreasing with increasing purity for all parameters?

These questions are now summed also to include the higher orders n. We come to an important thought - is it possible that the functions that come from the physical context of the purification protocols are restricted in some way? Is it possible that general rational polynomial functions can exhibit more exotic features? Do the physical laws manifest as certain restrictions to these functions? Can other rational polynomial functions be achieved by other physical settings?

In the third chapter, we have also detected bifurcation - a change in the number of attractors when the parameters of the protocol are changed. This effect is well known in chaotic dynamics. Its presence in the quantum purification protocols puts another piece of knowledge into the mosaic of quantum chaos.

The last important result from the third chapter was that the purification of state $|0\rangle$ is robust. I.e., when the state is perturbed and when even the protocol gates are perturbed, the output state also changes in a manner consistently small with the perturbations.

The fourth chapter, introduced further generalisation to the protocols. By considering mutliplets of qubits, we realised evolution driven by polynomials of higher degrees. Motivated by the idea that the degree of protocol can improve the convergence speed and therefore the purification capabilities, we have offered new protocol schemes and have also given corresponding evolution equations. In this way we produced the most general single-qubit protocol based on CNOT gate. We presented some basic findings on the nonlinear dynamics, mainly about the symmetries and phase transitions again. In the protocols of higher degree we have found a fundamental difference between protocols of odd and even degree while each of these groups share basic properties. This concerns also the generalised Mandelbrot set, we have not identified (by the box-counting method) the presence of Cantor dust fractal in the odd n degree protocols.

We mainly focused on protocols with a particular twirling with Hadamard type matrix; for these protocols we found that the odd - even dichotomy manifests in following way: All Pn protocols with n even have $\mathcal{C} \equiv |0\rangle \leftrightarrow |0\rangle + |1\rangle$ for attractor; protocols with n odd have 4-cycle $\mathcal{C} \equiv |0\rangle \rightarrow |0\rangle - |1\rangle \rightarrow |1\rangle \rightarrow |0\rangle - |1\rangle \rightarrow |0\rangle$ for

attractor. Also, we provided by numerical calculations that the fractal structure of the Hadamard twirling protocol is the same regardless of the degree n. The fractal in the three-dimensional Bloch space retains the dimension value near 2.20 and the slicing of the fractal still keeps the values near 1.56. The very slight decrease of the dimension estimate that can be detected is with high probability an artefact of numerical methods which work in rough precision ranges.

We have also analysed the convergence speed and compared it to the cost which is paid in the copies of qubits that are discarded during the protocol iteration. We have argued that the lower n may be much more suitable for practical applications.

The last chapter offered a direct use of previous research for two-qubit protocols. The protocols with Hadamard gates played a crucial role for two reasons - they purify the Bell states which is desirable for practical purposes, and their structure allowed to transfer single-qubit dynamics to particular subsets of more general two-qubit protocols. We argued that for the purpose of the entanglement purification the protocols with low n are a good compromise between the costs and gained purification. Still, the complete characterisation of the dynamics caused by arbitrary protocol in the two-qubit scenario is not viable because the chaotic dynamics in 15-dimensional space is still far beyond current state of the art, despite our significant advancements.

Let us formulate another set of questions for the future research

- What is the dynamics of the purification protocol $P2$ with Hadamard gate twirling in the 15-dimensional space? Can it be approximated at least numerically on some neighbourhood of the Bell state? Is the protocol robust to perturbations of both the state and the gates as we have shown in the single qubit case?

- What dynamical regimes can be found in the dynamics driven by rational polynomial functions of 15 variables, in the two-qubit states? Are there also states of saddle point and focus types? Are there more complicated bifurcations when the twirling parameters are changed?

- Are there some invariant sets of two-qubit states for protocols with other than Hadamard twirling that would allow to simplifying and analysing the dynamics?

- Is the phase transition also present in the two-qubit systems?

And one of the most important question rises from the fact that we used the CNOT gate to construct the protocol. This gate is one particular case of so called Controlled-U gates. These gates execute/execute not the U unitary gate on the target qubit based on the state of the control qubit. Our brief sketches suggest that such protocols can induce different evolution functions, although also rational polynomial.

- What dynamical regimes are present in the Controlled-U protocols?

- Can Controlled-U protocols be used as the purification protocols in the sense of mixedness of qubits?

- Are Controlled-U protocols capable of purifying entanglement? Can they be more efficient?
- Do Controlled-U protocols induce chaos? What fractal structures are generated? Do the structures also undergo phase transition?

In the very end we also propose to define the purification protocols on qudits and study the chaotic evolution in the corresponding spaces, this may be an acceptable next step in the field.

Succeeding in identification of the basic chaotic features in the quantum information processing, we believe that the field has much to offer not only to abstract mathematical studies but also to the physical applications leading to secure communication, faster information processing etc. in the near future.

Bibliography

[1] Alber, G., Delgado, A., Gisin, N., Jex, I.; *J. Phys. A: Math. Gen.* **34**, 8821, 2001.

[2] Arnold, V.I.; *Uspekhi Mat. Nauk*, **18**, 9, 1963.

[3] Beardon, F.A.; *Iteration of Rational Functions*, Springer-Verlag, New York,1991. ISBN 978-0-387-95151-5

[4] Bechmann-Pasquinucci, H. et. al.; *Phys. Lett. A* **242**, 198-204, 1998.

[5] Bell, J.S.; *Physics*, **1**, 195, 1964.

[6] Bennett, C.H., Brassard, G.; *Proc. Int. Conf. on Comp., Systems and Signals*, **175**, 8, 1984.

[7] Bennett, C.H., et al.; *Phys. Rev. Lett.*, **70**,1895, 1993.

[8] Berry, M.; *Physica Scripta*, **40**, 335, 1989.

[9] Biham E., et al.; *J. of Cryptology*, **19**, 381, 2006.

[10] Blank, J., Exner, P., Havlíček, M.; *Lineární operátory v kvantové fyzice*, Karolinum, 1993.

[11] Crescenzi, P., et al.; *A compendium of NP optimization problems*, KTH NAD, Stockholm, 2008.

[12] Davies, E.B.; *Quantum Thoery of Open Systems*, Academic Press, London, 1976.

[13] Deutsch, D., Jozsa, R.; *Proc. of the Royal Soc. of London A*, **439**, 553, 1992.

[14] Deutsch, D.; *Int. J. Theor. Phys.*, textbf24, 1, 1985.

[15] Deutsch, D.; *Proc. Royal Soc. of London*, textbf400, 97, 1985.

[16] Devaney, R.L.; *An Introduction to Chaotic Dynamical Systes*, 2^{nd} edition, Addison-Wesley Publishing Company, Inc., 1989.

[17] Ehrenfest, P.; *Proc. Royal Acad. Amsterdam*, **36**, 153, 1933.

[18] Einstein, A., Podolsky, B., Rosen, N.; *Phys. Rev.* **47**, 777, 1935.

[19] Falconer, K.; *Fractal Geometry*, John Wiley & Sons, Chichester, 2003, ISBN 0-470-84862-8

[20] Fano, U.; *Rev. Mod. Phys.*, **29**, 74, 1957.

[21] Fatou, M.P.; *Comptes Rendus del' Acad. des Sc. de Paris*, 164, 806, 1917

[22] Feinberg, M.; *Fibonacci Quarterly*, **1**, 71, 1963.

[23] Fornæs, J. E.; *Dynamics in several complex variables*, Amer. Math. Soc., 1994.

[24] Fornæs, J. E., Sibony,N.; *Ergodic Theory Dyn. Systems*, **11**, 687, 1991

[25] Gilyén, A., Kiss, T., Jex, I.; *Sci. Rep.*, **6**, 20076, 2016.

[26] González, A.; *Math. Geosci.* **42**, 49, 2010.

[27] Grebogi, C., McDonald, S.W., Ott, E., Yorke, J.A.; *Phys. Let. A*,**110**, 1985.

[28] Gutzwiller, M. C.; *Chaos in Classical and Quantum Mechanic*, Springer-Verlag, New York, 1990.

[29] Haroche, S., Raimond, J.-M.; *Exploring th Quantum*, Oxford Univeristy Press, Oxford, 2006. ISBN 978-0-19-850914-1

[30] Hausdorff, F.; *Math. An.*,. **79**, 157, 1919.

[31] Isaeva, O.B., Kuznetsov, S.P., Ponomarenko, V.I.; *Phys. Rev.* E64, 055201(R), 2021.

[32] Jaeger, G.; *Arch. for Hist. of Exact Sci.*, **53**, 51,1998.

[33] Julia, G.; *J. Math. Pures Appl.* **7**, 47-245 (1918).

[34] Kaplan, J.L., Yorke, J.A.; Conference paper, lecture notes available at DOI:10.1007/BFB0064319.

[35] Kiss, T., Jex, I., Alber, G., Vyměťal, S.; *Phys. Rev. A* **74**, 040301, 2006.

[36] Kiss, T., Vyměťal, S., Tóth, L.D., Gábris, A., Jex, I., Alber, G.; *Physical Review Letters* **107**, 100501, 2011.

[37] von Koch, H.; *Acta Math.*, **30**, 145, 1906.

[38] Kolmogorov, A.N.; *Dokl. Akad. Nauk SSR*, **98**, 1954.

[39] Malachov, M., *Chaotická dynamika purifikačních protokolů*, master's thesis, FNSPE CTU in Prague, 2015.

[40] Mandelbrot, B.B.; *The fractal geometry of nature*, W.H. Freeman and Company, New York, ISBN 0-7167-1186-9.

[41] Mandelbrot, B.B.; *Nonlinear Dynamics*, **357**, 249, 1980.

[42] Mañé, B., Sad, P., Sullivan, D.; *Ann. Sci., École Norm. Sup.*, **16**, 193, 1983.

[43] May, R.; *Nature*, **261**, 459, 1976.

[44] Milnor, J. W.; *Dynamics in One Complex Variable*, 3^{rd} edition, Princeton University Press, 2000.

[45] Morosawa, S., Nishimura, Y., Taniguchi, M., Ueda, T.; *Holomorphic dynamics*, Cambridge University Press, 2000, ISBN 0-521-66258-3

[46] Moser, J.; *Matematika*, **6**, 51, 1962.

[47] Nielsen, A. M., Chuang, I. L.; *Quantum Computation and Quantum Information*, Cambridge University Press, 2000.

[48] Onsager, L.; *Phys. Rev.*, **65**, 117, 1944.

[49] Peano, G.; *Math. An.*, **36**, 157, 1890.

[50] Peitgen, H.-O., Richter, P.H.; Conference paper, ISBN 978-3-540-39298-9

[51] Perron, O.; *Math. Z.*, 32, 703, 1930.

[52] Plenio, M.B., Virmani, S.; *Quantum Information & Computation* **7**, 1-51 (2007).

[53] Poincaré, H.; *Les Méthodes Nouvelles de la Méchanique Céleste*, Gauthier-Villars, Paris, 1892.

[54] Portmann, C., Renner, R.; arXiv:1409.3525

[55] Ruelle, D.; *The Math. Intelligencer*, **2**, 126, 1980.

[56] Sayama, H.; `https://math.libretexts.org/Bookshelves/Scientific_Computing_Simulations_and_Modeling/Book%3A_Introduction_to_the_Modeling_and_Analysis_of_Complex_Systems_(Sayama)/05%3A_DiscreteTime_Models_II__Analysis/5.07%3A_5.7_Linear_Stability_Analysis_of_Discrete-Time_Nonlinear_Dynamical_Systems`

[57] Shannon, C.E.; *Bell System Tech. J.*, **27**, 1948.

[58] Shishikura, M.; *Annals of Mat.*, **147**, 225, 1998.

[59] Shor, P.W.; *Comput. Soc. Press*, **70**,1895, 1993.

[60] Sierpinski, W.; *C.R. Acad. Sci. Paris*, textbf162, 629, 1916.

[61] Strogatz, S.H.; *Nonlinear Dynamics and Chaos*, 2^{nd} edition, Westview Press, 2015, ISBN 978-0738204536

[62] Turing, A.; *Mind*, **236**, 433, 1950.

[63] Verhulst, P.-F.; *Nouv. mém. de l'Academie Royale des Sci. et Belles-Lettres de Bruxelles* **18**, 1-41, 1845.

[64] Verhulst, P.-F.; *Mém. de l'Academie Royale des Sci., des Lettres et des Beaux-Arts de Belgique* **20**, 1-32, 1847.

A. Box-counting dimension

A.1 The idea of box-counting

The concept of the box-counting dimension was formally introduced as a mathematical definition in 2.3.36 where we also mentioned it can be taken as a reasonably efficient dimension estimate. However, the exact implementation is neither obvious nor easy process because the suggested algorithm inherently contains few caveats one must take care of. In this section we present the box-counting algorithm which we develop on our own (using only the basic idea of box covering). We have two reasons to write our own algorithm. First, we tailor the algorithm precisely to our use, we do not have any collisions with data types, and we know exactly how the program is written. We also can give the code so the process is controllable by other researchers who are invited to inspect the algorithm for eventual collaboration on this topic. The other reason is that the algorithm is based on a simple idea. Probably it is expected everyone can spend time to create their own.

First, we would like to remind that some books, e.g. [61] use similar but not the same approach to explain the idea itself. And yes, the idea is simple to understand. Therefore, we build our algorithm from the very beginning, which is also good to obtain some intuition of how the algorithm works and what problems we can expect. In order to avoid general troubles and minimise complications, we tested and 'calibrated' the method on various objects to be most accurate for our purposes. We have even performed three different codes with three different approaches to self-check the results. The following text is written into comprehensive though lengthy form because we wish that any reader can take this text for a guide from zero knowledge to full understanding of the algorithm and our code.

Let us first briefly explain our first approach based on the idea of image processing. For simplicity, we now restrict ourselves only to objects[1] with dimension $0 < \mathcal{D} < 2$ embedded into two-dimensional manifold (generalisation to higher dimensions will be obvious) which is clearly motivated for our use of attractor maps 2.7. We intend to apply the process to our attractor maps which are represented as matrices of certain size $n \times n$. The object of our interest is the structure (pixels) separating regions of different asymptotic regimes (colours). The first idea of box-counting is to relieve the optimality of the covering in the dimension formula 2.3.35. Instead, we split the matrix into a grid of $m \times m$ submatrices - boxes. Such boxes have side $\varepsilon = \frac{n}{m}$. We usually choose n to have many common divisors so that we avoid dividing matrix into uneven boxes. Such approach is also possible though, as well as with overlapping boxes, see [61]. But for the sake of simple programming, we do not choose to complicate the algorithm. In the case of general rectangular matrix of size $n_1 \times n_2$ we would divide the matrix into $m_1 \times m_2$ boxes and we would have to look for common divisors which is just a minor technical issue not changing the algorithm; without loss of generality we can continue with $n_1 = n_2 = n$. We calculate number of boxes N_ε that cover the

[1] Working in certain coordinate systems we identify the object with corresponding coordinate representation.

object, this is executed by checking if the submatrix (box) contains more than one unique value. For this reason, maximal suitable boxing layout can be done for $m = \frac{n}{2}$. a single pixel represents a set of states we consider to have the same dynamical regime and only a box of minimal size 2×2 can cover more asymptotic regimes and thus the structure of sensitive states.

The second idea of the box-counting approximates the scaling limit ε in 2.3.35. When we repeat preceding step for various (increasing) values of m, we decrease ε towards $2 \doteq 0$, we can simulate the limit in the dimension formula. The third idea simplifies determining $\mathcal{D}$ when the first two ideas are realised. From 2.3.35 we can see that the dimension $\mathcal{D}$ manifests as a slope of line $y = \mathcal{D}x$ when we denote $y = \log N_\varepsilon$ and $x = \log \frac{1}{\varepsilon}$. In this way we can estimate the dimension when fitting the set of such calculated points (x, y) with a line.

Here, we present the sketch of our first box-counting algorithm, merely to illustrate the algorithmic line of thought, in the way we realised it in the MATLAB software. The box-counting itself is realised with repeating following steps on a picture with resolution $n \times n$:

- Choose $m \in \hat{n}$ such that $m|n$. Divide the picture into $m \times m$ squares (containing $\varepsilon = \frac{n}{m}$ pixels);
- Create zero matrix M of size $m \times m$;
- For element of matrix M (indexing the boxes) we take the corresponding box in the $n \times n$ matrix (the attractor map) and check whether the submatrix contains more than unique value (i.e. covers the structure separating basins of attraction, structure of our interest). If yes, we inscribe value 1 to the matrix element in M.
- Sum elements of M, the sum equals to the number of covering boxes N_m.
- Create a point $(\log m, \log N_m) =: (x, y)$.

When these steps are iterated for all possible m we obtain a set of points which we fit with $y = \mathcal{D}x + R$ as suggested earlier;

$$y = \log N = \mathcal{D} \log \frac{1}{\varepsilon} = \mathcal{D} \log \frac{m}{n} = \mathcal{D} \log m - \mathcal{D} \log n = \mathcal{D}x + \tilde{R} \tag{A.1}$$

It is important to realise that in this procedure we approximate $\lim_{\varepsilon \to 0}$ (the size of the boxes goes to 0) with $\lim_{m \to \frac{n}{2} \doteq \infty}$, i.e. the image is divided into as many boxes as possible. This is one of the serious sources of error. For this reason, very detailed attractor maps must be created to ensure that $\varepsilon \to 2$ simulates the limit 0 well. We expressed the dimension as a slope fit in terms of m, the density of the box grid. This results into a new term $\tilde{R} = -\mathcal{D} \log n$ which is the shift of the line. Now, we remind that the dimension does not depend on the absolute size of the picture. This corresponds to the value of n. When we say the picture has 'size' $n = 1$ the shift term $\tilde{R}$ vanishes. We conclude the shift is not important for the dimension estimation, it can be simply related to the absolute size of the picture.

On the other hand, a shift is always present due to the numerical imprecision. We will comment this together with other problems now; the approximation of

the limit $\varepsilon \to 0$ is not the only source of error. Another source comes from omitting the optimality of the covering and also, we must not forget the finite precision of computation. In the following text, we also show some examples where the problems can be fatal for dimension estimation.

Since the first idea of the box-counting method reduces the optimal covering of the object to some rigid grid of boxes, this results in deviations from the line $y = \mathcal{D}x$ formulated earlier. These deviations can be not only random but also systematic because the rigid boxes cover the object in a far-from-optimal manner. For example, the rigid box grid can cover the object of interest with a vast number of boxes with only the tips of their corners: Imagine a square picture where our object of interest is its diagonal line. When we cut the square into $m \times m$ squares, m of them (lying exactly on the diagonal) would cover the line. The line would run through the corner points of these boxes precisely. When the line would be shifted slightly to a side, the line would outreach the squares, and we would need additional $m - 1$ squares to cover the whole line. In total, we would obtain

$$\mathcal{D} \sim \frac{\log(2m-1)}{\log m}. \tag{A.2}$$

This of course leads to $\mathcal{D} = 1$ when the limit $m \to \infty$ is performed. As we work numerically, we can only choose m far away from ∞. When we choose $m = 10^3$ the dimension estimate is deflected to $\mathcal{D} \sim 1.1$, for $m = 10^6$ the result would be $\mathcal{D} \sim 1.05$. But grids of orders of $10^6 \times 10^6$ pixels are not well manageable in common computers. It is vital to understand that the box-counting method can be very imprecise, yielding rather indicative values. It has no sense to present it to three decimal ciphers because the error can easily be deviated by 10%. However, this example is taken in a very specific way and the fractals in our calculations do not suffer from this effect that much. The issue springs from the alignment of the structure with the box grid. For most of the fractals and in particular fractals in our work such a situation does not occur. Another example of the systematic error in the method can be the Sierpinski carpet, [60] see figure A.1. In this case the structure of the fractal matches the box grid again and this leads to similar pathology of deviation of the dimension estimate.

The Sierpinski carpet is created in the following way: Starting with a square, divide it into nine equal squares and remove the middle one. This step is iterated on all subsequently obtained squares infinitely many times. In this way, each arbitrary piece of the surface gets eventually punctured at a certain step. Consider that each iteration reduces the area of the carpet to 8/9 of the original area. Executing this reduction infinitely many times we find that the carpet has zero area, similarly its perimeter grows to infinity. Truly, we will find below that the carpet is neither a surface nor a curve because its dimension will be $1 < \mathcal{D} < 2$. It can be proven that the carpet is equal to its border and for that reason we can look at the structure in two ways , as an area that is iteratively punctured, or square perimeters that are iteratively multiplied and rescaled.

Let us first take it as an area which is more suitable to the pixel representation. The construction of the Sierpinski carpet is very favourable when approached in pixelised form (in finite approximation, of course) - it is very easy to specify what pixel should have which colour (carpet present/not present). We use an easy idea to draw the carpet: Construct an elementary unit - a square (initially a pixel of

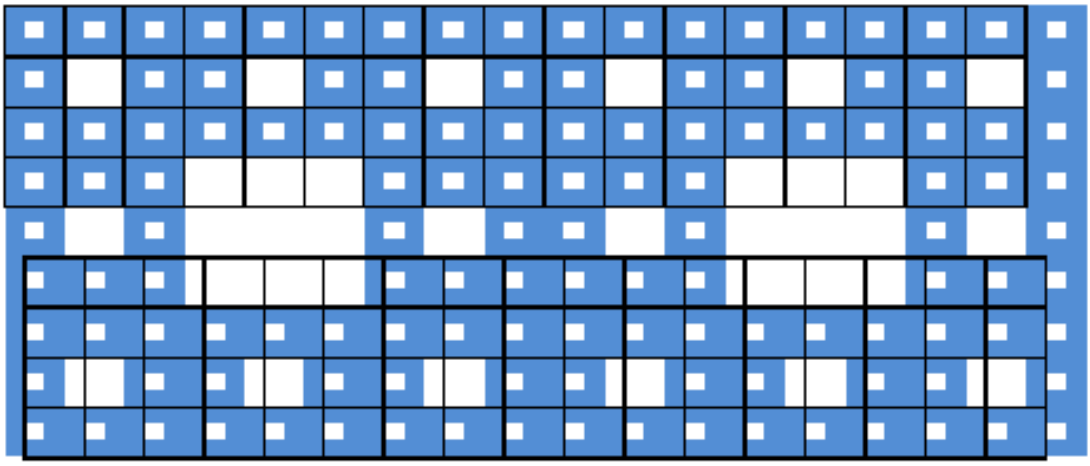

Figure A.1: Simplified model of the Sierpinski carpet simulates finite resolution of pictures in computer. Two possible coverings with identical box grid demonstrate the position dependence in the box-counting method. The grid at the top contains 12 boxes that do not cover the blue region. In contrast, the grid at the bottom contains only 4 such boxes. In case we would be interested in the curve separating blue and white regions, the upper grid coincides with the curve - the dimension cannot be estimated correctly in this case.

value 1). Set eight copies of the elementary unit along an empty unit (initially a pixel of value 0). Take this square of nine units as a new elementary unit and repeat. In this way, we weave the carpet to arbitrary size. At certain step, the initial square (pixel) becomes so small compared to the size of the whole carpet that it is indistinguishable from the true carpet element for the computer. When we reach this situation, we successfully simulate the carpet's structure.

Now, we want to determine the dimension of the Sierpinski carpet. We will use the box-counting method, the box covers the carpet when it contains at least one pixel of it, this is different to the situation when we aim at border structure, such box has to contain both of covering and not covering pixels. Suppose we have just performed the first iteration of the carpet's creation algorithm, we set the absolute measure by setting the side of the whole carpet to have length 1. The step of the creation algorithm divided it into nine equal squares and deleted the middle one. If we identify the structure of the carpet with the box-covering structure, we need 8 squares of side $1/3$ to cover the carpet. When we continue to another iteration we need 64 squares of side $1/9$. Proceeding to n iterations, we cover the carpet with grid of squares of side $1/3^n$, we need 8^n of such squares. In this line of thought, we can even perform the limit $n \to \infty$ and see that the box-counting dimension is $\log_3 8$. We would obtain this number even if we would allow the squares to float, not to be set in a fixed grid. This covering with squares is very well set but we illustrate now what happens when the grid of boxes would be shifted. As shown in the figure A.1 when we would displace the box grid for a unit, the covering would not be optimal, more boxes would be needed. This also demonstrates that the box-counting dimension depends on the location of the grid vs. the object.

To translate the situation back to the situation where we intend to detect the

border of a fractal, we understand previous pixels of the structure as covering pixels of the structure iterated to the next level. It can be easily imagined that each coloured pixel in figure A.1 stands for eight coloured and one uncoloured subpixels, therefore covers the structure of the carpet understood as a set of curves. This duality of the area and border curve will lead us to improvement of the first version of the box-counting algorithm.

Back to the topic of imprecise estimates, a pathological situation occurs when we would want to capture the dimension of the border of the model of the Sierpinski carpet from the figure as it is in A.1 in the aforementioned way. We mark the box as 'covering' when it contains pixels of both colours. We can see that in the figure A.1 the original and the shifted grid yield different number of covering boxes. If we would choose the box grid which is a level finer, each box would contain just a single colour and therefore no border would be detected. This situation when the box grid coincides with the fractal generally lowers the box-counting dimension, while the situation where the box grid is abundantly covering the object increases the value; both situations can generally happen in our later computation. But we can avoid this pitfall when we use different grids (which is equivalent to use rotated, shifted, even stretched pictures of the object) and decide the optimal dimension value.

We conclude there is an error connected to the setting of the object within the picture. This error (which comes from omitting the minimum and covering optimisation in the dimension definition) can lead to false dimension estimate. It also increases variance in the line fitting. To avoid this problem, we could use different pictures of the same fractal - shifted and rotated - to check how this issue affects the dimension estimate. We have two complementary options - either we modify the box grid, or an object. These two approaches are dual in the sense that the transformation of a deformed grid can be executed inversely to both the grid and the untouched structure by which we obtain the original grid and deformed structure. Such transformation must possess certain properties to guarantee that the structure dimension does not change, e.g. the structure is not deformed into a single point. It is not in our scope to find such properties but we can certainly propose following.

Proposition A.1.1. *For F Lipschitz continuous map with Lipschitz constant $\lambda > 0$ on a metric space X, $\mathcal{D}_{BC}(Y) = \mathcal{D}_{BC}(F(Y))$ is true for any Y subset of X.*

Proof. Taking the λ the Lipschitz constant of F and $\{U_i\}_i$ covering of Y. Then, diameters can be estimated $|F(U_i)| \leq \lambda |U_i|$. Therefore, when there were N_ε boxes of diametres at most ε, the same boxes mapped via F give the covering of diameter at most $\varepsilon' = \lambda\varepsilon$; the number of boxes does not change, $N'_{\varepsilon'} = N_\varepsilon$. Therefore, the dimension $\mathscr{D}'_{BC}$ calculated on the image $F(Y)$

$$\mathscr{D}'_{BC} = \lim_{\varepsilon' \to 0} \frac{\ln N'_{\varepsilon'}}{\ln \frac{1}{\varepsilon'}} = \lim_{\lambda\varepsilon \to 0} \frac{\ln N_\varepsilon}{\ln \frac{1}{\lambda\varepsilon}} = \lim_{\varepsilon \to 0} \frac{\ln N_\varepsilon}{\ln \frac{1}{\varepsilon}} = \mathscr{D}_{BC}, \tag{A.3}$$

just because λ is a nonzero constant. □

The second problem of box-counting approach has been already touched, it connects to the omitting of the limit in the dimension definition 2.3.36. For some

objects the limit can be reached very slowly and numerical threshold in m cannot get near. This can of course lead to defects in the dimension estimate.

The third problem is related to the picture of the object. We use matrices of pixels, i.e. the infinitely recurring fractal structure cannot inherently be captured. Finite resolution of the picture affects the resulting dimension in a following way. As the number of boxes approaches the resolution of the picture the object seems more and more coarse and the fractal fine structure is lost to the boxes, see A.2. In the extreme case when the number of the boxes is equal to the resolution size of the picture, we cannot capture the fractal as a curve separating two regions (each pixel contains a single colour, i.e. belongs to a single region). We remind this issue happened for model of the Sierpinski carpet for certain setting of the box grid.

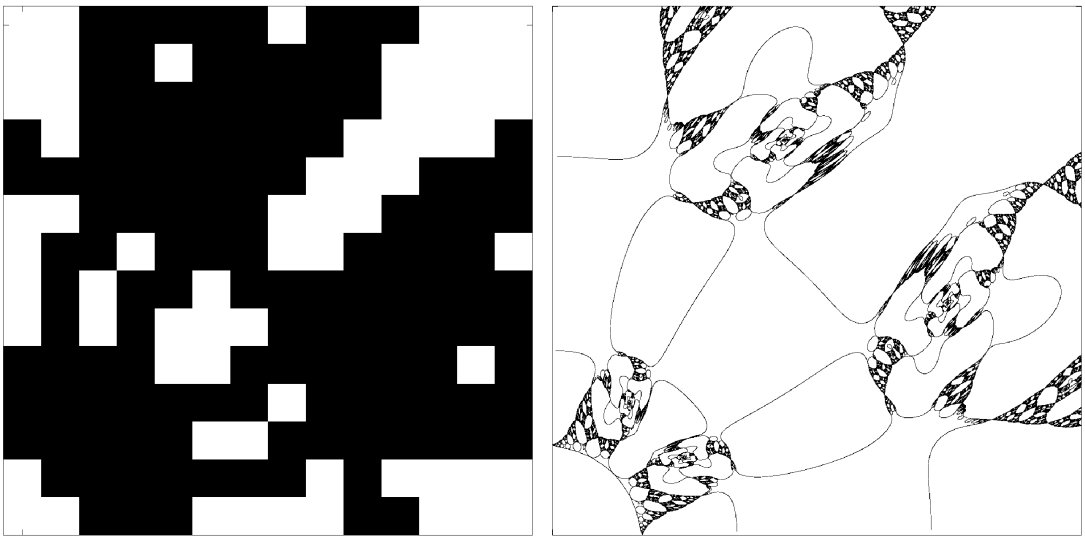

Figure A.2: Resolution of a picture affects the dimension estimate. When a poor picture is used or the box size approaches the size of a pixel, the box-counting method fails to detect borders between black and white regions. TheLeft picture represents a poor resolution picture. However, at the same time it represents a single box capturing a detail of the fractal when $\varepsilon = n/m = 15$.

In the figure A.3 we show points $[\log m, \log N_m]$ as m initiates at 1 (whole picture is taken as a single box) and then m is growing until $m \times m$ approaches resolution $n \times n$ of the picture of the fractal. We discuss now three significant regions, exact sizes of the regions must be decided from picture to picture, given values are just orientational:

- m small (ca. $m < \frac{n}{100}$) - in this mode the box grid is too rough to capture the details and self-similarity of a fractal. The position of the object in the picture strongly influences the N_m. Points fluctuate along the line determining the dimension;

- m intermediate - in this mode the boxes can capture the self similarity of a fractal. Also, each of the box contains enough pixels so the fractal actually has its shape. Because the grid is fine enough as well as each box contains fine details of the object, this region is the most reliable to extract the dimension from;

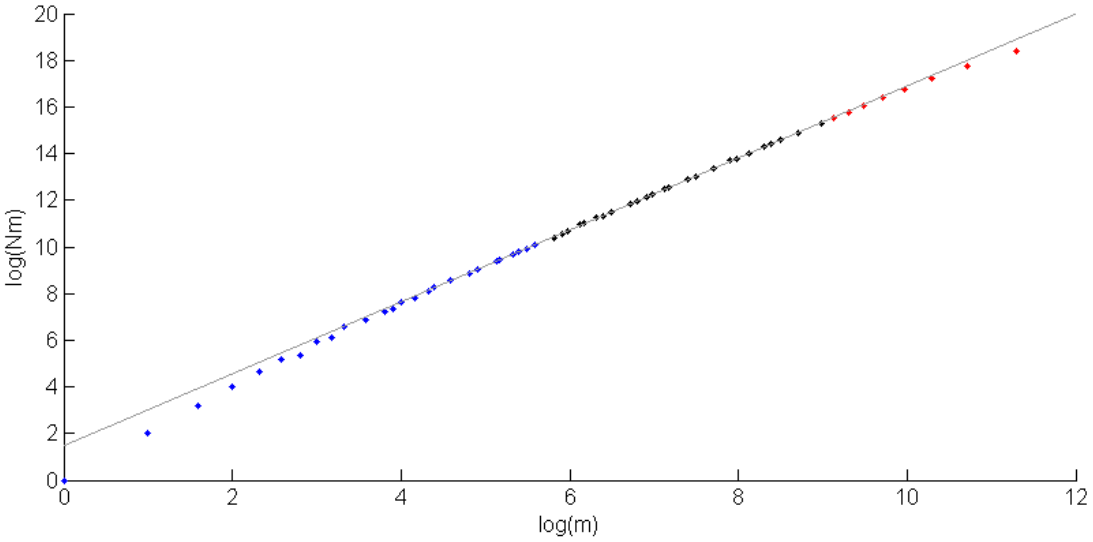

Figure A.3: Points $(\log m, \log N_m)$ form a line, its slope equals to box-counting dimension. Points with low m (blue colour) are affected by the object setting, points with high m (red colour) are deviated by the relative low resolution of the picture. Gray line is the fit of chosen intermediate m values (black colour).

- m big ($m \sim n$) - in this mode the resolution of the picture decreases the N_m because the boxes contain too few pixels to distinguish where object is and is not. This leads to underestimating the dimension when the fit is made in this region too. In extreme case the estimate might fail like in the Sierpinski carpet example. This mode is equivalent to using a picture with poor resolution, as illustrated in A.2.

To obtain the most accurate dimension estimate, we exploit the middle region $1 \ll m \ll n$. In order to have sufficiently many points to fit a line in this region we need to use a picture with high resolution. However, higher resolution naturally leads to longer computation times. We usually used pictures with resolution 5040×5040 pixels and we used $\frac{n}{100} < m \leq \frac{n}{10}$ in our calculations, experiments, and verifications.

The last note is that a similar approach can be generalised into a $d-$dimensional space by taking a (hyper-)cube of size n, divide it into m^D boxes of characteristic size $\varepsilon = \frac{n}{m}$ and then the process of the slope fitting is the same as discussed. We sum up that the box-counting method uses very simple ideas to approximate the fractal dimension. However, the ideas induce few troubles which we are aware of. We suggested and implemented few improvements to reduce the error. In spite of our effort, this implementation of box-counting algorithm remains very inaccurate and serves rather as an indicative instrument than an exact estimator.

A.2 Improved box-counting algorithm

Previous approach naively followed the ideas of the covering set by dimension definition 2.3.36. Yet it was too robust as it needed an image of high resolution which was later analysed. We now present our own idea and more efficient

implementation. To do so, we realise few issues that we further combine.

The basic thought of previous approach was that the pixel represented an elementary volume of a basin of attraction, a point and its immediate neighbourhood where we approximated that the dynamical regime is the same for all states. The smallest box to detect the border between two different regimes was of size 2×2 pixels which dramatically influenced necessary resolution. Now, we realise that two neighbouring pixels of different regimes (colors) imply existence of a point somewhere in between them that belongs to the border of basins of attraction, the structure of our interest. We relieve the idea of pixe as a volume representant but take it as a single initial state given by some coordinates. If two neighbouring pixels differ in their asymptotic evolution, it implies existence of point in between them that truly is the border point. For the purpose of numerical approximation, we can assign the point the average position of the two neighbouring points and include it into the structure we are investigating. In this way we can use each pair of pixels to be an efficient box instead of 2×2 box. Furthermore, this detection of the border states can be performed efficiently via `edge` command in MATLAB.

What we have just performed could be called duality of the representative and the box; it can be illustrated in figure A.5. Each box is represented by a state. Existence of grid of points implies existence of another grid of points which are positioned in the midst of neighbouring points, these can be taken as representatives of another boxing, this new conjugate boxing is efficiently taken for the algorithm. The point of the new grid is set to belong to the sensitive structure whenever the two (conjugate) neighbouring points differ in their asymptotic regime. This approach is far more successfull in capturing the object of our interest from the image of the same resolution. However, there is a major drawback - computational time. To compare all pairs of neighbouring points is very inefficient and for that reason we used the MATLAB `edge` command with Sobel's method and threshold 0.2 through our thesis which can detect such borders in a fast, optimised way. But a cost must be paid for this, the command creates a matrix if the same size as the input has (the new conjugate grid should be 1 pixel smaller in each size), thus the border states are slightly distorted. To justify the use of the distorted grid, it mainly represents the shift of the all points, such shift does not effect the dimension estimate. And the edge command is optimised to detect the borders.

The second major improvement to our box-counting algorithm gets inspiration from the fact that alignment of the fractal structure with the box structure can fail to detect borders precisely. For example, when the structure of Koch flake-like pinnacles penetrates only small parts of the boxes. The repositioning of the grid can uncover such pathology without making. For this reason we propose to randomise the points representing the original box grid where the evolution is calculated. The representative point can be taken anywhere in the box with uniform distribution. Such approach is correct, this statement can be sustained by following arguments. The box in the box counting method does not have to be a square generally, the definition requires coverings of certain size, not actual shapes. In literature, e.g. [61], spheres can be used generally, rectangles. Other grids can be thought of. Our suggestion is to use de facto boxes of random polygonal shapes completely filling the space. In the limit of good resolution

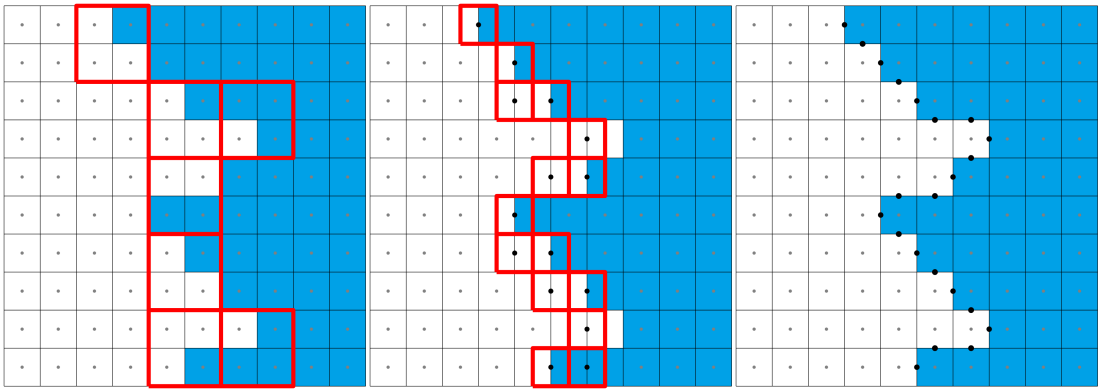

Figure A.4: The first approach of our box-counting algorithm uses boxes of at least 2×2 pixels; left. The improved algorithm uses command to detect borders of basins of attraction. The dual grid of new boxes symbolically shifted to dashed lines for better visualisation and can be understood as representatives of points of the structure; middle. The best option is any border point to the structure individually, each point can be understood as a single box; right.

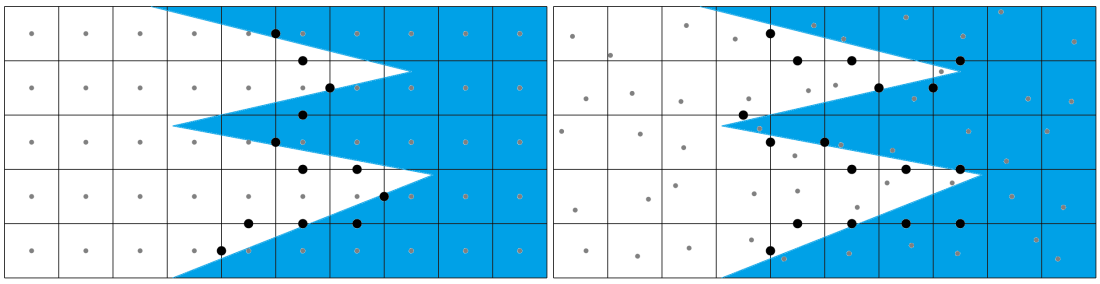

Figure A.5: Rigid boxes around uniform grid of points (gray dots) cannot capture complicated shape; left. Randomised points represent the same boxes but can offer better approximation of the structure (black dots), especially when the randomisation is repeated; right. Randomised boxes capture 5 more points of the structure and better simulate the fractal distribution in space in this case.

$\varepsilon \to 0$ the dimension estimate must agree for any shapes. Second and related argument is that more detailed resolution would detect a pathological structure, by the random repositioning of the representative point we virtually simulate higher resolution. The actual advantage of the randomised boxes lies in the repeating the process, in such case new positions can detect structure points not detected in previous setting. It is computationally more efficient (time, memory) to repeat the algorithm many times on a smaller matrix than one time on a large matrix. Another argument lies in the proposition A.1.1 which explains that certain well-behaved distortion does not change the dimension of the object. The distortion in our proposal is only chosen locally, not globally.

We now list the full code which we used to detect the structure of sensitive points and its dimension. We add comments to make it comprehensible, in particular we dedicate a few sentences to improvements. This MATLAB code could be transferred and is ready to use for the reader on their own. First of all, we write a help script that iterates the evolution function of one iteration of the general protocol P_n with twirling gate, 5.10, 4.7. This could be implemented as

a function but for the memory manipulation we chose the form of a script.

```
% ITERATE
D0=((1+W).^power+(1-W).^power)/2;
D1=((1+W).^power-(1-W).^power)/2;
D2=real((U+I*V).^power);
D3=imag((U+I*V).^power);

A=(cos(2*x)*D1+sin(2*x)*cos(psi)*D2+sin(2*x)*sin(psi)*D3)./D0;
B=((-sin(2*x)*cos(psi-tau))*D1+ ...
...+(sin(psi)*sin(psi-tau)+cos(psi)*cos(psi-tau)*cos(2*x))*D2+ ...
...+(-cos(psi)*sin(psi-tau)+sin(psi)*cos(psi-tau)*cos(2*x))*D3)./D0;
C=((-sin(2*x)*sin(psi-tau))*D1+ ...
...+(-sin(psi)*cos(psi-tau)+cos(psi)*sin(psi-tau)*cos(2*x))*D2+ ...
...+(cos(psi)*cos(psi-tau)+sin(psi)*sin(psi-tau)*cos(2*x))*D3)./D0;
```

This code transforms arrays of coordinates w, u, v using protocol parameters - the order of protocol (how many qubits are used) `power` and angles `x`, `psi`, `tau`, as intuitively suggested. We also need to manage the inputs and outputs. As the code must be given mentioned parameters; we can restrict the input states with discovered symmetries. We cast the inital set of all parameters into vector

```
ParameterSetting=[power,P,x,psi,tau,phi1,phi2,theta1,theta2];
```

where the P selects the purity of intial states and the spherical angles of in the initial state space are chosen in range $\varphi \in (\texttt{phi1}, \texttt{phi2}), \vartheta \in (\texttt{theta1}, \texttt{theta2})$.

The range however does not focus on fractal and can cover areas of basins of attraction which only effectively decrease the resolution of the box-counting. For that reason, we used following detection script that cuts off the areas where the structure of sensitive states is not present. We also developed a method of zooming on the areas with higher density of the structure based on Fourier transformation but we do not present it here because we did not use it. The reason is that we had to manually control whether the zooming converged well due to precision limitations. We only give the brief code that cuts off the areas without structure, in a form of script again.

```
%FRAMECUT
care=2;
% care=2 guarantees that the border of the structure is not
% cut off by setting a two pixel offset to the cut.
EDGE=(sum(M,1));
shiftor=find(EDGE,1)-care;
phi1new=phi1+(shiftor-1)*(phi2-phi1)/(phires-1);
EDGE=fliplr(EDGE);
shiftor=find(EDGE,1)-care;
phi2new=phi2-(shiftor-1)*(phi2-phi1)/(phires-1);

EDGE=(sum(M,2))';
shiftor=find(EDGE,1)-care;
theta1new=theta1+(shiftor-1)*(theta2-theta1)/(thetares-1);
```

```
EDGE=fliplr(EDGE);
shiftor=find(EDGE,1)-care;
theta2new=theta2-(shiftor-1)*(theta2-theta1)/(thetares-1);

changeindex=0;
% changeindex controls whether the cut effectively reduced the
% range of angles. If not, the cutting process is not iterated
% more  by the main body of the main programme.
if theta2new-theta1new>0
    if theta1<theta1new
     theta1=theta1new;changeindex=1;
    end
    if theta2>theta2new
     theta2=theta2new;changeindex=1;
    end
end
if phi2new-phi1new>0
    if phi1<phi1new
    phi1=phi1new;changeindex=1;
    end
    if phi2>phi2new
    phi2=phi2new;changeindex=1;
    end
end
```

Now we present the main body of the program, we expect the vector of the parameters `ParameterSetting` which was defined earlier to be loaded. If not, we add command

```
load('ParameterSetting.mat')
```

to the main body. We break the code of the program into blocks for better commenting.

```
% 2DIMSCALE
power=ParameterSetting(1); P=ParameterSetting(2);
x=ParameterSetting(3);
psi=ParameterSetting(4);
tau=ParameterSetting(5);

phi1=ParameterSetting(6); phi2=ParameterSetting(7);
theta1=ParameterSetting(8); theta2=ParameterSetting(9);

ResSizeHolder=[];
ResultVector=[];
repindex=10;
```

At this moment the setting is prepared for calculations and variables - `ResSizeHolder` to store the points $(\log m, \log N_m)$ to be fitted and `ResultVector` to store the results are created. Variable `repindex` determines how many times

the grid with randomised boxes will be constructed to reduce effect of numerical deviations. Its role will be specified below. Next part of the code creates the grid of initial states which is first compressed into complex variable `Z` which could be used to implement pure states dynamics easily. Because we focus on mixed states we do not write this case here.

```
resolution=5000;
xs=round(resolution*(x2-x1)/(y2-y1));
ys=round(resolution*(y2-y1)/(x2-x1));
if xs<resolution/50
     xs=round(resolution/50);ys=round(resolution/xs);
elseif ys<resolution/50
ys=round(resolution/50);xs=round(resolution/xs);
end
xspace=linspace(x1,x2,xs); yspace=linspace(y1,y2,ys);
[X,Y]=meshgrid(xspace,yspace);
Z=X+1i*Y;
```

When the grid of xs $\times$ ys pixels (states) is created, we introduce the random shift by uniform distribution in both directions with `rand` command. We perform the box-counting for a number of such disturbed grids to obtain a statistics. The number of attempts is fixed in `repindex` variable. Usually, we used value of 10 for prcise estimates as a compromise between statistics and computation time but for overviews we restricted to a single repetition. Qualitatively same results were also obtained when the grid was rotated and shifted globally but the rotations notably change the range of the ϕ, ϑ so we decided to use the random shift in each pixel.

```
for randrep=1:repindex
        Xran=real(Z)+(2*rand(ys,xs)-1)*(x2-x1)/(2*xs);
        Yran=imag(Z)+(2*rand(ys,xs)-1)*(y2-y1)/(2*ys);
        U=sqrt(2*P-1)*sin(Yran).*cos(Xran);
        V=sqrt(2*P-1)*sin(Yran).*sin(Xran);
        W=sqrt(2*P-1)*cos(Yran);
```

After creating the grid of w, u, v coordinates we let the states evolve and find the structure of sensitive states using the `edge` command. The iterations are calculated until the `edge` command yields the same structure. In such case, we take the convergence to be precise enough. The number of iteration is stored for later use. We note that the convergence deduced form unchanged edge structure does not imply the true convergence for cases where the convergence is too slow to cause changes in less than 100 iterations. However, such cases are extremely rare for rational polynomial maps and for that we neglect them. We could typically encounter such effects if we would investigate the evolution on a very small neighbourhood of a fixed point/cycle with eigenvalues of Jacobi matrix $|\lambda| \doteq 1$.

```
        itindex=0;
        for it=1:100
                Iterate
```

```
        end
        itindex=itindex+it;
        M1=edge(A,'sobel',0.2)+edge(B,'sobel',0.2)+ ...
                ... +edge(C,'sobel',0.2);
        M1(M1>1)=1;
        for it=1:100
                Iterate
        end
        itindex=itindex+it;
        M2=edge(A,'sobel',0.2)+edge(B,'sobel',0.2)+ ...
                ... +edge(C,'sobel',0.2);
        M2(M2>1)=1;

        while M1~=M2
        M1=M2;
        for it=1:100
                Iterate
        end
        itindex=itindex+it;
        M2=edge(A,'sobel',0.2)+edge(B,'sobel',0.2)+ ...
                ... +edge(C,'sobel',0.2);
        M2(M2>1)=1;
        end

        ResSizeHolder=vertcat(ResSizeHolder,  ...
                ... [sqrt(xs*ys),sum(sum(M2))]);
end
```

We would like to stress at this place that we use idea we mentioned earlier that the absolute size of an image projects only into the shift and not the slope of the fitting line. For this reason we can use characteristic length of the covering sets in definition 2.3.35 resp. 2.3.36; so we use $\sqrt{\texttt{xs} \cdot \texttt{ys}}$. The fact that the boxes can be rectangular and not only squares comes from the fact that scaling one side by certain factor cannot change the dimension of an object, we recall A.1.1. This factor plays a similar role as the absolute size of the image and proliferates only into the shift of the fit. We do not write explicit equations which are the same as but we put accent onto the intuition that an object cannot change its dimension by scaling; such scaling only changes the Hausdorff measure (length, area, volume). Alternatively, in the dimension definition one can substitute the diameter of the covering set with the square root of the area without disturbing convergences - the factors of proportionality only modify the value of the measure, not its convergence to zero or infinity which is the core of the dimension definition. For example when the covering sets would be squares then $\sqrt{A(U)} = \frac{1}{\sqrt{2}}|U|$ where A stands for area, for circles $\sqrt{A(U)} = \frac{\sqrt{\pi}}{2}|U|$, generally $\sqrt{A(U)} = \lambda|U|$ where $\lambda \in (0, \infty)$, therefore for covering $\{U_i\}_i$ we can identify infimum/supremum values

of all such factors λ_i, labeling them $0 < \lambda_{inf} \leq \lambda_{sup} < \infty$[2] and write

$$\sum_i \sqrt{A(U)}^d = \sum_i \lambda_i^d |U_i|^d \leq \lambda_{sup}^d \sum_i |U_i|^d, \sum_i \sqrt{A(U)}^d \geq \lambda_{inf}^d \sum_i |U_i|^d \qquad (A.4)$$

Because the only possibilities for quantity $\sum_i |U_i|^d$ are converging to 0, converging to infinity or converging to a finite nonzero number, the value $\sum_i \sqrt{A(U)}^d$ must also reach 0, ∞ or finite number respectively. We believe that these thoughts must have been written many times or taken for obvious so they are not explicitly written in todays literature. For that reason we do not cast the idea into formal proof but rather its sketch in this appendix. Formal proof is beyond the scope of this thesis and would require to discuss the area measure which for our case coincides with standard Lebesgue measure in Euclidean spaces. One could also use the Hausdorff d-measure which coincides with the Lebesgue measure for $d \in \mathbb{N}$. We just add a final note that this topic can be related to the proposition A.1.1 where the structure is deformed without changing its dimension.

The algorithm now created a single point $(\log m, \log N_m)$; to fit the linear trend we need more such points, therefore we repeat the process with other values of resolution. This resolution which determines the precision of the initial states can also be implemented by using command `round` and the box structure would be implemented by comparing the number of unique points under rounding to different levels of precision. We use the approach of setting the value of resolution to avoid more involved discussions of the scaling and also to obtain the statistics by randomising the boxes.

```
for resolution=4000:-1000:1000
xs=round(resolution*(x2-x1)/(y2-y1));
ys=round(resolution*(y2-y1)/(x2-x1));
if xs<resolution/50
xs=round(resolution/50);ys=round(resolution/xs);
elseif ys<resolution/50
ys=round(resolution/50);xs=round(resolution/xs);
end
xspace=linspace(x1,x2,xs); yspace=linspace(y1,y2,ys);
[X,Y]=meshgrid(xspace,yspace);
Z=X+1i*Y;

for randrep=1:repindex
Xran=real(Z)+(2*rand(ys,xs)-1)*(x2-x1)/(2*xs);
Yran=imag(Z)+(2*rand(ys,xs)-1)*(y2-y1)/(2*ys);
B=sqrt(2*P-1)*sin(Yran).*cos(Xran);
C=sqrt(2*P-1)*sin(Yran).*sin(Xran);
A=sqrt(2*P-1)*cos(Yran);
for it=1:itindex
Iterate
end
```

[2]These values cannot attain 0 or ∞ as the corresponding sets would cover 0 or infinite area. Such situation is not possible.

```
M2=edge(A,'sobel',0.2)+edge(B,'sobel',0.2)+edge(C,'sobel',0.2);
M2(M2>1)=1;

ResSizeHolder=vertcat(ResSizeHolder, ...
... [x,fi,omega,P,sqrt(xs*ys),sum(sum(M2))]);
end
end
```

The chosen values of resolution are a compromise between precision and computation time that was made after evaluating the dimension estimates for various fractals of our interest and for various values of the resolution. At this moment we have a set of points to fit as in A.3 which we do by linear model. Of course, only in case that the structure is present. The `ResultVector` that stores the result contains the slope of the linear fit, i.e. the dimension, the shift, sum of squared errors and root-mean-squared error. These results and the algorithm can be reforged to one's desired way of use, e.g. to work as a for cycle for various protocol settings etc., that is merely a cosmetic issue.

```
if sum(sum(M2))>0
mdl=fitlm(log(DetailSizeHolder(:,5)),log(DetailSizeHolder(:,6)));
ResultVector(1)=mdl.Coefficients.Estimate(2);
ResultVector(2)=mdl.Coefficients.Estimate(1);
ResultVector(3)=mdl.SSE;
ResultVector(4)=mdl.RMSE;
end
save("ResultVector.mat","ResultVector")
clearvars
```

A.3 Fast algorithm

The third alternative to previous algorithms uses a trick to implement the box grid. When the structure is determined, it is represented by point coordinates which are given to some precision. The precision itself forms a box! Rounding points naturally offers boxes of size 10^{-n}. Such boxes are too rough to provide good dimension estimate so we propose to use additional scaling. With this approach, we aim at determining the box-counting dimension in the three-dimensional space where creating $5000 \times 5000 \times 5000$ grid of points overwhelms RAM capacities of computers. Therefore, we can part by part determine positions of points of the structure as shown in the right scheme in A.5. These points are determined only a single time and for the highest resolution only. In our context of the Bloch space the three coordinates (w, u, v) are real numbers from $[-1; 1]$, 2.31, and these can be trustfully set to precision at most in the $\varepsilon = 10^{-15}$ order in double format standardly used in MATLAB. The following procedure is applied to the structure: for scaling factor $\lambda \in [1, 10^{15}]$ all the structure points are rescaled and rounded (marked with square brackets) $(w, u, v) \to ([\lambda w], [\lambda u], [\lambda v])$. Number of unique rescaled points N_λ is summed and a point is created $(\log \lambda, \log N_\lambda)$. Repeating this process for various lambdas is equivalent to the choice of various m earlier. Reader can easily grab the analogy when realising that for $\lambda = 1$ all points are rounded to points with integer

coordinates like $(0,0,0),(1,0,-1)$ etc. This essentially marks the occupation of 27 sub-cuboids that the cube $[-1;1]\times[-1;1]\times[-1;1]$ can be divided into. When the scaling factor is taken to reach the precision $\frac{1}{\varepsilon} = 10^{15}$, after rescaling each point has a distinct triplet of integers and the number N_λ represent the total number of points we have detected to approximate the structure.

A natural and significant advantage lies in only single calculation of the structure which is the demanding part. Still, the rounding executed with `round` command and finding N_λ with `unique` command are still computationally demanding in big structures. And there is the disadvantage in this approach that we are also relieving the randomised boxes that can approximate the structure better.

For practical reasons we do not choose a grid of fine resolution and calculate the structure from a grid of $2000\times2000\times2000$ equidistantly distributed points in the cube $[-1;1]\times[-1;1]\times[-1;1]$, the points outside the Bloch sphere are excluded then. With this precision the points are separated only by distance of orders of 10^{-4} at the closest and so the scaling λ is sufficient to be taken in range $\in[1,10^4]$. Symmetries can restrict the studied volume e.g. to octant $w,u,v\geq0$. and thus improve the algorithm. This method has been again tested and gave the same qualitative results for the case of fractals measured by previous methods.

With the scaling factor λ close to 1 and close to the resolution $\frac{1}{\varepsilon}$ we again encounter the effect shown in A.3. Therefore, only small set of λ is used to guarantee good estimate. Major advantage compared to the first naive algorithm is that the boxes were limited to $m|n$ to avoid problems with overlapping or cut boxes. The parameter λ can be chosen as an arbitrary real number.

We used this method as a faster alternative for determining the fractal dimensions in the three-dimensional Bloch space at the cost of worst dimension estimate and the lack of randomness exploited in the previous version of our box-counting algorithm. The cost is compensated by major advantage of computation feasibility which can be even parallelised in separate regions of the Bloch space.

A.4 Numerical methods and fractal structures

Of course, the box-counting dimension estimation relies on numerical methods. We now present short contemplation on the topic of rough numerical approach versus exponential instability of the chaos. The first question to object is: *"Is it correct and reliable to use the box-counting method?"* The answer is yes, when the fractal structure can be obtained with sufficiently high precision and the fractal is no pathological case, e.g. Sierpinski carpet. However, our improved algorithm succeeds even in such cases.

Of course, we should be aware of using numerical methods when creating the pictures of a fractal, searching for their structure. As sketched in the theory chapter wehre we explain our concept of attractor maps 2.5, the fractal will be a curve (surface) separating basins of attraction. The basins are formed by states with the same asymptotic state, the fractal states are inherently sensitive to perturbation. Second and the most important question to object is: *"Is it correct to use a computer to determine asymptotic evolution of a state?"* When we consider that the chaos equals to the exponential sensitivity of the evolution to the initial conditions, we must answer NO! Each computer can use only approximate calculations up to some precision (in our case of double format in MATLAB

it makes 10^{-15}). Even when we choose to start at a state the is determined exactly in this precision, after a single application of protocol we would most probably have to floor the result. In principle, this small deviation can drive this approximate result to another attractor due to the sensitivity to the initial conditions. However, we may ask the last question. *"Is the numerical imprecision in determining the fractal structure relevant for the dimension estimate?"* The states belonging to the fractals will actually never be acquired precisely in position and the border point can be assigned to a next neighbouring pixel. But because the box-counting only counts number of covering boxes and not exact position, a slight shift of a structure by one pixel due to numerical imprecision is not relevant as it does not change number N_ε. This argument justifies the utilisation of the method.

Another thought supporting the use of the box-counting and numerical methods comes from the evolution equations themselves. The functions 5.10, 4.7, driving the evolution of the mixed states are rational polynomial. Therefore, various inequalities could be derived which restrict behaviour to regular mode on wide domains. Because the evolution functions are continuous up to few poles we do not expect drastic changes when we lower the purity of the states up to some pathological phenomena that may occur at the poles of the functions. We could expect that the known picture 2.6 for pure states will change reasonably, possibly continuously, when the purity of the initial state would decrease. We have seen in the third and fourth chapters that such expectation is true even for generalised protocols. However, there are pathological exceptions in cases where the protocol evolves each state chaotically (for pure single-qubit states it means that the Julia set of the evolution function equals to $\mathbb{C}$) as mentioned in 2.3.28).

Attractors are characterised by the contractive behaviour on the open subsets of their basins of attraction - computational error is reduced during the evolution and the computer can be successful in determining the asymptotic evolution of the state. In contrast, a perturbation of the repulsive states expands a certain neighbourhood during the evolution. In this case, numerical calculations are not reliable. On the other hand, the inverse map must be contractive on that neighbourhood. In consequence, if we suspect that the protocol would induce chaotic behaviour (expanding) in all states, we could alternatively examine the inverse map which should be regular (contracting) in all states. The contractiveness of the map makes numerical calculations resistant and from numerical calculations the convergence is very fast. Together with the fact that the Julia set has zero area we see that numerical calculations are pretty reliable.

In any case, it is important to be aware of the intricate nature of the chaotic dynamics. Cautiousness is needed especially in case where we reach beyond theoretical support of [44] and in pathological cases.